UNIVERSIDADE DE LISBOA

Faculdade de Medicina de Lisboa

The role of A_{2A} receptors in cognitive decline – decoding the molecular shift towards neurodegeneration

Mariana Temido Mendes Ferreira

Orientadores:

Doutora Luísa Maria Vaqueiro Lopes

Professor Doutor Tiago Fleming de Oliveira Outeiro

Tese especialmente elaborada para obtenção do grau de Doutor em Ciências Biomédicas, Especialidade em Neurociências

2018

UNIVERSIDADE DE LISBOA

Faculdade de Medicina de Lisboa

The role of A_{2A} receptors in cognitive decline – decoding the molecular shift towards neurodegeneration

Mariana Temido Mendes Ferreira

Orientadores: Doutora Luísa Maria Vaqueiro Lopes
Professor Doutor Tiago Fleming de Oliveira Outeiro

Tese especialmente elaborada para obtenção do grau de Doutor em Ciências Biomédicas, Especialidade em Neurociências

Júri:
Presidente:
Doutor José Luís Bliebernicht Ducla Soares, Professor Catedrático em regime de *tenure* e membro do Conselho Científico da Faculdade de Medicina da Universidade de Lisboa
Vogais:
Doutor Christophe Bernard, Investigador Coordenador do Institut de Neurosciences des Systèmes, Aix-Marseille Université
Doutora Paula Isabel Antunes Pousinha, Professora Auxiliar do Institut de Pharmacologie Moléculaire et Cellulaire, Côte d'Azur Université
Doutora Ana Luísa Monteiro de Carvalho, Professora Auxiliar da Faculdade de Ciências e Tecnologia da Universidade de Coimbra
Doutora Ana Maria Ferreira de Sousa Sebastião, Professora Catedrática da Faculdade de Medicina da Universidade de Lisboa
Doutor Alexandre Valério de Mendonça, Investigador Coordenador da Faculdade de Medicina da Universidade de Lisboa
Doutora Luísa Maria Vaqueiro Lopes, Professora Associada Convidada da Faculdade de Medicina da Universidade de Lisboa *(Orientadora)*

Fundação para a Ciência e Tecnologia,
referência SFRH/BD/52228/2013

2018

As opiniões expressas nesta publicação são da exclusiva responsabilidade do seu autor, não cabendo qualquer responsabilidade à Faculdade de Medicina da Universidade de Lisboa pelos conteúdos nele apresentados.

A impressão desta dissertação foi aprovada pelo Conselho Científico da Faculdade de Medicina de Lisboa em reunião de 22 de Maio de 2018.

The experimental work herein described was performed at Instituto de Medicina Molecular - Faculdade de Medicina da Universidade de Lisboa except when otherwise stated, under the supervision of Luísa V. Lopes, PhD and Tiago F. Outeiro, PhD.

“It always seems impossible until it´s done”

Nelson Mandela

Abstract

Aging is associated with cognitive decline both in humans and animals. Importantly, aging is the main risk factor for nerurodegenerative diseases, namely Alzheimer's disease (AD), which primarily affects synapses in the temporal lobe and hippocampal formation. In fact, synaptic dysfunction plays a central role in AD, since it drives cognitive decline. Indeed, in age-related neurodegeneration, cognitive decline has a stronger correlation to early synapse loss than neuronal loss in patients. Despite the many clinical trials conducted to identify drug targets that could reduce protein toxicity in AD, such targets and strategies have proven unsuccessful.

Therefore, efforts focused on identifying the early mechanisms of disease pathogenesis, driven or exacerbated by the aging process, may prove more relevant to slow the progression rather than the current disease-based models.

A recent genetic study discovered a significant association of the adenosine A_{2A} receptor encoding gene (*ADORA2A)* with hippocampal volume in mild cognitive impairment and Alzheimer's disease. There is compelling evidence from animal models of a cortical and hippocampal upsurge of adenosine A_{2A} receptors ($A_{2A}R$) in glutamatergic synapses upon aging and AD. Importantly, the blockade of $A_{2A}R$ prevents hippocampus-dependent memory deficits and synaptic impairments in aged animals and in several AD models. Accordingly, in humans, several epidemiological studies have shown that regular caffeine consumption attenuates memory disruption during aging and decreases the risk of developing memory impairments in AD

patients. Together, these data suggest that $A_{2A}R$ might be a good candidate as trigger to synaptic dysfunction in aging and AD. The main goal of this dissertation was then to explore the synaptic function of $A_{2A}R$ in age-related conditions.

We have assessed the $A_{2A}R$ expression in human hippocampal slices and found a significant upsurge of $A_{2A}R$ in hippocampal neurons of aged humans, a phenotype aggravated in AD patients. Increased selective expression of $A_{2A}R$ driven by the CaMKII promoter in rat forebrain neurons was sufficient to mimic aging-like memory impairments, assessed by the Morris water maze task, and to uncover an LTD-to-LTP shift in the Schaffer collaterals-CA1 synapse of hippocampus. This shift was due to an increased NMDA receptor gating and associated to increased Ca^{2+} influx. The mGluR5-NMDAR interplay was identified as a key event in $A_{2A}R$-induced synaptic dysfunction. Moreover, chronic treatment with an $A_{2A}R$ selective antagonist, orally delivered for one month, rescued the aberrant NMDAR overactivation and the plasticity shift. Importantly, the same LTD-to-LTP shift was observed in memory-impaired aged rats and APP/PS1 mice modeling AD, a phenotype rescued upon $A_{2A}R$ blockade.

These data support a key role for over-active hippocampal $A_{2A}R$ in aging and AD-dependent synaptic and cognitive dysfunction and may underlie the significant genetic association of *ADORA2A* with AD. Importantly, this newly found interaction might prove a suitable alternative for regulating aberrant mGluR5/NMDAR signaling in AD without disrupting their constitutive activity.

Resumo

O envelhecimento está associado a défices cognitivos tanto em humanos como em animais. Para além disso, o envelhecimento é o principal fator de risco para as doenças neurodegenerativas, nomeadamente doença de Alzheimer (DA), a qual afecta de uma forma muito significativa as sinapses do lobo temporal e da formação hipocampal. Estes défices cognitivos estão associados a alterações estruturais e funcionais no hipocampo, nomeadamente disfunção sináptica.

A disfunção sináptica apresenta um papel central na DA, uma vez que leva a défices cognitivos. De facto, na neurodegeneração associada à idade, o declínio cognitivo apresenta uma correlação mais forte com a perda sináptica precoce do que com morte neuronal. Apesar do largo número de ensaios clínicos conduzidos no sentido de identificar alvos para fármacos que possam reduzir a toxicidade proteica em DA, tais alvos e estratégias terapêuticas têm-se revelado infrutíferos. Por conseguinte, esforços no sentido de identificar os mecanismos iniciais subjacentes à doença, os quais podem ser provocados ou exacerbados pelo processo de envelhecimento, poderão mostrar-se mais relevantes para retardar a progressão da doença do que os modelos actuais baseados na própria doença.

A gama de proteínas sinápticas é complexa e os mecanismos subjacentes à transmissão sináptica excitatória são rigorosamente regulados pela actividade sináptica. A activação dos receptores NMDA tem um papel fundamental uma vez que pode tanto induzir potenciação de longa duração (LTP) como depressão de longa duração (LTD),

sendo que alterações nestes receptores foram previamente reportadas no contexto de envelhecimento e doença de Alzheimer. Para além disso, foi também reportado um envolvimento dos receptores metabotrópicos de glutamato (mGluR) na disfunção sináptica mediada por Aβ, de tal forma que a proteína Aβ facilita LTD mediada por mGluR e inibe LTP, levando a uma diminuição na densidade das espinhas dendríticas.

O papel da LTP foi intensivamente estudado no contexto da aprendizagem e memória. Pelo contrário, a relação entre LTD e memória está muito menos estudada, tanto em condições fisiológicas como patológicas.

A LTD pode ser definida como um enfraquecimento duradouro de uma sinapse em resposta a um estímulo de baixa frequência. O estímulo desencadeador para a LTD dependente da actividade e induzida pós-sinapticamente é predominantemente um aumento no cálcio pós-sináptico (Ca^{2+}). Uma vez que aumentos pós-sinápticos de Ca^{2+} estão implicados na indução tanto de LTP como de LTD, o conceito de que um aumento elevado de Ca^{2+} intracelular resulta em LTP e um aumento modesto resulta em LTD encontra-se largamente aceite na comunidade científica. Alguns estudos científicos reportaram um aumento da susceptibilidade para LTD associado ao envelhecimento, enquanto outros não observaram diferenças na magnitude de LTD em animais envelhecidos. Estas discrepâncias em termos de resultados podem ser explicadas por diferenças em termos de estirpe de ratos utilizada, padrão de estimulação e rácio Ca^{2+}/Mg^{2+} no meio de perfusão das fatias de hipocampo. De facto, as diferenças relacionadas com a idade em termos de indução de LTD foram revertidas com a

manipulação do rácio Ca^{2+}/Mg^{2+}, consistente com a ideia de que alterações na regulação de Ca^{2+} com o envelhecimento desencadeiam este aumento na susceptibilidade para LTD. Contudo, os mecanismos que levam a alterações na regulação do Ca^{2+} no processo de LTD durante o envelhecimento fisiológico e também em patologias associadas ao envelhecimento continuam por esclarecer.

Recentemente, um estudo genético observou uma associação significativa entre o gene que codifica para os receptores da adenosina A_{2A} ($A_{2A}R$) (*ADORA2A*) e o volume hipocampal em défice cognitivo ligeiro e doença de Alzheimer. Existe evidência robusta de um aumento da expressão de $A_{2A}R$ em sinapses glutamatérgicas a nível cortical e hipocampal no envelhecimento e DA. Para além disso, o bloqueio de $A_{2A}R$ previne défices sinápticos e de memória dependentes do hipocampo em animais envelhecidos e modelos de DA. Em humanos, vários estudos epidemiológicos demonstraram que o consumo regular de cafeína atenua os défices de memória no envelhecimento e diminui o risco de desenvolver défices de memória em doentes de Alzheimer. Consequentemente, estes resultados sugerem que os $A_{2A}R$ são um potencial estímulo desencadeador de disfunção sináptica no envelhecimento e DA. Desta forma, o objectivo da presente dissertação foi explorar a função sináptica dos receptores $A_{2A}R$ em patologias associadas ao envelhecimento.

Avaliou-se a expressão de $A_{2A}R$ em secções humanas de hipocampo e observou-se um aumento significativo na expressão de $A_{2A}R$ em neurónios hipocampais de idosos, um fenótipo agravado em doentes de Alzheimer. Através de um modelo transgénico de rato com sobreexpressão dos receptores A_{2A} controlada através do promotor

CaMKII nos neurónios do prosencéfalo, observou-se que o aumento da expressão de $A_{2A}R$, maioritariamente pre-sinápticos, foi suficiente para desencadear défices de memória semelhantes aos observados no envelhecimento, os quais foram avaliados através do teste do labirinto de Morris. Para além disso, a sobreexpressão neuronal de $A_{2A}R$ leva a um aumento da probabilidade de libertação de glutamato e a uma sobreactivação dos receptores NMDAR. Em termos de plasticidade sináptica, estes animais apresentam uma potenciação da sinapse fibras de Schaffer-CA1 do hipocampo quando é aplicado um estímulo de baixa frequência que habitualmente induz LTD. Esta inversão de LTD para LTP encontra-se associada ao aumento da ativação do receptor NMDA, com um consequente aumento da entrada de Ca^{2+}. Identificou-se a interacção mGluR5-NMDAR como tendo um papel chave na disfunção sináptica induzida por $A_{2A}R$. O tratamento agudo quer com o antagonista selectivo SCH 58261 quer com o antagonista não selectivo cafeína reverte esta inversão na plasticidade. Para além disto, e de forma mais relevante, o tratamento crónico com um antagonista seletivo dos $A_{2A}R$, administrado por via oral durante um mês, reverteu a sobre-activação dos receptores NMDA e a inversão na plasticidade sináptica.

Foram também usados ratos envelhecidos (aproximadamente 18 meses de idade) com défices de memória e em ratinhos APP/PS1 com cerca de 12 meses de idade, um modelo de Doença de Alzheimer. Foram já previamente reportados défices de memória nestes ratinhos nesta idade. De forma muito relevante, esta mesma inversão sináptica foi observada em animais envelhecidos e em ratinhos APP/PS1. Para além disso, observou-se um aumento da expressão de $A_{2A}R$ no hipocampo

dos ratinhos APP/PS1, em comparação com ratinhos de estirpe selvagem. Consistente com o papel chave dos receptores $A_{2A}R$, o bloqueio agudo destes receptores reverte por completo estes défices sinápticos.

Em suma, a interacção NMDAR/mGluR5/$A_{2A}R$ descrita nesta dissertação pode constituir uma alternativa viável para regular a sinalização aberrante mGluR5/NMDAR em Doença de Alzheimer sem afetar a sua actividade constitutiva. Para além disso, todos estes resultados apontam para um papel chave da sobre-activação de $A_{2A}R$ a nível hipocampal na disfunção sináptica e cognitiva observada no envelhecimento e na DA e poderá estar subjacente à associação genética significativa do gene *ADORA2A* com DA.

Publications related to this dissertation

Temido-Ferreira M, Ferreira DG, Batalha VL, Marques-Morgado I, Coelho JE, Pereira P, Gomes R, Pinto A, Carvalho S, Canas PM, Cuvelier L, Buée-Scherrer V, Faivre E, Baqi Y, Müller CE, Pimentel J, Schiffmann SE, Buée L, Bader M, Outeiro TF, Blum D, Cunha RA, Marie H, Pousinha PA and Lopes LV (2018) Age-related shift in LTD is dependent on neuronal adenosine A_{2A} receptors interplay with mGluR5 and NMDA receptors; *Molecular Psychiatry*; doi: 10.1038/s41380-018-0110-9.

Temido-Ferreira M, Pousinha PA and Lopes LV; *The synaptic pathophysiology of aging: implications for cognitive defects*; Review; in preparation.

Other publications

Ferreira DG, **Temido-Ferreira M**, Miranda HV, Batalha VL, Coelho JE, Szegö ÉM, Marques-Morgado I, Vaz SH, Rhee JS, Schmitz M, Zerr I, Lopes LV, Outeiro TF (2017) α-synuclein interacts with PrPC to induce cognitive impairment through mGluR5 and NMDAR2B. *Nature Neuroscience* 20(11):1569-1579.

Batalha VL, Ferreira DG, Coelho JE, Valadas JS, Gomes RA, **Temido-Ferreira M**, Shmidt T, Baqi Y, Buée L, Müller CE, Hamdane M, Outeiro TF, Bader M, Meijsing SH, Sadri-Vakili G, Blum D, Lopes LV. (2016) The caffeine-binding adenosine A_{2A} receptor induces age-

like HPA-axis dysfunction by targeting glucocorticoid receptor function. *Scientific Reports* 11;6:31493.

Table of Contents

ABBREVIATION LIST

A_1R – Adenosine A_1 receptors

$A_{2A}R$ – Adenosine A_{2A} receptors

Act-β – Actin-β

AD – Alzheimer's disease

AMPA – α-Amino-3-hydroxy-5-methyl-4isoxazolepropionic acid

ANOVA – Analysis of variance

AP5 - 2-Amino-5-phosphonopentanoic acid

ATP – Adenosine triphosphate

BDNF – Brain derived neurotrophic factor

BiFC – Bimolecular fluorescence complementation

BSA – Bovine serum albumin

C57BL6/J – "Black Six" or B6 Strain Mice

CA1 – *Cornu ammonis* 1

CA2 – *Cornu ammonis* 2

CA3 – *Cornu ammonis* 3

CaMKII – Calcium calmodulin dependent protein kinase II

cAMP – 3'-5'-cyclic adenosine monophosphate

CaN - Calcineurin

CGS 21680 - 2-(4-(2-Carboxyethyl)phenethylamino)-5'-N-ethylcarboxamidoadenosine

CNS – Central nervous system

CREB – cAMP response element-binding protein

CTR – Control

CypA – Cyclophilin A

DG – Dentate gyrus

DHPG – (*S*)-3,5-Dihydroxyphenylglycine

DMEM – Dulbecco's modified Eagle's medium

DMSO – Dimethylsulfoxide

DNA – Deoxyribonucleic acid

DNQX - 6,7-Dinitro-1,4-dihydroquinoxaline-2,3-dione

DTT – Ditiotreitol

EC – Entorhinal cortex

EDTA – Ethylenediaminetetraacetic acid

EPM – Elevated plus maze

fEPSP – field Excitatory postsynaptic potential

FBS – Fetal bovine serum

GABA – Gamma-aminobutyric acid

GFAP – Glial fibrillary acidic protein

GPCR – G-Protein coupled receptor

HBSS – Hank's balanced salt solution

HRP – Horseradish peroxidase

Iba1 – Ionized calcium binding adaptor molecule 1

ICC – Immunocytochemistry

IHC – Immunohistochemistry

IP_3 - Inositol-1,4,5-triphosphate

KW6002 – 8-[(E)-2-(3,4-Dimethoxyphenyl)ethenyl]-1,3-diethyl-7-methyl-purine-2,6-dione

LFS - Low frequency stimulation

LTD – Long-term depression

LTP – Long-term potentiation

MAP2 – Microtubule-associated protein 2

MCI – Mild cognitive impairment

mGluR5 – Metabotropic glutamate receptor 5

MPEP – 2-Methyl-6-(phenylethynyl)pyridine

MTL – Medial temporal lobe

MWM – Morris water maze

NaCl – Sodium chloride

NMDA - N-Methyl-D-aspartate

OF – Open field test

PI - Phosphatidylinositol-4,5-biphosphate

PBS – Phosphate buffered saline

PFA – Paraformaldehyde

PFC – Pre-frontal cortex

PKA – Protein kinase A

PKC – Protein kinase C

PSD – Postsynaptic density

RIPA – Radioimmunoprecipitation assay buffer

RT – Room temperature

RT-qPCR – Real-time quantitative polymerase chain reaction

SEM – Standard error of mean

SCH 58261 – 2-(Furan-2-yl)-7-phenethyl-7H-pyrazolo[4,3-e][1,2,4]triazolo[1,5-c]pyrimidin-5-amine

SDS – Sodium dodecyl sulfate

TBS – Tris buffered saline

Tg(CaMKII-hA_{2A}R) – Transgenic rats overexpressing human adenosine A_{2A}R Receptor under the control of the CaMKII promoter

VDCC – Voltage-dependent calcium channels

WHO – World health organization

WT – Wild-type

CHAPTER I

Introduction

1. State of the art

1.1. Memory and the hippocampus

Encoding, consolidation and retrieval of mnemonic information is critically dependent on a large reciprocal network of regions that includes neocortical association regions, subcortical nuclei, the medial temporal lobe (MTL), parahippocampal areas and the hippocampal formation. The hippocampus is considered the central node in this circuit. It receives input from almost all neocortical association areas via perirhinal and parahippocampal cortices and finally through the entorhinal cortex (EC) (Bartsch and Wulff, 2015) (Figure 1.1).

The gross anatomical analysis of the hippocampal formation dates back to Arantius who first described the appearance of human hippocampal formation and gave it the name hippocampus (derived from the Greek word for sea horse). The term *cornu ammonis* was introduced by the neuroanatomist Lorente de Nó (Lorente de No, 1934).

The hippocampal formation comprises four relatively simple cortical regions. These include the dentate gyrus, the hippocampus proper (which can be divided into three sub-fields, namely CA3, CA2 and CA1), the subicular complex (which can also be divided into three subdivisions: the subiculum, presubiculum and parasubiculum) and the entorhinal cortex which, particularly in the rodents, is generally divided into medial and lateral subdivisions (Amaral and Witter, 1989).

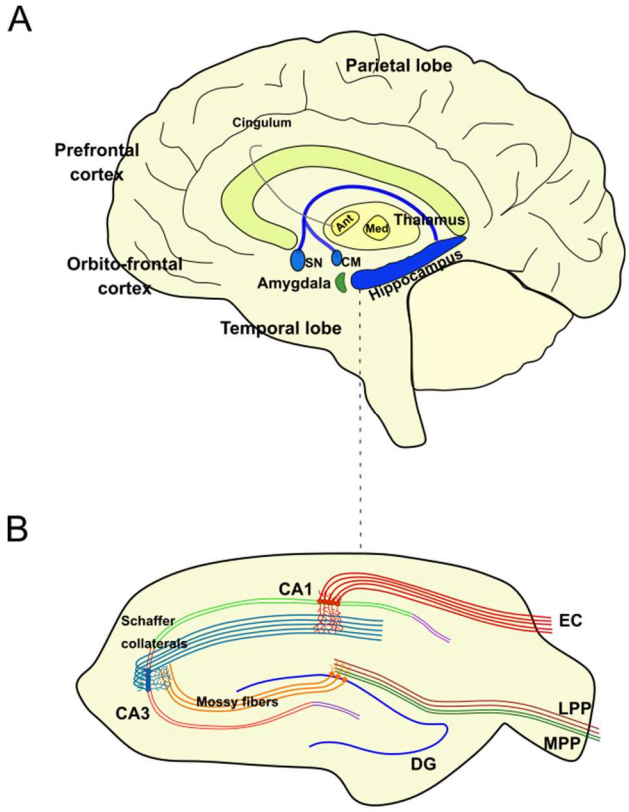

Figure 1.1. Hippocampal anatomy. (A) Principal anatomy of the hippocampal memory systems and the brain regions involved in learning and memory. (B) Hippocampal slice. Abbreviations: Ant, anterior thalamic nuclei; CA, *cornu ammonis*; CM, *corpus mammillaris*; DG, dentate gyrus; EC, entorhinal cortex; LPP, lateral performant pathway; Med, medial thalamic nuclei; MPP, medial performant pathway; Mtt, mamillothalamic tract; SN: septal nucleus.

1.1.1. Structural composition

The human hippocampus can be divided into the fields CA3, CA2 and CA1. These hippocampal fields have essentially one cellular layer,

called the pyramidal cell layer – *stratum pyramidale*. The limiting surface with the ventricular lumen is formed by axons of the pyramidal cells – the alveus. Between it and the pyramidal cell layer, the *stratum oriens* mainly contains the basal dendrites of the pyramidal cells as well as several types of interneurons. The region superficial to the pyramidal cell layer (toward the hippocampal fissure) contains the apical dendrites of the pyramidal cells and interneurons. This region has historically been divided into (1) the *stratum lucidum*, (2) the *stratum radiatum* and (3) the *stratum lacunosum-moleculare* corresponding to the most superficial portion of this region, adjacent to the hippocampal fissure. The apical dendrites of pyramidal neurons make up the *stratum radiatum* (Figure 1.2) (Schultz and Engelhardt, 2014).

In the *stratum lucidum* of CA3, the mossy fibers travel and form synapses with proximal dendrites just above the pyramidal cell layer of CA3. In the human hippocampus a fraction of the mossy fibers also travels within the CA3 pyramidal cell layer. *Stratum lucidum* is absent in CA2 and CA1 regions, which do not receive mossy fiber input (Schultz and Engelhardt, 2014).

The hallmark of CA3 neurons is that their proximal dendrites are contacted by mossy fibers which correspond to the dentate granule cell axons. The mossy fibers traverse the *stratum lucidum* immediately above the CA3 pyramidal cell layer. In CA1, the projections from CA3 and CA2 – the so-called Schaffer collaterals – terminate in the *stratum radiatum* and *stratum oriens* (Figure 1.2) (Schultz and Engelhardt, 2014).

The CA2 region has a relatively compact and narrow pyramidal cell layer. The borders of this region are difficult to establish in routine preparations of the human hippocampus (Schultz and Engelhardt, 2014).

The pyramidal cell layer of CA1 becomes thicker and more heterogeneous in monkeys and humans as compared to rodents. Stereological studies estimate the total number of CA1 neurons as approximately 14 x 10^6. The appearance of CA1 varies along its transverse and rostrocaudal axes. Based on pigmentoarchitectonic studies, the human pyramidal cell layer can be subdivided into an outer and inner pyramidal cell layer. Close to the CA2 border, the CA1 cells of both sublayers appear most tightly packed and the pyramidal cell layer is at its thinnest. The border of CA1 with CA2 is very difficult to define because some CA2 pyramidal cells appear to extend over the emerging CA1 pyramidal cell layer. The pyramidal layer of CA1 overlaps that of the subiculum in an oblique manner (Schultz and Engelhardt, 2014).

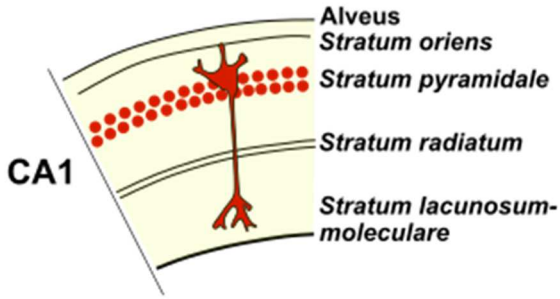

Figure 1.2. Section of CA1 with different layers. Abbreviations: CA1, *cornu ammonis* 1. (Adapted from (Amaral and Witter, 1989)).

1.1.2. Connectivity

The hippocampus is a three-layered structure that is reciprocally connected to other cortical and subcortical areas. The principal neurons of the hippocampus are organized in layers and receive unidirectional input from the EC, where layer II neurons project to granule cells in the dentate gyrus (DG) via the perforant path (Bartsch and Wulff, 2015; Strange et al., 2014). The trisynaptic pathway from the DG to the CA3 via mossy fibers and onward to CA1 via Schaffer collaterals is the principal feed-forward circuit involved in the process of information through the hippocampus (Bartsch and Wulff, 2015). Additionally, layer III neurons from the EC directly project to CA1 neurons via the temporoammonic path (perforant path to CA1) (Bartsch and Wulff, 2015). CA1 pyramidal cells – the major output neurons – project via the subicular complex back to deep layers of the EC and to various subcortical and cortical areas (Bartsch and Wulff, 2015b; Murray et al., 2011). Importantly, the structure of this feed-forward circuit with its limited redundancy may be critical for learning and memory but may also contribute to its vulnerability during insults (Bartsch and Wulff, 2015; Lavenex and Amaral, 2000).

The DG, with three distinct layers (molecular, granular, and polymorphic), consists mainly of granule cells and receives input from the EC. The axons of the DG granule cells form the mossy fiber system and project to the CA3 (Amaral et al., 2007; Bartsch and Wulff, 2015). Mossy fibers also project back onto granule cells, thus forming a recurrent network. Additionally, the DG receives information from the contralateral hippocampus via commissural projections (Amaral et

al., 2007; Bartsch and Wulff, 2015). Axon collaterals of CA3 pyramidal neurons synapse onto other CA3 neurons, forming a recurrent autoassociative network, whereas CA3 neurons projecting back to the dentate network form a heteroassociative network (Bartsch and Wulff, 2015; Lisman, 1999). CA1 pyramidal neurons receive information which has been pre-processed in the subnetworks of the DG and CA3, but also receives direct projections from the EC, suggesting that the function of the CA1 neurons includes comparing new information from the EC with stored information via CA3 in terms of mismatch, error and novelty detection (Figure 1.3) (Bartsch and Wulff, 2015; Lisman and Otmakhova, 2001).

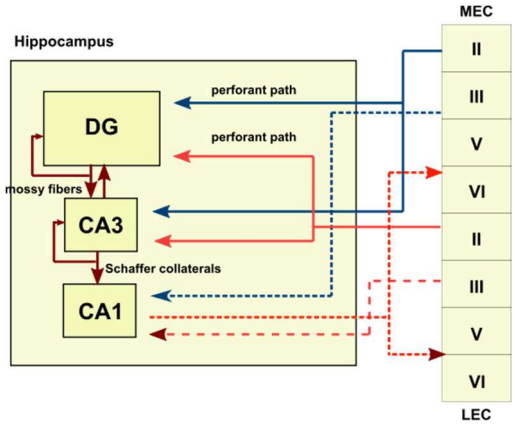

Figure 1.3. Schematic representation of the hippocampal trisynaptic circuit. Firstly, granule neurons in the hippocampal dentate gyrus receive afferent inputs, via the performant path, from the layer II of the lateral and medial entorhinal cortex. Next, granule neurons project to the CA3 pyramidal neurons via mossy fibers and, ultimately, CA1 neurons receive inputs from the CA3 by the Schaffer collaterals, by the contralateral hippocampus through associational/commissural fibers or direct inputs from the performant path. To close the hippocampal synaptic loop, CA1 pyramidal neurons project back to the entorhinal cortex. Abbreviations: CA1, CA2

and CA3, *cornu ammonis* 1, 2 and 3; DG, dentate gyrus; LEC, lateral entorhinal cortex; MEC, medial entorhinal cortex (Adapted from (Alves, 2017)).

1.2. Synaptic Plasticity

Neural plasticity is the ability of the brain or brain structures to adapt in response to intrinsic or extrinsic stimuli such as changes in the environment, development or lesions (Bartsch and Wulff, 2015; Kolb and Muhammad, 2014). Neural plasticity can occur on various functional and structural levels, such as changes in membrane excitability, synaptic plasticity and changes in dendritic and axonal structure (Bartsch and Wulff, 2015; Kolb and Gibb, 2014). Neural plasticity can also occur as structural and functional adaptations and reorganization of neuronal populations, which is reflected in modifications of recruitment and strength of connectivity of networks and circuits. Furthermore, neural plasticity can show a time- and age-dependency and can result in positive or negative adaptive effects (Bartsch and Wulff, 2015; Kolb and Gibb, 2014).

The hippocampus has been for long considered a classic example for the study of neural plasticity as many paradigms of synaptic plasticity such as Long-term potentiation (LTP) and Long-term depression (LTD), excitatory postsynaptic potential (EPSP)-spike potentiation and spike-timing dependent plasticity, have been identified and demonstrated in hippocampal circuits (Malenka, 1994).

Synaptic plasticity can be defined as activity-dependent modifications in the efficacy and strength of synaptic transmission of pre-existing

synapses (Citri and Malenka, 2008). Long-term synaptic plasticity can last from minutes to several days and even years (Abraham et al., 1994, 2002; Staubli and Scafidi, 1997) and therefore may be associated with the formation of long-term memories (Dong et al., 2013; Ge et al., 2010). Long-term potentiation (LTP) and long-term depression (LTD) are the two main forms of long-term synaptic plasticity thought to play a role in hippocampal functioning (Pinar et al., 2017). LTP is defined as the long-lasting enhancement in signal transmission between two neurons after continuous stimulation and has been for long considered the cellular and molecular basis of memory (Citri and Malenka, 2008). However, much less is known about LTD and its role on learning and memory, either in physiological or pathological conditions, although some reports have already described an association between LTD impairments and cognitive deficits, namely in animal models of stress and Alzheimer's Disease (AD) (Lanté et al., 2015; Wong et al., 2007).

One of the earliest reports of lasting activity-dependent depression of transmission at central synapses concerned the phenomenon of heterosynaptic depression (Lynch et al., 1977). This study demonstrated that in the CA1 region of the hippocampus *in vitro*, stimuli delivered to one pathway that induced LTP resulted in a reversible depression in the non-tetanised pathway (Lynch et al., 1977). However, this phenomenon was ignored for many years until the 1990s, when it was demonstrated that low-frequency stimulation (LFS) was effective at inducing LTD without the requirement for the induction of LTP, a process called homosynaptic *de novo* LTD (Dudek and Bear, 1992; Mulkey and Malenka, 1992).

Initial reports demonstrated that the induction of LTD in the CA1 region of the hippocampus was dependent on the synaptic activation of NMDAR, NMDAR-dependent LTD, which is usually induced by LFS (Dudek and Bear, 1992; Fujii et al., 1991; Kemp et al., 2000; Mulkey and Malenka, 1992). Furthermore, application of NMDA by itself has also been shown to induce lasting synaptic depression, a form of chemical-LTD, which appears to share common mechanisms with LFS-induced LTD (Lee et al., 1998). However, these two forms of LTD also have important differences (Kameyama et al., 1998; Morishita et al., 2001).

A second major form of LTD requires the activation of mGluRs (Bashir and Collingridge, 1994; Bashir et al., 1993). Additionally, LTD can be obtained by brief application of mGluR agonist DHPG, designated DHPG-LTD (Huber et al., 2001; Palmer et al., 1997). The patterns of activation that are required to induce mGluR-LTD are generally similar to those required to induce NMDAR-LTD, although there are differences depending on the synapse type. For example, NMDAR-LTD is usually induced at CA1 synapses by single-shock LFS, whereas mGluR-LTD is usually induced by paired-pulse LFS (Collingridge et al., 2010; Massey and Bashir, 2007).

However, it should be noted that with very few exceptions (Cho et al., 2000; Palmer et al., 1997; Wang and Gean, 1999) the requirement of NMDA and mGlu receptor activation in LTD is mutually exclusive; thus in virtually all cases of LTD, where there is a requirement for NMDAR activation, there is no role for mGluR activation and vice versa (Kemp and Bashir, 2001).

The trigger for postsynaptically induced, activity-dependent LTD is predominantly an increase in calcium (Ca^{2+}). Since postsynaptic rises in Ca^{2+} are implicated in the induction of both LTD and LTP (Bliss and Collingridge, 1993; Lynch et al., 1983), particular properties of the Ca^{2+} signal (temporal, spatial or magnitude) may determine whether LTP or LTD is induced. The suggestion of Lisman et al (Lisman, 1989) that large increases in intracellular Ca^{2+} result in LTP induction and modest increases in intracellular Ca^{2+} result in LTD induction extended the theory of Bienenstock et al., who had proposed that some function of postsynaptic activity controlled the direction (increase or decrease) of synaptic plasticity (Bienenstock et al., 1982).

The increase in postsynaptic Ca^{2+} that results in LTD can arise from a variety of sources. For example, several reports describe Ca^{2+} influx through NMDAR as fundamental for LTD induction (Ahmed et al., 2011; Dudek and Bear, 1992). Moreover, there is evidence that calcium entry through voltage-dependent Ca^{2+} channels (VDCC) can also be important in LTD induction (Christie et al., 1997; Cummings et al., 1996; Oliet et al., 1997; Otani and Connor, 1998; Wang et al., 1997). However, this is still controversial, since other studies showed no effect of nifedipine, a VDCC blocker, in LTD magnitude (Udagawa et al., 2006). mGlu receptor-mediated release of Ca^{2+} from intracellular stores also contributes to LTD. Group I mGlu receptors are coupled to phosphatidylinositol-4,5-biphosphate (PI) hydrolysis. One of the products of PI hydrolysis, inositol-1,4,5-triphosphate (IP_3), causes release of calcium from intracellular stores (Pin and Duvoisin, 1995) (Figure 1.4).

Despite NMDAR, VDCC and group I mGluR drive Ca^{2+} influx to induce LTD, their relative contribution depends significantly on the pattern of stimulation, Ca^{2+}/Mg^{2+} ratio in the bath medium and age of the animals (Kumar and Foster, 2014; Norris et al., 1996).

How does the increase in Ca^{2+} mediate long-lasting changes in synaptic transmission? One important Ca^{2+}-dependent cascade involves the binding of Ca^{2+} to calmodulin, thus forming a calcium-calmodulin complex. This complex subsequently activates both calcium-calmodulin dependent protein kinase (CaMKII) and calcium-calmodulin dependent protein phosphatase, calcineurin (CaN; also known as PP2B). Moderate increases in postsynaptic Ca^{2+}, such as those expected from LFS, activates calcineurin, which will then lead to the activation of protein phosphatase 1 and/or phosphatase 2 (PP1/2) and subsequent LTD via dephosphorylation of AMPA receptors and other substrates (Lee et al., 2000; Mulkey et al., 1993, 1994; O'Dell and Kandel, 1994) (Figure 1.4). Protein phosphatases can also dephosphorylate and inactivate CaMKII, thereby facilitating LTD. Consistent with this hypothesis, a CaMKII antagonist facilitated DHPG-induced LTD in the CA1 region (Schnabel et al., 1999). However, Mockett et al. showed that mGluR-LTD, induced by DHPG or paired-pulse synaptic stimulation, was dependent on CaMKII activation (Mockett et al., 2011). Given these contradictory results, the role of CaMKII in regulating LTD is not completely understood.

Additionally, group I mGluR-dependent activation of phospholipase C (PLC) leads not only to Ca^{2+} release from intracellular stores but also to PKC activation. The activation of PKC can lead to phosphorylation of the GluA2 subunit at the serine 880 residue and lead to AMPAR

lateral diffusion and subsequent internalization (Gladding et al., 2009; Lüscher and Huber, 2010) (Figure 1.4).

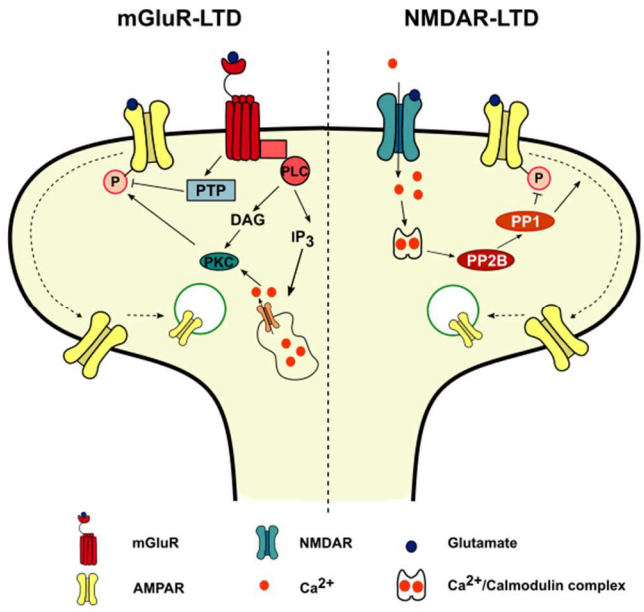

Figure 1.4. mGluR and NMDAR-LTD exhibit different underlying mechanisms. mGluR activation results in Ca^{2+} release from intracellular stores and a PKC-dependent AMPAR internalization. NMDAR activation drives Ca^{2+} influx, which activates protein phosphatases, leading to subsequent AMPAR dephosphorylation and internalization. Abbreviations: DAG: Diacylglycerol; IP3: Inositol-1,4,5-triphosphate; PKC: Protein kinase C; PLC: Phospholipase C; PP1: Protein phosphatase 1; PP2B: Protein phosphatase 2B; PTP: Protein tyrosine phosphatase.

LTD can also be mediated by persistent presynaptic changes, and the proportion of presynaptic *versus* postsynaptic alterations probably depends on various factors, including the brain region, the animal and its developmental stage. There is evidence that LTD (Enoki et al.,

2009), including NMDAR-LTD (Stanton et al., 2003) and mGlu-LTD (Foy et al., 1987), can involve a reduction in the probability of glutamate release, which can be triggered by changes in the presynaptic terminal or by postsynaptic changes that are communicated across the synapse via a retrograde messenger (Feinmark et al., 2003; Stanton et al., 2003).

1.3. Aging and Synaptic dysfunction

Nowadays, the world's population is aging: the number and proportion of older persons in the societies is growing significantly. According to the World Health Organization (WHO), by 2020, the number of people aged 60 years and older will outnumber children younger than 5 years. Moreover, between 2015 and 2050, the proportion of the world's population over 60 years will nearly double from 12% to 22%. Importantly, aging is the main risk factor for Alzheimer's disease (AD) (Reitz et al., 2011). These profound demographic changes place understanding the aging process as one of the big challenges for scientific research nowadays. Although aging affects the entire body, its impact on brain and cognition has a profound effect on the life quality of the individuals. Given the critical role of the hippocampus in learning and memory, it is very important to comprehend the aging-related alterations in this brain structure (Burke and Barnes, 2010). Importantly, memory capabilities that depend on proper hippocampal function appear to be of particular vulnerability to the aging process (McEwen, 1997). Much work has been focused on the hippocampus,

as age-related decline in performance dependent on this region is consistently found across species and tasks (Barnes, 1979; Colombo et al., 1997; Erickson and Barnes, 2003; Mabry et al., 1996; Oler and Markus, 1998; Tanila et al., 1997). These age-related memory impairments can be explained in part by changes in neural plasticity or cellular alterations that directly affect mechanisms of plasticity (Burke and Barnes, 2006). Although several age-related neurological changes have been identified during normal aging, these tend to be subtle compared with the ones observed in age-associated disorders, such as Alzheimer's and Parkinson's disease (Burke and Barnes, 2006). Consequently, understanding age-related changes in cognition sets a background against which it is possible to assess the effects of the disease (Burke and Barnes, 2006).

1.3.1. Neuronal loss

For a long time, aging had been associated with neuronal loss independently of brain region (Ball, 1977; Brizzee et al., 1980; Brody, 1955; Coleman and Flood, 1987). However, the methods used in those studies question the accuracy of such results (Burke and Barnes, 2006; Morrison and Hof, 1997) and subsequent studies have conclusively shown that the cell number is preserved in aging in several brain areas including the hippocampus (Gazzaley et al., 1997; Keuker et al., 2003; Merrill et al., 2000; Pakkenberg and Gundersen, 1997; Peters et al., 1994; West, 1993). Rather than neuronal loss, alterations in dendritic branching and spine density seem to be a better correlate of aging in

terms of neuronal morphology (Foster et al., 1991; Pyapali and Turner, 1996; Scheibel et al., 1976). In fact, dendritic branching is greater in the dentate gyrus and in the layer II of the parahippocampal gyrus of aged individuals (Buell and Coleman, 1979, 1981, Flood et al., 1985, 1987a), while no age-associated changes were observed in CA3 (Flood et al., 1987b) and CA1 (Hanks and Flood, 1991). Further non-human studies confirmed the results observed in the CA1 (Markham et al., 2005; Pyapali and Turner, 1996; Turner and Deupree, 1991). Unlike hippocampus, the morphology of neurons from pre-frontal cortex (PFC) seems to be vulnerable to the aging process (Burke and Barnes, 2006), where a decrease of dendritic branching was reported in aged rats (Grill and Riddle, 2002) and humans (de Brabander et al., 1998; Uylings and de Brabander, 2002). Similar to the dendritic branching results, no alterations were found in synaptic density in DG and CA1 across species (Curcio and Hinds, 1983; Markham et al., 2005; Williams and Matthysse, 1986). There is, however, one study that observed a reduction in spine density in the subiculum of aged monkeys (Uemura, 1985). Loss of CA1 synapses is characteristic of AD and, to a lesser extent, mild cognitive impairment in humans (Scheff et al., 2007). Altogether this data highlight the differences between normal aging, characterized by structural preservation in the MTL, and AD, which is associated with neuronal and synaptic loss in the MTL and in the hippocampus in particular (Morrison and Baxter, 2012).

1.3.2. Synaptic dysfunction

Since cell number is not affected in aging, there must be other alterations that are in the genesis of age-associated memory deficits. Deficits in neurogenesis could account for these age-related synaptic impairments. Although aged rats exhibit decreased neurogenesis (Kuhn et al., 1996), this alteration does not correlate with memory performance, since old rats with lower neurogenesis rates actually perform better in spatial memory tasks (Bizon and Gallagher, 2005; Bizon et al., 2004).

Age-associated impairments can be due to synaptic changes that would then lead to altered mechanisms of plasticity (Burke and Barnes, 2006, 2010). Although the total number of Schaffer collaterals-CA1 synapses is preserved across different age groups (Bear et al., 1987), the amplitude of the Schaffer collaterals-induced field EPSP (fEPSP) recorded in CA1 was reduced in aged memory-impaired animals (Barnes et al., 1992; Landfield et al., 1986; Rosenzweig et al., 1997). Furthermore, the postsynaptic density (PSD) area of axospinous synapses was significantly reduced in aged learning-impaired rats (Nicholson et al., 2004). However, at the CA3-CA1 synapse, the size of the unitary EPSP remains constant during aging (Barnes et al., 1997). Together, these data suggest that aging might not be associated with alterations in the strength of individual synaptic connections but instead with an increase in non-functional or silent synapses in the hippocampus (Burke and Barnes, 2006, 2010).

Furthermore, biophysical properties of hippocampal neurons such as the resting membrane potential, membrane time constant, input

resistance, threshold to action potential are largely preserved over the lifespan (Burke and Barnes, 2010; Rosenzweig and Barnes, 2003). A notable exception is age-related changes in calcium regulation in aged hippocampal neurons, which have an increased Ca^{2+} influx through L-type Ca^{2+} channels. The pathophysiological role of L-type Ca^{2+} channels in age-related synaptic dysfunction will be further explored below.

1.3.3. Synaptic plasticity

The alterations observed at individual synapses have a significant impact on synaptic plasticity. Long-term synaptic plasticity processes (LTP and LTD) have been correlated with memory performance for a long time and are proposed as a main neurophysiological correlate of memory (Citri and Malenka, 2008; Lynch, 2004). Importantly, age-associated memory deficits correlate with impairments in either LTP or LTD (Ge et al., 2010; Tombaugh et al., 2002).

In aged animals, LTP has been found to be reduced (Barnes, 1979; Deupree et al., 1993, 1993; Rex et al., 2005; Sankar et al., 2000), not altered (Costenla et al., 1999; Kumar et al., 2007; Landfield and Lynch, 1977; Landfield et al., 1978; Norris et al., 1996; Rex et al., 2005) or even strengthened (Costenla et al., 1999; Diógenes et al., 2011; Huang and Kandel, 2006; Kumar and Foster, 2004; Pinho et al., 2017). This is inconsistent with the classical correlation between increased LTP magnitude and better performance on hippocampal-dependent memory tasks. The synaptic circuit that is being potentiated

(Rex et al., 2005) and the stimulation protocol (Burke and Barnes, 2006; Costenla et al., 1999) may then account for the differences observed in LTP magnitude. Generally, age-associated alterations in LTP are only observed when weaker stimulus protocols are used, either an increase (Costenla et al., 1999; Diógenes et al., 2011; Huang and Kandel, 2006; Pinho et al., 2017) or decrease (Tombaugh et al., 2002) in LTP.

Some authors report increased susceptibility to LTD during aging (Norris et al., 1996), whereas others fail to observe alterations in LTD magnitude in aged animals (Foster and Kumar, 2007; Kumar et al., 2007). These discrepancies can be explained by differences in animal strain, stimulation pattern or Ca^{2+}/Mg^{2+} ratio. Accordingly, paired-pulse LFS (PP-LFS) does not induce changes in LTD between young and aged animals (Foster and Kumar, 2007), suggesting that different mechanisms may be involved in the induction of LTD by LFS and PP-LFS. Also, age-related differences in LTD induction could be rescued by manipulating the extracellular Ca^{2+}/Mg^{2+} ratio. Indeed, the fact that induction of LTD is a function of age and the level of Ca^{2+} in the recording medium strongly support an age-related Ca^{2+} dysregulation and a shift in Ca^{2+}-dependent induction mechanisms rather than in the LTD intrinsic capacity (Foster and Kumar, 2007; Kumar et al., 2007). It had been hypothesized that postsynaptic intracellular levels of Ca^{2+} are involved in setting the synaptic modification curve, which determines the probability that a synapse will be depressed or potentiated for a given pattern of input (Bear et al., 1987; Foster and Kumar, 2002). Accordingly, since Ca^{2+} homeostasis is disrupted in aged animals (discussed further below) (Foster and Norris, 1997;

Thibault and Landfield, 1996), we can expect alterations in the probability for a given synapse to undergo potentiation or depression. All these observations support the *calcium hypothesis* of aging, which implicates raised intracellular Ca^{2+} as the major source of functional impairment and degeneration in aged neurons (Khachaturian, 1989, 1994; Verkhratsky and Toescu, 1998).

1.3.4. Calcium homeostasis

To avoid excessive intracellular levels of calcium ($[Ca^{2+}]_i$) elevations, neurons are equipped with complex machinery that permanently modulates the temporal and spatial patterns of Ca^{2+} signaling (Arundine and Tymianski, 2003; Delorenzo et al., 2005). Brief elevations of $[Ca^{2+}]_i$ are essential in controlling membrane excitability and modulating synaptic plasticity mechanisms, gene transcription and other major cellular functions (Arundine and Tymianski, 2003; Delorenzo et al., 2005). However, long-lasting elevation of $[Ca^{2+}]_i$ triggers neurotoxic signaling pathways that ultimately drive cell death (Arundine and Tymianski, 2003; Delorenzo et al., 2005).

Several studies reported an age-associated increase in basal $[Ca^{2+}]_i$ levels (Hajieva et al., 2009; Raza et al., 2007) and action potential-evoked calcium influx (Oh et al., 2013). Also, hippocampal slice neurons from aged rats display an increase in calcium spike duration (Pitler and Landfield, 1990). The fact that this increase in calcium spike duration is accompanied by a prolongation of Ca^{2+}-dependent after hyperpolarization (Landfield and Pitler, 1984) suggests that this is

due to increased voltage-dependent Ca^{2+} influx (discussed further below) (Pitler and Landfield, 1990). Furthermore, another study reported an age-associated increase in $[Ca^{2+}]_i$ levels upon synaptic activation, although resting free Ca^{2+} ions were unaltered (Thibault et al., 2001). Consistent with an upsurge of $[Ca^{2+}]_i$ levels, BAPTA treatment, a calcium chelator, improves spatial learning in aged animals (Tonkikh et al., 2006) and enhances fEPSP in aged slices, an effect that is lost when Ca^{2+} influx is partially blocked (Ouanounou et al., 1999).

However, there are also reports of no change in resting free Ca^{2+} ions in aging subjects (Gant et al., 2006; Gibson et al., 1986; Murchison and Griffith, 1998). Hence, there are conflicting reports regarding which elements of calcium homeostasis change with aging and the direction of these changes. In some cases, the contradictory results may result from different rodent species or strain, tissue preparations, duration for which neurons/slices are kept *in vitro* before Ca^{2+} determination, cell type, Ca^{2+} indicator, method of loading indicator, and calibration (Oh et al., 2013; Raza et al., 2007).

Alterations in mechanisms that tightly control $[Ca^{2+}]_i$ levels, such as buffering (de Jong et al., 1996; Satrústegui et al., 1996; Villa and Meldolesi, 1994), extrusion (Martinez-Serrano et al., 1992; Michaelis et al., 1984, 1992; Raza et al., 2007) and uptake (Gibson et al., 1986) may also account for the age-related disruption of Ca^{2+} homeostasis.

Reductions in the expression of the calcium-buffering proteins calbindin D-28K and parvalbumin have been observed in the aging brain (Armbrecht et al., 1999; Bu et al., 2003; Geula et al., 2003; de Jong et al., 1996; Kishimoto et al., 1998) and such impairments were

associated with faster age-related decline in hippocampal metabolism (Moreno et al., 2012). Also, endogenous buffer capacity was shown to be reduced in intact hippocampal neurons from aged rats (Tonkikh et al., 2006). However, there are also reports of an enhanced endogenous buffer capacity in dissociated basal forebrain neurons of aged rats (Murchison and Griffith, 1998) and in the proximal apical dendrite of CA1 pyramidal neurons in acute slices of aged rats (Oh et al., 2013). These results indicate that increasing calcium buffering blunts the enhanced calcium accumulation in aged rats, but fails to prevent the aging-related increase in calcium influx following a burst of action potentials (Oh et al., 2013).

Alterations in voltage-dependent calcium channels may also underlie the increased Ca^{2+} influx. There is compelling evidence of an age-associated increase in L-type Ca^{2+} channels expression (Núñez-Santana et al., 2014; Thibault and Landfield, 1996; Veng and Browning, 2002) that can be further correlated with performance in hippocampus-dependent memory tests (Thibault and Landfield, 1996). Furthermore, a significant increase in voltage-gated Ca^{2+} currents in CA1 hippocampal neurons was found in aged rats (Campbell et al., 1996). Consistent with the enhanced role of VDCC in Ca^{2+} dysregulation, L-type Ca^{2+} channel blocker MEM 1003 rescued deficits in trace eye-blink conditioning in aged rabbits, an hippocampal-dependent task (Rose et al., 2007). Plus, treatment with nimodipine, an L-type Ca^{2+} channel blocker, improved spatial working memory in aged rats (Veng et al., 2003).

Given the key role of NMDAR in synaptic plasticity and memory (Tsien et al., 1996), putative alterations in NMDAR may account for Ca^{2+} dysregulation.

In aged CA1 pyramidal neurons there is an increased duration of NMDAR-mediated responses (Jouvenceau et al., 1998). Consistent with this hypothesis, aged animals display an NMDAR overactivation upon glutamate or glycine stimulation, despite a decrease in the density of these receptors (Serra et al., 1994). Accordingly, several studies report a decrease in NMDAR expression in the hippocampus, by western blotting analysis and binding of both NMDAR agonists and antagonists (Clayton et al., 2002; Kito et al., 1990; Magnusson et al., 2002; Pittaluga et al., 1993; Tamaru et al., 1991; Wenk et al., 1991). Furthermore, physiological studies indicate the NMDAR-mediated excitatory postsynaptic potentials in the Schaffer collateral pathway of the hippocampus are reduced by approximately 50-60% in spatial memory-impaired aged animals (Barnes et al., 1997; Billard and Rouaud, 2007; Brim et al., 2013). However, such decrease in NMDAR-mediated responses may be due to the previously described increase in non-functional synapses with aging. There is also an increased MK-801 binding in animals with learning and retention deficits (Ingram et al., 1992; Topic et al., 2007). Since MK-801 only labels open channels, an increase in NMDAR channel open time may act as a compensatory mechanism for the apparent decrease in receptor number (Kumar, 2015).

These discrepant results can also be explained in part by strain effects and differences in technical approaches. NMDAR channels are blocked by extracellular Mg^{2+} (Mayer et al., 1984; Nowak et al.,

1984), and recent data have suggested an age-related increase in NMDAR sensitivity to Mg^{2+} blockade (Eckles and Browning, 1997). While in one study, NMDAR-mediated fEPSPs were recorded in a Mg^{2+}-free medium (Jouvenceau et al., 1998), another measured fEPSPs in the presence of 0.2 mM of Mg^{2+} (Barnes et al., 1997). Accordingly, Barnes *et al.* did not find impairments of NMDAR activation in aged animals when the pyramidal cells were directly depolarized by current injection, thus releasing the NMDAR-related channels of their Mg^{2+} blockade (Barnes et al., 1996). Furthermore, differences in protein levels can be due to subregions specificities. For example, Liu *et al.* showed that a decrease in NR1 (constitutive NMDAR subunit) protein levels was only present in CA2/3 regions of the hippocampus, while no changes were observed for CA1 and DG (Liu et al., 2008). On the other hand, differences in NMDAR density were more significative in the intermediate hippocampus, rather than in the dorsal portion (Magnusson et al., 2006).

Furthermore, NMDAR antagonist treatment enhances neurogenesis in aged rat hippocampus, which could have an impact in cognition (Nacher et al., 2003). Accordingly, an increased activation of NMDAR in other pathological conditions has been already described (Auffret et al., 2010a, 2010b; Ferreira et al., 2017a; Pousinha et al., 2017). Altogether, these age-related alterations in NMDAR expression and activation further strengthens an instrumental role of NMDAR in this age-associated Ca^{2+} dysregulation.

Besides age-associated alterations in sources of Ca^{2+} dysregulation, previous studies focused on putative impairments in signaling

pathways that translate changes in Ca^{2+} regulation into altered neuronal function and cognition (Foster et al., 2001). Concretely, several studies described alterations in the activity of protein kinases and phosphatases involved in the expression of synaptic plasticity (Davis et al., 2000; Foster et al., 2001; Karege et al., 2001). These kinases and phosphatases are thought to act on AMPAR to mediate the expression of LTP and LTD, respectively. Although in most cases the expression of a particular kinase or phosphatase is unaltered, their basal activity is decreased, localization is shifted or stimulation induced activation is impaired upon aging (Foster, 2004).

CaMKII is an enzyme crucial for synaptic plasticity (Lisman et al., 2002). Aged rats display impairments in activity-dependent regulation of CaMKII transcription (Davis et al., 2000). Furthermore, an age-associated decrease in the activation/translocation of CaMKII was also described (Eckles et al., 1997; Mullany et al., 1996; Parfitt et al., 1991).

Postsynaptic inhibition of protein phosphatase 1 (PP1) increased synaptic transmission in aged animals, supporting the hypothesis that increase PP1 activity may underlie the age-related decrease in synaptic transmission (Norris et al., 1998). PP1 activity is not directly regulated by Ca^{2+} but by calcineurin (CaN), the unique phosphatase that is directly regulated by the level of intracellular Ca^{2+} (Foster et al., 2001). Hippocampal CaN and PP1 activity increase with aging and is associated with L-type calcium channels function (Foster et al., 2001). Furthermore, this impaired CaN activity drives increased dephosphorylation of CaN substrate proteins, such as bcl-2 family member protein (BAD) and cAMP response element binding protein

(CREB), which is associated with decreased cell viability, susceptibility to neurotoxicity (Walton and Dragunow, 2000) and impairments in terms of maintenance of LTP and memory (Impey et al., 1998; Silva et al., 1998). Consistently, performance in hippocampus-dependent memory tasks can be correlated with CaN activity in aged animals, further stressing hippocampal CaN activity as a useful marker of cognitive decline, since CaN activity can link Ca^{2+} homeostasis disruption with memory impairments through mechanisms controlling synaptic modification (Foster et al., 2001).

Altogether, these data support a shift in the balance of activity of Ca^{2+}-dependent kinase/phosphatase enzymes as an important marker for age-associated changes in neuronal function and cognition (Figure 1.5).

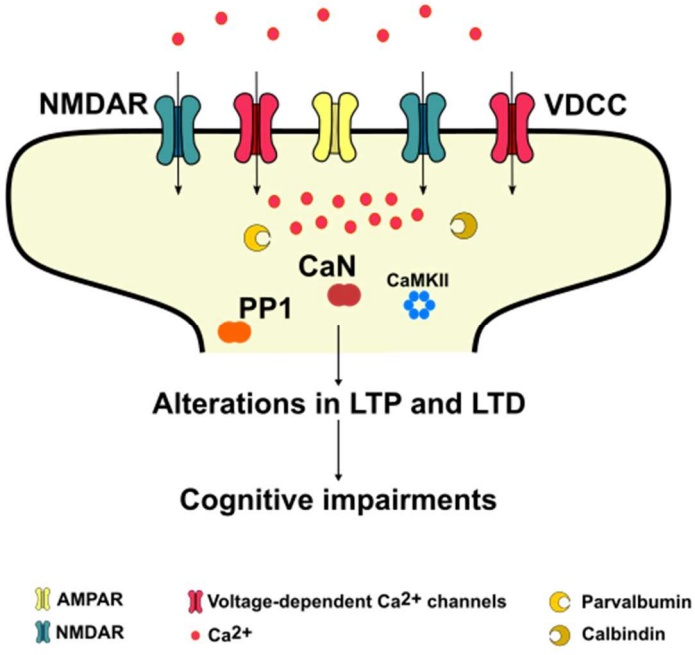

Figure 1.5. Aging is associated with increased intracellular levels of calcium caused by an aberrant contribution of NMDAR, Voltage-dependent calcium channels and impairments in calcium buffering mechanisms. This increase in Ca^{2+} leads to the disruption of the balance kinases/phosphatases and thus to alterations in LTP and LTD, which can be further correlated with cognitive deficits. Abbreviations: CaMKII: Ca^{2+}/calmodulin-dependent protein kinase II; CaN: calcineurin; PP1: Protein phosphatase 1; VDCC: Voltage-dependent calcium channels.

1.4. Physiopathological role of $A_{2A}R$ in the hippocampus

1.4.1. Adenosine

Adenosine is an endogenous nucleotide mainly produced by the degradation of ATP, being present in all cells as a metabolite (Stone et al., 1985). In situations of compromised energy charge or when cells demand an increased consume of ATP, the intracellular concentration of adenosine, estimated to be in the nanomolar range, increases up to micromolar concentrations (Bardenheuer and Schrader, 1986; Nordström et al., 1977) and this metabolite acts with a homeostatic role in the control of cellular metabolism (Arch and Newsholme, 1978). Adenosine has been shown to play a role in the regulation of physiological activity in several organs and tissues, such as purinergic nucleic acid base synthesis, amino acid metabolism and modulation of cellular metabolic status (Daly, 1982; Stone et al., 1985; Williams, 1989).

In the central nervous system, adenosine has important neuromodulatory actions and acts as a fine-tuner of synaptic communication, since it is a relevant player in neuron-glia communication and can affect the release and action of many neurotransmitters and other neuromodulators (Ribeiro and Sebastião, 2010). In fact, adenosine can exert its actions either presynaptically - inhibiting or facilitating neurotransmitter release - or postsynaptically - modulating neurotransmitter receptors activity, through the activation of different membrane receptors with opposite actions (Ribeiro and Sebastião, 2010). Consequently, the effects of adenosine depend on the expression pattern and signaling of such receptors, the brain region and the pathophysiological condition. Accordingly, the neuromodulatory role of adenosine is mediated by a balance between the inhibitory and excitatory actions via A_1 and A_{2A} receptors (A_1R and $A_{2A}R$), respectively. Adenosine can also activate adenosine A_{2B} and A_3 receptors. However, those receptors are mainly involved in the peripheral effects of adenosine (Cunha, 2001; Ribeiro and Sebastião, 2010).

1.4.2. Adenosine A_{2A} receptors

Adenosine mediates its effects mainly through activation of A_1 and $A_{2A}R$ receptors, metabotropic G-protein coupled receptors (GPCR). A_1R are usually coupled to adenylate cyclase inhibitory proteins (Gi/Go) and $A_{2A}R$ to adenylate cyclase excitatory proteins (Gs) (Linden, 2001). The distribution pattern of adenosine receptors in the

brain has a direct impact on adenosine differential modulation in the brain. A_1R are widely distributed, being more abundant in the cortex, cerebellum and hippocampus (Reppert et al., 1991). On the opposite, $A_{2A}R$ display a more restricted expression pattern: $A_{2A}R$ is highly expressed in the olfactory bulb and striatum (Jarvis and Williams, 1989), whereas in the neocortex and hippocampus they are present at residual levels (Cunha et al., 1994a; Kirk and Richardson, 1995) (Figure 1.6). Both A_1R and $A_{2A}R$ are mostly located in synapses (Rebola et al., 2003a, 2005a), in particular in excitatory (glutamatergic) synapses (Rebola et al., 2005b; Tetzlaff et al., 1987), although both receptors were shown to be also present in other synapses, such as GABAergic (Cunha and Ribeiro, 2000; Rombo et al., 2015; Shindou et al., 2002) and dopaminergic (Borycz et al., 2007; Garção et al., 2013).

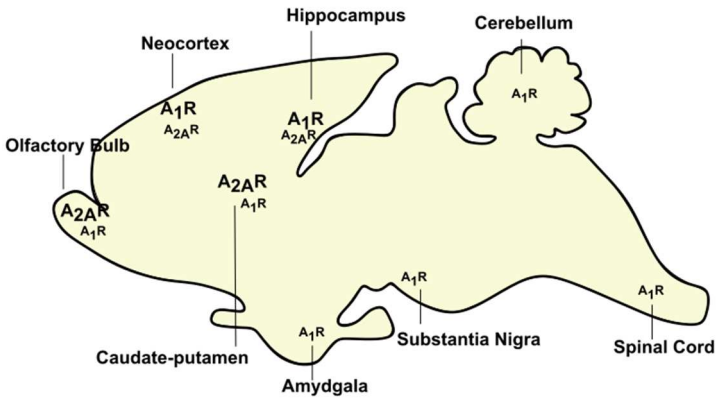

Figure 1.6. Distribution of adenosine receptors A_1 and A_{2A} in the brain. The hippocampus displays high levels of A_1R and low levels of $A_{2A}R$. (Adapted from (Ribeiro et al., 2003)).

$A_{2A}R$ have an important role on astrocytes, microglia and neurons. $A_{2A}R$ were shown to be localized in astrocytes (Brambilla et al., 2003; Cristóvão-Ferreira et al., 2013; Matos et al., 2012a; Orr et al., 2015), where they control uptake of glutamate (Matos et al., 2012a, 2012b) and mediate glucose metabolism, astrogliosis, proliferation, cellular volume and the release of neurotrophic factors and interleukins (Boison et al., 2010; Daré et al., 2007). Plus, different brain insults cause an upregulation of the expression and density of $A_{2A}R$ in activated microglia (Yu et al., 2008). Both *in vitro* and *in vivo* studies further support a role for $A_{2A}R$ in controlling several important functions operated by microglia, such as process retraction (Gyoneva et al., 2014; Orr et al., 2009), synthesis and release of inflammatory mediators, levels of inflammatory enzymes and proliferation (Santiago et al., 2014).

In neurons, under basal conditions, adenosine preferentially stimulates A_1R, which shows a higher affinity for adenosine than $A_{2A}R$ (Fredholm et al., 2001), leading to inhibition of glutamatergic synaptic transmission in the hippocampus (Sebastião et al., 1990). Adenosine can also activate $A_{2A}R$, which decreases A_1R binding and thus an inhibition of A_1R actions (Lopes et al., 2002). Accordingly, $A_{2A}R$, predominantly presynaptic (Rebola et al., 2005a), increase the release of glutamate in the hippocampus (Cunha et al., 1994b; Lopes et al., 2002), possibly by inducing Ca^{2+} uptake (Gonçalves et al., 1997) and PKA-dependent Ca^{2+} currents through P-type Ca^{2+} channels in the presynaptic CA3 neurons (Mogul et al., 1993) that project onto the CA1 pyramidal cells (Figure 1.7).

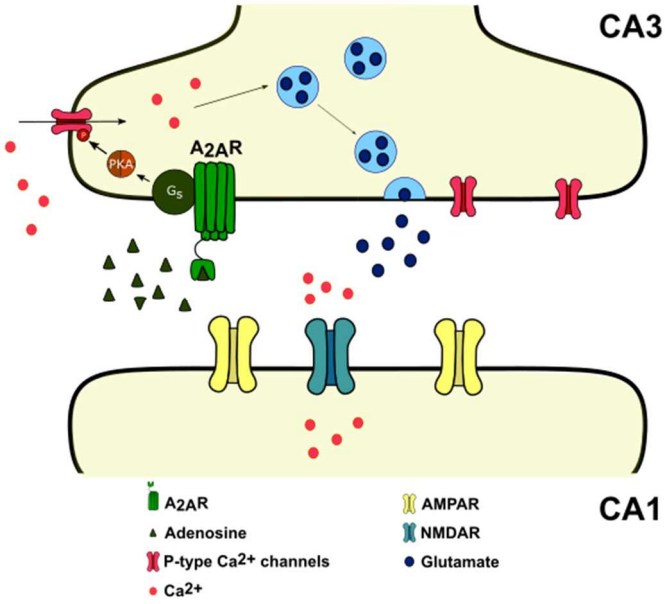

Figure 1.7. Presynaptic effects of $A_{2A}R$ in the glutamatergic synapses of the hippocampus. $A_{2A}R$ increase the release of glutamate in the hippocampus, possibly by inducing Ca^{2+} uptake and PKA-dependent Ca^{2+} currents through P-type Ca^{2+} channels in the presynaptic CA3 neurons that project onto the CA1 pyramidal cells. Abbreviations: CA1 and CA3: *Cornu ammonis* 1 and 3; PKA: Protein kinase A.

Postsynaptically, $A_{2A}R$ promote the function of AMPAR (Dias et al., 2012) and NMDAR (Ferreira et al., 2017a; Rebola et al., 2008; Sarantis et al., 2015). Concretely, previous studies hinted at a possible $A_{2A}R$-NMDAR interaction, since $A_{2A}R$ can control expression (Ferreira et al., 2017b, 2017a), recruitment (Rebola et al., 2008) and the rate of desensitization (Sarantis et al., 2015) of NMDAR. Group I metabotropic glutamate receptors, namely mGluR5, are postsynaptic and tightly coupled to NMDA receptors (Ferreira et al., 2017a; Jia et al., 1998; Takagi et al., 2010), conferring them the ability to either

protect or exacerbate NMDAR mediated toxicity depending upon the model or cell type (Lea et al., 2002). Upon activation by glutamate release, preferentially upon strong synaptic activation, mGluR5 increase NMDAR-mediated Ca^{2+} currents (Mannaioni et al., 2001), by reducing the Mg^{2+} block (Lea et al., 2002) and triggering the phosphorylation of NMDAR (Takagi et al., 2010). There is compelling evidence of an A_{2A}R-mGluR5 synergistic interaction in the modulation of NMDAR-mediated effects (Ferreira et al., 2017a; Kouvaros and Papatheodoropoulos, 2016; Sarantis et al., 2015; Tebano et al., 2005). This data suggests that mGluR5 might be a link between A_{2A}R and NMDAR.

Furthermore, A_{2A}R activation is important for LTP in the hippocampus (Fontinha et al., 2009; Rebola et al., 2008).

A_{2A}R also act as fine-tuners of other neuromodulatory systems, since A_{2A}R activation is required to observe synaptic effects of neuropeptides (Sebastião et al., 2000) or growth factors, namely for the facilitatory actions of brain derived neurotrophic factor (BDNF) on synaptic transmission (Diógenes et al., 2004, 2007a; Tebano et al., 2008) and on LTP (Fontinha et al., 2008). Furthermore, A_{2A}R activation decreases the efficiency of presynaptic inhibitory systems, namely cannabinoid CB1 receptors (Ferreira et al., 2015; Martire et al., 2011).

Aging is associated with cognitive decline both in humans and animals. Importantly, aging is the main risk factor for Alzheimer's disease (AD) (Reitz et al., 2011), which primarily affects synapses in the temporal lobe and hippocampal formation (Scheff et al., 2006).

These cognitive impairments are associated with structural and functional alterations in the hippocampus, that directly affect neural plasticity mechanisms (Burke and Barnes, 2006; Foster and Norris, 1997), leading to synaptic dysfunction and the subsequent memory deficits.

Synaptic dysfunction plays a central role in Alzheimer's Disease (AD), since it drives the cognitive decline (Walsh and Selkoe, 2004). Indeed, in age-related neurodegeneration, cognitive decline has a stronger correlation to early synapse loss than neuronal loss in patients (DeKosky and Scheff, 1990). Despite the many clinical trials conducted to identify drug targets that could reduce protein toxicity in AD, such targets and such strategies proven unsuccessful. Therefore, efforts focused on identifying the early mechanisms of disease pathogenesis, driven or exacerbated by the aging process, may prove more relevant to slow the progression rather than the current disease-based models.

The array of synaptic proteins is complex and the mechanisms underlying excitatory synaptic transmission are finely tuned by synaptic activity. The activation of N-methyl-D-aspartate (NMDA) receptors plays a pivotal role, because it can induce either long-term potentiation (LTP) or long-term depression (LTD), depending on the extent of the resultant intracellular [Ca^{2+}] rise in the dendritic spines and the downstream activation of specific intracellular cascades (Kullmann and Lamsa, 2007). Indeed, the Aβ-triggered synaptic failure involves the removal of AMPA receptors from the synaptic membrane and the degradation of PSD-95 protein at glutamatergic synapses (Almeida et al., 2005; Roselli et al., 2005). In addition to NMDA

receptors and AMPA receptors, an involvement of the metabotropic glutamate receptors (mGlu receptors) in Aβ mediated synaptic dysfunction has been suggested (Shankar et al., 2008). Shankar and colleagues demonstrated that different sources of Aβ (synthetic, extracted from human brain or from cells) can facilitate mGlu receptor-mediated LTD and can inhibit LTP leading to a reduced dendritic spine density (Shankar et al., 2008).

In pathophysiological conditions, such as aging and AD, there is compelling evidence of a cortical and hippocampal $A_{2A}R$ in glutamatergic synapses (Canas et al., 2009; Diógenes et al., 2007a; Lopes et al., 1999a, 2011a; Rebola et al., 2003b). Such $A_{2A}R$ overactivation induces glutamate release via PKA/cAMP/CREB signaling (Li et al., 2015a; Lopes et al., 1999a, 2002; Rebola et al., 2003b), calcium influx (Gonçalves et al., 1997) and leads to cognitive deficits (Batalha et al., 2016; Orr et al., 2015; Pagnussat et al., 2015a).

In aging, upsurge of $A_{2A}R$ and down-regulation of A_1R corresponds to a modified modulation of hippocampal synaptic transmission by $A_{2A}R$ and A_1R, with an enhanced role of $A_{2A}R$ in the facilitation of basal synaptic transmission and LTP in the hippocampus of aged rats (Costenla et al., 2011; Rebola et al., 2003b). This age-associated hippocampal $A_{2A}R$ upsurge, associated with high basal levels of adenosine (Cunha et al., 1995), impacts also on the transduction mechanisms associated with these receptors (Lopes et al., 1999b). Accordingly, in aged rats, $A_{2A}R$-dependent activation of glutamate release becomes more pronounced and shifts from a protein kinase C (PKC) mediated signaling to protein kinase A (PKA), c-AMP dependent effects (Lopes et al., 1999b; Rebola et al., 2003b).

In the striatum, $A_{2A}R$ and A_1R form heteromers and, under physiological conditions, adenosine preferentially activate A_1R (Ciruela et al., 2006; Ferré et al., 2007), which controls glutamatergic neurotransmission, namely by a decrease in NMDAR-mediated responses (Canhão et al., 1994; Klishin et al., 1995). In the hippocampus, associated to the $A_{2A}R$ overexpression, there is a loss of this $A_{2A}R$-A_1R cross-talk upon aging (Lopes et al., 1999b) and an excitatory effect on glutamatergic transmission, which suggests that it may be mediated by non-heteromerized $A_{2A}R$. However, due to the physiological residual levels of $A_{2A}R$ in the hippocampus and lack of experimental tools and techniques, the question of A_1R-$A_{2A}R$ heterodimerization in physiology and an aging-associated switch to $A_{2A}R$ homodimerization was not addressed so far.

The fact that aged rats display behavior and synaptic deficits hints an $A_{2A}R$ molecular switch in the genesis of age-related cognitive impairments. Accordingly, a recent genetic study discovered a significant association of the adenosine A_{2A} receptor encoding gene (*ADORA2A)* with hippocampal volume in mild cognitive impairment and Alzheimer's disease (Horgusluoglu-Moloch et al., 2017).

Furthermore, in animal models of several other pathologies, there is a clear correlation of hippocampal $A_{2A}R$ up-regulation with cognitive deficits, such as in acute or chronic stress (Batalha et al., 2013; Cunha et al., 2006; Kaster et al., 2015), Parkinson's (Varani et al., 2010) or Huntington's diseases (Li et al., 2015c; Tyebji et al., 2015). However, the exact mechanism by which neuronal $A_{2A}R$ overactivation could trigger or increase the susceptibility for memory dysfunction in these multiple pathologies is not completely understood.

Aberrant astrocytic $A_{2A}R$ expression in late-stage AD has been associated with cognitive decline in AD, and indeed astrocytic $A_{2A}R$ can lead to alterations of synaptic $A_{2A}R$-mediated functions (Matos et al., 2015). However, neuronal contribution is highlighted by recent evidence showing that stimulation of neuronal opto-$A_{2A}R$ in the hippocampus induces changes in synaptic plasticity and CREB activation (Li et al., 2015a). Moreover, silencing $A_{2A}R$ in neurons of the associative/commissural pathway rescues the aberrant LTP in APP/PS1 mice (Figure 1.7) (Viana da Silva et al., 2016). Furthermore, neuronal $A_{2A}R$ overexpression also induces alterations in microglia, including a microglia-primed phenotype, triggering morphological alterations that resemble early stages of activation process (Marques-Morgado, 2016). On the opposite, GFAP immunoreactivity was decreased, suggesting an asthenic astrocytic phenotype (Marques-Morgado, 2016) (Figure 1.7). These findings demonstrate that neuronal $A_{2A}R$ overactivation is sufficient to induce synaptic dysfunction and cognitive impairments, suggesting that synaptic dysfunction in aging and early AD is driven predominantly by a neuronal $A_{2A}R$ progressive increase, whereas at later Braak stages of AD, astrocytic $A_{2A}R$ and inflammation might also play an important role (Laurent et al., 2016; Orr et al., 2015).

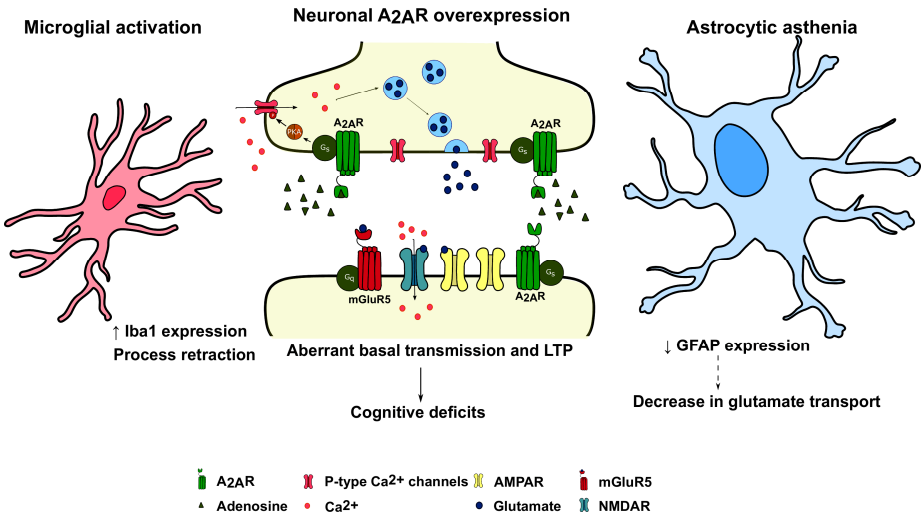

Figure 1.8. Functional interrelations between neuronal, astrocytic and microglial systems in pathological conditions with increased neuronal levels of $A_{2A}R$. Neuronal $A_{2A}R$ overexpression induces aberrant basal synaptic transmission and LTP, ultimately leading to cognitive deficits. Plus, it also drives a microglia-primed phenotype, triggering morphological alterations that resemble early stages of activation process. On the opposite, GFAP immunoreactivity was decreased, suggesting an asthenic astrocytic phenotype. Abbreviations: GFAP: Glial fibrillary acidic protein; Iba1: Ionized calcium binding adaptor molecule 1; PKA: Protein kinase 1.

Consistent with the pathophysiological role of $A_{2A}R$ in hippocampus-dependent cognitive impairments, the blockade of $A_{2A}R$ with caffeine prevented memory deficits in aged animals (Costa et al., 2008; Prediger et al., 2005). Also, the blockade of $A_{2A}R$ with either caffeine or more selective antagonists (SCH 58261, KW6002 or MSX-3) has a protective effect in hippocampal memory impairments, namely by the rescue of behavior and synaptic deficits (Arendash et al., 2006; Cunha et al., 2008; Dall'Igna et al., 2007; Laurent et al., 2016; Viana da Silva

et al., 2016) and by the decrease of Aβ and phosphorylated tau levels (Arendash et al., 2006; Laurent et al., 2016). Furthermore, knocking-out $A_{2A}R$ can rescue stress and AD-related synaptic dysfunction (Kaster et al., 2015; Laurent et al., 2016).

Altogether, these data observed in animal models strongly support a potential role of $A_{2A}R$ blockade, namely caffeine, in at least slowing the process of neurodegeneration. Consequently, it is crucial to address the putative neuroprotective role of caffeine on cognitive deficits in humans.

Caffeine is the world's most popular psychoactive drug and is consumed by millions of people. While short-term central nervous system stimulating effects of caffeine are well-known (Smith, 2002), the long-term impact remains not completely clear. The Finland, Italy and the Netherlands Elderly (FINE) Study showed that coffee intake was inversely associated with cognitive decline. In fact, elderly men (70 ± 10 years) who consumed coffee had a two times smaller 10-year cognitive decline than non-consumers (van Gelder et al., 2007). Accordingly, there was also an inverse association between the number of cups of coffee consumed per day and 10-year cognitive decline, with the least decline for men consuming three cups per day (van Gelder et al., 2007). Furthermore, in the Three City Study, with a sample of subjects aged 65 years and over, consumption of at least three cups of coffee per day was associated with less decline in verbal memory in women (Ritchie et al., 2007). On the opposite, coffee had no significant protective effect in women with under two daily units (Ritchie et al., 2007).

Importantly, other studies support a role for caffeine in the prevention of AD. A retrospective study reported an inverse correlation between coffee consumption and disease onset – AD patients had an average daily caffeine intake of 73.9 ± 97.9 mg during the 20 years before AD diagnosis, whereas the control had an average daily caffeine intake of 198.7 ± 135.7 mg during the corresponding 20 years of their lifetimes (Maia and de Mendonça, 2002). In a prospective study, daily coffee drinking decreased the risk of AD by 31% during a 5-year follow up (Lindsay et al., 2002). In line with those findings, moderate coffee drinkers (3-5 cups of coffee per day) had a 65-70% decreased risk of dementia and a 62-64% decreased risk of AD compared with low coffee consumers (Eskelinen et al., 2009). Furthermore, another prospective study showed that plasma caffeine levels at study onset were substantially lower (-51%) in mild cognitive impairment (MCI) subjects who later progressed to dementia compared to levels in stable MCI subjects. Also, plasma caffeine levels greater than 1200 ng/ml (≈6 μM) in MCI subjects were associated with no conversion to dementia during the ensuing 2/4 year follow-up period (Cao et al., 2012). However, coffee and caffeine intake in midlife were not associated with cognitive impairment, dementia, or individual neuropathologic lesions (Gelber et al., 2011). It is noteworthy that higher caffeine intake was associated with lower odds of having any neuropathological lesions at autopsy, including AD-related lesions, microvascular ischemic lesions, cortical Lewy bodies, hippocampal sclerosis, or generalized atrophy (Gelber et al., 2011).

Altogether, this data strongly emphasizes the role of caffeine in slowing down cognitive decline in aged population and reducing the

risk of developing Alzheimer's disease. This is also the case of Parkinson's disease, since epidemiological studies show an inverse relation between the consumption of caffeine and the risk of developing PD (Ascherio et al., 2001).

The following scheme summarizes the alterations that occur in the CA3-CA1 synapse of the hippocampus in aging and that impact in synaptic plasticity and ultimately in memory.

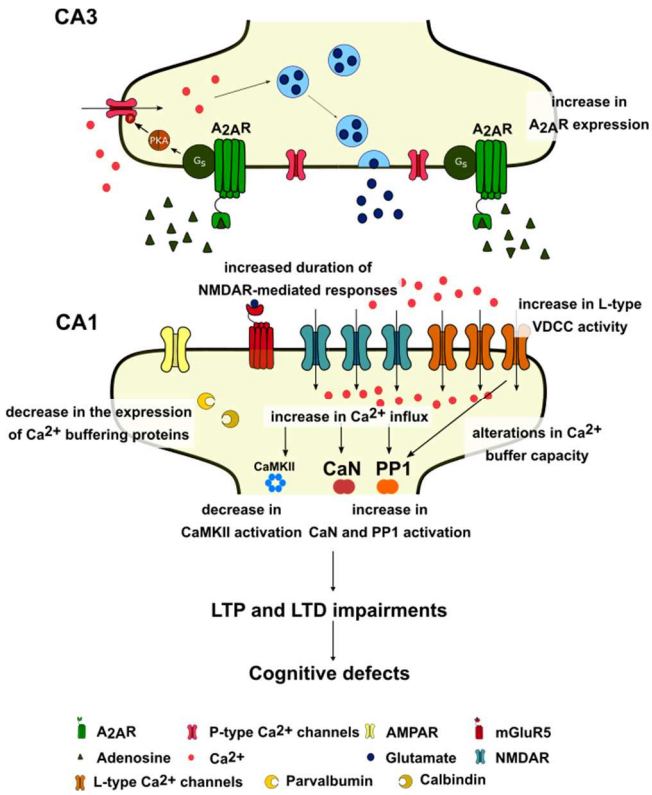

Figure 1.9. Aging is associated with pre- and postsynaptic alterations. There is an increase in $A_{2A}R$ expression, leading to Ca^{2+} uptake and PKA-dependent Ca^{2+} currents through P-type Ca^{2+} channels in the presynaptic CA3 neurons. Postsynaptically, aberrant contribution of NMDAR, L-type calcium channels and

impairments in calcium buffering mechanisms drive increased intracellular levels of calcium. This increase in Ca^{2+} leads to the disruption of the balance kinases/phosphatases and thus to impairments in LTP and LTD, which can be further correlated with cognitive deficits. Abbreviations: CA1 and CA3: *Cornu ammonis* 1 and 3; CaMKII: Ca^{2+}/calmodulin-dependent protein kinase II; CaN: calcineurin; PP1: Protein phosphatase 1; PKA: Protein kinase A; VDCC: Voltage-dependent calcium channels.

2. Aims

Aging is associated with cognitive decline both in humans and animals. Importantly, aging is the main risk factor for AD, which primarily affects synapses in the temporal lobe and hippocampal formation. These cognitive impairments are associated with structural and functional alterations in the hippocampus, which directly affect neural plasticity mechanisms, leading to synaptic dysfunction and the subsequent memory deficits.

There is compelling evidence from animal models of a cortical and hippocampal upsurge of $A_{2A}R$ in glutamatergic synapses of aged animals and AD models, leading to hippocampus-dependent cognitive deficits. The main goal of the present work is to investigate the underlying mechanism of neuronal $A_{2A}R$ upon hippocampal synaptic dysfunction in aging and AD.

Thus, the major aims of this study were to:

1. Assess whether in human aging and AD there is increased levels of $A_{2A}R$ and in which cell type this occurs.
2. Test if $A_{2A}R$ overexpression drives age-like modification in memory performance and synaptic plasticity, using a transgenic approach and, in this case, unravel the underlying synaptic mechanism.
3. Investigate if the synaptic alterations observed in transgenic animals are also present in aged animals and in an AD model.

3. Technical approaches

3.1. Electrophysiology

Electrophysiology is the study of the electrical properties of biological cells and tissues by measuring voltage changes or electrical current. It begun in the 1700's, when Luigi Galvani, using a frog neuromuscular preparation, discovered that the function of the nervous system was tightly linked with electrical activity (Piccolino, 1997).

Nowadays electrophysiological techniques allow scientists to measure from single channel conductivities to whole cells (patch-clamp) and cell population (extracellular recordings) responses. It was the development of electrophysiology that allowed many of the now basic concepts of neuroscience to be discovered and its through electrophysiological techniques that many are still revealed.

Due to the organized and preserved structure of the hippocampal slice, it is possible to stimulate the different afferent fibers, as the Schaffer collaterals, and record the innervated cells, in this case CA1 cells, either single cell recording, by patch clam techniques, or extracellularly, thus performing extracellular recordings.

3.1. 1. Extracellular recordings

In figure 1.10 is a schematic representation of the hippocampus and how the electrodes are positioned when performing extracellular

recording of field excitatory postsynaptic potentials (fEPSP) in the CA3-CA1 synapse.

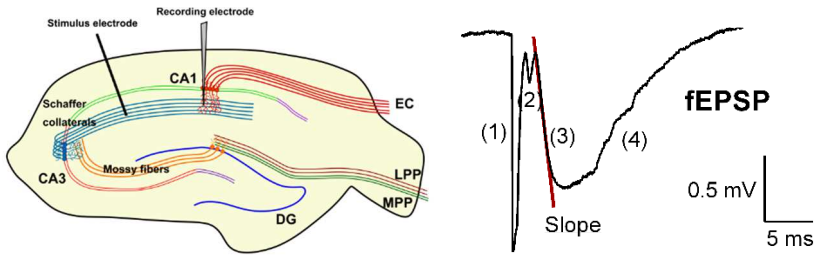

Figure 1.10. Left: Schematic representation of the simplified circuitry of the hippocampus. One stimulation electrode is placed in the Schaffer collaterals, while the recording electrode is in CA1 dendritic area. Right: a representative field Excitatory PostSynaptic Potential (fEPSP). (1) Stimulus artifact; (2) Fiber volley; (3) Early EPSP, (4) Late EPSP. Abbreviations: CA, *cornu ammonis*; DG, dentate gyrus; EC, entorhinal cortex; LPP, lateral performant pathway; MPP, medial performant pathway.

To perform extracellular recordings, the recording electrode is placed in the dendritic area of the innervated cells and the response of the population of cells that is being stimulated is measured. The result is a field Excitatoty Postsynaptic potential (fEPSP) (Figure 1.10). The main neurotransmitter released by hippocampal neurons is glutamate. Therefore, the fEPSP obtained when performing extracellular recordings in the hippocampus results from the depolarization of the postsynaptic population as a result of ion influx caused by the glutamate release. In figure 1.10 it is possible to observe a typical waveform of the fEPSP. It has mainly three components, the stimulus artifact (1), followed by the "fiber volley" (2) and finally the EPSP itself (3) and (4). This is composed by two phases, the first (3), a result

of the postsynaptic response to glutamate and the second (4) the repolarization part of the EPSP in which the main neurotransmitter involved is GABA. The "fiber volley" (2) results from the presynaptic action potential arriving at the recording site, and it therefore the first to be recorded. This can give an indicator of how healthy the slices are, since a small fiber volley amplitude means that less afferent fibers are being recruited to obtain a given fEPSP. The EPSP itself is the manifestation of the postsynaptic depolarization induced by the glutamate released from the stimulated fibers and its slope and amplitude can be used to evaluate glutamate release. Usually the parameter evaluated is the slope since the peak amplitude of the fEPSP is more prone to contamination and more affected by the GABAergic contribution (Sweatt, 2010). This technique is widely used to evaluate the efficiency of synaptic transmission and the way it is modified in different situations, namely long-term potentiation and long-term depression.

3.1.2. Patch-clamp

Especially in neuroscience, the physiology of ion channels has always been an imporatnt topic of interest. The development of the patch-clamp technique in the 1970s has given electrophysiologists new prospects. It allows high-resolution current recordings not only of whole cells, but also of excised cellular patches.

Figure 1.11 depicts a schematic representation of the hippocampus and how the electrodes are positioned when performing patch-clamp in CA1 pyramidal cells.

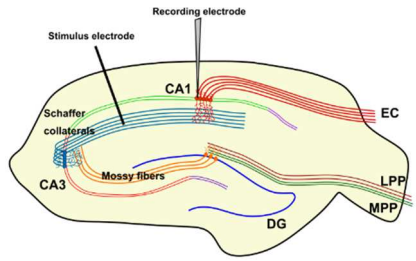

Figure 1.11. Schematic representation of the simplified circuitry of the hippocampus. One stimulation electrode is placed in the Schaffer collaterals, while the recording electrode is in one CA1 pyramidal cell. Abbreviations: CA, *cornu ammonis*; DG, dentate gyrus; EC, entorhinal cortex; LPP, lateral performant pathway; MPP, medial performant pathway.

Based upon the formation of a high resistance (gigaohm) seal with the membrane of the cell being studied, the tip of a microelectrode is then inserted inside the cell and measures voltage or current alterations across the cell membrane.

The **voltage clamp** technique involves the clamping of a cell potential at a chosen value, making it possible to measure the ionic current that crosses a cell's membrane at that voltage. This is important because many of the ion channels in the membrane of a neuron are voltage-gated ion channels, which open only when the membrane voltage is within a certain range.

The **current clamp** technique records the membrane potential by injecting current into a cell through the recording electrode. Unlike in the voltage clamp mode, where the membrane potential is held at a

level determined by the experimenter, in current clamp mode the membrane potential is free to vary, and the amplifier records whatever voltage the cell generates on its own or as a result of stimulation. This technique is used to study how a cell responds to electric current. This is important for instance for understanding how neurons respond to neurotransmitters that act by opening membrane ion channels.

CHAPTER II

Methods

1. Human samples

The use of human samples was conducted in accordance with the Helsinki Declaration as well as national ethical guidelines. Protocols were approved by the Local Ethics Committee and the National Data Protection Committee. Human AD samples were provided by Valerie Buée-Scherrer (INSERM UMR-S1172 "Alzheimer & Tauopathies", Lille Neurobank, Jean-Pierre Aubert Research Centre Univ. Lille-Nord de France, France) or by Pedro Pereira and José Pimentel (Laboratório de Neuropatologia, Hospital de Santa Maria, CHLN, EPE, Lisboa, Portugal). Samples were collected from brains at 36h *post mortem.* Aged and young human samples were collected by Beatriz S. da Silva (National Institute of Legal Medicine and Forensic Sciences, Coimbra, Portugal) and prepared by Paula M. Canas (CNC-Center for Neurosciences and Cell Biology, Univ. Coimbra, Coimbra, Portugal). After validation of their quality (Pliássova et al., 2016) young (20-40 years old), aged (60-75 years old) and AD (60-75 years old, Braak stages 5-6) human forebrain and hippocampus were used for histological analysis, Western blotting and qPCR as indicated.

2. Animals

Animal procedures were performed in accordance with the European Community guidelines (Directive 2010/63/EU), Portuguese law on animal care (DL 113/2013), and approved by the Instituto de Medicina Molecular Internal Committee and the Portuguese Animal Ethics

Committee (Direcção Geral de Veterinária). Environmental conditions were kept constant: food and water *ad libitum*, 21 ± 0.5°C, 60 ± 10% relative humidity, 12 h light/dark cycles, 2 to 3 rats per cage or 3 to 4 mice per cage. Only male animals were used in all experiments. Mice were sacrificed by cervical dislocation and rats were sacrificed by decapitation after anesthesia under halothane atmosphere. Male Tg(CaMKII-hA_{2A}R) Sprague-Dawley rats and their WT littermates with matched age (8-14 weeks old) or aged WT males (18-20 months old) were used for behavior and electrophysiology experiments. Male WT and APP/PS1 mice (11-12 months old) were used for electrophysiology experiments.

3. Generation and maintenance of transgenic animals

Transgenic rats with an overexpression of human A_{2A}R cDNA under the control of the Ca^{2+}/calmodulin-dependent protein kinase II (CaMKII) promoter, Tg(CaMKII-hA_{2A}R), were generated as previously described (Batalha et al., 2016). Expression of A_{2A}R was achieved in forebrain areas, mainly in the hippocampus and cortex. Relevantly, the endogenous rA_{2A}R mRNA levels were not modified in the hippocampus (Batalha et al., 2016). Furthermore, there was no changes in adenosine A1 receptor levels in the hippocampus of Tg(CaMKII-hA_{2A}R) animals (Batalha et al., 2016). Genotyping: Transgenic rats were identified by PCR (30 cycles, 58 °C annealing temperature) of their genomic DNA isolated from ear biopsies by the use of the CaMKII-hA_{2A}R transgene-specific primers and rat β-actin

primers as an internal control (Invitrogen, USA; see Table 2.1). APP/PS1dE9 transgenic mice on C57Bl6/J background have been described elsewhere (Jankowsky et al., 2001). Genotyping was done by PCR analysis of tail DNA (30 cycles, 60 °C annealing temperature) using transgene-specific primers (APP and PrP) and tau as an internal control (Table 2.1).

4. Oral administration of the drug

KW6002 (istradefylline), a selective $A_{2A}R$ antagonist (Hockemeyer et al., 2004; Yang et al., 2007), was diluted in the drinking water (0.025% methylcellulose) and was orally administered to WT, Tg(CaMKII-$hA_{2A}R$) and aged animals, being continuously available. The experimenter was blinded to genotype for the duration of KW6002 administration. The weight of the animals and the volume intake were assessed twice a week and the concentration of the solution was adjusted so that the drug intake was maintained at 5 mg kg^{-1} per day. The treatment started at 5–7 weeks of age in WT and Tg(CaMKII-$hA_{2A}R$) and at 16 months of age in aged animals, and lasted for 1 month or 3 weeks, respectively, until sacrifice.

5. RNA extraction and quantitative real time PCR analysis (RT-qPCR)

Total RNA was extracted and purified using the RNeasy Lipid Tissue Mini Kit (Qiagen, Germany). RNA quality was assessed by NanoDrop 2000 (Thermo Scientific, USA) analysis (A260/A280 ≈ 2; 260/235 > 1.8). Total RNA (2 μg) was reverse-transcribed using random primers and SuperScript™ First-Strand Synthesis System for RT-PCR (Invitrogen, USA). RT-qPCR analysis was performed on a Corbett Rotor-gene 6000 apparatus (Qiagen, Germany) using Power SYBR Green PCR Master Mix (Applied Biosystems, UK), 0.2 μM of each primer and 1/20 dilutions of total cDNA (final concentration 0.4 ng/μl). The thermal cycler conditions were 10 min at 95°C, 40 cycles of a two-step PCR, 95°C for 15 s followed by 60°C for 25 s with a final thermal ramp from 72 to 95ºC. Primer efficiencies (E=1±0.02) were obtained from standard curves of serial dilutions (slope and R^2 respectively around -3.3 and 0.99). Sequences of primers used (all from Invitrogen, UK, HPLC purified) are listed in the Table 2.1. Reference genes were PPIA (cyclophilin A) and β-actin for human tissues. Amplifications were carried out in triplicate in two independent runs, and according to the MIQE guidelines (Bustin et al., 2009). The relative expression of target genes was determined by the comparative CT method (Schmittgen and Livak, 2008).

Primer	Target Gene	Organism	Forward Primer	Reverse Primer	Amplicon Size
CypA	PPIA peptidylprolyl isomerase A (cyclophilin A)	human	TATCTGCACTGCC AAGACTGAGTG	CTTCTTGCTGGTC TTGCCATTCC	126bp
hACTB	Human Actin-β	human	GGACTTCGAGCA AGAGATGG	AGCACTGTGTTGG CGTACAG	233bp
A2AH	Human Adenosine A2A Receptor	human	AACCTGCAGAAC GTCAC	GTCACCAAGCCA TTGTACCG	245bp
Act-B	Actin-β	rat	AGCCATGTACGT AGCCAT	CTCTCAGCTGTGG TGGTGAA	228bp
CaMKII-hA_{2A}	calmodulin-dependent protein kinase II promoter and human Adenosine Receptor A2A	transgene	GACTAAGTTTGTT CGCATCCC	GTGACACCACAA AGTAGTTGG	450bp
tau	microtubule-associated protein tau isoform X4	mouse	CCAGTTGTGTATG TCCACCC	CTCAGCATCCCAC CTGTAAC	187bp
APP	Amyloid precursor protein	transgene	CCGAGATCTCTGA AGTGAAGATGGA TG	AGCCTAGACCAC GAGAATGC	400bp

Table 2.1: Primers used for genotyping and qPCR.

6. *In situ* hibridization

The *in situ* hybridization technique was adapted from previously described methods (Schiffmann and Vanderhaeghen, 1993). The sections mounted on RNAse free poly-L-lysine-coated slides were fixed in freshly prepared 4% paraformaldehyde solution for 30 min and rinsed in phosphate buffer saline (PBS: 130 mM NaCl, 7 mM

Na_2HPO_4, 3 mM NaH_2PO_4) All sections were dehydrated and dipped for 3 min in chloroform. After air drying, the sections were incubated overnight at 42°C with $0.35x10^6$ cpm per section of ^{35}S-labelled probes diluted in hybridization buffer, which consisted of 50% formamide, 4xSSC (1xSSC: 0.15 M NaCl, 0.015 M sodium citrate, pH 7.4), 1 x Denhardt's solution (0.02% polyvinylpyrrolidone, 0.02% BSA, 0.02% Ficoll, 1% sarcosyl, 0.02 M sodium phosphate at pH 7.4, 10% dextran sulfate, 500 µg/ml yeast tRNA, 100 µg /ml salmon sperm DNA, and 60 mM dithiothreitol). After hybridization, the sections were rinsed for 4x15 min in 1xSSC at 55°C, dehydrated and covered with Hyperfilm-βmax film (Amersham, Belgium) for 2 or 3 weeks. The oligonucleotide probes were synthesized on an Applied Biosystems 381A DNA synthesizer or Eurogentec (Belgium) with a GC to AT ratio between 45 and 65%. The human $A_{2A}R$ oligonucleotide probe (CAGCCCTGGGAGTGGTTCTTGCCCTCCTTTGGCTGACC-GCA) is complementary to nucleotides 123-166 in a partial human cDNA sequence (Libert et al., 1989) and has been previously used on human brain sections (Schiffmann et al., 1991). The rat $A_{2A}R$ probe (CCGCTCCCCTGGCAGGGGCTGGCTCTCCATC-TGCTTCAGCTG) is complementary to nucleotides 604–645 of the rat cDNA sequence (Fink et al., 1992). Oligonucleotides were labelled with α-^{35}S dATP (DuPont-NEN, Belgium) at their 3' end by terminal DNA deoxynucleotidylexotransferase (Gibco, Belgium) and purified with a G50 column (Pharmacia, Belgium) according to the manufacturer's instructions.

7. Behavioral assessments

Rats were first handled for 5 days prior to behavioral tests. Mazes were cleaned with a 30% ethanol solution between each animal. Animals were randomized prior to behavioral assessment and the experimenter blinded to genotype for the duration of behavioral testing. All behavioral tests were performed during the light phase between 8 a.m. and 6 p.m. in a sound attenuated room.

7.1. Morris water maze

Spatial memory ability was evaluated in the MWM test, as previously described (Batalha et al., 2013). The test was performed in a circular pool (1.8m diameter, 0.6m height), filled with water opacified with non-toxic black paint and kept at 25±2ºC. A round 8-cm in diameter platform was hidden 1 cm beneath the surface of the water at a fixed position. Four positions around the edge of the tank were used, dividing the tank into four quadrants: target quadrant (T, quadrant here the platform was hidden), left quadrant (L, quadrant on the left of the target quadrant), right quadrant (R, quadrant of the right of the target quadrant) and opposite quadrant (O, quadrant on the opposite side of the target quadrant). During the acquisition phase, each animal was given four swimming trials per day (30-min inter-trial interval). A trial consisted of placing the animal into the water facing the outer edge of the pool and allowing the animal to explore and reach for the hidden platform. If the animal reached the platform before 60 secs, it was

allowed to remain there for 10 sec. If the animal failed to find the target before 60 sec, it was manually guided to the platform, where it was allowed to remain for 20 sec. After the end of each trial, animals were removed from the pool and placed back to their home cages beneath heat lamps in order to prevent temperature loss. On the probe test, the platform was removed and animals were allowed to swim freely for 60 sec while recording the percentage of time spent on each quadrant. The latency to find the platform during the acquisition phase and the percentage of time in the platform quadrant in the probe test were recorded and analysed using the Smart 2.5 tracking system (PanLab, Barcelona) and used to evaluate hippocampal-dependent memory. Swimming speed was also registered, as a measure of possible motor deficits that could interfere with the ability to perform the task.

7.2. Y-maze behavior test

Short-term reference memory was assessed in a spontaneous novelty-based spatial preference Y-maze test. The Y-maze was performed in a two-trial recognition test in a Y-shaped maze with 3 arms (each with 35 cm length x 10 cm width x 20 cm height), angled at 120° and with opaque walls. Different cues were placed on the surrounding walls. Allocation of arms was counterbalanced within each group. On the first trial (learning trial), the animal explored the maze for 10 min with only two arms opened (“start” and “other” arm). Access to the third arm of the maze (“novel” arm) was blocked by an opaque door. The rat

was then removed from the maze and returned to its home cage. After 1 h, the animal was placed again in the "start" arm of the maze, the door of the "novel" arm was removed and the mouse was allowed to explore the maze for 5 min (test trial). Rat tracings were continuously monitored by an automated tracking system (Smart 2.5, PanLab, Barcelona). Preference for the novel arm is considered a measure of short-term reference memory. To exclude the possible confounding effect of alterations of locomotor activity, we used the frequency of entrance into the arms (number of transitions) as an indirect indicator of the general locomotor activity.

8. Electrophysiology experiments

8.1. Field potential recordings

After decapitation the brain was rapidly removed and the hippocampi were dissected free in ice-cold Krebs solution, which is composed of (mM): NaCl 124; KCl 3; NaH_2PO_4 1.25; $NaHCO_3$ 26; $MgSO_4$ 1; $CaCl_2$ 2 and D-glucose 10, previously gassed with 95% O_2 and 5% CO_2, pH 7.4. Transverse hippocampal slices (400 µm thick) were obtained with a McIlwain tissue shopper and field excitatory postsynaptic potentials (fEPSPs) were recorded in the *stratum radiatum* of the CA1 area as previously described (Batalha et al., 2013). Tested drugs, SCH58261 (50 nM and 100 nM), caffeine (30 µM), MPEP (5 µM) or AP5 (15 µM, 50 or 100 µM), were added to the Krebs superfusion solution after obtaining a stable 10 min baseline.

Long term depression (LTD) was induced as previously (Laurent et al., 2016) with 3 trains of 2 Hz during 10 min separated by a 10-min interval, or 1200 pulses at 0.5, 1 or 2 Hz, with basal fEPSPs of 0.5 mV/ms. LTD magnitude was calculated as percentage of change of fEPSP slope 50-60 min after LTD induction compared to baseline fEPSP (10 min before LTD induction). Recordings were performed at 32ºC, 3 ml/min.

8.2. Patch-clamp recordings

Transverse hippocampal slices (300 µm) were cut in an oxygenated ice-cold solution containing (mM): 234 sucrose, 2.5 KCl, 1.25 NaH_2PO_4, 0.5 $CaCl_2$, 10 $MgSO_4$, 11 glucose, 26 $NaHCO_3$. They were incubated at 37ºC for 1h and then maintained at room temperature for 0.5-5h in an oxygenated physiological solution (ACSF) containing (in mM): 119 NaCl, 2.5 KCl, 1.25 NaH_2PO_4, 2.5 $CaCl_2$, 1.3 $MgSO_4$, 11 glucose, 26 $NaHCO_3$, pH 7.4. For recording, slices were transferred into a recording chamber perfused with oxygenated ACSF at 3 ml min^{-1} at 32ºC and visualized under IR-DIC on a slidescope at x60 magnification (Scientifica Ltd., UK). Recordings were made using a patchstar micromanipulator (Scientifica Ltd.) connected to a Multiclamp700B amplifier, Digidata 1440 acquisition system and pClamp 10 software (Axon instruments, Molecular Devices Ltd., USA). Patch pipettes were made of borosilicate glass and shaped to a final resistance of approximately 5 MΩ.

8.2.1. Current clamp experiments

Whole-cell patch clamp experiments were performed in the current clamp configuration (Marcantoni et al., 2014) using a pipette solution containing (in mM): 135 gluconic acid (potassium salt: K-gluconate), 5 NaCl, 2 $MgCl_2$, 10 HEPES, 0.5 EGTA, 2 ATP-Tris and 0.4 Tris-GTP. After a tight seal (>1 GΩ) on the cell body of the selected neuron was obtained, whole-cell patch clamp configuration was established, and cells were left to stabilize for approximately 2 min before recordings began. The resting (V_m) membrane potential was first measured in the absence of any spontaneous firing, and only cells with V_m more negative than −55 mV were considered. We then injected a minimum amount of current (150 pA) to stimulate a sustained firing that we recorded for a few minutes. Using this tonic firing, we measured the fast and medium afterhyperpolarization potentials (fAHP and mAHP, respectively) (Figure 3.7A, B). The maximum rising slope, the overshoot and the action potential (AP) halfwidth were also considered (Figure 3.7A, B). The half-width value was calculated considering the AP width measured at 50% of the peak amplitude. These AP parameters were estimated without taking into account the voltage drop across the pipette resistance. To study the relationship between firing frequency and current input (Figure 3.7C, D), we first adjusted the membrane potential to −60 mV and then injected 16 pulses of increasing intensity (from 100 to 850 pA, 200 ms duration). We also used these recordings to measure the instantaneous firing frequency at the beginning (onset frequency, f_o, corresponding to the firing frequency measured between the first and second APs in the spike

train) and at the end of the spike train (steady-state frequency, f_{ss}, corresponding to the firing frequency measured between the last two APs in the spike train) (Figure 3.7C). By plotting f_o and f_{ss} as a function of injected current (Figure 3.7E, F), we obtained information on the spike frequency adaptation of these neurons. To quantify the inward rectification time-dependent potential, we first adjusted the membrane potential (V_h) to −60 mV and injected 20 pulses of increasing intensity (from −100 pA to −2 nA, 600 ms duration). During the pulse, we observed that the hyperpolarization reached a maximum value (peak) and then decreased to stabilize to a steady-state value (Figure 3.7G). We plotted the difference between the peak and the steady-state values as a function of injected current to obtain indirect information on the hyperpolarization-activated inward current (I_h) (Figure 3.7H).

8.2.2. Voltage clamp experiments

Whole-cell patch clamp experiments were performed in the voltage clamp configuration (Marchetti et al., 2010) using a pipette solution containing (in mM): 117.5 caesium methanesulfonate, 15 CsCl, 10 Tetraethylammonium Chloride (TEACl), 8 NaCl, 10 HEPES, 0.25 EGTA, 4 MgATP, 0.3 NaGTP; the pH was adjusted to 7.3 with CsOH. For all experiments, slices were superfused with the oxygenated ACSF at 32°C in the continuous presence of 50 µM picrotoxin (dissolved in DMSO, Sigma-Aldrich) to block GABAergic transmission. The Schaffer collateral pathway was stimulated at 0.10 Hz using electrodes

(glass pipettes filled with ACSF) placed in the *stratum radiatum*. After a tight seal (>1 GΩ) on the cell body of the selected neuron was obtained, whole-cell patch clamp configuration was established, and cells were left to stabilize for approximately 2 min before recordings began. To measure the paired-pulse ratio (PPR), two stimuli were delivered with inter-spike intervals between 50 and 200 ms. PPRs were calculated as the ratio between the peak amplitude of $EPSC_2$ and of $EPSC_1$ (20 sweeps average per inter-spike interval) (Figure 3.8). To calculate the AMPAR/NMDAR ratio (Figure 3.9A), cells were held at -65 mV to record AMPAR EPSCs and at +40 mV to record NMDAR EPSCs. AMPAR EPSCs amplitudes were calculated by averaging 30 consecutive EPSCs recorded at -65 mV and measuring the peak compared to the baseline. NMDAR EPSCs amplitudes were calculated by averaging 30 consecutive EPSCs recorded at +40 mV and measuring the amplitude 60 ms after EPSC onset compared to the baseline. Before starting I-V relationship measurements, stimulus intensity was set to evoke an EPSC of approximately 100 pA at -60 mV, normalizing the response and thus the number of recruited fibers. Liquid junction potential was not corrected for whole-cell voltage-clamp recordings. For $EPSC_{NMDAR}$ I-V relationship measurements, pharmacologically isolated NMDAR EPSCs were obtained in the presence of 6,7-dinitroquinoxaline-2,3-dione (DNQX, 100 µM dissolved in 1% DMSO, Sigma-Aldrich). NMDAR EPSCs amplitudes were calculated by averaging 15 consecutive EPSCs recorded at voltages ranging from -70 mV to +40 mV in 10 mV steps. I-V relationships were normalized to the NMDAR EPSC amplitude at +40 mV (as +1). AMPAR I-V relationships were recorded using an

identical procedure, but in presence of R-2-amino-5-phosphonopentanoate (AP5, 50 μM dissolved in DMSO, Sigma-Aldrich) and were normalized to the AMPAR EPSC amplitude at -70 mV (as -1). The decay time of pharmacologically isolated NMDAR EPSC, recorded from cells voltage clamped at +40 mV, was fit with a double exponential function, using Clampfit software, to calculate both slow and fast decay time constants, τs_{low} and τ_{fast}, respectively. The weighted time constant ($\tau_{weighted}$) was calculated using the relative contribution from each of these components, applying the formula: $\tau_w = [(a_f.\tau_f) + (a_s.\ \tau_s)]/(a_f + a_s)$, where a_f and a_s are the relative amplitudes of the two exponential components, and τ_f and τ_s are the corresponding time constants.

9. Primary neuronal cultures

Hippocampal neurons were cultured from 18 day Sprague Dawley rat embryos (Harlan, Barcelona, Spain) as previously described (Valadas et al., 2012). Briefly, embryos were collected in Hank's Balanced Salt Solution (HBSS, Corning, USA) and rapidly decapitated. Meninges were removed, and whole cortices (hippocampi and attached cortex) were dissociated and incubated for 15 minutes in HBSS with 0.025% trypsin. Cells were washed once with HBSS with 30% Fetal Bovine Serum (FBS), centrifuged three times, re-suspended in Neurobasal Medium (Gibco – Life Technologies, USA) supplemented with 2% B-27 supplement, 25 μM Glutamate, 0.5 mM glutamine, and 2 U/ml Penicillin/Streptomycin, gently dissociated and filtered through a

70µm strainer (VWR, USA). Cells were plated on poly-D-lysine-coated plates and grown for 14 days at 37°C in a 5% CO_2-humidified atmosphere in the previously described supplemented Neurobasal medium, in the absence of any positive selection for neurons.

10. Transfection of primary neuronal cultures

At DIV (day *in vitro*) 13, neurons were transfected as previously described (Sariyer, 2013). A 33 ± 4% efficiency of transfection was obtained. At DIV 14, Ca^{2+} imaging experiments and immunocytochemistry to confirm transfection were performed.

11. Construct generation

Venus-A_{2A}R construct was generated with the In-fusion HD Cloning Kit (Clontech Takara, USA). Venus and A_{2A}R fragments were produced by using, respectively, the pair of primers 5'-GTTTAAACTTAAGCTTATGGTGAGCAAGGGCGAG-3' and 5'-GCTGCCCATGGTGGCCTTGTACAGCTCGTCCATG-3', and the pair of primers 5'-GCCACCATGGGCAGCAGC-3' and 5'-AAACGGGCCCTCTAGATCAGCTGGGGGCGAACTC-3'. PCR fragments were cloned into the vector pcDNA3.1(+) linearized with HindIII and XbaI, and the resulting construct was verified by DNA sequencing (GATC Biotech, Germany). Venus plasmid was provided by Tiago F. Outeiro and David Blum provided the A_{2A}R plasmid.

12. Ca^{2+} imaging

Primary neuronal cultures were plated at a density of 50 x 10^3 cells per well in 35 mm glass bottom culture dishes (MatTek Corporation, USA) previously coated with poly-D-lysine. At DIV 14, neurons were loaded with Fura-2 AM (5 µM, in external physiological solution with the following composition in mM: NaCl 125, KCl 3, NaH_2PO_4 1.25, $CaCl_2$ 2, $MgSO_4$ 1, D-(+)-glucose 10 and HEPES 10; pH 7.4 adjusted with NaOH) and incubated at 37ºC for 1 h. Cells were then placed on a heated chamber installed in an inverted microscope with epifluorescent optics and equipped with a high speed multiple excitation fluorimetric system (Lambda DG4, with a 175W Xenon arc lamp). Fura-2 AM loaded neurons were sequentially excited both at 340 nm and 380 nm, for 250 ms at each wavelength, and the emission fluorescence was recorded at 510 nm with a CDD camera. Experiments were performed on cells with a baseline fluorescence ratio around 0.5, which corresponds approximately to a $[Ca^{2+}]i$ of about 100nM, considered the normal $[Ca^{2+}]i$ (Barhoumi et al., 2010; Knot et al., 2005). Cells with a baseline fluorescence ratio above 1 were discarded. Experiments were performed at 37ºC in a 5% CO_2-humidified atmosphere. Drugs were applied directly to the cells medium. All cells were challenged with ionomycin (a Ca^{2+} ionophore; 2 µM) at the end of the experiment and only those that responded were included, confirming neuronal viability. Image data were recorded and analyzed using the MetaFluor software (Universal Imaging, West Chester, PA, USA).

13. Immunocytochemistry

Twenty-four hours after transfection, primary neurons were washed with PBS and fixed with 4% paraformaldehyde for 10 min at RT, followed by a permeabilization step with 0.5% Triton X-100 (Sigma–Aldrich) for 20 min at RT. After blocking in 10% FBS for 30 min, the cells were incubated with mouse anti-$A_{2A}R$ primary antibody (1:100, mouse monoclonal, mab70192, Covalab, France) overnight at 4°C. After a 30-min washing with PBS, cells were incubated with the secondary antibody Alexa Fluor 568 goat anti-mouse IgG (Life Technologies-Invitrogen) for 1 h at RT. Finally, the cells were stained with Hoechst 33258 (1 mg/mL, Life Technologies; 1:5000 in PBS) for 5 min and mounted in Dako mounting medium. Z-stack images at 63x magnification were acquired with a Zeiss LSM 880 Confocal Microscope.

14. Immunohistochemistry

Brains were removed, stored in formaldehyde 4% aqueous solution (VWR, USA) for three days, embedded in paraffin, and cut into coronal sections of 2 μm. Slides were deparaffinized, rehydrated and antigen retrieval was performed by microwave heating in 0.01 M citrate buffer pH=6.0. For fluorescence analysis, slices were then incubated with primary antibodies selective for $A_{2A}R$ (1:100, mouse monoclonal, mab70192, Covalab, France) and GFAP (1:250, rabbit polyclonal IgG, G9269, Sigma-Aldrich, USA), MAP2 (1:500, rabbit

polyclonal IgG, ab32454, Abcam, UK), SNAP25 (1:5000, rabbit polyclonal IgG, S9684, Sigma-Aldrich), synaptophysin (1:200, mouse monoclonal, S7568, Sigma-Aldrich) or PSD95 (1:100, rabbit polyclonal IgG, D27E11, Cell Signaling Technology, UK) overnight at RT and washed for 20 min with PBS before being incubated overnight at RT with secondary antibodies (Alexa Fluor 488 donkey anti-rabbit and Alexa Fluor 568 donkey anti-mouse 1:400, Life Technologies, USA). After washing for 20 min, the sections were incubated with Hoechst (12 μg/ml final concentration; Hoechst 33342, Thermo Scientific, USA), washed once and mounted in Dako Mounting Medium (Agilent, USA). Z-stack images at 63x magnification were acquired with a Zeiss LSM 880 Confocal Microscope with Airyscan. The images were acquired with a 63x objective, model Plan-Apochromat, a numerical aperture of 1.40 and a working distance of 0.19mm. The images were acquired with a voxel size of x:132nm, y:132nm, z:316nm, and the point spread function (PSF) monitored with beads of 175nm was XY = min 205 ± 4 nm, max 234 ± 3 nm and Z 478 ± 30 nm (emission wavelength 525 nm). Colocalization analysis between $A_{2A}R$ and SNAP25/PSD95 was performed in single plans with colocalization threshold tool in Fiji software (Costes et al., 2004), which calculates several colocalization parameters and generates an image with colocalized pixels stained in white. Compositional images of hippocampal formation were produced by tile stitching of images at 10x magnification acquired using Zeiss Axio Observer Widefield Microscope. For human samples, coronal sections were stained with anti-$A_{2A}R$ (1:100, mab70192, Covalab) and developed using amplification (NovoLink™ Polymer Detection System, Leica

Biosystems, Germany) and Horseradish peroxidase–diaminobenzidine (HRP-DAB) detection systems. In parallel, an age-matched control section was used as a negative control, where no primary antibody was used. Samples were then mounted in Entellan® Mounting Medium (Sigma-Aldrich). Optical density was measured using ImageJ software in 1 field of 20x magnification and 3 fields of 40x magnification.

15. Electron microscopy

Tg(CaMKII-hA_{2A}R) animals were anesthetized using isoflurane and fixed using perfusion pump with 0.1 M phosphate buffer containing 2% paraformaldehyde and 0.2% glutaraldehyde. After removal of the brain, 500µm slices of hippocampus were collected using a Vibratome (Leica, Germany). Immuno-electron microscopy of hippocampal slices was performed according to Tokuyasu (Tokuyasu, 1980). Slides were chemically fixed in 0.1 M phosphate buffer containing 2% paraformaldehyde and 0.2% glutaraldehyde, embedded in gelatine (Royal® food grade gelatine) and cryo-preserved in 2.3 M sucrose. Gelatine blocks were frozen in liquid nitrogen and sectioned at −120°C using a cryo-ultramicrotome (UC7 and FC7, Leica) to generate 70 nm sections, sections were collected and thaw in a mixture of 2.3M sucrose and 2% methylcellulose. Immuno-labelling was done in 1% Bovine Serum Albumin and 0,8% gelatine from cold water fish skin in PBS with polyclonal rabbit anti-A_{2A}R primary antibody (pab70273, 1:50, Covalab) and 15nm gold coupled Protein A (CMC Utrecht, 1:50). After immuno-labelling, the sections were stained and mounted

in a mixture of 3% (aq.) uranyl acetate and 2% methylcellulose. Images were taken using a Hitachi H-7650 electron microscope at 100 kV acceleration. We counted the immunogold particles in 40 micrographs (total of 72 synapses) of the CA1 area of Tg(CaMKII-hA_{2A}R) animals (according to (Elsaesser et al., 2011)) and evaluated blindly by two pathologists. We found an average of 2.4 particles/synapse. The gold labeling in synapses elements was categorized into pre or post (<30 nm within the active zone) and perisynaptic (<30 nm outside the active zone). No particles were found in the nucleus.

16. Fractionation

Subcellular fractionation was performed as described previously (Burnouf et al., 2013). Briefly, WT and Tg(CaMKII-hA_{2A}R) frozen hippocampi were homogenized with Potter in a buffer containing sucrose 0.32M and HEPES 10mM. After centrifugation (1000g for 10min), the pellet was dissolved in a buffer containing HEPES 4mM and EDTA 1mM. After centrifugation (12000g for 20min), the pellet was dissolved in a buffer containing HEPES 20mM, NaCl 100mM, triton X-100 0.5%. After centrifugation (12000g for 20min), the supernatant is the non-postsynaptic density membrane fraction (non-PSD95 enriched fraction), as confirmed by the detection of enriched SNAP25 and the absence of PSD95. The pellet was dissolved in a buffer containing HEPES 20mM, NaCl 0.15mM, triton X-100 1%, deoxycholic acid 1%, SDS 1% and centrifuged for 15min at 10000g.

The supernatant is the postsynaptic density membrane fraction (PSD95-enriched fractions), as demonstrated by the detection of enriched PSD95 and sparse SNAP25. Equal volumes of non-PSD95 and PSD-95-enriched fractions were diluted in sample buffer (see Western Blotting section) and denatured by heating to 65ºC for 20 min and used for western blot analysis.

17. Western blotting

Tissue was homogenized by sonication using RIPA buffer (50 mM Tris, 1 mM EDTA, 150 mM NaCl, 0.1% SDS, 1% Tergitol-type NP-40, pH 8.0). The protein concentration was determined using a BioRad DC Protein assay Kit [based on (Lowry et al., 1951)]. The appropriate volume of each sample was diluted in water and sample buffer (70 mM Tris pH 6.8, 6% glycerol, 2% SDS, 120 mM dithiothreitol and 0.0024% Bromophenol blue). The samples were denatured at 65°C for 20 min. Based on the protocol of Towbin *et al.* (Towbin et al., 1979), samples and molecular weight markers were separated by SDS-PAGE (10% for resolving and a 5% for stacking gels) in denaturing conditions and electro-transferred to PVDF membranes (GE Healthcare, UK). Membranes were blocked with 3% bovine serum albumin (BSA) in TBS-T 0.1% (Tris Buffer Saline with 0.1% Tween-20 solution, 200 nM Tris, 1.5 M NaCl) for 1 hour and incubated with primary antibody (diluted in TBS-T, 3% BSA and 0.1% NaN_3) overnight at 4°C. Primary antibodies were mouse anti-$A_{2A}R$ (1:2000, 05-717, Upstate/Millipore, Germany), rabbit anti-SNAP25 (1:10000,

S9684, Sigma), rabbit anti-pan-cadherin (1:20000, ab6529, Abcam), rabbit anti-PSD-95 (1:1000, D27E11 Cell Signaling Technology) and mouse anti-α-tubulin (1:1000, sc-8035, Santa Cruz Biotechnology, USA). After 3 washing periods of 10 min with TBS-T, membranes were incubated with horseradish peroxidase (HRP) - conjugated anti-mouse or anti-rabbit secondary antibodies (1:10 000; Santa Cruz Biotechnology) (in 5% nonfat dry milk) for 1 h at RT. After 30 minutes of washing with TBS-T, chemiluminescent detection was performed with ECL western blotting detection reagent (GE Healthcare) using X-Ray films (Fujifilm, Japan). Optical density was determined with Image-J software and normalized to the respective pan-cadherin or tubulin band density.

18. Drugs

The $A_{2A}R$ selective antagonist, 2-(2-furanyl)-7-(2-phenylethyl)-7H-pyrazolo[4,3-e][1,2,4]triazolo[1,5-c]¬pyrimi¬din-5-amine (SCH 58261) and $A_{2A}R$ selective agonist 2-[*p*-(2-Carboxyethyl)-phenylethylamino]-5'-*N*-ethylcarboxamidoadenosine (CGS 21680) were purchased from Tocris (UK). GABA receptor antagonist picrotoxin, AMPA receptor antagonist 6,7-dinitroquinoxaline-2,3-dione (DNQX) and NMDA receptor antagonist (2*R*)-amino-5-phosphonovaleric acid (AP5) were purchased from Sigma-Aldrich. mGluR5 antagonist 6-methyl-2-(phenylethylnyl)-pyridine hydrochloride (MPEP) was purchased from Enzo Life Sciences (USA). These drugs were diluted in the assay solution from 5 mM or 1 mM

stock aliquots made in DMSO or water stored at -20ºC. All other reagents used were of the highest purity available either from Merck or Sigma Aldrich.

19. Statistics

All statistical analyses were performed with GraphPad Prism software. Values are presented as mean ± s.e.m. in figure legends. Statistical analyses were designed using the assumption of normal distribution and similar variance among groups, as previously tested. Statistical comparisons included two-sided unpaired *t* test, one or two-way ANOVA followed by a Bonferroni's multiple comparison post hoc tests as specified in the figure legends. P-values of < 0.05 were considered to be statistically significant. The sample size was determined based on Power Analysis or similar experiments carried-out in the past. Power Analysis was performed using G-power in order to estimate the number of animals required, for a signal-to-noise ratio of 1.4 and 80% to 90% power assuming a 5% significance level.

CHAPTER III

Results

Author contributions

Mariana Temido-Ferreira designed and performed all the experimental work, except the immunohistochemical assays, performed by Inês Marques-Morgado. The in-frame Venus-$A_{2A}R$ construct was made by Mariana Temido-Ferreira starting from a Venus plasmid (provided by Tiago Outeiro) and a $A_{2A}R$ plasmid (provided by David Blum). The patch-clamp experiments were performed by Mariana Temido-Ferreira at the Institut de Pharmacologie Moléculaire et Cellulaire (IPMC), Centre National de la Recherche Scientifique (CNRS), Université de Nice Sophia Antipolis, Valbonne, France, in a PhD exchange period with assistance and collaboration of Paula Pousinha and Hélène Marie.

Michael Bader (Max-Delbrück-Center for Molecular Medicine (MDC), Berlin, Germany; Charité-University Medicine, Berlin, Germany and Institute of Biology, University of Lübeck, Lübeck, Germany) generated the Tg(CaMKII-h$A_{2A}R$) animals.
Pedro Pereira and José Pimentel (Laboratory of Neuropathology, Department of Neurosciences, Hospital de Santa Maria, CHLN, EPE, Lisbon, Portugal) and David Blum (Université de Lille, Institut National de la Santé et de la Recherche Medicale (INSERM), CHU Lille, UMR-S 1172 JPArc, "Alzheimer & Tauopathie", LabEx DISTALZ Lille, France) provided the human samples and assisted with the histology procedures. The *in situ* hybridization control presented for the Tg(CaMKII-h$A_{2A}R$) was provided by Serge N. Schiffmann (Laboratory of Neurophysiology, ULB Neuroscience Institute, Université Libre de Bruxelles (ULB), Brussels, Belgium).

1. Increased levels of $A_{2A}R$ in human aged and Alzheimer's disease brain

There is a genetic association of the adenosine $A_{2A}R$ receptor encoding gene (*ADORA2A*) with hippocampal volume in mild cognitive impairment and Alzheimer's disease (Horgusluoglu-Moloch et al., 2017). Plus, $A_{2A}R$ upregulation in cortex and hippocampus is associated with memory dysfunction in different animal models (Batalha et al., 2013; Espinosa et al., 2013). We now probed this increase in human brain of aged and AD subjects. $A_{2A}R$ expression was measured in young (20-40 years old), aged (60-75 years old) and AD (60-75 years old, Braak stages 5-6) forebrain. There was a significant increase in $A_{2A}R$ protein levels in the aged forebrain that was further enhanced in samples from AD patients (Figure 3.1A, B). The mRNA quantification by qPCR indicates a 4.9±0.3 (n=3) fold increase in $A_{2A}R$ transcripts in AD samples compared to aged samples (Figure 3.1C). To assess the cellular origin of this $A_{2A}R$ upregulation, we performed a histological analysis of the hippocampi from AD patients and age-matched controls. We detected a DAB-specific staining for $A_{2A}R$ in aging and AD sections (Figure 3.1D, E), absent in the negative control (Figure 3.1D, E). In both conditions, we observed a neuron-specific $A_{2A}R$ positive staining (brown arrows; characterized by a large hypochromatic nucleus with nucleolar inclusions). We did not detect any significant $A_{2A}R$ signal in astrocytes (black arrows; nuclei typically have pale, finely granular chromatin patterns and relatively small or indistinct nucleoli), oligodendrocytes (blue arrows; small, round, relatively dark nuclei) or microglia (green arrows; rod-

shaped and often irregularly contoured nuclei) (Garman, 2011) (Figure 3.1E).

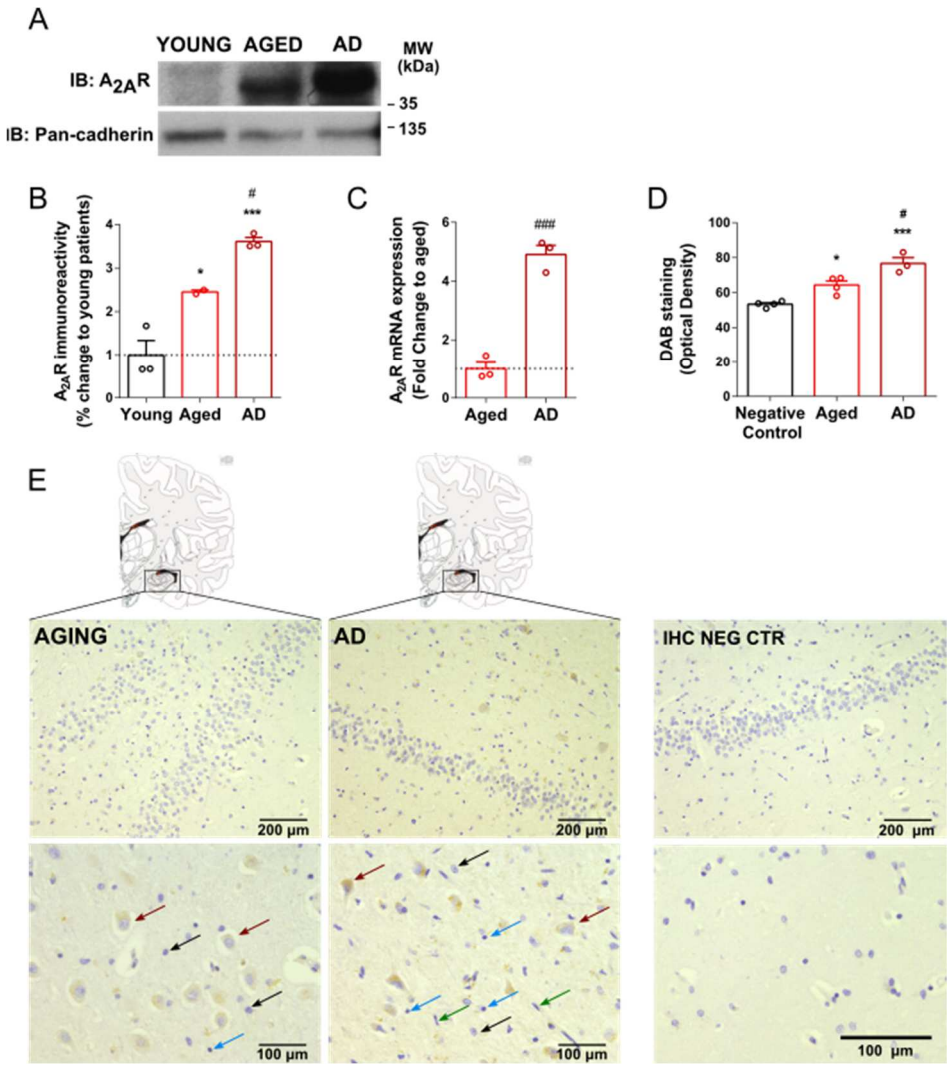

Figure 3.1. Increased levels of $A_{2A}R$ in human aged and AD brain.

(A) Representative image of the western blot for $A_{2A}R$ in human prefrontal cortex and the internal control Pan-cadherin. **(B)** $A_{2A}R$ immunoreactivity in young, aged and AD human cortex. (*$p < 0.05$, ***$p < 0.001$ comparing to young subjects, #$p < 0.05$ comparing to aged subjects, one-way ANOVA followed by a Tukey's multiple

comparisons post hoc test) (n = 2-3). **(C)** Increase in $A_{2A}R$ mRNA in AD human brain when compared with age-matched control subjects ($^{###}p < 0.001$ comparing to healthy age-matched subjects, unpaired t test) (n = 3). **(D)** DAB immunostaining quantification in negative control, aged and AD samples. A specific staining for $A_{2A}R$ is observed in aged and AD conditions ($^{*}p < 0.05$, $^{***}p < 0.001$ comparing to negative control, $^{\#}p < 0.05$ comparing to aged, one-way ANOVA followed by a Bonferroni's multiple comparisons *post hoc* test) (n = 3-4). $A_{2A}R$ labelling in AD is stronger than the labelling observed in the aged condition ($^{\#}p < 0.05$ comparing to aged, one-way ANOVA followed by a Bonferroni's multiple comparisons *post hoc* test) (n = 3-4). **(E)** In human AD and age-matched control hippocampal sections, positive staining for $A_{2A}R$ is present (scale bar: 200 µm). Within hippocampus, $A_{2A}R$ upsurge is neuronal specific, since positive labelling is observed in neurons (brown arrows; cells with large hypochromatic nucleus with nucleolar inclusions), while in astrocytes (black arrows; astrocytic nuclei typically have pale, finely granular chromatin patterns and relatively small or indistinct nucleoli), oligodendrocytes (blue arrows; characterized by small, round, relatively dark nuclei) and microglia (green arrows; cells with rod-shaped and often irregularly contoured nuclei) $A_{2A}R$ is not detected (scale bar: 100 µm). Such staining is specific for $A_{2A}R$, since in the negative control of the immunohistochemistry (no primary antibody anti-$A_{2A}R$ was used) no labelling was found (representative picture of n = 3 for each condition). All values are mean ± SEM.

2. Physiopathological levels of $A_{2A}R$ in neurons impair hippocampus-dependent spatial memory

Given that $A_{2A}R$ upregulation is associated with decreased cognitive performance characteristic of aging and AD, we studied a rat transgenic model with $A_{2A}R$ overexpression to address the underlying mechanism. These transgenic rats selectively overexpress the human

$A_{2A}R$ in neurons under the control of the CaMKIIα promoter [Tg(CaMKII-h$A_{2A}R$); Figure 3.2A], mainly in the cortex and hippocampus, in an aging-like pattern of expression (Batalha et al., 2016; Lopes et al., 1999a). The hippocampus displays a significant overexpression of $A_{2A}R$, particularly the DG and CA1, as reported by the *in situ* $A_{2A}R$ mRNA human probe (Figure 3.2A) and immunostaining (Figure 3.2B) and negligible expression in other brain areas (see also (Batalha et al., 2016)). Importantly, at 12-16 weeks of age, Tg(CaMKII-h$A_{2A}R$) animals present a 5–8 fold increase of hippocampal $A_{2A}R$ immunoreactivity (Batalha et al., 2016), which is of the same magnitude as the increase found in our human aged and AD samples (Figure 3.1B), and equivalent to that of aged rats (Diógenes et al., 2007a). To further evaluate the profile of $A_{2A}R$ expression, co-staining for $A_{2A}R$, GFAP and MAP2 was performed in hippocampal slices, confirming the upsurge in the neuropil and discarding the possibility of astrocytic $A_{2A}R$ expression in this model (Figure 3.2B). Biochemical fractionation of hippocampal tissue revealed a clear enrichment of $A_{2A}R$ in the SNAP25 positive fraction, in contrast to the low levels in the PSD95-enriched fraction, favoring a mainly presynaptic localization (Figure 3.2C), as occurs for native $A_{2A}R$ in the rodent hippocampus (Costenla et al., 2011; Rebola et al., 2005a).

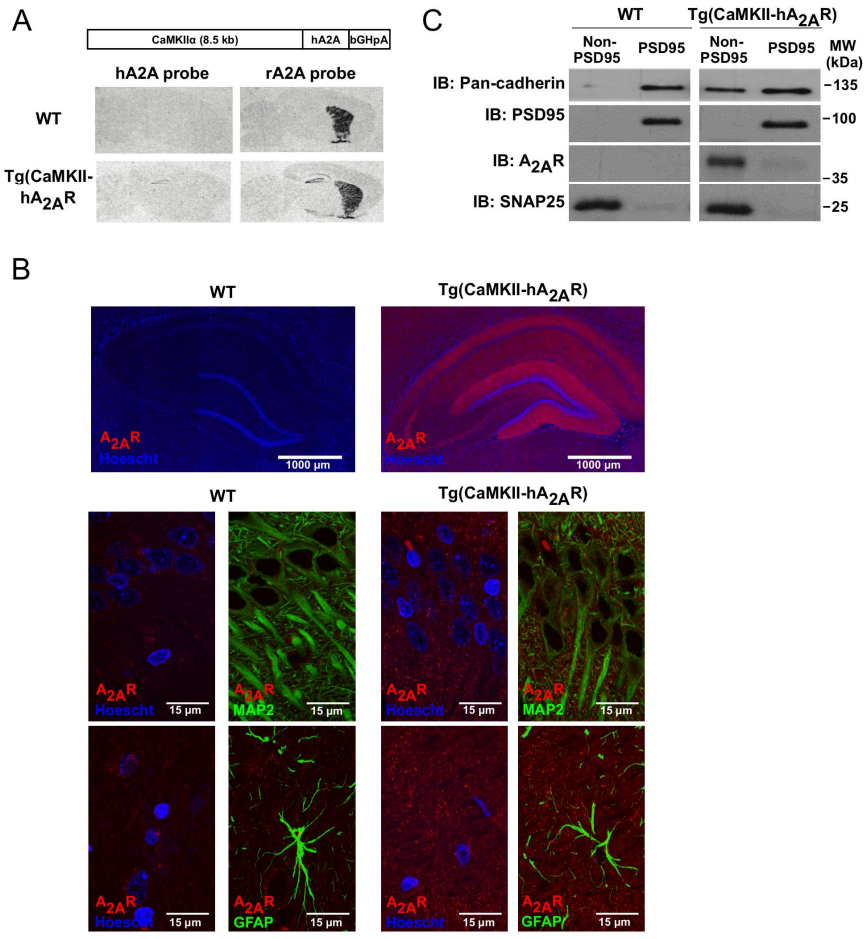

Figure 3.2. Tg(CaMKII-hA_{2A}R) animals display a neuronal-selective A_{2A}R overexpression, mainly presynaptically.

(**A**) Construct used to generate Tg(CaMKII-hA_{2A}R) rats; Tg(CaMKII-hA_{2A}R) animals present an overexpression of total A_{2A}R in the hippocampus evaluated by *in situ* hybridization (both with the hA_{2A}R probe and through cross-hybridization of the rat A_{2A}R probe to the human A_{2A}R mRNA). (**C**) Compositional images of fluorescence immunohistochemistry of hippocampus of WT and Tg(CaMKII-hA_{2A}R) animals (scale bar: 1000µm). Nuclei are labelled in blue (with Hoechst) and A_{2A}R in red. A_{2A}R staining is present in hippocampal areas of Tg(CaMKII-hA_{2A}R) animals but not in WT littermates. Within the hippocampus, positive labelling can be

observed in CA3 axonal projections and strong staining is also observed in the neuropil of DG and CA1 areas. At the middle panel, z-stack maximum intensity projection images taken at 63x magnification in CA1 area of hippocampus are presented (scale bar: 15 μm). MAP2 positive cells are identified by green fluorescence. $A_{2A}R$ staining can be observed in the neuropil of CA1 area in Tg(CaMKII-h$A_{2A}R$) hippocampal slices. At the bottom panel, a z-stack maximum intensity projection image taken at 63x magnification in CA1 area of hippocampus is presented (scale bar: 15μm). GFAP positive cells are identified by green fluorescence. No co-localization is found between $A_{2A}R$ and GFAP staining. (**C**) Immunoblotting analysis after subcellular localization of hippocampal tissue from WT and Tg(CaMKII-h$A_{2A}R$) animals.

This was further confirmed by immunohistochemical analysis, in which the $A_{2A}R$ signal overlaps with that of SNAP25, and not with PSD95 signal (Figure 3.3 and 3.4A). This is not due to lack of resolution since our system was able to resolve a control section labelled for both a pre- and a postsynaptic protein (Figure 3.4B).

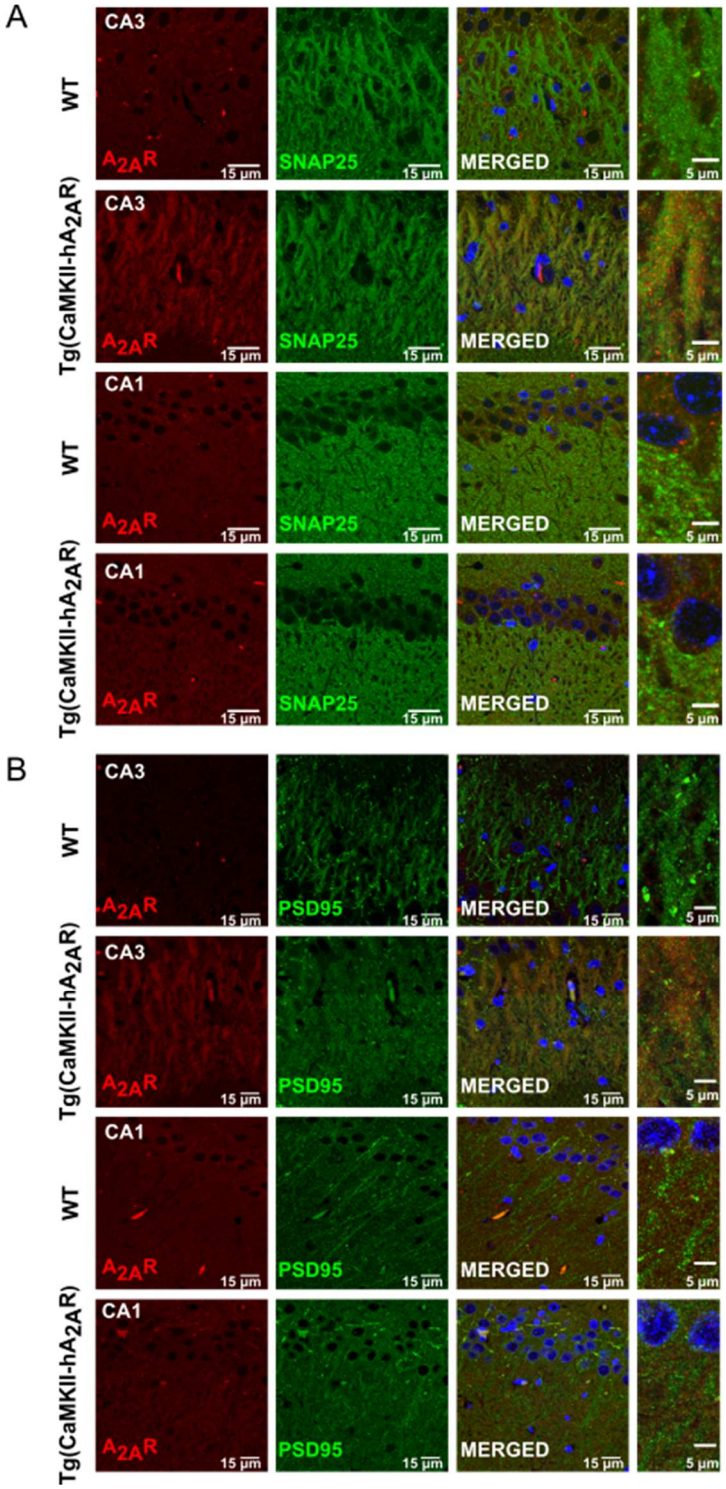
A
CA3
WT
A2AR
SNAP25
MERGED
15 µm
5 µm
Tg(CaMKII-hA2AR)
CA1
B
PSD95

Figure 3.3. Immunohistochemical analysis of $A_{2A}R$, SNAP25 and PSD95 in WT and Tg(CaMKII-h$A_{2A}R$) hippocampal slices.

(**A**) Z-stack maximum intensity projection images taken at 63x magnification in CA1 and CA3 areas of hippocampus are presented (scale bars: 15 μm and 5 μm). Nuclei are stained with Hoechst (blue), $A_{2A}R$ are labeled with red and SNAP25 positive cells are stained in green. (**B**) Z-stack maximum intensity projection images taken at 63x magnification in CA1 and CA3 areas of hippocampus are presented (scale bars: 15 μm and 5 μm). Nuclei are stained with Hoechst (blue), $A_{2A}R$ are labeled with red and PSD95 positive cells are stained in green.

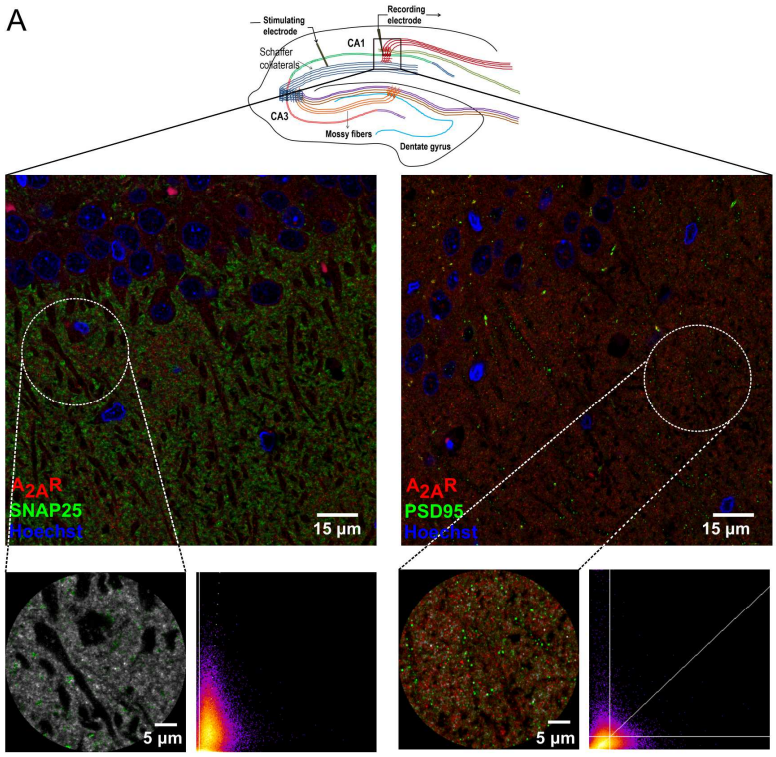

	tM $A_{2A}R$	tM SNAP25/ PSD95	Ncoloc	%$A_{2A}R$ Vol	%SNAP25/ PSD95 Vol	%$A_{2A}R$ Int	%SNAP25/ PSD95 Int	%$A_{2A}R$ int > thres	%SNAP25/ PSD95 int > thres
$A_{2A}R$ + SNAP25	1 ± 0	0,98 ± 0,01	66135 ± 428	98,29% ± 0,13	93,56% ± 0,61	99,42% ± 0,15	96,63% ± 0,46	99,71% ± 0,06	96,63% ± 0,46
$A_{2A}R$ + PSD95	0,22 ± 0,04	0,36 ± 0,03	4165 ± 437	20,32% ± 3,59	32,04% ± 2,51	10,38% ± 1,32	15,85% ± 0,84	21,28% ± 3,73	33,37% ± 2,09
p	< 0,0001	< 0,0001	< 0,0001	< 0,0001	< 0,0001	< 0,0001	< 0,0001	< 0,0001	< 0,0001

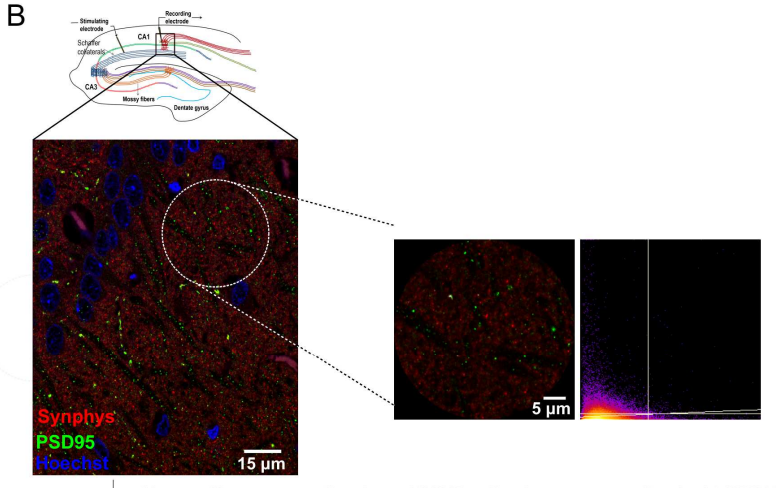

	tM synphys	tM PSD95	Ncoloc	%synphys Vol	%PSD95 Vol	%synphys Int	%PSD95 Int	%synphys int > thres	%PSD95 int > thres
Synphys + PSD95	0,25 ± 0,02	0,16 ± 0,06	1942 ± 894	23,84% ± 2,13	12,34% ± 5,12	6,27% ± 2,60	11,97% ± 4,78	24,19% ± 2,24	16,33% ± 6,19

Figure 3.4. In Tg(CaMKII-hA_{2A}R) animals, A_{2A}R is mainly expresses presynaptically.

(**A**) On top, images taken at 63x magnification in CA1 area of hippocampus are presented (scale bar: 15 μm). Nuclei are stained with Hoechst (blue), A_{2A}R are labeled with red and SNAP25 positive cells (left) or PSD95 positive cells (right) are stained in green. At center left, amplification of the upper image, where colocalized pixels are stained in white (scale bar: 5 μm). At center right, scatter plot (channel 1 (red; A_{2A}R) along the x-axis; channel 2 (green; SNAP25/PSD95) along the y-axis) with both the linear regression as well as the thresholds marked. We observe a stronger white labelling for A_{2A}R/SNAP25 than for A_{2A}R/PSD95, suggesting that A_{2A}R is mainly expressed presynaptically. On bottom, table with colocalization parameters measured in A_{2A}R/SNAP25 and in A_{2A}R/PSD9; *tM1* - channel 1: red, A_{2A}R; *tM2* - channel 2; green, SNAP25/PSD95 (Mander's adjusted to thresholds for each channel); *Ncoloc* (Number of colocalized voxels, number of voxels which have both channel 1 and channel 2 intensities above threshold); *%Ch1 Vol*, *%Ch2 Vol* (Percentage of voxels colocalized, number of voxels for each channel which have both channel 1 and channel 2 intensities above threshold, expressed as percentage of the total number of voxels for each channel above their respective thresholds); *%Ch1 Int*, *%Ch2 Int* (Percentage of intensity colocalized for each channel, this value is equal to the sum of the pixel intensities, with intensities above both channel 1 and channel 2 thresholds expressed as a percentage of the sum of all channel 1 intensities); *%Ch1 Int > thres*, *%Ch2 Int > thres* (percentage of intensities above threshold colocalized, for each channel, this value is equal to the sum of the pixel intensities with intensities above both channel 1 and channel 2 thresholds expressed as a percentage of the sum of all channel 1 intensities above the threshold for channel 1). We observe that for SNAP25-A_{2A}R, Mander's adjusted to threshold for both channels are close to 1, indicating colocalization, while this value is significantly lower for PSD95-A_{2A}R (A_{2A}R: 0.22 ± 0.04, PSD95: 0.36 ± 0.03). All the other colocalization parameters further confirm colocalization between A_{2A}R and SNAP25 and lack of colocalization between A_{2A}R and PSD95. (**B**) On top, image taken at 63x magnification in CA1 area of hippocampus is presented (scale bar: 15 μm). Nuclei are stained with Hoechst (blue), synaptophysin (synphys) is labeled with red and PSD95 positive cells are stained in green. At center left, amplification of the upper

image, where colocalized pixels are stained in white (scale bar: 5 μm). At center right, scatter plot with both the linear regression as well as the thresholds marked. On bottom, table with colocalization parameters measured. We observe a lack of co-localization between synaptophysin and PSD95 signals. All values are mean ± SEM.

Accordingly, immunoelectron micrographs of the CA1 area of Tg(CaMKII-hA_{2A}R) reveal a preferential presynaptic localization of A_{2A}R (Figure 3.5).

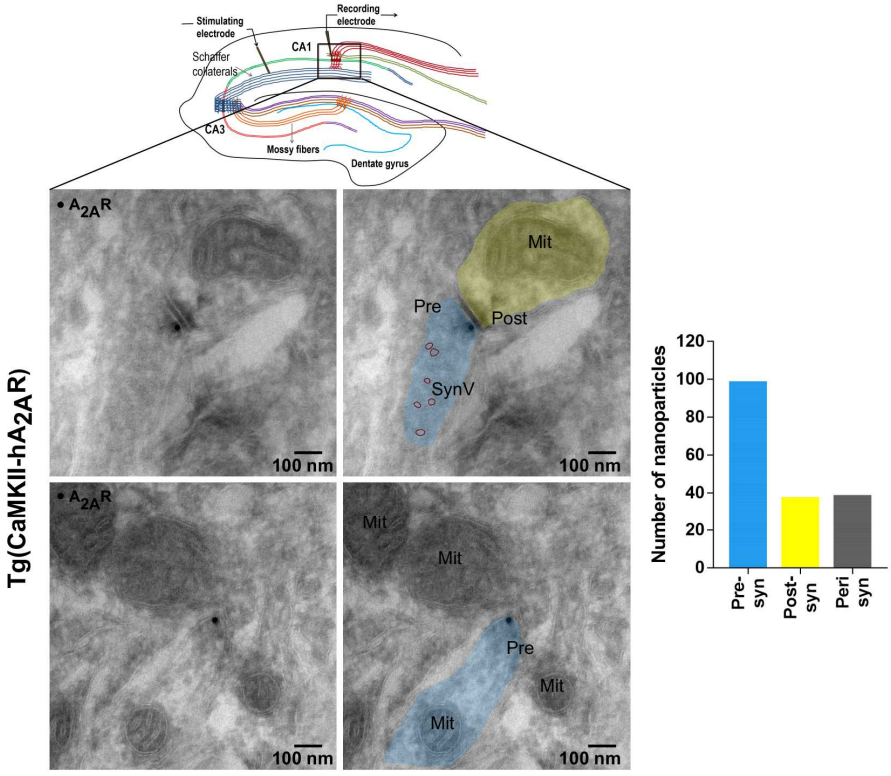

Figure 3.5. Immunoelectron micrographs of the CA1 area of Tg(CaMKII-hA_{2A}R) animals reveal a preferential synaptic localization of A_{2A}R.

Electron micrographs of the area where recordings were conducted in the hippocampus of Tg(CaMKII-hA_{2A}R) animals showing immunogold particles for A_{2A}R in the presynaptic neuron. On top, intracellular distribution of nanoparticles

reveal a preferential localization of $A_{2A}R$. On the right, duplicates of the images with the identification of the subcellular structures. Pre, presynaptic neuron; Post, postsynaptic neuron; Mit, mitochondria; SynV, synaptic vesicle. All values are mean ± SEM.

We then evaluated hippocampus-dependent spatial memory using the Morris water maze (MWM) test. Transgenic animals displayed a decrease in acquisition (Figure 3.6A) and a lack of preference for the target quadrant during the probe test (Figure 3.6B). We did not find differences in swimming speed between groups (Figure 3.6C).

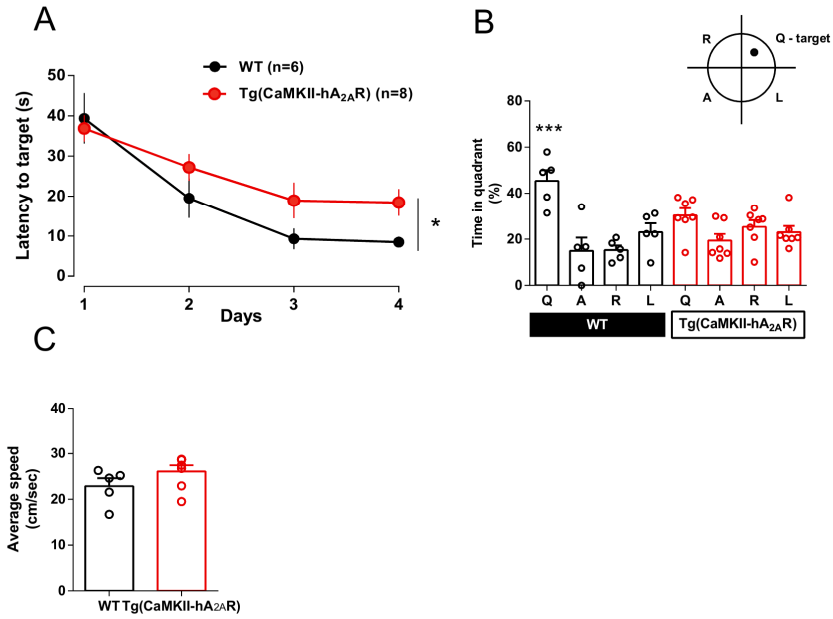

Figure 3.6. Tg(CaMKII-hA$_{2A}$R) animals exhibit memory impairments in the Morris water maze test.

(**A**, **B**) Hippocampal-dependent memory performance was assessed by the MWM test, in which acquisition (**A**) (*p < 0.05, two-way ANOVA) (n = 6-8) and retention (**B**) (***p < 0.001, one-way ANOVA followed by a Bonferroni's multiple

comparisons *post hoc* test within groups) (n = 6-8) were evaluated. (**C**) No changes in swimming speed during probe test between WT and Tg(CaMKII-hA_{2A}R) animals (n = 6-8). All values are mean ± SEM.

3. Increased levels of A_{2A}R enhance glutamate release probability

To further dissect the mechanism by which A_{2A}R impair memory performance, whole-cell patch-clamp recordings were performed. We first measured the intrinsic excitability of CA1 neurons from Tg(CaMKII-hA_{2A}R) and WT rats. No changes were observed in passive properties (resting membrane potential or membrane resistance), nor in single spike analysis of the studied populations of neurons (Figure 3.7A, B). Moreover, neurons from WT and Tg(CaMKII-hA_{2A}R) animals exhibited similar behavior when submitted to steps of current injection (Figure 3.7C-H). Thus, A_{2A}R overexpression does not impact on the passive or intrinsic excitability properties of CA1 neurons.

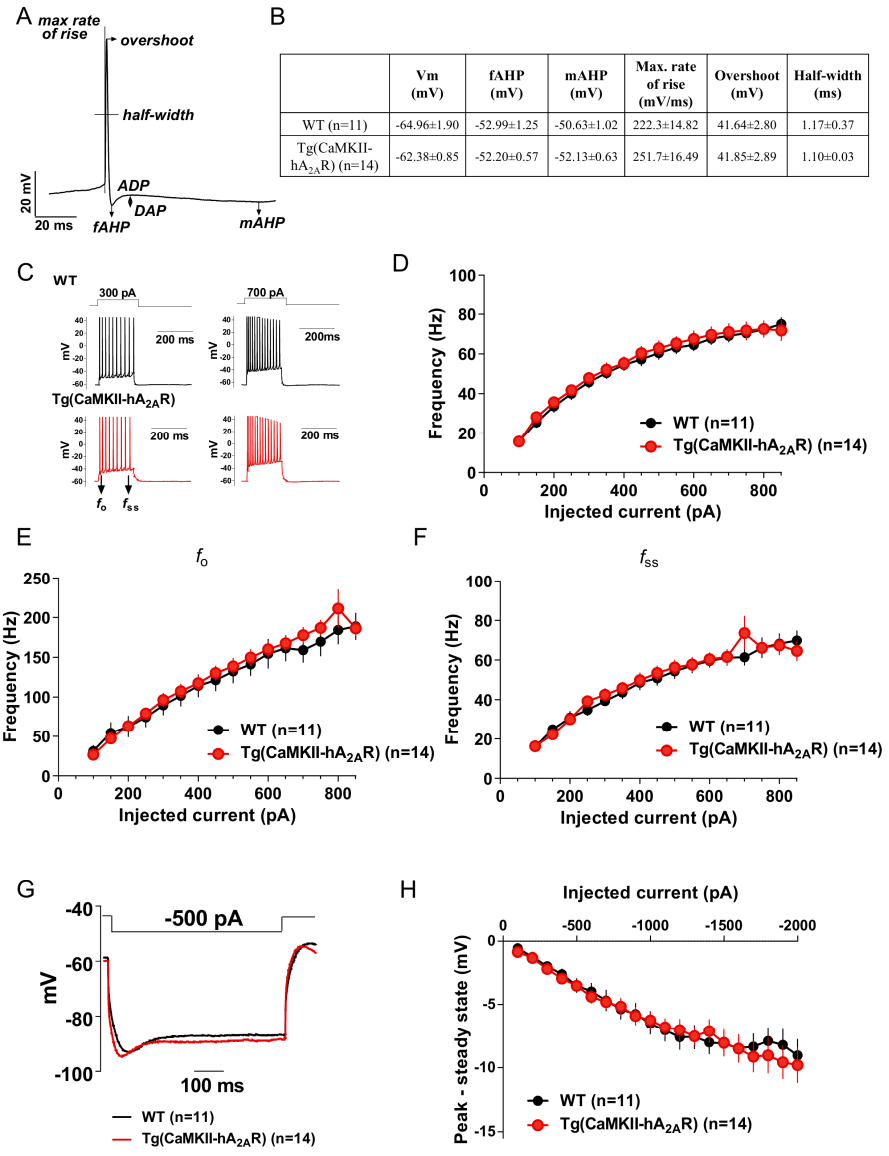

	Vm (mV)	fAHP (mV)	mAHP (mV)	Max. rate of rise (mV/ms)	Overshoot (mV)	Half-width (ms)
WT (n=11)	-64.96±1.90	-52.99±1.25	-50.63±1.02	222.3±14.82	41.64±2.80	1.17±0.37
Tg(CaMKII-hA$_{2A}$R) (n=14)	-62.38±0.85	-52.20±0.57	-52.13±0.63	251.7±16.49	41.85±2.89	1.10±0.03

Figure 3.7. Increased levels of A$_{2A}$R do not alter neuronal intrinsic excitability. **(A)** Action potentials parameters evaluated as summarized in (B). **(B)** Summary of action potential (AP) parameters measured during tonic firing in CA1 neurons from WT and Tg(CaMKII-hA$_{2A}$R) animals. No differences can be observed in these parameters (n = 11-14). **(C)** Representative traces of AP trains in response to 300 and

700 pA current steps recorded from neurons from WT (top) and Tg(CaMKII-hA_{2A}R) (bottom) animals. **(D)** Mean firing frequency *versus* injected current for WT and Tg(CaMKII-hA_{2A}R). No differences were observed between groups (n = 11-14). **(E)** The instantaneous firing frequency (f_o) measured between the first and second APs of the spike train plotted *versus* the injected current is similar in WT e Tg(CaMKII-hA_{2A}R) conditions (n = 11-14). **(F)** The instantaneous firing frequency (fss) measured between the last two APs of the spike train recorded in neurons from in WT and Tg(CaMKII-hA_{2A}R) is not different (n = 11-14). **(G)** Representative trace of the time-dependent inward rectification potential measured in WT and Tg(CaMKII-hA_{2A}R) during a 500 pA hyperpolarization current injection lasting 600 ms. **(H)** The difference between the peak and the steady-state values plotted *versus* the negative current amplitude (from -100 to -2000 pA) suggests that the hyperpolarization pattern is not changed in Tg(CaMKII-hA_{2A}R) (n = 11-14). All values are mean ± SEM.

We then performed afferent-evoked EPSCs from CA1 pyramidal neurons (V_h=-70 mV), in the presence of $GABA_A$ receptor antagonist picrotoxin (50 μM). A_{2A}R blockade significantly inhibited excitatory postsynaptic currents (EPSCs), an effect that was not observed in WT animals (Figure 3.8A, B). Thus, there is a gain of function of A_{2A}R upon their overexpression, whereby A_{2A}R tonically control basal synaptic transmission in Tg(CaMKII-hA_{2A}R) animals, which does not occur in WT animals.

To test if tonic A_{2A}R modulation of neuronal function occurs at a presynaptic level, we evaluated the glutamate release probability. A facilitation of the paired-pulse ratio (PPR) was observed in neurons from WT animals at all inter-stimulation intervals, more evident for the shorter intervals (Figure 3.8C). The magnitude of facilitation was reduced in Tg(CaMKII-hA_{2A}R) rats when compared to WT neurons (Figure 3.8C), albeit maintaining the same facilitatory profile. These

data suggest that neuronal $A_{2A}R$ overexpression increases glutamate release probability (Cunha et al., 1994b; Rombo et al., 2015). These PPR alterations in Tg(CaMKII-h$A_{2A}R$) rats were completely rescued by the $A_{2A}R$ selective antagonist, SCH 58261 (Figure 3.8C). As expected, $A_{2A}R$ blockade does not alter PPR values in WT animals (Figure 3.8C).

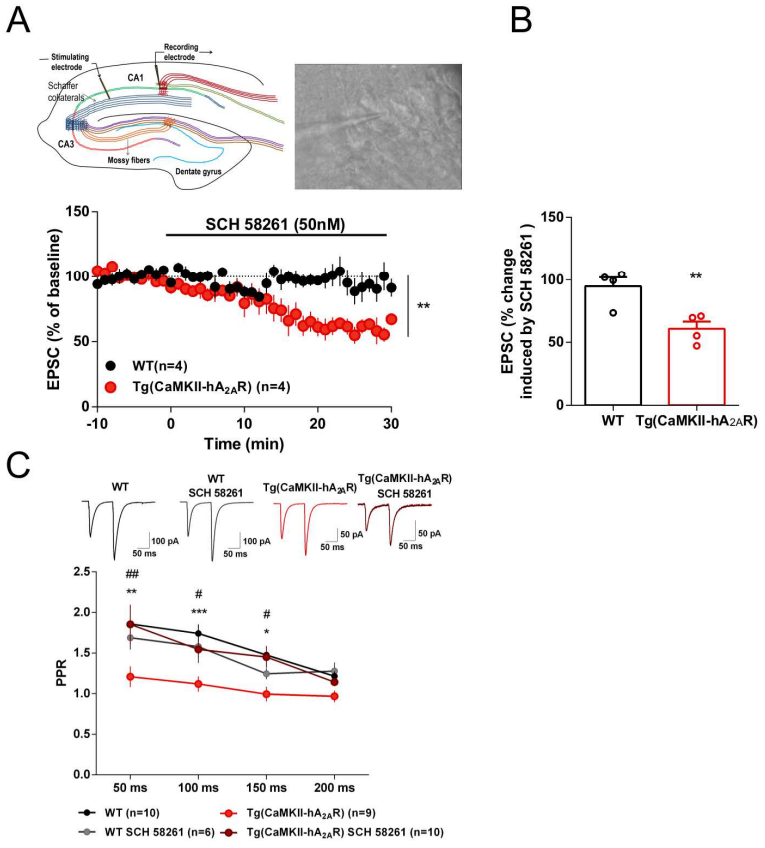

Figure 3.8. $A_{2A}R$ control basal synaptic transmission and enhance glutamate release probability in Tg(CaMKII-h$A_{2A}R$) animals.

(**A**) Top left: schematic representation of the simplified circuitry of the hippocampus. A stimulation electrode is placed in the Schaffer collaterals and a recording electrode

patches a pyramidal cell of the CA1 area. Top right: CA1 pyramidal layer with a recording electrode patching one cell; Graph: Average time course of Excitatory Postsynaptic currents after perfusion with SCH 58261 (50 nM) for 30 min, in neurons from WT and Tg(CaMKII-hA_{2A}R) animals (**p < 0.01, unpaired t test) (n = 4). Black traces represent baseline, while grey traces correspond to the EPSCs 20-30 minutes after SCH 58261 application (**B**) Averaged EPSCs (change in EPSCs from the last 10 min of SCH 58261 application) from acute SCH 58261 perfusion experiments (**p < 0.01, unpaired t test) (n = 4). (**C**) PPR values in neurons from WT and Tg(CaMKII-hA_{2A}R) animals, treated and non-treated with SCH 58261 (50 nM). For the interspike intervals between 50 and 150 ms, a decrease in PPR in Tg(CaMKII-hA_{2A}R) is observed, in comparison with the values obtained from WT neurons (*p < 0.05, two-way ANOVA followed by a Bonferroni's multiple comparisons *post hoc* test) (n = 9-10). This decrease is lost when the interspike interval is 200 ms. When neurons from Tg(CaMKII-hA_{2A}R) animals are acutely treated with SCH 58261 (50 nM), the PPR values are completely reverted back to the WT levels ($^{\#}$p < 0.05 comparing to Tg(CaMKII-hA_{2A}R), two-way ANOVA followed by a Bonferroni's multiple comparisons *post hoc* test) (n = 10-12); representative traces of EPSCs with an inter-spike interval of 100 ms, for WT and Tg(CaMKII-hA_{2A}R) animals, with and without SCH 58261 perfusion. All values are mean ± SEM.

4. A_{2A}R increase NMDAR-mediated currents in CA1 pyramidal neurons

A_{2A}R were proposed to mainly modulate NMDA receptors (NMDAR) (Ferreira et al., 2017a; Rebola et al., 2008; Sarantis et al., 2015), which are minor contributors to excitatory synaptic transmission under basal conditions in the hippocampus (Collingridge et al., 1983). We tested possible alterations of the AMPA and NMDA receptor contribution, by

quantifying the AMPAR/NMDAR ratio. The AMPA/NMDA receptor ratio was decreased in Tg(CaMKII-hA_{2A}R) *versus* WT animals (Figure 3.9A). To assess if this could be attributed to changes in the gating properties of the receptors, we performed current-voltage (I-V) relationships in pharmacologically isolated AMPAR and NMDAR responses. While the I-V relationships of the NMDAR were significantly increased in neurons from Tg(CaMKII-hA_{2A}R) animals (Figure 3.9B), the AMPAR voltage-dependency was unaltered in Tg(CaMKII-hA_{2A}R) neurons (Figure 3.9C). Moreover, we calculated the ratio between NMDAR current recorded at +40 mV and at -60 mV, and observed it was significantly increased in Tg(CaMKII-hA_{2A}R) neurons.

In the hippocampus, NMDARs are heteromeric assemblies mainly composed of a constitutive GluN1 subunit and GluN2A or GluN2B subunits (Rosenmund et al., 1998). The deactivation time course of GluN1/GluN2B heteromers is higher than the one observed for GluN1/GluN2A heteromers (Paoletti et al., 2013). To test if NMDAR overactivation was due to alterations in NMDAR subunit composition, we analyzed the deactivation kinetics of pharmacologically isolated NMDAR EPSCs. Time constants for fast, slow and weighted components (τ_{fast}, τ_{slow} and $\tau_{weighted}$) were obtained by fitting the pharmacologically isolated NMDAR EPSCs (V_h=+40 mV) to a double exponential function (Levenberg-Marquandt method). No differences were found between groups for all parameters evaluated (Figure 3.9E), suggesting that the enhancement of NMDAR conductance observed in Tg(CaMKII-hA_{2A}R) neurons is not related to alterations in NMDAR subunit composition.

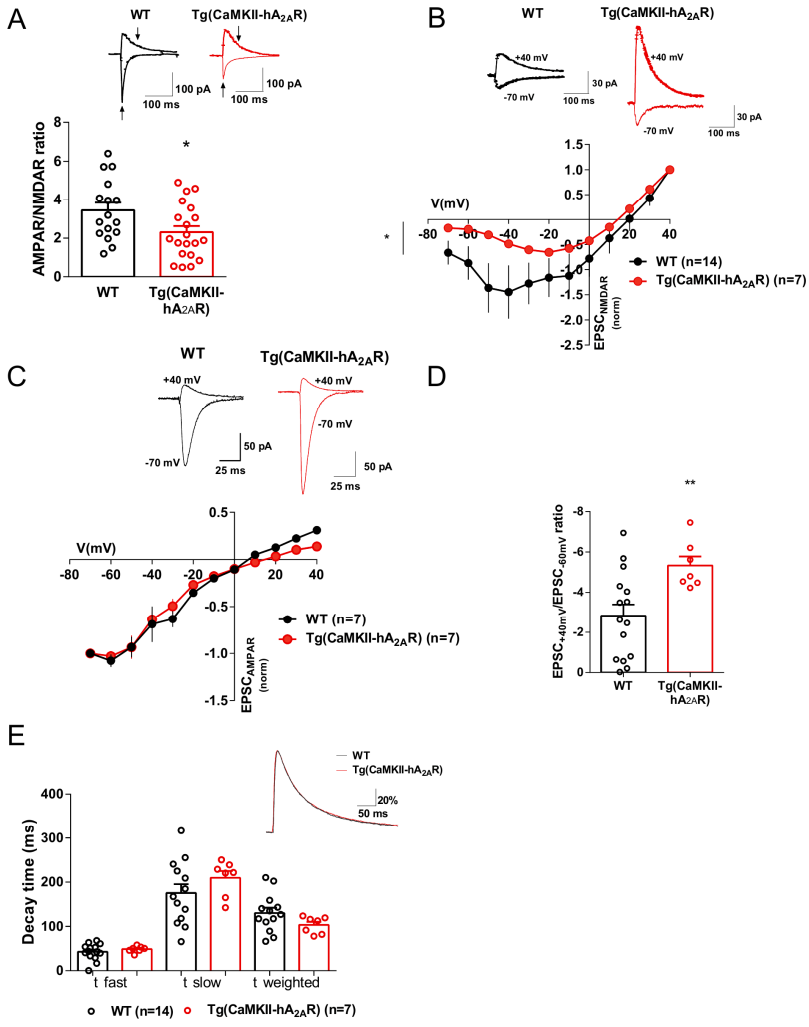

Figure 3.9. Physiopathological levels of $A_{2A}R$ increase NMDAR-mediated currents in CA1 pyramidal neurons.

(A) AMPAR/NMDAR ratio in neurons from Tg(CaMKII-hA_{2A}R) animals is decreased, when compared to WT animals (*p < 0.05, unpaired t-test) (n = 16-20); representative traces of EPSCs recorded at -70 mV and +40 mV, arrows indicate the amplitudes considered to calculate AMPAR/NMDAR ratio. **(B)** Plots of normalized $EPSC_{NMDA}$ current-voltage relationships recorded in the presence of DNQX (100

μM) from WT and Tg(CaMKII-hA_{2A}R) neurons (*p < 0.05, two-way ANOVA followed by a Bonferroni's multiple comparisons *post hoc* test) (n = 7-14); representative traces of NMDAR EPSCs recorded at -70 mV and +40 mV. (**C**) Tg(CaMKII-hA_{2A}R) animals do not exhibit alterations in AMPAR activation (n = 7); representative traces of AMPAR EPSCs recorded at -70 mV and +40 mV. (**D**) NMDAR $EPSC_{+40mV}/EPSC_{-60mV}$ ratio from WT and Tg(CaMKII-hA_{2A}R) neurons (**p < 0.01, unpaired t test) (n = 7-14). (**E**) Average time constants for fast and slow components (τ_{fast} and τ_{slow}) of NMDAR EPSCs representative traces recorded in WT and Tg(CaMKII-hA_{2A}R) animals. All values are mean ± SEM.

5. Physiological levels of A_{2A}R lead to a NMDAR-mediated LTD-to-LTP shift

In view of the key role of NMDAR in the control of synaptic plasticity we next focused on the impact of A_{2A}R overexpression on long-term depression (LTD) in the CA1 area of the dorsal hippocampus. LTD is altered in association with memory deficits in aging (Foster and Kumar, 2007) and animal models of stress (Wong et al., 2007) or AD (Lanté et al., 2015). In the hippocampus, LTD can be experimentally induced using several different protocols, including both electrical and pharmacological stimulation (Abraham et al., 1996). For our purpose, we selected a low frequency stimulation (LFS) protocol particularly efficient in inducing robust LTDs in adult animals - 3 trains of 1200 pulses, 2 Hz, 10-min interval (Ahmed et al., 2011; Laurent et al., 2016).

We observed a significant alteration of the pattern of induction of LTD: whereas this protocol triggered a typical LTD in WT animals, it

generated instead a significant LTP in Tg(CaMKII-hA_{2A}R) animals (Figure 3.10A).

The pattern of activation of NMDAR controls the entry of calcium into the postsynaptic compartment, determining the output of plasticity (Lisman, 1989; Yang et al., 1999). The robust recruitment of NMDAR causes a large calcium influx driving LTP, whereas the engagement of a lower number of NMDAR causes a more discrete calcium influx culminating in LTD (Lisman, 1989; Yang et al., 1999). To confirm a greater NMDAR role in this LTD-to-LTP shift in Tg(CaMKII-hA_{2A}R) animals, we induced LTD and titrated the recruitment of NMDAR using increasing concentrations of the NMDAR antagonist, AP5 (Figure 3.10B, C). With a low concentration of AP5 (15 µM), the LTP observed in Tg(CaMKII-hA_{2A}R) animals was abolished. Further increase of the AP5 concentration to 50 µM converted the LTP into LTD, fully rescuing the abnormal plasticity profile in Tg(CaMKII-hA_{2A}R) to a WT-like phenotype. Further increase of AP5 concentration to a supra-maximal value of 100 µM, abolished LTD, confirming that LTD in Tg(CaMKII-hA_{2A}R) animals is still strictly NMDAR-dependent (Figure 3.10C). In WT animals, LTD magnitude did not change with 15 µM of AP5 (Figure 3.10C), but when NMDAR were blocked with AP5 at 50 µM, no LTD was elicited, as expected (Figure 3.10C). Consistent with an aberrant NMDAR contribution to basal transmission in Tg(CaMKII-hA_{2A}R) animals, we observed a decrease in fEPSPs slope with AP5 (50 µM) in Tg(CaMKII-hA_{2A}R) animals, but not in WT animals (Figure 3.10D). Acute blockade of A_{2A}R directly on slices rescued the LTD shift observed in Tg(CaMKII-hA_{2A}R) animals. In fact, LFS stimulation of Tg(CaMKII-hA_{2A}R) slices

with either SCH 58261 (50 nM) or the non-selective adenosine antagonist, caffeine (30 μM) triggered an LTD similar to that found in WT animals (Figure 3.10E-G). As expected, in WT animals, this $A_{2A}R$ blockade did not change LTD magnitude (Figure 3.10G). Accordingly, SCH 58261, 50 nM, significantly decreased basal fEPSPs in Tg(CaMKII-h$A_{2A}R$) animals, while no effect was observed in WT (Figure 3.10H), confirming that the effects seen in Tg(CaMKII-h$A_{2A}R$) animals are indeed due to $A_{2A}R$ overactivation.

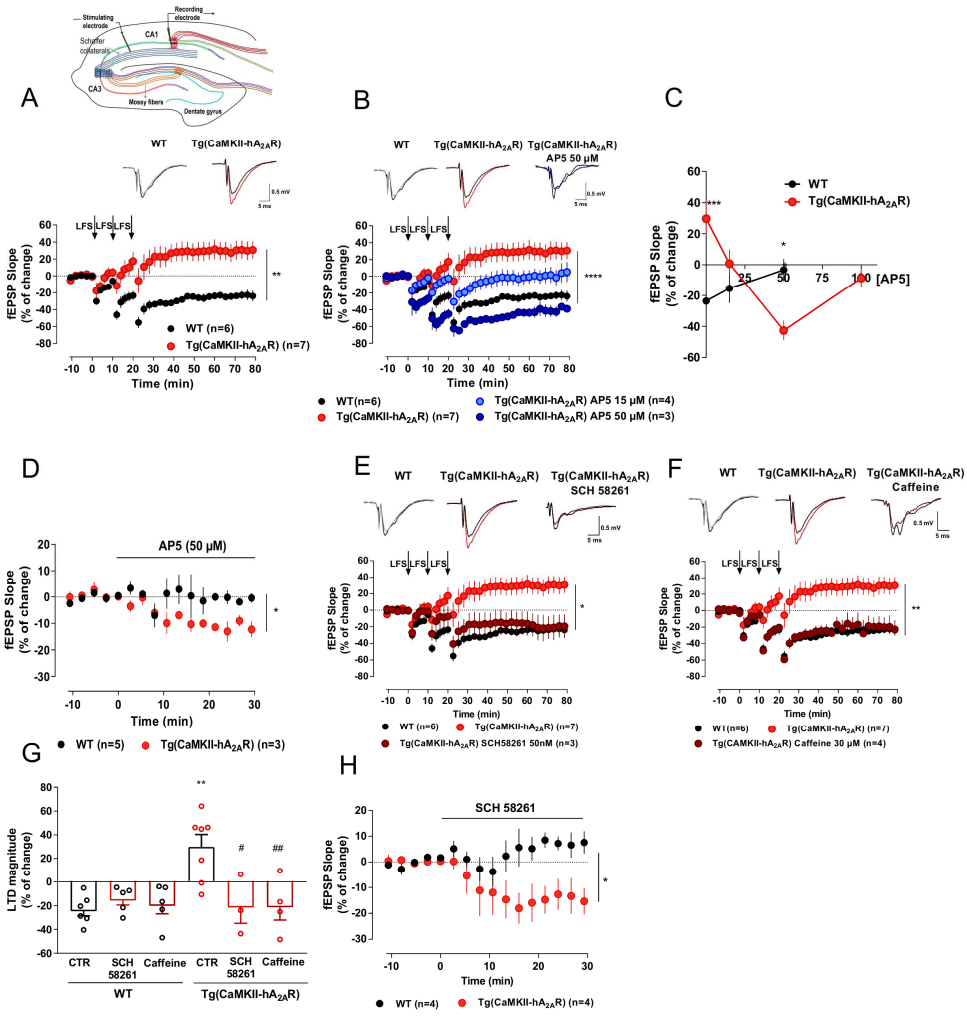

Figure 3.10. Physiopathological levels of $A_{2A}R$ lead to a NMDAR-mediated LTD-to-LTP shift.

(**A**) Top left: schematic representation of the simplified circuitry of the hippocampus. A stimulation electrode is placed in the Schaffer collaterals and a recording electrode in the CA1 dendritic area; Graph: Changes in fEPSP slope induced by LFS stimulation (3 trains of 1200 pulses, 2 Hz) recorded from WT and Tg(CaMKII-hA_{2A}R) hippocampal slices (**p < 0.01, unpaired t test) (n = 6-7); representative traces of fEPSPs before (black) and 50-60 min after (grey, red) LTD induction in WT and Tg(CaMKII-hA_{2A}R) animals. **(B)** Changes in fEPSP slope induced by LFS

stimulation (3 trains of 1200 pulses, 2 Hz) recorded from WT and Tg(CaMKII-$hA_{2A}R$) hippocampal slices after partial and complete NMDAR blockade with AP5 (15 and 50 μM, respectively) (****$p < 0.0001$ comparing to Tg(CaMKII-$hA_{2A}R$), two-way ANOVA followed by Bonferroni's multiple comparisons *post hoc* test) (n = 3-4); representative traces of fEPSPs before (black) and 50-60 minutes after (grey, red, blue) LTD induction in WT, Tg(CaMKII-$hA_{2A}R$) and Tg(CaMKII-$hA_{2A}R$) animals with NMDAR complete blockade. **(C)** Effect of increasing AP5 concentrations (0-100 μM) on synaptic strength after low frequency stimulation (changes after 50-60min) in WT and Tg(CaMKII-$hA_{2A}R$) animals. (n=3-4). **(D)** AP5 decreases fEPSP basal transmission in Tg(CaMKII-$hA_{2A}R$) animals (*$p < 0.05$, unpaired t test) (n=3-5). **(E)** Changes in fEPSP slope induced by LFS stimulation recorded from WT, Tg(CaMKII-$hA_{2A}R$) and Tg(CaMKII-$hA_{2A}R$) hippocampal slices perfused with SCH 58261 (50 nM) (*$p < 0.05$ comparing to Tg(CaMKII-$hA_{2A}R$), two-way ANOVA followed by Bonferroni's multiple comparisons *post hoc* test) (n = 3-7); representative traces of fEPSPs before (black) and 50-60 min after (grey, red, dark red) LTD induction in WT, Tg(CaMKII-$hA_{2A}R$) and Tg(CaMKII-$hA_{2A}R$) animals with SCH 58261. **(F)** Changes in fEPSP slope induced by LFS stimulation recorded from WT, Tg(CaMKII-$hA_{2A}R$) and Tg(CaMKII-$hA_{2A}R$) hippocampal slices perfused with caffeine (30 μM) (**$p < 0.01$ comparing to Tg(CaMKII-$hA_{2A}R$), two-way ANOVA followed by Bonferroni's multiple comparisons *post hoc* test) (n = 4-7); representative traces of fEPSPs before (black) and 50-60 min after (grey, red, dark red) LTD induction in WT, Tg(CaMKII-$hA_{2A}R$) and Tg(CaMKII-$hA_{2A}R$) animals with caffeine. **(G)** Changes in fEPSP slope induced by LFS stimulation recorded from WT and Tg(CaMKII-$hA_{2A}R$) perfused with SCH 58261 (50 nM) or caffeine (30 μM) (**$p < 0.01$ comparing to WT, $^{\#}p < 0.05$, $^{\#\#}p < 0.01$ comparing to Tg(CaMKII-$hA_{2A}R$), two-way ANOVA followed by Bonferroni's multiple comparisons *post hoc* test) (n = 3-7). All values are mean ± SEM.

Group I metabotropic glutamate receptors, namely mGluR5, are postsynaptic and tightly coupled to NMDA receptors (Ferreira et al., 2017a; Jia et al., 1998; Takagi et al., 2010), conferring them the ability to exacerbate NMDAR mediated toxicity. Upon activation by

glutamate release, preferentially upon strong synaptic activation, they increase NMDAR-mediated Ca^{2+} currents (Mannaioni et al., 2001). When we blocked mGluR5 with MPEP (5 µM), the LTD-to-LTP shift observed in Tg(CaMKII-hA_{2A}R) animals was prevented (Figure 3.11A), while MPEP does not change LTD magnitude in WT animals (Figure 3.11B). Consistent with their activation upstream of NMDAR, the aberrant NMDAR component in Tg(CaMKII-hA_{2A}R) disappeared upon mGluR5 blockade (Figure 3.11C, D), while no effect was observed in WT animals (Figure 3.11D), disclosing the role of mGluR5 as a player in A_{2A}R-induced synaptic dysfunction.

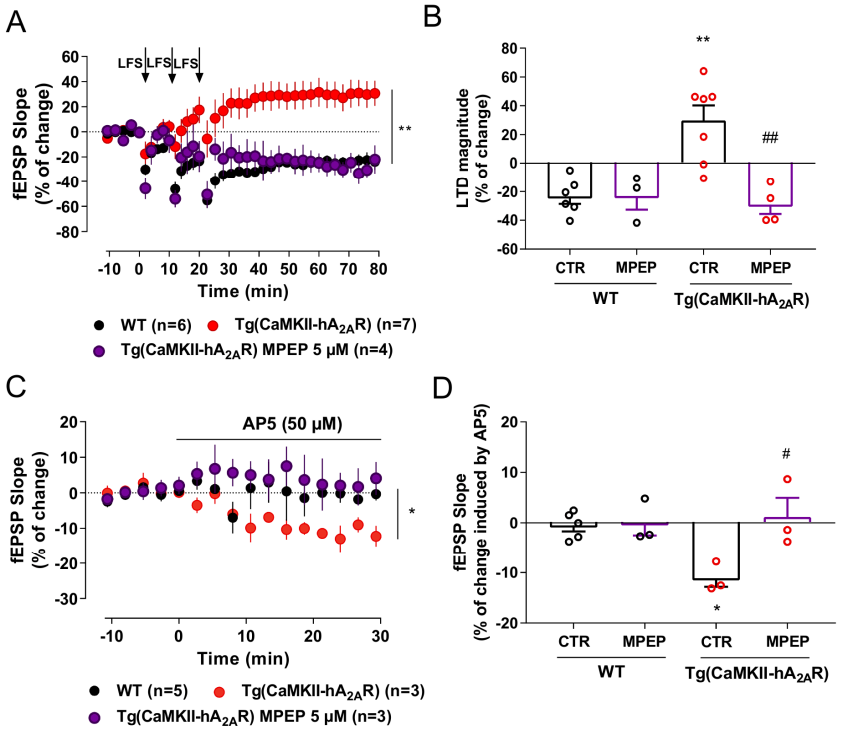

Figure 3.11. mGluR5 activation drives the NMDAR-mediated LTD-to-LTP shift.

(**A**) Changes in fEPSP slope induced by LFS stimulation recorded from WT, Tg(CaMKII-hA_{2A}R) and Tg(CaMKII-hA_{2A}R) hippocampal slices perfused with mGluR5 antagonist MPEP (5 μM) (**p < 0.01 comparing to Tg(CaMKII-hA_{2A}R), one-way ANOVA followed by Bonferroni's multiple comparisons *post hoc* test) (n = 3-5). (**B**) MPEP rescues LtD-to-LTP shift in Tg(CaMKII-hA_{2A}R) animals, while no effect is observed in WT animals (**p < 0.01 comparing to WT, $^{\#\#}$p < 0.01 comparing to Tg(CaMKII-hA_{2A}R), two-way ANOVA followed by Bonferroni's multiple comparisons *post hoc* test) (n = 3-5). (**C**) MPEP abolishes the effect of AP5 on basal transmission in Tg(CaMKII-hA_{2A}R) animals (*p < 0.05 comparing to WT, one-way ANOVA followed by Bonferroni's multiple comparisons *post hoc* test) (n = 3-5). (**D**) mGluR5 antagonist rescues NMDAR aberrant component on basal transmission (*p < 0.05 comparing to WT, $^{\#}$p < 0.05 comparing to Tg(CaMKII-hA_{2A}R), two-way ANOVA followed by Bonferroni's multiple comparisons *post hoc* test) (n = 3-5). All values are mean ± SEM.

To further study the alterations in the threshold for LTD in Tg(CaMKII-hA_{2A}R) animals, we elicited LTD using decreasing frequencies of stimulation maintaining the total number of pulses of one train (1200): 2 Hz, 1 Hz and 0.5 Hz. In contrast to what we observed for 3 x trains of 1200 pulses (2 Hz), a lower 0.5 Hz frequency was more effective in inducing LTD in Tg(CaMKII-hA_{2A}R) than in WT animals (Figure 3.12A, B). Furthermore, frequencies of 1 and 2 Hz failed to elicit LTD in both WT and Tg(CaMKII-hA_{2A}R) (Figure 3.12C, D)- More importantly, the magnitude of LTD in Tg(CaMKII-hA_{2A}R) animals correlated significantly with the frequency of stimulation (Figure 3.12A), consistent with a shift to the left in the LTD threshold.

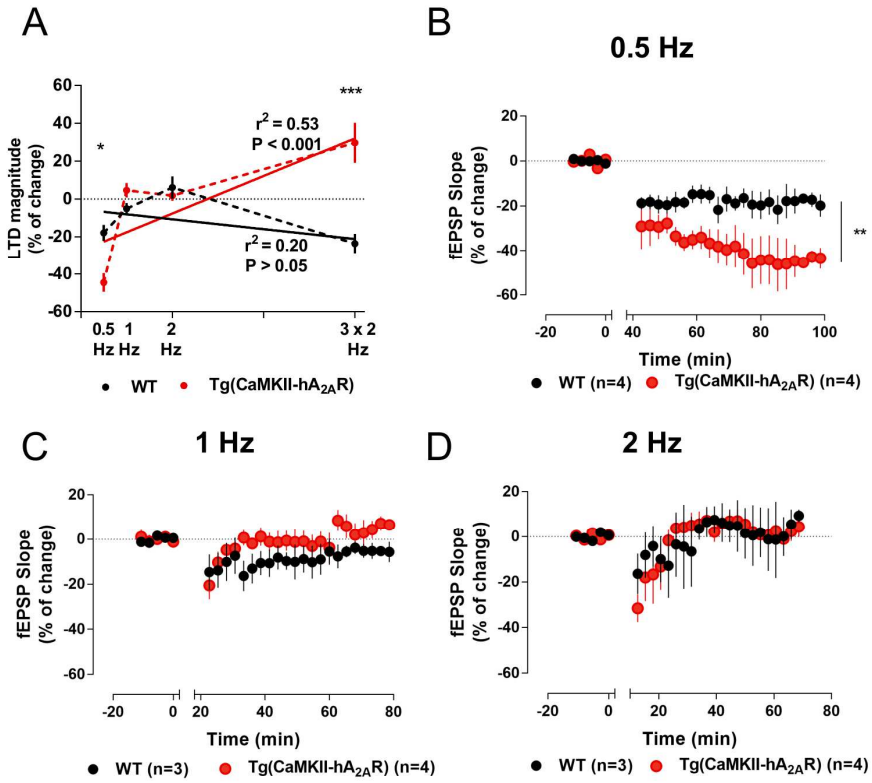

Figure 3.12. Tg(CaMKII-hA$_{2A}$R) animals exhibit a shift to the left in LTD threshold.

(**A**) Changes in fEPSP slope induced by increasing frequencies of LFS stimulation in WT and Tg(CaMKII-hA$_{2A}$R) (*p < 0.05, ***p < 0.0001, two-way ANOVA followed by Bonferroni's multiple comparisons *post hoc* test) (n = 3-7). (**B**), (**C**), (**D**) Changes in fEPSP slope induced by LFS stimulation (0.5, 1 and 2 Hz, respectively) in WT and Tg(CaMKII-hA$_{2A}$R) animals (**p < 0.01, unpaired t test) (n = 3-4). All values are mean ± SEM.

6. Blockade of $A_{2A}R$ *in vivo* rescues the LTD-to-LTP shift in Tg(CaMKII-h$A_{2A}R$) animals

To establish that $A_{2A}R$ overactivation is indeed the trigger for the aberrant NMDAR recruitment, we treated Tg(CaMKII-h$A_{2A}R$) animals with the $A_{2A}R$ selective antagonist KW6002 (5 mg/kg/day), in the drinking water for 4 weeks. In Tg(CaMKII-h$A_{2A}R$) treated animals, LFS induced an LTD comparable to WT animals, rescuing the LTD-to-LTP shift (Figure 3.13A, B). Furthermore, the KW6002 treatment normalized NMDAR overactivation, as confirmed by the reinstatement of AP5 ability to fully block LTD in Tg(CaMKII-h$A_{2A}R$) (Figure 3.13A, B). The treatment with KW6002 did not change LTD magnitude in WT animals (Figure 3.13B), nor $A_{2A}R$ mRNA relative expression in both WT and Tg(CaMKII-h$A_{2A}R$) (Figure 3.13C). The increased NMDAR contribution to basal transmission observed in Tg(CaMKII-h$A_{2A}R$) animals disappeared upon chronic KW6002 treatment (Figure 3.13D).

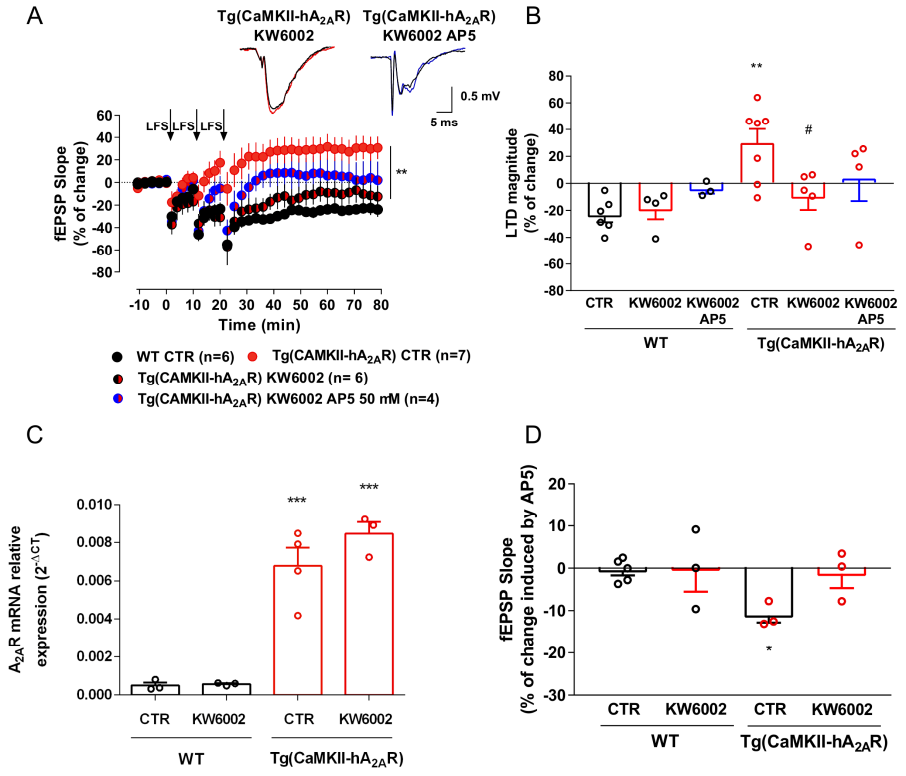

Figure 3.13. Blockade of $A_{2A}R$ activation *in vivo* rescues the LTD-to-LTP shift in Tg(CaMKII-hA_{2A}R) animals

(A) Changes in fEPSP slope induced by LFS stimulation (3 trains of 1200 pulses, 2 Hz) in WT and Tg(CaMKII-hA_{2A}R) animals non-treated (CTR) and treated with KW6002 (**p < 0.01 comparing to Tg(CaMKII-hA_{2A}R), two-way ANOVA followed by Bonferroni's multiple comparisons *post hoc* test) (n = 6). AP5 (50 µM) abolished LTD in Tg(CaMKII-hA_{2A}R animals treated with KW6002 (n = 4); representative traces of fEPSPs before (black) and 50-60 min after (red, blue) LTD induction in Tg(CaMKII-hA_{2A}R) chronically treated with KW6002 in the absence and presence of AP5. (**B**) Changes in fEPSP slope induced by LFS stimulation (3 trains of 1200 pulses, 2 Hz) in WT and Tg(CaMKII-hA_{2A}R) animals non-treated (CTR) and treated with KW6002, in the presence and absence of AP5 (50 µM) (**p < 0.01 comparing to WT, $^{\#}$p < 0.05 comparing to Tg(CaMKII-hA_{2A}R), two-way ANOVA followed by Bonferroni's multiple comparisons *post hoc* test) (n = 3-7). (**C**) $A_{2A}R$ mRNA relative

expression in WT and Tg(CaMKII-hA_{2A}R) animals non-treated and treated with KW6002 (***p < 0.001 comparing to WT, two-way ANOVA followed by Bonferroni's multiple comparisons *post hoc* test) (n = 3-4). (**D**) Chronic KW6002 treatment reverts the effect of AP5 on basal transmission in Tg(CaMKII-hA_{2A}R) animals (*p < 0.05 comparing to WT, one-way ANOVA followed by Bonferroni's multiple comparisons *post hoc* test) (n = 3-5). All values are mean ± SEM.

7. Increased levels of A_{2A}R impair calcium homeostasis

To investigate whether A_{2A}R-mediated NMDAR hyperactivation disrupted Ca^{2+} signaling, we measured variations in intracellular calcium concentrations ($[Ca^{2+}]i$) in primary neuronal cultures transfected with A_{2A}R. For this, we used a construct encoding a Venus-A_{2A}R fusion protein. We confirmed the co-localization of the Venus signal with the immunostaining for A_{2A}R (Figure 3.14A). Changes in $[Ca^{2+}]i$ were detected by Ca^{2+} imaging using Fura 2-acetoxymethyl ester (Fura-2 AM) (Figure 3.14B). Application of the A_{2A}R agonist CGS 21680, 30 nM, elevated intracellular Ca^{2+} levels in Venus-A_{2A}R transfected neurons, whereas in non-transfected neurons lower changes in fluorescence were detected (Figure 3.14C, G). This A_{2A}R-evoked increase in $[Ca^{2+}]i$ was prevented by the NMDAR antagonist, AP5, 50 μM (Figure 3.10D, H), the A_{2A}R antagonist, SCH 58261, 50 nM (Figure 3.14E, I) or mGluR5 antagonist MPEP, 5 μM (Figure 3.14F, J). These results show for the first time a crosstalk between A_{2A}R and NMDAR that impacts on Ca^{2+} influx in glutamatergic neurons.

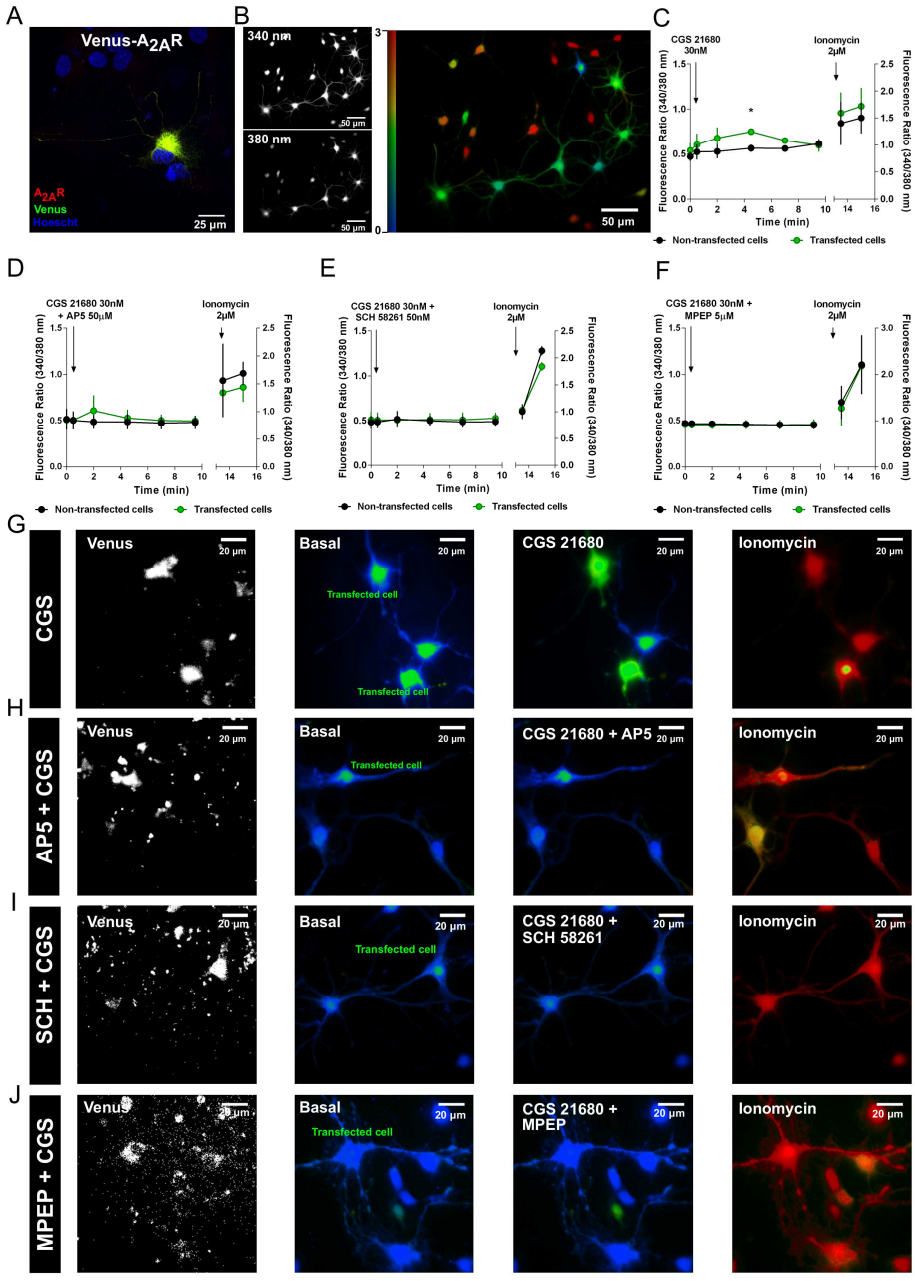

Figure 3.14. Increased levels of $A_{2A}R$ impair calcium homeostasis.

(A) Control immunocytochemistry analysis of neurons transfected with Venus-$A_{2A}R$ construct confirmed co-expression of Venus and $A_{2A}R$. **(B)** Representative images of

Ca^{2+} imaging. Bright regions indicate the location of cytoplasm and organelles, where the concentration of Ca^{2+} is higher than in the dark regions indicating the extracellular medium, where diffusion processes take place. The right image corresponds to the ratio between the radiation emitted at 510 nm, when cells are excited at 340 nm, over emission upon excitation at 380 nm (F340/F380). **(C)** Time course of Ca^{2+}-dependent fluorescence recorded and averaged per minute from Fura-2 AM neurons transfected with Venus-A_{2A}R construct in response to CGS 21680, 30 nM, and ionomycin, 2 µM. Application of A_{2A}R agonist CGS 21680, 30 nM, elevated intracellular Ca^{2+} levels in Venus-A_{2A}R transfected neurons, whereas lower changes in fluorescence were detected in non-transfected neurons (*$p<0.05$, unpaired t test). Time of application of drugs are shown by arrows (4-15 responsive cells per experimental condition from 3 independent cultures). **(D)** Time course of Ca^{2+}-dependent fluorescence recorded and averaged from Fura-2 AM neurons transfected with Venus-A_{2A}R construct in response to AP5, 50 µM, CGS 21680, 30 nM, and ionomycin, 2 µM. The A_{2A}R-evoked increase in $[Ca^{2+}]i$ observed in (C) was prevented by NMDAR antagonism. Time of application of drugs are shown by arrows. (4-15 responsive cells per experimental condition from 2 independent cultures). **(E)** Time course Ca^{2+}-dependent fluorescence recorded and averaged from Fura-2 AM neurons transfected with Venus-A_{2A}R construct in response to SCH 58261, 50 nM, CGS 21680, 30 nM, and ionomycin, 2µM. The A_{2A}R-evoked increase in $[Ca^{2+}]i$ observed in (C) was prevented by A_{2A}R antagonism. Time of application of drugs are shown by arrows (4-15 responsive cells per experimental condition from 2 independent cultures). (**F**) Time course Ca^{2+}-dependent fluorescence recorded and averaged from Fura-2 AM neurons transfected with Venus-A_{2A}R construct in response to MPEP, 5 µM, CGS 21680, 30 nM, and ionomycin, 2µM. The A_{2A}R-evoked increase in $[Ca^{2+}]i$ observed in (C) was prevented by mGluR5 antagonism. Time of application of drugs are shown by arrows (4-15 responsive cells per experimental condition from 2 independent cultures). (**G**), (**H**), (**I**), (**J**) Representative images of the different conditions showed in (C), (D), (E) and (F), respectively. All values are mean ± SEM.

8. LTD-to-LTP shift in aged and APP/PS1 animals is rescued by $A_{2A}R$ blockade

Aging and AD are associated with an up-regulation of $A_{2A}R$ in the hippocampus as we report here (Figure 3.1) and others have shown previously (Canas et al., 2009; Costenla et al., 2011; Diógenes et al., 2011; Lopes et al., 1999a). We evaluated putative LTD impairments in aged animals and in an APP/PS1 mouse model of AD, both models displaying $A_{2A}R$ increased levels (Figure 3.15A, B).

Aged animals displayed the same LTD-to-LTP shift to that observed in our Tg(CaMKII-h$A_{2A}R$) animals, while in young animals a robust LTD was achieved (Figure 3.15C, D). The LTD-to-LTP shift was completely rescued with $A_{2A}R$ blockade by SCH 58261 (Figure 3.15C, D), whereas SCH 58261 did not alter LTD profile in young animals (Figure 3.15D). Within the aged group, we identified a subset of age-impaired animals that performed worse than young rats in the Y-maze test, revealing no preference for the novel arm (Figure 3.15E). Interestingly, these same animals seem to be distinguished by an LTD-to-LTP shift, also observed in Tg(CaMKII-h$A_{2A}R$) (Figure 3.15E). In contrast, age-unimpaired animals performed within the range of young rats (Figure 3.15E) and could be distinguished by their lack of response to LFS (Figure 3.15F). Consistent with the enhanced role of $A_{2A}R$ upon aging (Diógenes et al., 2007a; Lopes et al., 2002; Rebola et al., 2003b), SCH 58261 decreased basal transmission in hippocampal slices of aged animals, while no effect was observed in young animals (Figure 3.15G). We observed a tendency towards an increased effect of

SCH 58261 in age-impaired subset (Figure 3.15H), when compared with age-unimpaired animals, in spite of the lower n. This larger tonic effect of adenosine suggests that an increased $A_{2A}R$ activation in age-impaired animals. Importantly, we found that plasticity profile correlated significantly with the behavioral memory index in aged animals (Figure 3.15I), whereby a higher LTD-to-LTP shift corresponded to a worse Y-maze performance. Notably, a 3-week treatment with the selective $A_{2A}R$ antagonist (KW6002; 5 mg/kg/day; oral) restored memory impairments, as observed by the increased time spent in the novel arm (Figure 3.15E). This KW6002 treatment did not affect $A_{2A}R$ mRNA expression in aged animals (Figure 3.15A), consistent to what was observed for Tg(CaMKII-h$A_{2A}R$) (Figure 3.13C).

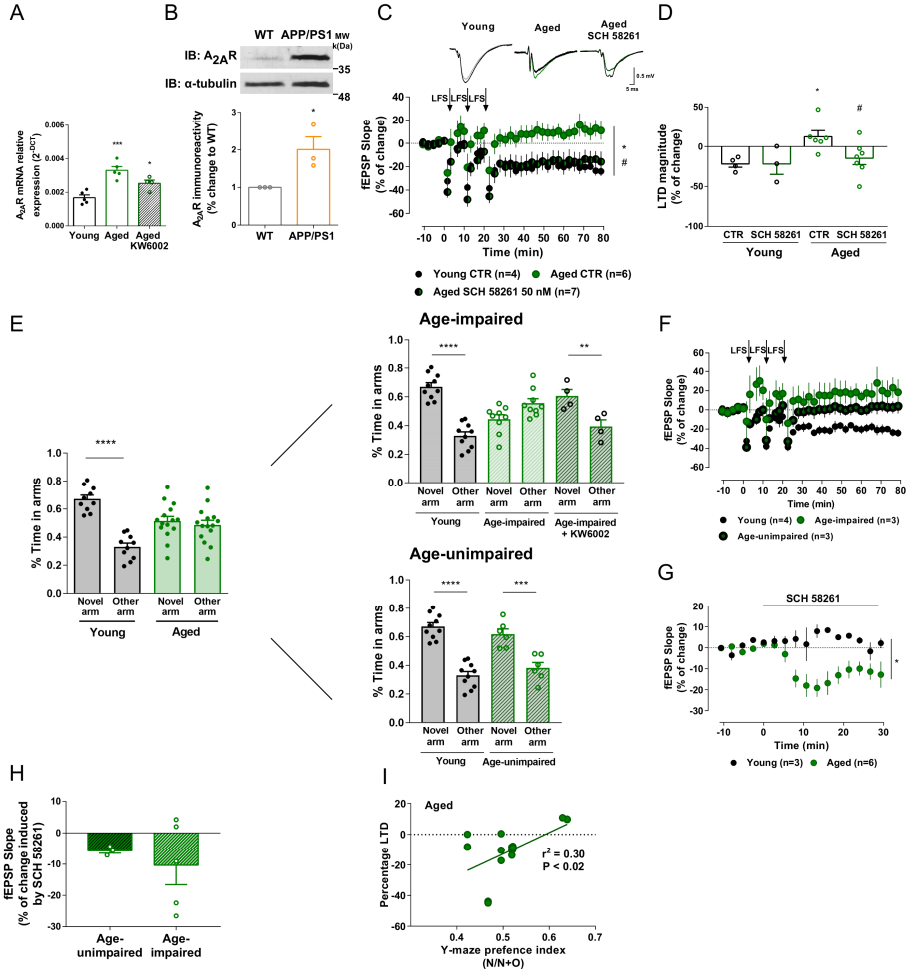

Figure 3.15. LTD-to-LTP shift in aged animals is rescued by $A_{2A}R$ blockade.

(A) $A_{2A}R$ mRNA relative expression in young and aged animals non-treated and treated with KW6002 (*p < 0.05, ***p < 0.001 comparing to young, one-way ANOVA followed by Bonferroni's multiple comparisons *post hoc* test) (n = 4-5). (**B**) APP/PS1 mice display $A_{2A}R$ hippocampal overexpression, as compared to WT animals (*p < 0.05, unpaired t test) (n = 3). (**C**), (**D**) Changes in fEPSP slope induced by LFS stimulation recorded from young and aged animals upon acute $A_{2A}R$ blockade (SCH 58261, 50 nm) (*p < 0.05 comparing to young, #p < 0.05 comparing to aged, two-way ANOVA followed by Tukey's multiple comparisons post hoc test) (n = 3-7); representative traces of fEPSPs before (black) and 50-60 minutes after

(grey, green, dark green) LTD induction in young, aged and aged animais treated with SCH 58261, respectively. (**E**) Spatial memory performance was assessed by the Y-Maze test. Aged animals displayed a loss of preference for the novel arm (***p < 0.001, ****p < 0.0001, novel arm comparing to other arm, two-way ANOVA followed by Bonferroni's multiple comparisons post hoc test) (young: n = 10; aged: n = 15). The pool of aged rats included a substantial subset of rats that performed within the range of young rats, labeled age-unimpaired rats (n = 6), while other clearly showed impairment, labeled age-impaired rats (n = 9), that is rescued upon chronic KW6002 treatment (**p<0.01, novel arm comparing to other arm, two-way ANOVA followed by Bonferroni's multiple comparisons post hoc test) (n = 4). (**F**) Age-impaired animals exhibited an LTD-to-LTP shift (*p < 0.05 comparing to WT, one-way ANOVA followed by a Bonferroni's multiple comparisons post hoc test) (n = 3). Age-unimpaired animals can be distinguished by their lack of response to LFS (n = 3). (**G**) SCH 58261, 50 nM, decreased basal transmission in aged animals, while no effect is observed in young animals (*p < 0.05, unpaired t test) (n = 3-6). (**H**) There is a tendency towards an increase in SCH 58261 effect on basal transmission in age-impaired animals (n = 5), when compared to age-unimpaired animals (n = 3). (**I**) LTD magnitude observed in aged animals significantly correlates with Y-maze preference index (3 replicates of n = 6 animals, $r^2 = 0.03$, $p < 0.05$). All values are mean ± SEM.

In 11-12 months-old APP/PS1 mice, these animals display memory deficits (Cramer et al., 2012) and LFS elicited LTP instead of LTD (Figure 3.16A, B), as seen in Tg(CaMKII-hA_{2A}R) animals. Importantly, acute blockade of A_{2A}R with 100 nM SCH 58261, was able to revert the LTD-to-LTP shift back to the LTD characteristic of WT mice (Figure 3.16A, B).

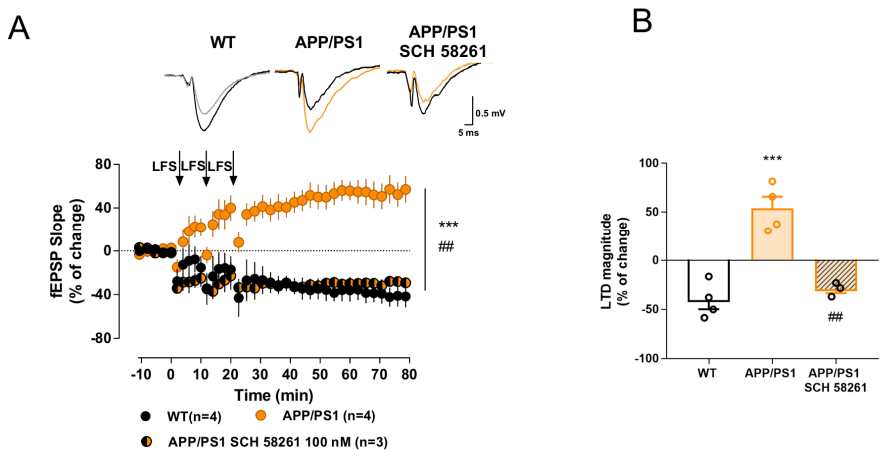

Figure 3.16. LTD-to-LTP shift in APP/PS1 animals is rescued by $A_{2A}R$ blockade.

(**A**), (**B**) Changes in fEPSP slope induced by LFS stimulation recorded from WT, APP/PS1 and APP/PS1 hippocampal slices perfused with SCH 58261 (100 nM) (***$p < 0.001$ comparing to WT, $^{\#\#}p < 0.01$ comparing to APP/PS1, one-way ANOVA followed by a Bonferroni's multiple comparisons post hoc test) (n = 3-4); representative traces of fEPSPs before (black) and 50-60 minutes after (grey, orange) LTD induction in WT, APP/PS1 and APP/PS1 SCH 58261 100 nM. All values are mean ± SEM.

CHAPTER IV

Conclusions

1. Discussion

We show that the $A_{2A}R$ upsurge, described in different pathological situations in rodent models, such as hypoxia, ischemia, stress, diabetes and even upon aging (Cunha, 2016), is also characteristic of the human aged brain and is aggravated in Alzheimer's disease (AD) (Albasanz et al., 2008). Moreover, we describe that an increase in neuronal $A_{2A}R$ is sufficient to drive deficits in synaptic plasticity, leading to an LTD-to-LTP shift and impairments of hippocampal-dependent learning and memory. This is a consequence of an $A_{2A}R$-induced increase in postsynaptic Ca^{2+} influx *via* NMDAR, which is dependent on mGluR5 activation (see Figure 4.1 for a summary). We reveal that the same synaptic plasticity shift occurs in the hippocampus of aged and APP/PS1 animals, which is rescued upon $A_{2A}R$ blockade.

The findings in human hippocampal samples confirm the observations made in animal models, in which $A_{2A}R$ density is increased upon aging (Canas et al., 2009; Cunha et al., 1995; Diógenes et al., 2007a; Lopes et al., 1999a, 2011a). Accordingly, in humans, several epidemiological studies have shown that regular caffeine consumption attenuates memory disruption during aging and decreases the risk of developing memory impairments in AD patients (Arendash and Cao, 2010; Eskelinen et al., 2009; van Gelder et al., 2007; Maia and de Mendonça, 2002; Ritchie et al., 2007). Furthermore, in animal models of several other pathologies, there is a clear correlation of hippocampal $A_{2A}R$ up-regulation with cognitive deficits, such as in acute or chronic stress (Batalha et al., 2013; Cunha et al., 2006; Kaster et al., 2015), Alzheimer's (Viana da Silva et al., 2016), Parkinson's (Varani et al.,

2010) or Huntington's diseases (Li et al., 2015c; Tyebji et al., 2015). However, the exact mechanism by which neuronal $A_{2A}R$ overactivation could trigger or increase the susceptibility for memory dysfunction in these multiple pathologies was not known.

A previous study using a model of $A_{2A}R$ overexpression under the control of the neuron-specific enolase promoter reported working memory deficits (Giménez-Llort et al., 2007). However, that study could not distinguish $A_{2A}R$-related embryonic effects from those elicited by postnatal alterations. In contrast, our model of overexpression, driven by a CaMKII promoter, allows a progressive postnatal and forebrain-specific expression, bypassing developmental effects and closer to an age-like $A_{2A}R$ distribution. These animals exhibit depressive-like behavior, hyperlocomotion, and altered exploratory behavior, consistent with the depressive signs found in aging, chronic stress, and Alzheimer's disease (Coelho et al., 2014a). Importantly, they do not present changes in adenosine A_1 receptor levels nor adenosine levels in the hippocampus (Batalha et al., 2016). Furthermore, at 12 week-old, the Tg(CaMKII-h$A_{2A}R$) animals display a 5–8 fold increase of $A_{2A}R$ immunoreactivity (Batalha et al., 2016), which is in the same magnitude of that found in our human aged and AD samples, and equivalent to that of aged rats (Canas et al., 2009; Costenla et al., 2011; Diógenes et al., 2007a; Rebola et al., 2003b). Importantly, this $A_{2A}R$ overexpression occurs in the hippocampus and cortex, recapitulating the pattern observed in our aged and AD human samples and consistent with previous reports (Albasanz et al., 2008). In the Tg(CaMKII-h$A_{2A}R$) model there is no evidence of $A_{2A}R$ overexpression in astrocytes, strengthening the idea

that the observed memory and synaptic impairments are due to a neuronal-specific $A_{2A}R$ overexpression. The fact that in aged and AD human samples we observed a clear $A_{2A}R$ overexpression in neurons further emphasizes neuronal $A_{2A}R$ as key mediators in synaptic glutamatergic dysfunction observed in aging and AD (Orr et al., 2015). Aberrant astrocytic $A_{2A}R$ expression in late-stage AD has been associated to cognitive decline, and indeed astrocytic $A_{2A}R$ can lead to alterations of synaptic $A_{2A}R$-mediated functions (Matos et al., 2015). However, neuronal contribution is highlighted by recent evidence showing that stimulation of neuronal opto-$A_{2A}R$ in the hippocampus induces changes in synaptic plasticity and CREB activation. Moreover, silencing $A_{2A}R$ in neurons of the associative/commissural pathway rescues the aberrant LTP in APP/PS1 mice in a non-NMDAR dependent mechanism (Li et al., 2015a; Viana da Silva et al., 2016). Our findings demonstrate that neuronal A_{2A} overactivation is sufficient to induce synaptic dysfunction and cognitive impairments. This suggests that synaptic dysfunction in aging and early AD may be driven predominantly by a neuronal $A_{2A}R$ progressive dysfunction, whereas at later Braak stages of AD, astrocytic $A_{2A}R$ and inflammation might become more relevant (Laurent et al., 2016; Orr et al., 2015).

Both aging and AD comprehend functional and structural alterations in the hippocampus that drive cognitive decline (Burke and Barnes, 2006; Walsh and Selkoe, 2004). Furthermore, they are also characterized by an abnormal Ca^{2+} signaling. Several studies reported an age-associated increase in basal $[Ca^{2+}]i$ levels (Hajieva et al., 2009; Raza et al., 2007) and action potential-evoked calcium influx (Oh et al., 2013) and a reduction in the expression of calcium-buffering proteins. In AD

mouse models, increased levels of intracellular Ca^{2+} (Lopez et al., 2008) distorts the normal Ca^{2+} signaling and Ca^{2+}-dependent mechanisms and can indeed trigger the amyloidogenic pathway (Pierrot et al., 2004, 2006). Concretely, the AD brain is characterized by a clear loss of synaptic processes and neuronal cell bodies in the limbic and association cortices (reviewed in (Walsh and Selkoe, 2004)). In normal aging there is still a considerable structural preservation in several brain areas including the hippocampus (Burke and Barnes, 2006; Keuker et al., 2003; Merrill et al., 2000; Pakkenberg and Gundersen, 1997). Therefore it is conceivable to hypothesize that the shift from normal aging to AD could be related to dysregulation of the integrated homeostatic network caused by differences either in the levels of the endogenous ligand – adenosine (Sebastião et al., 2000), or in the expression of $A_{2A}R$ that are increased upon aging and further exacerbated in AD (Figure 3.1). To specifically check the endogenous activation of $A_{2A}R$, we have quantified the effect of blocking $A_{2A}R$ in basal transmission, in age-impaired and age-unimpaired animals. The fact that we observe a tendency towards an increased effect of SCH 58261 in age-impaired subset, without significant differences in the bulk mRNA levels within the aged group, supports the first hypothesis. $A_{2A}R$ and A_1R form heteromers and, under physiological conditions, adenosine preferentially activate A_1R (Ciruela et al., 2006; Ferré et al., 2007) in the hippocampus, which control glutamatergic neurotransmission, namely by a decrease in NMDAR-mediated responses (Canhão et al., 1994; Klishin et al., 1995). In conditions where hippocampal transmission is dysfunctional, there is an up-regulation of $A_{2A}R$ (reviewed in (Cunha, 2016)) together with an

increased release of ATP as a danger signal (Rodrigues et al., 2015), which is the main source of the extracellular adenosine activating $A_{2A}R$ (Augusto et al., 2013). The signaling of these up-regulated $A_{2A}R$ is shifted from a PKC-dependent, controlled by inhibitory adenosine A_1 receptors, towards a more disinhibited PKA-dependent mechanism in aging and pathology (Batalha et al., 2016; Lopes et al., 1999b; Rebola et al., 2003b), leading to impaired synaptic plasticity and compromised memory performance (Batalha et al., 2013; Kaster et al., 2015; Laurent et al., 2016; Viana da Silva et al., 2016).

This dysfunction is associated to an excitatory effect on glutamatergic transmission, which we can postulated that it may be mediated by non-heteromerized $A_{2A}R$. Our results in Tg(CaMKII-h$A_{2A}R$) are in line with this hypothesis, since we observe an aberrant constitutive activation of $A_{2A}R$, dependent on PKA (Batalha et al., 2016), and consequent NMDAR, both contributing to basal synaptic transmission, that could not be observed in WT animals.

Long-term synaptic plasticity processes (LTP and LTD) are the main neurophysiological correlate of memory (Citri and Malenka, 2008; Lynch, 2004). Although the relation between hippocampal LTP and memory is the most explored (Marchetti and Marie, 2011), there is also robust evidence that altered hippocampal LTD affects memory performance (Dong et al., 2013; Ge et al., 2010), as shown in animal models of stress (Wong et al., 2007) or of AD (Ahmed et al., 2015; Lanté et al., 2015). We now report that Tg(CaMKII-h$A_{2A}R$) animals display memory impairments together with a newly described LTD-to-LTP shift as a result of an increase in Ca^{2+} influx dependent on NMDAR activation. In fact, we observed a dose-dependent rescue of

LTD in slices from Tg(CaMKII-hA_{2A}R) rats with the NMDAR antagonist AP5. The concentration that fully restored LTD in Tg(CaMKII-hA_{2A}R) prevented it in WT animals. This LTD in Tg(CaMKII-hA_{2A}R) is NMDAR-dependent, since a higher concentration of AP5, 100 μM, was able to completely abolish LTD. Accordingly, in primary cultures of hippocampal neurons, A_{2A}R activation directly increased Ca^{2+} intracellular levels through NMDAR activation, blocked by its selective antagonist AP5. These data strongly indicate an A_{2A}R – NMDAR interaction, consistent with our synaptic plasticity results. Although in our paper we observe a Ca^{2+} influx-dependent LTD-to-LTP shift, there are reports that metabotropic NMDAR activity, independent of calcium influx, can also induce LTD (Nabavi et al., 2013). More relevant, we have shown that the blockade of A_{2A}R can restore a similar LTD-to-LTP shift in aged and AD mice models, strongly emphasizing A_{2A}R as the pathophysiological mediator involved in this synaptic shift.

We can postulate that NMDA receptor gating properties are directly modulated by such an increase in glutamate available to activate the ionotropic receptor. In such a case, however, AMPA mediated currents in Tg(CaMKII-hA_{2A}R) would be similarly increased, which we do not find. Moreover, when we transfected neurons with A_{2A}R we could only observe an increase in Ca^{2+} transients in transfected cells, but not in the adjacent non-transfected neurons. If an overall increase in glutamate were the only mechanism, then we might expect some non-transfected neurons to be affected. Therefore, other postsynaptic modifications due to an A_{2A}R-related increase in glutamate release and/or postsynaptic A_{2A}R contribution must be considered. Indeed, a

postsynaptic activation of $A_{2A}R$ can lead to downstream activation of CREB in the hippocampus (Li et al., 2015a), and $A_{2A}R$ and mGluR5 can directly interact and regulate NMDAR activity (Sarantis et al., 2015; Tebano et al., 2005).

Group I metabotropic glutamate receptors, namely mGluR5, are postsynaptic and tightly coupled to NMDA receptors (Ferreira et al., 2017a; Jia et al., 1998; Takagi et al., 2010), conferring them the ability to either protect or exacerbate NMDAR mediated toxicity depending upon the model or cell type (Lea et al., 2002). Upon activation by glutamate release, preferentially upon strong synaptic activation, mGluR5 increase NMDAR-mediated Ca^{2+} currents (Mannaioni et al., 2001), by reducing the Mg^{2+} block (Lea et al., 2002) and triggering the phosphorylation of NMDAR (Takagi et al., 2010). Previous studies hinted at a possible $A_{2A}R$-NMDAR crosstalk, since $A_{2A}R$ can control expression (Ferreira et al., 2017b, 2017a), recruitment (Rebola et al., 2008) and the rate of desensitization (Sarantis et al., 2015) of NMDAR. We and others have provided compelling evidence of an $A_{2A}R$-mGluR5 synergistic interaction in the modulation of NMDAR-mediated effects (Ferreira et al., 2017a; Kouvaros and Papatheodoropoulos, 2016; Sarantis et al., 2015; Tebano et al., 2005). Thus, mGluR5 is a likely candidate to act as a switch between $A_{2A}R$ and NMDAR, by sensing glutamate and translating it into NMDAR overactivation. Consistent with this hypothesis, we observe that mGluR5 blockade prevents the downstream NMDAR aberrant contribution in basal transmission and the LTD-to-LTP shift, supporting the mGluR5-NMDAR interplay as key player in the observed $A_{2A}R$-induced physiopathology.

Aging is associated with a decline in cognitive function that can, in part, be explained by changes in the mechanisms of plasticity (Burke and Barnes, 2006). While some studies report increased susceptibility to LTD during aging (Norris et al., 1996), others do not observe alterations in LTD magnitude between young and aged animals (Kumar et al., 2007). These discrepancies can be easily explained by differences in rat strain, stimulation pattern and Ca^{2+}/Mg^{2+} ratio. In fact, the stimulation pattern used in those studies (900 pulses, 1 Hz) does not elicit LTD in young animals (Kumar and Foster, 2005; Norris et al., 1996), while we and others observe a robust LTD with our LFS protocol (Ahmed et al., 2015; Laurent et al., 2016). Moreover, those age differences were reverted under elevated Ca^{2+}/Mg^{2+} ratio suggesting that aging is associated with a shift in the threshold for LTD-induction rather than in the LTD intrinsic capacity (Foster and Kumar, 2007; Kumar et al., 2007). Notably, the significant correlation between LTD magnitude and the frequency of LFS in Tg(CaMKII-$hA_{2A}R$) animals confirms an age-associated decrease in the threshold for LTD induction.

The fact that in aged CA1 pyramidal neurons there is an increased duration of NMDAR-mediated responses (Jouvenceau et al., 1998) which display an altered Ca^{2+} metabolism typified by larger increases upon repeated stimulation (Oh et al., 2013; Thibault et al., 2001) further strengthens our hypothesis. This increase in Ca^{2+} observed in aging can lead to CREB dephosphorylation due to an increase in calcineurin (PP2B) activity, strongly suggesting differential phosphatases and kinases activation as a key mediator in these impairments (Foster et al., 2001; Norris et al., 1998). Alterations in

phosphatases and kinases could directly account for the observed LTD-to-LTP shift. Importantly, we not only showed that susceptibility to induction of LTD is associated with memory impairments in aging, but also that the LTD magnitude could be positively correlated with behavior performance, consistent with previous data (Foster and Kumar, 2007; Lee et al., 2005).

The fact that an acute $A_{2A}R$ blockade is sufficient to rescue the LTD-to-LTP shift favors the hypothesis that $A_{2A}R$ blockade reestablishes the physiological signaling of adenosine, rather than the receptor expression which is unlikely to occur at such a short time frame. Accordingly, we have prior data showing that chronic KW6002 treatment rescues cognitive and synaptic impairments induced by stress, without altering $A_{2A}R$ levels (Batalha et al., 2013), as observed now in KW6002 treated Tg(CaMKII-h$A_{2A}R$) and aged animals.

There is a growing awareness of AD beginning as a synaptic pathology (Selkoe, 2002), but very little is known concerning LTD in these animals (Chang et al., 2006; D'Amelio et al., 2011; Yang et al., 2016). We now demonstrate that, as our Tg(CaMKII-h$A_{2A}R$) model, APP/PS1 animals exhibit this LTD-to-LTP shift. Alterations in NMDAR have been consistently linked to AD pathology (Auffret et al., 2010a, 2010b; Lanté et al., 2015; Pousinha et al., 2017; Snyder et al., 2005; Zhang et al., 2016) that we now report to be dependent on $A_{2A}R$ activation. This abnormal $A_{2A}R$/NMDAR cross-talk may underlie the efficiency of $A_{2A}R$ blockade in reverting memory deficits in animal models of AD (Dall'Igna et al., 2007; Laurent et al., 2016; Viana da Silva et al., 2016).

The combined evidence of an increased $A_{2A}R$ expression in hippocampal neurons from humans (aged individuals and AD patients) and from animal models of these physiopathological conditions (Figure 3.1; (Albasanz et al., 2008; Espinosa et al., 2013; Viana da Silva et al., 2016)) and the complete rescue of the LTD-to-LTP shift upon $A_{2A}R$ acute blockade stresses out $A_{2A}R$ as a pathological mediator involved in calcium dysfunction underlying age- and AD-related cognitive deficits, involving an aberrant recruitment of mGluR5/NMDAR coupled to an altered Ca^{2+} influx (see Figure 4.1 for a summary). These findings provide a neurophysiological basis to clarify the instrumental role of $A_{2A}R$ in pathology and strongly support the development of new $A_{2A}R$ antagonists in therapeutics.

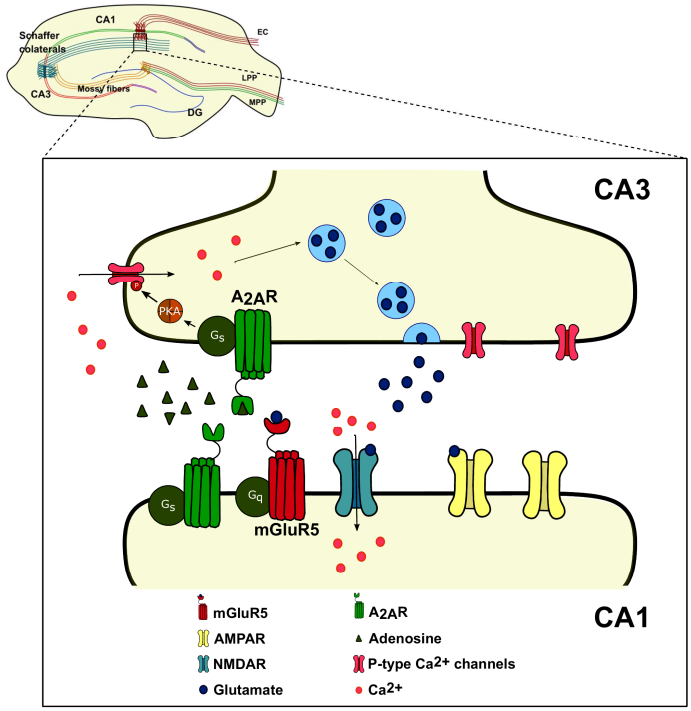

Figure 4.1. $A_{2A}R$/NMDAR/mGluR5 interplay in age-related synaptic dysfunction in the hippocampus. $A_{2A}R$ induce glutamate release possibly by a PKA-dependent P-type Ca^{2+} channels activation. Postsynaptically, mGluR5 may act as a glutamate sensor, translating it into NMDAR overactivation, which drives an increase in Ca^{2+} intracellular levels.

2. Future Perspectives

In this present study, I show that aging and AD are associated with increased levels of neuronal $A_{2A}R$. Moreover, such increase in neuronal $A_{2A}R$ is sufficient to drive deficits in synaptic plasticity, leading to an LTD-to-LTP shift and impairments of hippocampal-dependent learning and memory. This is a consequence of an $A_{2A}R$-induced increase in postsynaptic Ca^{2+} influx *via* mGluR5-dependent NMDAR dysfunction.

However, it also raised major questions that, in my opinion, need to be answered. Now that we described the pathophysiological role of $A_{2A}R$ in aging-associated synaptic deficits, what is the relative contribution to pathology of $A_{2A}R$ in other cell types, such as astrocytes? What is the structural identity of $A_{2A}R$? Which are the (epi)genetic/cellular/molecular drivers of this $A_{2A}R$ upsurge in the hippocampus in aging and pathology?

The fact that neuronal $A_{2A}R$ is sufficient to drive memory and synaptic defects does not exclude other cellular contributions of $A_{2A}R$. In fact, $A_{2A}R$ have a role in glutamate uptake in astrocytes (Matos et al., 2013) and can indeed lead to alterations of synaptic $A_{2A}R$-mediated functions (Matos et al., 2015). In the context of disease, astrocytic $A_{2A}R$ control amyloid-β peptide-induced decrease of glutamate uptake (Matos et al., 2012b) and AD is associated with increased levels of $A_{2A}R$ in astrocytes, both in humans and mice (Orr et al., 2015). However, in this last study, putative neuronal $A_{2A}R$ contribution to pathology was never addressed. Furthermore, stimulation of neuronal opto-$A_{2A}R$ in

the hippocampus induces changes in synaptic plasticity and CREB activation (Li et al., 2015a) and silencing $A_{2A}R$ in neurons of the associative/commissural pathway rescues the aberrant LTP in APP/PS1 mice (Viana da Silva et al., 2016).

All these data suggest that synaptic dysfunction in aging and early AD is driven predominantly by a neuronal $A_{2A}R$ progressive increase, whereas at later Braak stages of AD, astrocytic $A_{2A}R$ and inflammation might also play an important role (Laurent et al., 2016; Orr et al., 2015). Also, from a pure biological point of view, given that ATP is a ubiquitous molecule in the brain, $A_{2A}R$ are expressed in neurons, astrocytes and microglia and AD is associated with alterations in all these cells, we may expect that they all contribute to pathology. But which one appears first? Does neuronal $A_{2A}R$ increased levels drive an upsurge in astrocytes or microglia? Do they have the same relative contribution? All these questions still need to be clarified.

In addition to the increase in $A_{2A}R$ levels, upon aging and disease, this overexpression is accompanied by modifications in $A_{2A}R$ signaling. Concretely, $A_{2A}R$-dependent activation of glutamate release becomes more pronounced as aging progresses and shifts from a protein kinase C-mediated signaling to a cAMP-dependent effect (Lopes et al., 1999b).

$A_{2A}R$ has the ability to integrate both Gi- and Gs-dependent signals by forming heteromeric complexes at the presynapse. This remarkable property of such concentration-sensing device allows for fine-tuning the release of neurotransmitters. In the striatum, A_1R and $A_{2A}R$ are known to form heteromers whose main biochemical characteristic is

the ability of $A_{2A}R$ to reduce the affinity of A_1R, providing a switch mechanism by which low and high concentrations of adenosine inhibit and stimulate, respectively, glutamate release (Ciruela et al., 2006). In the hippocampus, although heteromers were never proven, activation of $A_{2A}R$ decreases A_1R binding, consequently inhibiting A_1R actions in young animals (Lopes et al., 1999b). Interestingly, this $A_{2A}R/A_1R$ receptor cross talk disappears in aged rats (Lopes et al., 1999b) and $A_{2A}R$-mediated responses are amplified, suggesting a change in heteromer formation. The fact that A_1R KO lose a significant amount of $A_{2A}R$ in the neuronal membrane, favours this hypothesis (Lopes et al., 2004). If a stoichiometric upsurge favouring non-heteromer forming $A_{2A}R$ results in Gs-dominant signaling (Chiodi et al., 2016), then an $A_{2A}R$ assembly switch could be the primary event driving this pathological glutamate output. Altogether, multiple evidences point towards a molecular shift in $A_{2A}R$. The clarification of transcriptional, post-transcriptional and post-translational regulation of the $A_{2A}R$ in youth *versus* aging is crucial. Also, the detection of A_1R-$A_{2A}R$ heteromers/$A_{2A}R$-$A_{2A}R$ homodimers in the hippocampus, by native gel or proximity ligation assay (PLA) techniques, will help to unravel the structural entity of the "pathological" $A_{2A}R$.

3. Acknowledgements

Esta tese não ficaria completa se não agradecesse a todos aqueles que permitiram que a realizasse com sucesso.

Em primeiro lugar, aos meus orientadores, Luísa e Tiago, por aceitarem percorrer este caminho comigo. Luísa, obrigada por me ter feito sempre ir mais além, que vibrou verdadeiramente com os meus sucessos e conquistas. Obrigada pela paixão que me transmitiu pelos nossos receptores da adenosina, pela boa disposição, pelos momentos inesquecíveis de *brainstorming*, por me dar independência e por me fazer sentir uma pessoa importante para o laboratório.

Minhas mentoras Joana e Diana, investigadoras de mão cheia. Obrigada pelos ensinamentos, sorrisos, alegria no trabalho!! Mais que tudo isso, obrigada pela vossa amizade.

Meus queridos *Loucus lopilis*, vocês trouxeram cor (e chocolates) aos meus dias! Obrigada por serem o meu pilar do dia-a-dia, nesta caminhada ingreme, tortuosa, mas com direito a alguns *sprints*.

Obrigada minha querida co-orientadora não oficial Paula, por me ter dado a conhecer o maravilhoso mundo das sinapses. O acompanhamento por terras de Napoleão foi fundamental e considero que marcou o início do desenrolar do novelo que foi este doutoramento.

A ti, Mário, por mesmo longe (e agora bem mais perto), seres um grande apoio, apoiares-me nas longas horas no laboratório, viveres as

minhas conquistas científicas com grande entusiasmo e seres um excelente ouvinte. Partilhar a vida contigo é um grande privilégio.

Nunca vou conseguir agradecer o suficiente aos meus pais e à minha irmã, Maria José. Serão sempre poucas as palavras que ilustrem o apoio incondicional que recebi, o entusiasmo que comigo partilharam. Orgulhosos de mim desde cedo, prometo não os desiludir.

A todos os restantes amigos e família com quem partilhei esta minha aventura e que ficavam deveras impressionados com a minha vertente de domadora de roedores. Obrigada por mostrarem interesse, ouvirem os meus desabafos e se rirem das minhas piadas palermas.

CHAPTER IV

References

Abraham, W.C., Christie, B.R., Logan, B., Lawlor, P., and Dragunow, M. (1994). Immediate early gene expression associated with the persistence of heterosynaptic long-term depression in the hippocampus. Proc. Natl. Acad. Sci. U. S. A. *91*, 10049–10053.

Abraham, W.C., Mason-Parker, S.E., and Logan, B. (1996). Low-frequency stimulation does not readily cause long-term depression or depotentiation in the dentate gyrus of awake rats. Brain Res. *722*, 217–221.

Abraham, W.C., Logan, B., Greenwood, J.M., and Dragunow, M. (2002). Induction and experience-dependent consolidation of stable long-term potentiation lasting months in the hippocampus. J. Neurosci. Off. J. Soc. Neurosci. *22*, 9626–9634.

Ahmed, T., Sabanov, V., D'Hooge, R., and Balschun, D. (2011). An N-methyl-D-aspartate-receptor dependent, late-phase long-term depression in middle-aged mice identifies no GluN2-subunit bias. Neuroscience *185*, 27–38.

Ahmed, T., Blum, D., Burnouf, S., Demeyer, D., Buée-Scherrer, V., D'Hooge, R., Buée, L., and Balschun, D. (2015). Rescue of impaired late-phase long-term depression in a tau transgenic mouse model. Neurobiol. Aging *36*, 730–739.

Albasanz, J.L., Perez, S., Barrachina, M., Ferrer, I., and Martín, M. (2008). Up-regulation of adenosine receptors in the frontal cortex in Alzheimer's disease. Brain Pathol. Zurich Switz. *18*, 211–219.

Almeida, C.G., Tampellini, D., Takahashi, R.H., Greengard, P., Lin, M.T., Snyder, E.M., and Gouras, G.K. (2005). Beta-amyloid accumulation in APP mutant neurons reduces PSD-95 and GluR1 in synapses. Neurobiol. Dis. *20*, 187–198.

Alves, N.D. (2017). Adult neural plasticity in the pathophysiology of depression: new insights from an animal model of recurrence. Universidade do Minho.

Amaral, D.G., and Witter, M.P. (1989). The three-dimensional organization of the hippocampal formation: a review of anatomical data. Neuroscience *31*, 571–591.

Amaral, D.G., Scharfman, H.E., and Lavenex, P. (2007). The dentate gyrus: fundamental neuroanatomical organization (dentate gyrus for dummies). Prog. Brain Res. *163*, 3–22.

Arch, J.R., and Newsholme, E.A. (1978). The control of the metabolism and the hormonal role of adenosine. Essays Biochem. *14*, 82–123.

Arendash, G.W., and Cao, C. (2010). Caffeine and coffee as therapeutics against Alzheimer's disease. J. Alzheimers Dis. JAD *20 Suppl 1*, S117-126.

Arendash, G.W., Schleif, W., Rezai-Zadeh, K., Jackson, E.K., Zacharia, L.C., Cracchiolo, J.R., Shippy, D., and Tan, J. (2006). Caffeine protects Alzheimer's mice against cognitive impairment and reduces brain beta-amyloid production. Neuroscience *142*, 941–952.

Armbrecht, H.J., Boltz, M.A., Kumar, V.B., Flood, J.F., and Morley, J.E. (1999). Effect of age on calcium-dependent proteins in hippocampus of senescence-accelerated mice. Brain Res. *842*, 287–293.

Arundine, M., and Tymianski, M. (2003). Molecular mechanisms of calcium-dependent neurodegeneration in excitotoxicity. Cell Calcium *34*, 325–337.

Ascherio, A., Zhang, S.M., Hernán, M.A., Kawachi, I., Colditz, G.A., Speizer, F.E., and Willett, W.C. (2001). Prospective study of caffeine consumption and risk of Parkinson's disease in men and women. Ann. Neurol. *50*, 56–63.

Auffret, A., Mariani, J., and Rovira, C. (2010a). Age-related progressive synaptic dysfunction: the critical role of presenilin 1. Rev. Neurosci. *21*, 239–250.

Auffret, A., Gautheron, V., Mattson, M.P., Mariani, J., and Rovira, C. (2010b). Progressive age-related impairment of the late long-term potentiation in Alzheimer's disease presenilin-1 mutant knock-in mice. J. Alzheimers Dis. JAD *19*, 1021–1033.

Augusto, E., Matos, M., Sévigny, J., El-Tayeb, A., Bynoe, M.S., Müller, C.E., Cunha, R.A., and Chen, J.-F. (2013). Ecto-5'-

nucleotidase (CD73)-mediated formation of adenosine is critical for the striatal adenosine A2A receptor functions. J. Neurosci. Off. J. Soc. Neurosci. *33*, 11390–11399.

Ball, M.J. (1977). Neuronal loss, neurofibrillary tangles and granulovacuolar degeneration in the hippocampus with ageing and dementia. A quantitative study. Acta Neuropathol. (Berl.) *37*, 111–118.

Bardenheuer, H., and Schrader, J. (1986). Supply-to-demand ratio for oxygen determines formation of adenosine by the heart. Am. J. Physiol. *250*, H173-180.

Barnes, C.A. (1979). Memory deficits associated with senescence: a neurophysiological and behavioral study in the rat. J. Comp. Physiol. Psychol. *93*, 74–104.

Barnes, C.A., Rao, G., Foster, T.C., and McNaughton, B.L. (1992). Region-specific age effects on AMPA sensitivity: electrophysiological evidence for loss of synaptic contacts in hippocampal field CA1. Hippocampus *2*, 457–468.

Barnes, C.A., Rao, G., and McNaughton, B.L. (1996). Functional integrity of NMDA-dependent LTP induction mechanisms across the lifespan of F-344 rats. Learn. Mem. Cold Spring Harb. N *3*, 124–137.

Barnes, C.A., Rao, G., and Shen, J. (1997). Age-related decrease in the N-methyl-D-aspartateR-mediated excitatory postsynaptic potential in hippocampal region CA1. Neurobiol. Aging *18*, 445–452.

Bartsch, T., and Wulff, P. (2015). The hippocampus in aging and disease: From plasticity to vulnerability. Neuroscience *309*, 1–16.

Bashir, Z.I., and Collingridge, G.L. (1994). An investigation of depotentiation of long-term potentiation in the CA1 region of the hippocampus. Exp. Brain Res. *100*, 437–443.

Bashir, Z.I., Jane, D.E., Sunter, D.C., Watkins, J.C., and Collingridge, G.L. (1993). Metabotropic glutamate receptors contribute to the induction of long-term depression in the CA1 region of the hippocampus. Eur. J. Pharmacol. *239*, 265–266.

Batalha, V.L., Pego, J.M., Fontinha, B.M., Costenla, A.R., Valadas, J.S., Baqi, Y., Radjainia, H., Müller, C.E., Sebastião, A.M., and Lopes, L.V. (2013). Adenosine A(2A) receptor blockade reverts hippocampal stress-induced deficits and restores corticosterone circadian oscillation. Mol. Psychiatry *18*, 320–331.

Batalha, V.L., Ferreira, D.G., Coelho, J.E., Valadas, J.S., Gomes, R., Temido-Ferreira, M., Shmidt, T., Baqi, Y., Buée, L., Müller, C.E., et al. (2016). The caffeine-binding adenosine A2A receptor induces age-like HPA-axis dysfunction by targeting glucocorticoid receptor function. Sci. Rep. *6*, 31493.

Bear, M.F., Cooper, L.N., and Ebner, F.F. (1987). A physiological basis for a theory of synapse modification. Science *237*, 42–48.

Bienenstock, E.L., Cooper, L.N., and Munro, P.W. (1982). Theory for the development of neuron selectivity: orientation specificity and binocular interaction in visual cortex. J. Neurosci. Off. J. Soc. Neurosci. *2*, 32–48.

Billard, J.-M., and Rouaud, E. (2007). Deficit of NMDA receptor activation in CA1 hippocampal area of aged rats is rescued by D-cycloserine. Eur. J. Neurosci. *25*, 2260–2268.

Bizon, J.L., and Gallagher, M. (2005). More is less: neurogenesis and age-related cognitive decline in Long-Evans rats. Sci. Aging Knowl. Environ. SAGE KE *2005*, re2.

Bizon, J.L., Lee, H.J., and Gallagher, M. (2004). Neurogenesis in a rat model of age-related cognitive decline. Aging Cell *3*, 227–234.

Bliss, T.V., and Collingridge, G.L. (1993). A synaptic model of memory: long-term potentiation in the hippocampus. Nature *361*, 31–39.

Boison, D., Chen, J.-F., and Fredholm, B.B. (2010). Adenosine signaling and function in glial cells. Cell Death Differ. *17*, 1071–1082.

Borota, D., Murray, E., Keceli, G., Chang, A., Watabe, J.M., Ly, M., Toscano, J.P., and Yassa, M.A. (2014). Post-study caffeine administration enhances memory consolidation in humans. Nat. Neurosci. *17*, 201–203.

Borycz, J., Pereira, M.F., Melani, A., Rodrigues, R.J., Köfalvi, A., Panlilio, L., Pedata, F., Goldberg, S.R., Cunha, R.A., and Ferré, S. (2007). Differential glutamate-dependent and glutamate-independent adenosine A1 receptor-mediated modulation of dopamine release in different striatal compartments. J. Neurochem. *101*, 355–363.

de Brabander, J.M., Kramers, R.J., and Uylings, H.B. (1998). Layer-specific dendritic regression of pyramidal cells with ageing in the human prefrontal cortex. Eur. J. Neurosci. *10*, 1261–1269.

Brambilla, R., Cottini, L., Fumagalli, M., Ceruti, S., and Abbracchio, M.P. (2003). Blockade of A2A adenosine receptors prevents basic fibroblast growth factor-induced reactive astrogliosis in rat striatal primary astrocytes. Glia *43*, 190–194.

Brim, B.L., Haskell, R., Awedikian, R., Ellinwood, N.M., Jin, L., Kumar, A., Foster, T.C., and Magnusson, K.R. (2013). Memory in aged mice is rescued by enhanced expression of the GluN2B subunit of the NMDA receptor. Behav. Brain Res. *238*, 211–226.

Brizzee, K.R., Ordy, J.M., and Bartus, R.T. (1980). Localization of cellular changes within multimodal sensory regions in aged monkey brain: possible implications for age-related cognitive loss. Neurobiol. Aging *1*, 45–52.

Brody, H. (1955). Organization of the cerebral cortex. III. A study of aging in the human cerebral cortex. J. Comp. Neurol. *102*, 511–516.

Bu, J., Sathyendra, V., Nagykery, N., and Geula, C. (2003). Age-related changes in calbindin-D28k, calretinin, and parvalbumin-immunoreactive neurons in the human cerebral cortex. Exp. Neurol. *182*, 220–231.

Buell, S.J., and Coleman, P.D. (1979). Dendritic growth in the aged human brain and failure of growth in senile dementia. Science *206*, 854–856.

Buell, S.J., and Coleman, P.D. (1981). Quantitative evidence for selective dendritic growth in normal human aging but not in senile dementia. Brain Res. *214*, 23–41.

Burke, S.N., and Barnes, C.A. (2006). Neural plasticity in the ageing brain. Nat. Rev. Neurosci. *7*, 30–40.

Burke, S.N., and Barnes, C.A. (2010). Senescent synapses and hippocampal circuit dynamics. Trends Neurosci. *33*, 153–161.

Burnouf, S., Martire, A., Derisbourg, M., Laurent, C., Belarbi, K., Leboucher, A., Fernandez-Gomez, F.J., Troquier, L., Eddarkaoui, S., Grosjean, M.-E., et al. (2013). NMDA receptor dysfunction contributes to impaired brain-derived neurotrophic factor-induced facilitation of hippocampal synaptic transmission in a Tau transgenic model. Aging Cell *12*, 11–23.

Bustin, S.A., Benes, V., Garson, J.A., Hellemans, J., Huggett, J., Kubista, M., Mueller, R., Nolan, T., Pfaffl, M.W., Shipley, G.L., et al. (2009). The MIQE guidelines: minimum information for publication of quantitative real-time PCR experiments. Clin. Chem. *55*, 611–622.

Campbell, L.W., Hao, S.Y., Thibault, O., Blalock, E.M., and Landfield, P.W. (1996). Aging changes in voltage-gated calcium currents in hippocampal CA1 neurons. J. Neurosci. Off. J. Soc. Neurosci. *16*, 6286–6295.

Canas, P.M., Duarte, J.M.N., Rodrigues, R.J., Köfalvi, A., and Cunha, R.A. (2009). Modification upon aging of the density of presynaptic modulation systems in the hippocampus. Neurobiol. Aging *30*, 1877–1884.

Canhão, P., de Mendonça, A., and Ribeiro, J.A. (1994). 1,3-Dipropyl-8-cyclopentylxanthine attenuates the NMDA response to hypoxia in the rat hippocampus. Brain Res. *661*, 265–273.

Cao, C., Loewenstein, D.A., Lin, X., Zhang, C., Wang, L., Duara, R., Wu, Y., Giannini, A., Bai, G., Cai, J., et al. (2012). High Blood caffeine levels in MCI linked to lack of progression to dementia. J. Alzheimers Dis. JAD *30*, 559–572.

Chang, E.H., Savage, M.J., Flood, D.G., Thomas, J.M., Levy, R.B., Mahadomrongkul, V., Shirao, T., Aoki, C., and Huerta, P.T. (2006). AMPA receptor downscaling at the onset of Alzheimer's disease pathology in double knockin mice. Proc. Natl. Acad. Sci. U. S. A. *103*, 3410–3415.

Chiodi, V., Ferrante, A., Ferraro, L., Potenza, R.L., Armida, M., Beggiato, S., Pèzzola, A., Bader, M., Fuxe, K., Popoli, P., et al. (2016). Striatal adenosine-cannabinoid receptor interactions in rats over-expressing adenosine A2A receptors. J. Neurochem. *136*, 907–917.

Cho, K., Kemp, N., Noel, J., Aggleton, J.P., Brown, M.W., and Bashir, Z.I. (2000). A new form of long-term depression in the perirhinal cortex. Nat. Neurosci. *3*, 150–156.

Christie, B.R., Schexnayder, L.K., and Johnston, D. (1997). Contribution of voltage-gated Ca2+ channels to homosynaptic long-term depression in the CA1 region in vitro. J. Neurophysiol. *77*, 1651–1655.

Ciruela, F., Casadó, V., Rodrigues, R.J., Luján, R., Burgueño, J., Canals, M., Borycz, J., Rebola, N., Goldberg, S.R., Mallol, J., et al. (2006). Presynaptic control of striatal glutamatergic neurotransmission by adenosine A1-A2A receptor heteromers. J. Neurosci. Off. J. Soc. Neurosci. *26*, 2080–2087.

Citri, A., and Malenka, R.C. (2008). Synaptic plasticity: multiple forms, functions, and mechanisms. Neuropsychopharmacol. Off. Publ. Am. Coll. Neuropsychopharmacol. *33*, 18–41.

Clayton, D.A., Grosshans, D.R., and Browning, M.D. (2002). Aging and surface expression of hippocampal NMDA receptors. J. Biol. Chem. *277*, 14367–14369.

Coelho, J.E., Alves, P., Canas, P.M., Valadas, J.S., Shmidt, T., Batalha, V.L., Ferreira, D.G., Ribeiro, J.A., Bader, M., Cunha, R.A., et al. (2014a). Overexpression of Adenosine A2A Receptors in Rats: Effects on Depression, Locomotion, and Anxiety. Front. Psychiatry *5*, 67.

Coelho, J.E., Alves, P., Canas, P.M., Valadas, J.S., Shmidt, T., Batalha, V.L., Ferreira, D.G., Ribeiro, J.A., Bader, M., Cunha, R.A., et al. (2014b). Overexpression of Adenosine A2A Receptors in Rats: Effects on Depression, Locomotion, and Anxiety. Front. Psychiatry *5*, 67.

Coleman, P.D., and Flood, D.G. (1987). Neuron numbers and dendritic extent in normal aging and Alzheimer's disease. Neurobiol. Aging *8*, 521–545.

Collingridge, G.L., Kehl, S.J., and McLennan, H. (1983). Excitatory amino acids in synaptic transmission in the Schaffer collateral-commissural pathway of the rat hippocampus. J. Physiol. *334*, 33–46.

Collingridge, G.L., Peineau, S., Howland, J.G., and Wang, Y.T. (2010). Long-term depression in the CNS. Nat. Rev. Neurosci. *11*, 459–473.

Colombo, P.J., Wetsel, W.C., and Gallagher, M. (1997). Spatial memory is related to hippocampal subcellular concentrations of calcium-dependent protein kinase C isoforms in young and aged rats. Proc. Natl. Acad. Sci. U. S. A. *94*, 14195–14199.

Costa, M.S., Botton, P.H., Mioranzza, S., Souza, D.O., and Porciúncula, L.O. (2008). Caffeine prevents age-associated recognition memory decline and changes brain-derived neurotrophic factor and tirosine kinase receptor (TrkB) content in mice. Neuroscience *153*, 1071–1078.

Costenla, A.R., de Mendonça, A., and Ribeiro, J.A. (1999). Adenosine modulates synaptic plasticity in hippocampal slices from aged rats. Brain Res. *851*, 228–234.

Costenla, A.R., Diógenes, M.J., Canas, P.M., Rodrigues, R.J., Nogueira, C., Maroco, J., Agostinho, P.M., Ribeiro, J.A., Cunha, R.A., and de Mendonça, A. (2011). Enhanced role of adenosine A(2A) receptors in the modulation of LTP in the rat hippocampus upon ageing. Eur. J. Neurosci. *34*, 12–21.

Costes, S.V., Daelemans, D., Cho, E.H., Dobbin, Z., Pavlakis, G., and Lockett, S. (2004). Automatic and quantitative measurement of protein-protein colocalization in live cells. Biophys. J. *86*, 3993–4003.

Cramer, P.E., Cirrito, J.R., Wesson, D.W., Lee, C.Y.D., Karlo, J.C., Zinn, A.E., Casali, B.T., Restivo, J.L., Goebel, W.D., James, M.J., et al. (2012). ApoE-directed therapeutics rapidly clear β-amyloid and reverse deficits in AD mouse models. Science *335*, 1503–1506.

Cristóvão-Ferreira, S., Navarro, G., Brugarolas, M., Pérez-Capote, K., Vaz, S.H., Fattorini, G., Conti, F., Lluis, C., Ribeiro, J.A., McCormick, P.J., et al. (2013). A1R-A2AR heteromers coupled to Gs and G i/0 proteins modulate GABA transport into astrocytes. Purinergic Signal. *9*, 433–449.

Cummings, J.A., Mulkey, R.M., Nicoll, R.A., and Malenka, R.C. (1996). Ca2+ signaling requirements for long-term depression in the hippocampus. Neuron *16*, 825–833.

Cunha, R.A. (2001). Adenosine as a neuromodulator and as a homeostatic regulator in the nervous system: different roles, different sources and different receptors. Neurochem. Int. *38*, 107–125.

Cunha, R.A. (2016). How does adenosine control neuronal dysfunction and neurodegeneration? J. Neurochem. *139*, 1019–1055.

Cunha, R.A., and Ribeiro, J.A. (2000). Purinergic modulation of [(3)H]GABA release from rat hippocampal nerve terminals. Neuropharmacology *39*, 1156–1167.

Cunha, G.M.A., Canas, P.M., Oliveira, C.R., and Cunha, R.A. (2006). Increased density and synapto-protective effect of adenosine A2A receptors upon sub-chronic restraint stress. Neuroscience *141*, 1775–1781.

Cunha, G.M.A., Canas, P.M., Melo, C.S., Hockemeyer, J., Müller, C.E., Oliveira, C.R., and Cunha, R.A. (2008). Adenosine A2A receptor blockade prevents memory dysfunction caused by beta-amyloid peptides but not by scopolamine or MK-801. Exp. Neurol. *210*, 776–781.

Cunha, R.A., Johansson, B., van der Ploeg, I., Sebastião, A.M., Ribeiro, J.A., and Fredholm, B.B. (1994a). Evidence for functionally important adenosine A2a receptors in the rat hippocampus. Brain Res. *649*, 208–216.

Cunha, R.A., Milusheva, E., Vizi, E.S., Ribeiro, J.A., and Sebastião, A.M. (1994b). Excitatory and inhibitory effects of A1 and A2A adenosine receptor activation on the electrically evoked [3H]acetylcholine release from different areas of the rat hippocampus. J. Neurochem. *63*, 207–214.

Cunha, R.A., Constantino, M.C., Sebastião, A.M., and Ribeiro, J.A. (1995). Modification of A1 and A2a adenosine receptor binding in aged striatum, hippocampus and cortex of the rat. Neuroreport *6*, 1583–1588.

Curcio, C.A., and Hinds, J.W. (1983). Stability of synaptic density and spine volume in dentate gyrus of aged rats. Neurobiol. Aging *4*, 77–87.

Dall'Igna, O.P., Fett, P., Gomes, M.W., Souza, D.O., Cunha, R.A., and Lara, D.R. (2007). Caffeine and adenosine A(2a) receptor antagonists prevent beta-amyloid (25-35)-induced cognitive deficits in mice. Exp. Neurol. *203*, 241–245.

Daly, J.W. (1982). Adenosine receptors: targets for future drugs. J. Med. Chem. *25*, 197–207.

D'Amelio, M., Cavallucci, V., Middei, S., Marchetti, C., Pacioni, S., Ferri, A., Diamantini, A., De Zio, D., Carrara, P., Battistini, L., et al. (2011). Caspase-3 triggers early synaptic dysfunction in a mouse model of Alzheimer's disease. Nat. Neurosci. *14*, 69–76.

Daré, E., Schulte, G., Karovic, O., Hammarberg, C., and Fredholm, B.B. (2007). Modulation of glial cell functions by adenosine receptors. Physiol. Behav. *92*, 15–20.

Davis, S., Salin, H., Helme-Guizon, A., Dumas, S., Stéphan, A., Corbex, M., Mallet, J., and Laroche, S. (2000). Dysfunctional regulation of alphaCaMKII and syntaxin 1B transcription after induction of LTP in the aged rat. Eur. J. Neurosci. *12*, 3276–3282.

DeKosky, S.T., and Scheff, S.W. (1990). Synapse loss in frontal cortex biopsies in Alzheimer's disease: correlation with cognitive severity. Ann. Neurol. *27*, 457–464.

Delorenzo, R.J., Sun, D.A., and Deshpande, L.S. (2005). Cellular mechanisms underlying acquired epilepsy: the calcium hypothesis of the induction and maintainance of epilepsy. Pharmacol. Ther. *105*, 229–266.

Deupree, D.L., Bradley, J., and Turner, D.A. (1993). Age-related alterations in potentiation in the CA1 region in F344 rats. Neurobiol. Aging *14*, 249–258.

Dias, R.B., Ribeiro, J.A., and Sebastião, A.M. (2012). Enhancement of AMPA currents and GluR1 membrane expression through PKA-coupled adenosine A(2A) receptors. Hippocampus *22*, 276–291.

Diógenes, M.J., Fernandes, C.C., Sebastião, A.M., and Ribeiro, J.A. (2004). Activation of adenosine A2A receptor facilitates brain-derived neurotrophic factor modulation of synaptic transmission in hippocampal slices. J. Neurosci. Off. J. Soc. Neurosci. *24*, 2905–2913.

Diógenes, M.J., Assaife-Lopes, N., Pinto-Duarte, A., Ribeiro, J.A., and Sebastião, A.M. (2007a). Influence of age on BDNF modulation of hippocampal synaptic transmission: interplay with adenosine A2A receptors. Hippocampus *17*, 577–585.

Diógenes, M.J., Assaife-Lopes, N., Pinto-Duarte, A., Ribeiro, J.A., and Sebastião, A.M. (2007b). Influence of age on BDNF modulation of hippocampal synaptic transmission: Interplay with adenosine A2A receptors. Hippocampus *17*, 577–585.

Diógenes, M.J., Costenla, A.R., Lopes, L.V., Jerónimo-Santos, A., Sousa, V.C., Fontinha, B.M., Ribeiro, J.A., and Sebastião, A.M. (2011). Enhancement of LTP in aged rats is dependent on endogenous BDNF. Neuropsychopharmacol. Off. Publ. Am. Coll. Neuropsychopharmacol. *36*, 1823–1836.

Dong, Z., Bai, Y., Wu, X., Li, H., Gong, B., Howland, J.G., Huang, Y., He, W., Li, T., and Wang, Y.T. (2013). Hippocampal long-term depression mediates spatial reversal learning in the Morris water maze. Neuropharmacology *64*, 65–73.

Dudek, S.M., and Bear, M.F. (1992). Homosynaptic long-term depression in area CA1 of hippocampus and effects of N-methyl-D-aspartate receptor blockade. Proc. Natl. Acad. Sci. U. S. A. *89*, 4363–4367.

Eckles, K.E., and Browning, M.D. (1997). Functional changes in the NMDA receptor of aged F344 rats. In Soc Neuosci Abstr, p. 23:575.

Eckles, K.E., Dudek, E.M., Bickford, P.C., and Browning, M.D. (1997). Amelioration of age-related deficits in the stimulation of synapsin phosphorylation. Neurobiol. Aging *18*, 213–217.

Elsaesser, A., Barnes, C.A., McKerr, G., Salvati, A., Lynch, I., Dawson, K.A., and Howard, C.V. (2011). Quantification of nanoparticle uptake by cells using an unbiased sampling method and electron microscopy. Nanomed. *6*, 1189–1198.

Enoki, R., Hu, Y.-L., Hamilton, D., and Fine, A. (2009). Expression of long-term plasticity at individual synapses in hippocampus is graded, bidirectional, and mainly presynaptic: optical quantal analysis. Neuron *62*, 242–253.

Erickson, C.A., and Barnes, C.A. (2003). The neurobiology of memory changes in normal aging. Exp. Gerontol. *38*, 61–69.

Eskelinen, M.H., Ngandu, T., Tuomilehto, J., Soininen, H., and Kivipelto, M. (2009). Midlife coffee and tea drinking and the risk of late-life dementia: a population-based CAIDE study. J. Alzheimers Dis. JAD *16*, 85–91.

Espinosa, J., Rocha, A., Nunes, F., Costa, M.S., Schein, V., Kazlauckas, V., Kalinine, E., Souza, D.O., Cunha, R.A., and Porciúncula, L.O. (2013). Caffeine consumption prevents memory impairment, neuronal damage, and adenosine A2A receptors upregulation in the hippocampus of a rat model of sporadic dementia. J. Alzheimers Dis. JAD *34*, 509–518.

Feinmark, S.J., Begum, R., Tsvetkov, E., Goussakov, I., Funk, C.D., Siegelbaum, S.A., and Bolshakov, V.Y. (2003). 12-lipoxygenase metabolites of arachidonic acid mediate metabotropic glutamate receptor-dependent long-term depression at hippocampal CA3-CA1 synapses. J. Neurosci. Off. J. Soc. Neurosci. *23*, 11427–11435.

Ferré, S., Ciruela, F., Quiroz, C., Luján, R., Popoli, P., Cunha, R.A., Agnati, L.F., Fuxe, K., Woods, A.S., Lluis, C., et al. (2007). Adenosine receptor heteromers and their integrative role in striatal function. ScientificWorldJournal *7*, 74–85.

Ferreira, D.G., Temido-Ferreira, M., Miranda, H.V., Batalha, V.L., Coelho, J.E., Szegö, É.M., Marques-Morgado, I., Vaz, S.H., Rhee, J.S., Schmitz, M., et al. (2017a). α-synuclein interacts with PrP(C) to induce cognitive impairment through mGluR5 and NMDAR2B. Nat. Neurosci. *20*, 1569–1579.

Ferreira, D.G., Batalha, V.L., Vicente Miranda, H., Coelho, J.E., Gomes, R., Gonçalves, F.Q., Real, J.I., Rino, J., Albino-Teixeira, A., Cunha, R.A., et al. (2017b). Adenosine A2A Receptors Modulate α-Synuclein Aggregation and Toxicity. Cereb. Cortex N. Y. N 1991 *27*, 718–730.

Ferreira, S.G., Gonçalves, F.Q., Marques, J.M., Tomé, Â.R., Rodrigues, R.J., Nunes-Correia, I., Ledent, C., Harkany, T., Venance, L., Cunha, R.A., et al. (2015). Presynaptic adenosine A2A receptors dampen cannabinoid CB1 receptor-mediated inhibition of corticostriatal glutamatergic transmission. Br. J. Pharmacol. *172*, 1074–1086.

Fink, J.S., Weaver, D.R., Rivkees, S.A., Peterfreund, R.A., Pollack, A.E., Adler, E.M., and Reppert, S.M. (1992). Molecular cloning of the rat A2 adenosine receptor: selective co-expression with D2 dopamine receptors in rat striatum. Brain Res. Mol. Brain Res. *14*, 186–195.

Flood, D.G., Buell, S.J., Defiore, C.H., Horwitz, G.J., and Coleman, P.D. (1985). Age-related dendritic growth in dentate gyrus of human brain is followed by regression in the "oldest old." Brain Res. *345*, 366–368.

Flood, D.G., Buell, S.J., Horwitz, G.J., and Coleman, P.D. (1987a). Dendritic extent in human dentate gyrus granule cells in normal aging and senile dementia. Brain Res. *402*, 205–216.

Flood, D.G., Guarnaccia, M., and Coleman, P.D. (1987b). Dendritic extent in human CA2-3 hippocampal pyramidal neurons in normal aging and senile dementia. Brain Res. *409*, 88–96.

Fontinha, B.M., Diógenes, M.J., Ribeiro, J.A., and Sebastião, A.M. (2008). Enhancement of long-term potentiation by brain-derived neurotrophic factor requires adenosine A2A receptor activation by endogenous adenosine. Neuropharmacology *54*, 924–933.

Fontinha, B.M., Delgado-García, J.M., Madroñal, N., Ribeiro, J.A., Sebastião, A.M., and Gruart, A. (2009). Adenosine A(2A) receptor modulation of hippocampal CA3-CA1 synapse plasticity during associative learning in behaving mice. Neuropsychopharmacol. Off. Publ. Am. Coll. Neuropsychopharmacol. *34*, 1865–1874.

Foster, T.C. (2004). Age-related changes in synaptic phosphorylation and dephosphorylation. In Advances in Cell Aging and Gerontology, (Elsevier), pp. 133–152.

Foster, T.C., and Kumar, A. (2002). Calcium dysregulation in the aging brain. Neurosci. Rev. J. Bringing Neurobiol. Neurol. Psychiatry *8*, 297–301.

Foster, T.C., and Kumar, A. (2007). Susceptibility to induction of long-term depression is associated with impaired memory in aged Fischer 344 rats. Neurobiol. Learn. Mem. *87*, 522–535.

Foster, T.C., and Norris, C.M. (1997). Age-associated changes in Ca(2+)-dependent processes: relation to hippocampal synaptic plasticity. Hippocampus *7*, 602–612.

Foster, T.C., Barnes, C.A., Rao, G., and McNaughton, B.L. (1991). Increase in perforant path quantal size in aged F-344 rats. Neurobiol. Aging *12*, 441–448.

Foster, T.C., Sharrow, K.M., Masse, J.R., Norris, C.M., and Kumar, A. (2001). Calcineurin links Ca2+ dysregulation with brain aging. J. Neurosci. Off. J. Soc. Neurosci. *21*, 4066–4073.

Foy, M.R., Stanton, M.E., Levine, S., and Thompson, R.F. (1987). Behavioral stress impairs long-term potentiation in rodent hippocampus. Behav. Neural Biol. *48*, 138–149.

Fredholm, B.B., IJzerman, A.P., Jacobson, K.A., Klotz, K.N., and Linden, J. (2001). International Union of Pharmacology. XXV. Nomenclature and classification of adenosine receptors. Pharmacol. Rev. *53*, 527–552.

Fujii, S., Saito, K., Miyakawa, H., Ito, K., and Kato, H. (1991). Reversal of long-term potentiation (depotentiation) induced by tetanus stimulation of the input to CA1 neurons of guinea pig hippocampal slices. Brain Res. *555*, 112–122.

Gant, J.C., Sama, M.M., Landfield, P.W., and Thibault, O. (2006). Early and simultaneous emergence of multiple hippocampal biomarkers of aging is mediated by Ca2+-induced Ca2+ release. J. Neurosci. Off. J. Soc. Neurosci. *26*, 3482–3490.

Garção, P., Szabó, E.C., Wopereis, S., Castro, A.A., Tomé, Â.R., Prediger, R.D., Cunha, R.A., Agostinho, P., and Köfalvi, A. (2013). Functional interaction between pre-synaptic α6β2-containing nicotinic and adenosine A2A receptors in the control of dopamine release in the rat striatum. Br. J. Pharmacol. *169*, 1600–1611.

Garman, R.H. (2011). Histology of the central nervous system. Toxicol. Pathol. *39*, 22–35.

Gazzaley, A.H., Thakker, M.M., Hof, P.R., and Morrison, J.H. (1997). Preserved number of entorhinal cortex layer II neurons in aged macaque monkeys. Neurobiol. Aging *18*, 549–553.

Ge, Y., Dong, Z., Bagot, R.C., Howland, J.G., Phillips, A.G., Wong, T.P., and Wang, Y.T. (2010). Hippocampal long-term depression is required for the consolidation of spatial memory. Proc. Natl. Acad. Sci. U. S. A. *107*, 16697–16702.

Gelber, R.P., Petrovitch, H., Masaki, K.H., Ross, G.W., and White, L.R. (2011). Coffee intake in midlife and risk of dementia and its neuropathologic correlates. J. Alzheimers Dis. JAD *23*, 607–615.

van Gelder, B.M., Buijsse, B., Tijhuis, M., Kalmijn, S., Giampaoli, S., Nissinen, A., and Kromhout, D. (2007). Coffee consumption is inversely associated with cognitive decline in elderly European men: the FINE Study. Eur. J. Clin. Nutr. *61*, 226–232.

Geula, C., Bu, J., Nagykery, N., Scinto, L.F.M., Chan, J., Joseph, J., Parker, R., and Wu, C.-K. (2003). Loss of calbindin-D28k from aging human cholinergic basal forebrain: relation to neuronal loss. J. Comp. Neurol. *455*, 249–259.

Gibson, G., Perrino, P., and Dienel, G.A. (1986). In vivo brain calcium homeostasis during aging. Mech. Ageing Dev. *37*, 1–12.

Giménez-Llort, L., Schiffmann, S.N., Shmidt, T., Canela, L., Camón, L., Wassholm, M., Canals, M., Terasmaa, A., Fernández-Teruel, A., Tobeña, A., et al. (2007). Working memory deficits in transgenic rats overexpressing human adenosine A2A receptors in the brain. Neurobiol. Learn. Mem. *87*, 42–56.

Gladding, C.M., Collett, V.J., Jia, Z., Bashir, Z.I., Collingridge, G.L., and Molnár, E. (2009). Tyrosine dephosphorylation regulates AMPAR internalisation in mGluR-LTD. Mol. Cell. Neurosci. *40*, 267–279.

Gonçalves, M.L., Cunha, R.A., and Ribeiro, J.A. (1997). Adenosine A2A receptors facilitate 45Ca2+ uptake through class A calcium channels in rat hippocampal CA3 but not CA1 synaptosomes. Neurosci. Lett. *238*, 73–77.

Grill, J.D., and Riddle, D.R. (2002). Age-related and laminar-specific dendritic changes in the medial frontal cortex of the rat. Brain Res. *937*, 8–21.

Gyoneva, S., Shapiro, L., Lazo, C., Garnier-Amblard, E., Smith, Y., Miller, G.W., and Traynelis, S.F. (2014). Adenosine A2A receptor antagonism reverses inflammation-induced impairment of microglial process extension in a model of Parkinson's disease. Neurobiol. Dis. *67*, 191–202.

Hajieva, P., Kuhlmann, C., Luhmann, H.J., and Behl, C. (2009). Impaired calcium homeostasis in aged hippocampal neurons. Neurosci. Lett. *451*, 119–123.

Hanks, S.D., and Flood, D.G. (1991). Region-specific stability of dendritic extent in normal human aging and regression in Alzheimer's disease. I. CA1 of hippocampus. Brain Res. *540*, 63–82.

Hockemeyer, J., Burbiel, J.C., and Müller, C.E. (2004). Multigram-scale syntheses, stability, and photoreactions of A2A adenosine receptor antagonists with 8-styrylxanthine structure: potential drugs for Parkinson's disease. J. Org. Chem. *69*, 3308–3318.

Horgusluoglu-Moloch, E., Nho, K., Risacher, S.L., Kim, S., Foroud, T., Shaw, L.M., Trojanowski, J.Q., Aisen, P.S., Petersen, R.C., Jack, C.R., et al. (2017). Targeted neurogenesis pathway-based gene analysis identifies ADORA2A associated with hippocampal volume in mild cognitive impairment and Alzheimer's disease. Neurobiol. Aging *60*, 92–103.

Huang, Y.-Y., and Kandel, E.R. (2006). Age-related enhancement of a protein synthesis-dependent late phase of LTP induced by low

frequency paired-pulse stimulation in hippocampus. Learn. Mem. Cold Spring Harb. N *13*, 298–306.

Huber, K.M., Roder, J.C., and Bear, M.F. (2001). Chemical induction of mGluR5- and protein synthesis--dependent long-term depression in hippocampal area CA1. J. Neurophysiol. *86*, 321–325.

Impey, S., Smith, D.M., Obrietan, K., Donahue, R., Wade, C., and Storm, D.R. (1998). Stimulation of cAMP response element (CRE)-mediated transcription during contextual learning. Nat. Neurosci. *1*, 595–601.

Ingram, D.K., Garofalo, P., Spangler, E.L., Mantione, C.R., Odano, I., and London, E.D. (1992). Reduced density of NMDA receptors and increased sensitivity to dizocilpine-induced learning impairment in aged rats. Brain Res. *580*, 273–280.

Jankowsky, J.L., Slunt, H.H., Ratovitski, T., Jenkins, N.A., Copeland, N.G., and Borchelt, D.R. (2001). Co-expression of multiple transgenes in mouse CNS: a comparison of strategies. Biomol. Eng. *17*, 157–165.

Jarvis, M.F., and Williams, M. (1989). Direct autoradiographic localization of adenosine A2 receptors in the rat brain using the A2-selective agonist, [3H]CGS 21680. Eur. J. Pharmacol. *168*, 243–246.

Jia, Z., Lu, Y., Henderson, J., Taverna, F., Romano, C., Abramow-Newerly, W., Wojtowicz, J.M., and Roder, J. (1998). Selective abolition of the NMDA component of long-term potentiation in mice lacking mGluR5. Learn. Mem. Cold Spring Harb. N *5*, 331–343.

de Jong, G.I., Naber, P.A., Van der Zee, E.A., Thompson, L.T., Disterhoft, J.F., and Luiten, P.G. (1996). Age-related loss of calcium binding proteins in rabbit hippocampus. Neurobiol. Aging *17*, 459–465.

Jouvenceau, A., Dutar, P., and Billard, J.M. (1998). Alteration of NMDA receptor-mediated synaptic responses in CA1 area of the aged rat hippocampus: contribution of GABAergic and cholinergic deficits. Hippocampus *8*, 627–637.

Kameyama, K., Lee, H.K., Bear, M.F., and Huganir, R.L. (1998). Involvement of a postsynaptic protein kinase A substrate in the

expression of homosynaptic long-term depression. Neuron *21*, 1163–1175.

Karege, F., Lambercy, C., Schwald, M., Steimer, T., and Cissé, M. (2001). Differential changes of cAMP-dependent protein kinase activity and 3H-cAMP binding sites in rat hippocampus during maturation and aging. Neurosci. Lett. *315*, 89–92.

Kaster, M.P., Machado, N.J., Silva, H.B., Nunes, A., Ardais, A.P., Santana, M., Baqi, Y., Müller, C.E., Rodrigues, A.L.S., Porciúncula, L.O., et al. (2015). Caffeine acts through neuronal adenosine A2A receptors to prevent mood and memory dysfunction triggered by chronic stress. Proc. Natl. Acad. Sci. U. S. A. *112*, 7833–7838.

Kemp, N., and Bashir, Z.I. (2001). Long-term depression: a cascade of induction and expression mechanisms. Prog. Neurobiol. *65*, 339–365.

Kemp, N., McQueen, J., Faulkes, S., and Bashir, Z.I. (2000). Different forms of LTD in the CA1 region of the hippocampus: role of age and stimulus protocol. Eur. J. Neurosci. *12*, 360–366.

Keuker, J.I.H., Luiten, P.G.M., and Fuchs, E. (2003). Preservation of hippocampal neuron numbers in aged rhesus monkeys. Neurobiol. Aging *24*, 157–165.

Khachaturian, Z.S. (1989). The role of calcium regulation in brain aging: reexamination of a hypothesis. Aging Milan Italy *1*, 17–34.

Khachaturian, Z.S. (1994). Calcium hypothesis of Alzheimer's disease and brain aging. Ann. N. Y. Acad. Sci. *747*, 1–11.

Kirk, I.P., and Richardson, P.J. (1995). Further characterization of [3H]-CGS 21680 binding sites in the rat striatum and cortex. Br. J. Pharmacol. *114*, 537–543.

Kishimoto, J., Tsuchiya, T., Cox, H., Emson, P.C., and Nakayama, Y. (1998). Age-related changes of calbindin-D28k, calretinin, and parvalbumin mRNAs in the hamster brain. Neurobiol. Aging *19*, 77–82.

Kito, S., Miyoshi, R., and Nomoto, T. (1990). Influence of age on NMDA receptor complex in rat brain studied by in vitro

autoradiography. J. Histochem. Cytochem. Off. J. Histochem. Soc. *38*, 1725–1731.

Klishin, A., Lozovaya, N., and Krishtal, O. (1995). A1 adenosine receptors differentially regulate the N-methyl-D-aspartate and non-N-methyl-D-aspartate receptor-mediated components of hippocampal excitatory postsynaptic current in a Ca2+/Mg(2+)-dependent manner. Neuroscience *65*, 947–953.

Kolb, B., and Gibb, R. (2014). Searching for the principles of brain plasticity and behavior. Cortex J. Devoted Study Nerv. Syst. Behav. *58*, 251–260.

Kolb, B., and Muhammad, A. (2014). Harnessing the power of neuroplasticity for intervention. Front. Hum. Neurosci. *8*, 377.

Kouvaros, S., and Papatheodoropoulos, C. (2016). Major dorsoventral differences in the modulation of the local CA1 hippocampal network by NMDA, mGlu5, adenosine A2A and cannabinoid CB1 receptors. Neuroscience *317*, 47–64.

Kuhn, H.G., Dickinson-Anson, H., and Gage, F.H. (1996). Neurogenesis in the dentate gyrus of the adult rat: age-related decrease of neuronal progenitor proliferation. J. Neurosci. Off. J. Soc. Neurosci. *16*, 2027–2033.

Kullmann, D.M., and Lamsa, K.P. (2007). Long-term synaptic plasticity in hippocampal interneurons. Nat. Rev. Neurosci. *8*, 687–699.

Kumar, A. (2015). NMDA Receptor Function During Senescence: Implication on Cognitive Performance. Front. Neurosci. *9*, 473.

Kumar, A., and Foster, T.C. (2004). Enhanced long-term potentiation during aging is masked by processes involving intracellular calcium stores. J. Neurophysiol. *91*, 2437–2444.

Kumar, A., and Foster, T.C. (2005). Intracellular calcium stores contribute to increased susceptibility to LTD induction during aging. Brain Res. *1031*, 125–128.

Kumar, A., and Foster, T.C. (2014). Interaction of DHPG-LTD and synaptic-LTD at senescent CA3-CA1 hippocampal synapses. Hippocampus *24*, 466–475.

Kumar, A., Thinschmidt, J.S., Foster, T.C., and King, M.A. (2007). Aging effects on the limits and stability of long-term synaptic potentiation and depression in rat hippocampal area CA1. J. Neurophysiol. *98*, 594–601.

Landfield, P.W., and Lynch, G. (1977). Impaired monosynaptic potentiation in in vitro hippocampal slices from aged, memory-deficient rats. J. Gerontol. *32*, 523–533.

Landfield, P.W., and Pitler, T.A. (1984). Prolonged Ca2+-dependent afterhyperpolarizations in hippocampal neurons of aged rats. Science *226*, 1089–1092.

Landfield, P.W., McGaugh, J.L., and Lynch, G. (1978). Impaired synaptic potentiation processes in the hippocampus of aged, memory-deficient rats. Brain Res. *150*, 85–101.

Landfield, P.W., Pitler, T.A., and Applegate, M.D. (1986). The effects of high Mg2+-to-Ca2+ ratios on frequency potentiation in hippocampal slices of young and aged rats. J. Neurophysiol. *56*, 797–811.

Lanté, F., Chafai, M., Raymond, E.F., Pereira, A.R.S., Mouska, X., Kootar, S., Barik, J., Bethus, I., and Marie, H. (2015). Subchronic glucocorticoid receptor inhibition rescues early episodic memory and synaptic plasticity deficits in a mouse model of Alzheimer's disease. Neuropsychopharmacol. Off. Publ. Am. Coll. Neuropsychopharmacol. *40*, 1772–1781.

Laurent, C., Eddarkaoui, S., Derisbourg, M., Leboucher, A., Demeyer, D., Carrier, S., Schneider, M., Hamdane, M., Müller, C.E., Buée, L., et al. (2014). Beneficial effects of caffeine in a transgenic model of Alzheimer's disease-like tau pathology. Neurobiol. Aging *35*, 2079–2090.

Laurent, C., Burnouf, S., Ferry, B., Batalha, V.L., Coelho, J.E., Baqi, Y., Malik, E., Mariciniak, E., Parrot, S., Van der Jeugd, A., et al.

(2016). A2A adenosine receptor deletion is protective in a mouse model of Tauopathy. Mol. Psychiatry *21*, 97–107.

Lavenex, P., and Amaral, D.G. (2000). Hippocampal-neocortical interaction: a hierarchy of associativity. Hippocampus *10*, 420–430.

Lea, P.M., Custer, S.J., Vicini, S., and Faden, A.I. (2002). Neuronal and glial mGluR5 modulation prevents stretch-induced enhancement of NMDA receptor current. Pharmacol. Biochem. Behav. *73*, 287–298.

Lee, H.K., Kameyama, K., Huganir, R.L., and Bear, M.F. (1998). NMDA induces long-term synaptic depression and dephosphorylation of the GluR1 subunit of AMPA receptors in hippocampus. Neuron *21*, 1151–1162.

Lee, H.K., Barbarosie, M., Kameyama, K., Bear, M.F., and Huganir, R.L. (2000). Regulation of distinct AMPA receptor phosphorylation sites during bidirectional synaptic plasticity. Nature *405*, 955–959.

Lee, H.-K., Min, S.S., Gallagher, M., and Kirkwood, A. (2005). NMDA receptor-independent long-term depression correlates with successful aging in rats. Nat. Neurosci. *8*, 1657–1659.

Li, P., Rial, D., Canas, P.M., Yoo, J.-H., Li, W., Zhou, X., Wang, Y., van Westen, G.J.P., Payen, M.-P., Augusto, E., et al. (2015a). Optogenetic activation of intracellular adenosine A2A receptor signaling in the hippocampus is sufficient to trigger CREB phosphorylation and impair memory. Mol. Psychiatry *20*, 1339–1349.

Li, P., Rial, D., Canas, P.M., Yoo, J.-H., Li, W., Zhou, X., Wang, Y., van Westen, G.J.P., Payen, M.-P., Augusto, E., et al. (2015b). Optogenetic activation of intracellular adenosine A2A receptor signaling in the hippocampus is sufficient to trigger CREB phosphorylation and impair memory. Mol. Psychiatry *20*, 1339–1349.

Li, W., Silva, H.B., Real, J., Wang, Y.-M., Rial, D., Li, P., Payen, M.-P., Zhou, Y., Muller, C.E., Tomé, A.R., et al. (2015c). Inactivation of adenosine A2A receptors reverses working memory deficits at early stages of Huntington's disease models. Neurobiol. Dis. *79*, 70–80.

Libert, F., Parmentier, M., Lefort, A., Dinsart, C., Van Sande, J., Maenhaut, C., Simons, M.J., Dumont, J.E., and Vassart, G. (1989).

Selective amplification and cloning of four new members of the G protein-coupled receptor family. Science *244*, 569–572.

Linden, J. (2001). Molecular approach to adenosine receptors: receptor-mediated mechanisms of tissue protection. Annu. Rev. Pharmacol. Toxicol. *41*, 775–787.

Lindsay, J., Laurin, D., Verreault, R., Hébert, R., Helliwell, B., Hill, G.B., and McDowell, I. (2002). Risk factors for Alzheimer's disease: a prospective analysis from the Canadian Study of Health and Aging. Am. J. Epidemiol. *156*, 445–453.

Lisman, J. (1989). A mechanism for the Hebb and the anti-Hebb processes underlying learning and memory. Proc. Natl. Acad. Sci. U. S. A. *86*, 9574–9578.

Lisman, J.E. (1999). Relating hippocampal circuitry to function: recall of memory sequences by reciprocal dentate-CA3 interactions. Neuron *22*, 233–242.

Lisman, J.E., and Otmakhova, N.A. (2001). Storage, recall, and novelty detection of sequences by the hippocampus: elaborating on the SOCRATIC model to account for normal and aberrant effects of dopamine. Hippocampus *11*, 551–568.

Lisman, J., Schulman, H., and Cline, H. (2002). The molecular basis of CaMKII function in synaptic and behavioural memory. Nat. Rev. Neurosci. *3*, 175–190.

Liu, P., Smith, P.F., and Darlington, C.L. (2008). Glutamate receptor subunits expression in memory-associated brain structures: regional variations and effects of aging. Synap. N. Y. N *62*, 834–841.

Lopes, L.V., Cunha, R.A., and Ribeiro, J.A. (1999a). Increase in the number, G protein coupling, and efficiency of facilitatory adenosine A2A receptors in the limbic cortex, but not striatum, of aged rats. J. Neurochem. *73*, 1733–1738.

Lopes, L.V., Cunha, R.A., and Ribeiro, J.A. (1999b). Cross talk between A(1) and A(2A) adenosine receptors in the hippocampus and cortex of young adult and old rats. J. Neurophysiol. *82*, 3196–3203.

Lopes, L.V., Cunha, R.A., Kull, B., Fredholm, B.B., and Ribeiro, J.A. (2002). Adenosine A(2A) receptor facilitation of hippocampal synaptic transmission is dependent on tonic A(1) receptor inhibition. Neuroscience *112*, 319–329.

Lopes, L.V., Halldner, L., Rebola, N., Johansson, B., Ledent, C., Chen, J.F., Fredholm, B.B., and Cunha, R.A. (2004). Binding of the prototypical adenosine A(2A) receptor agonist CGS 21680 to the cerebral cortex of adenosine A(1) and A(2A) receptor knockout mice. Br. J. Pharmacol. *141*, 1006–1014.

Lopes, L.V., Sebastião, A.M., and Ribeiro, J.A. (2011a). Adenosine and related drugs in brain diseases: present and future in clinical trials. Curr. Top. Med. Chem. *11*, 1087–1101.

Lopes, L.V., Sebastião, A.M., and Ribeiro, J.A. (2011b). Adenosine and related drugs in brain diseases: present and future in clinical trials. Curr. Top. Med. Chem. *11*, 1087–1101.

Lopez, J.R., Lyckman, A., Oddo, S., Laferla, F.M., Querfurth, H.W., and Shtifman, A. (2008). Increased intraneuronal resting [Ca2+] in adult Alzheimer's disease mice. J. Neurochem. *105*, 262–271.

Lorente de No, R. (1934). Studies on the structure of the cerebral cortex II: continuation of the study of the ammonic system. J Psychol Neurol Leipz *46*, 113–177.

Lüscher, C., and Huber, K.M. (2010). Group 1 mGluR-dependent synaptic long-term depression: mechanisms and implications for circuitry and disease. Neuron *65*, 445–459.

Lynch, M.A. (2004). Long-term potentiation and memory. Physiol. Rev. *84*, 87–136.

Lynch, G., Larson, J., Kelso, S., Barrionuevo, G., and Schottler, F. (1983). Intracellular injections of EGTA block induction of hippocampal long-term potentiation. Nature *305*, 719–721.

Lynch, G.S., Dunwiddie, T., and Gribkoff, V. (1977). Heterosynaptic depression: a postsynaptic correlate of long-term potentiation. Nature *266*, 737–739.

Mabry, T.R., McCarty, R., Gold, P.E., and Foster, T.C. (1996). Age and stress history effects on spatial performance in a swim task in Fischer-344 rats. Neurobiol. Learn. Mem. *66*, 1–10.

Magnusson, K.R., Nelson, S.E., and Young, A.B. (2002). Age-related changes in the protein expression of subunits of the NMDA receptor. Brain Res. Mol. Brain Res. *99*, 40–45.

Magnusson, K.R., Kresge, D., and Supon, J. (2006). Differential effects of aging on NMDA receptors in the intermediate versus the dorsal hippocampus. Neurobiol. Aging *27*, 324–333.

Maia, L., and de Mendonça, A. (2002). Does caffeine intake protect from Alzheimer's disease? Eur. J. Neurol. *9*, 377–382.

Malenka, R.C. (1994). Synaptic plasticity in the hippocampus: LTP and LTD. Cell *78*, 535–538.

Mannaioni, G., Marino, M.J., Valenti, O., Traynelis, S.F., and Conn, P.J. (2001). Metabotropic glutamate receptors 1 and 5 differentially regulate CA1 pyramidal cell function. J. Neurosci. Off. J. Soc. Neurosci. *21*, 5925–5934.

Marcantoni, A., Raymond, E.F., Carbone, E., and Marie, H. (2014). Firing properties of entorhinal cortex neurons and early alterations in an Alzheimer's disease transgenic model. Pflugers Arch. *466*, 1437–1450.

Marchetti, C., and Marie, H. (2011). Hippocampal synaptic plasticity in Alzheimer's disease: what have we learned so far from transgenic models? Rev. Neurosci. *22*, 373–402.

Marchetti, C., Tafi, E., Middei, S., Rubinacci, M.A., Restivo, L., Ammassari-Teule, M., and Marie, H. (2010). Synaptic adaptations of CA1 pyramidal neurons induced by a highly effective combinational antidepressant therapy. Biol. Psychiatry *67*, 146–154.

Markham, J.A., McKian, K.P., Stroup, T.S., and Juraska, J.M. (2005). Sexually dimorphic aging of dendritic morphology in CA1 of hippocampus. Hippocampus *15*, 97–103.

Marques-Morgado, I. (2016). Contribution of different cellular subsets to the Adenosine A2A Receptor overexpression in the rat brain. Universidade de Lisboa.

Martinez-Serrano, A., Blanco, P., and Satrústegui, J. (1992). Calcium binding to the cytosol and calcium extrusion mechanisms in intact synaptosomes and their alterations with aging. J. Biol. Chem. *267*, 4672–4679.

Martire, A., Tebano, M.T., Chiodi, V., Ferreira, S.G., Cunha, R.A., Köfalvi, A., and Popoli, P. (2011). Pre-synaptic adenosine A2A receptors control cannabinoid CB1 receptor-mediated inhibition of striatal glutamatergic neurotransmission. J. Neurochem. *116*, 273–280.

Massey, P.V., and Bashir, Z.I. (2007). Long-term depression: multiple forms and implications for brain function. Trends Neurosci. *30*, 176–184.

Matos, M., Augusto, E., Santos-Rodrigues, A.D., Schwarzschild, M.A., Chen, J.-F., Cunha, R.A., and Agostinho, P. (2012a). Adenosine A2A receptors modulate glutamate uptake in cultured astrocytes and gliosomes. Glia *60*, 702–716.

Matos, M., Augusto, E., Machado, N.J., dos Santos-Rodrigues, A., Cunha, R.A., and Agostinho, P. (2012b). Astrocytic adenosine A2A receptors control the amyloid-β peptide-induced decrease of glutamate uptake. J. Alzheimers Dis. JAD *31*, 555–567.

Matos, M., Augusto, E., Agostinho, P., Cunha, R.A., and Chen, J.-F. (2013). Antagonistic Interaction between Adenosine A2A Receptors and Na+/K+-ATPase- 2 Controlling Glutamate Uptake in Astrocytes. J. Neurosci. *33*, 18492–18502.

Matos, M., Shen, H.-Y., Augusto, E., Wang, Y., Wei, C.J., Wang, Y.T., Agostinho, P., Boison, D., Cunha, R.A., and Chen, J.-F. (2015). Deletion of adenosine A2A receptors from astrocytes disrupts glutamate homeostasis leading to psychomotor and cognitive impairment: relevance to schizophrenia. Biol. Psychiatry *78*, 763–774.

Mayer, M.L., Westbrook, G.L., and Guthrie, P.B. (1984). Voltage-dependent block by Mg2+ of NMDA responses in spinal cord neurones. Nature *309*, 261–263.

McEwen, B.S. (1997). Possible mechanisms for atrophy of the human hippocampus. Mol. Psychiatry *2*, 255–262.

Merrill, D.A., Roberts, J.A., and Tuszynski, M.H. (2000). Conservation of neuron number and size in entorhinal cortex layers II, III, and V/VI of aged primates. J. Comp. Neurol. *422*, 396–401.

Michaelis, M.L., Johe, K., and Kitos, T.E. (1984). Age-dependent alterations in synaptic membrane systems for Ca2+ regulation. Mech. Ageing Dev. *25*, 215–225.

Michaelis, M.L., Foster, C.T., and Jayawickreme, C. (1992). Regulation of calcium levels in brain tissue from adult and aged rats. Mech. Ageing Dev. *62*, 291–306.

Mockett, B.G., Guévremont, D., Wutte, M., Hulme, S.R., Williams, J.M., and Abraham, W.C. (2011). Calcium/calmodulin-dependent protein kinase II mediates group I metabotropic glutamate receptor-dependent protein synthesis and long-term depression in rat hippocampus. J. Neurosci. Off. J. Soc. Neurosci. *31*, 7380–7391.

Mogul, D.J., Adams, M.E., and Fox, A.P. (1993). Differential activation of adenosine receptors decreases N-type but potentiates P-type Ca2+ current in hippocampal CA3 neurons. Neuron *10*, 327–334.

Moreno, H., Burghardt, N.S., Vela-Duarte, D., Masciotti, J., Hua, F., Fenton, A.A., Schwaller, B., and Small, S.A. (2012). The absence of the calcium-buffering protein calbindin is associated with faster age-related decline in hippocampal metabolism. Hippocampus *22*, 1107–1120.

Morishita, W., Connor, J.H., Xia, H., Quinlan, E.M., Shenolikar, S., and Malenka, R.C. (2001). Regulation of synaptic strength by protein phosphatase 1. Neuron *32*, 1133–1148.

Morrison, J.H., and Baxter, M.G. (2012). The ageing cortical synapse: hallmarks and implications for cognitive decline. Nat. Rev. Neurosci. *13*, 240–250.

Morrison, J.H., and Hof, P.R. (1997). Life and death of neurons in the aging brain. Science *278*, 412–419.

Mulkey, R.M., and Malenka, R.C. (1992). Mechanisms underlying induction of homosynaptic long-term depression in area CA1 of the hippocampus. Neuron *9*, 967–975.

Mulkey, R.M., Herron, C.E., and Malenka, R.C. (1993). An essential role for protein phosphatases in hippocampal long-term depression. Science *261*, 1051–1055.

Mulkey, R.M., Endo, S., Shenolikar, S., and Malenka, R.C. (1994). Involvement of a calcineurin/inhibitor-1 phosphatase cascade in hippocampal long-term depression. Nature *369*, 486–488.

Mullany, P., Connolly, S., and Lynch, M.A. (1996). Ageing is associated with changes in glutamate release, protein tyrosine kinase and Ca2+/calmodulin-dependent protein kinase II in rat hippocampus. Eur. J. Pharmacol. *309*, 311–315.

Müller, T. (2013). Suitability of the adenosine antagonist istradefylline for the treatment of Parkinson's disease: pharmacokinetic and clinical considerations. Expert Opin. Drug Metab. Toxicol. *9*, 1015–1024.

Murchison, D., and Griffith, W.H. (1998). Increased calcium buffering in basal forebrain neurons during aging. J. Neurophysiol. *80*, 350–364.

Nabavi, S., Kessels, H.W., Alfonso, S., Aow, J., Fox, R., and Malinow, R. (2013). Metabotropic NMDA receptor function is required for NMDA receptor-dependent long-term depression. Proc. Natl. Acad. Sci. U. S. A. *110*, 4027–4032.

Nacher, J., Alonso-Llosa, G., Rosell, D.R., and McEwen, B.S. (2003). NMDA receptor antagonist treatment increases the production of new neurons in the aged rat hippocampus. Neurobiol. Aging *24*, 273–284.

Nicholson, D.A., Yoshida, R., Berry, R.W., Gallagher, M., and Geinisman, Y. (2004). Reduction in size of perforated postsynaptic densities in hippocampal axospinous synapses and age-related spatial learning impairments. J. Neurosci. Off. J. Soc. Neurosci. *24*, 7648–7653.

Nordström, C.H., Rehncrona, S., Siesjö, B.K., and Westerberg, E. (1977). Adenosine in rat cerebral cortex: its determination, normal

values, and correlation to AMP and cyclic AMP during shortlasting ischemia. Acta Physiol. Scand. *101*, 63–71.

Norris, C.M., Korol, D.L., and Foster, T.C. (1996). Increased susceptibility to induction of long-term depression and long-term potentiation reversal during aging. J. Neurosci. Off. J. Soc. Neurosci. *16*, 5382–5392.

Norris, C.M., Halpain, S., and Foster, T.C. (1998). Alterations in the balance of protein kinase/phosphatase activities parallel reduced synaptic strength during aging. J. Neurophysiol. *80*, 1567–1570.

Nowak, L., Bregestovski, P., Ascher, P., Herbet, A., and Prochiantz, A. (1984). Magnesium gates glutamate-activated channels in mouse central neurones. Nature *307*, 462–465.

Núñez-Santana, F.L., Oh, M.M., Antion, M.D., Lee, A., Hell, J.W., and Disterhoft, J.F. (2014). Surface L-type Ca2+ channel expression levels are increased in aged hippocampus. Aging Cell *13*, 111–120.

O'Dell, T.J., and Kandel, E.R. (1994). Low-frequency stimulation erases LTP through an NMDA receptor-mediated activation of protein phosphatases. Learn. Mem. Cold Spring Harb. N *1*, 129–139.

Oh, M.M., Oliveira, F.A., Waters, J., and Disterhoft, J.F. (2013). Altered calcium metabolism in aging CA1 hippocampal pyramidal neurons. J. Neurosci. Off. J. Soc. Neurosci. *33*, 7905–7911.

Oler, J.A., and Markus, E.J. (1998). Age-related deficits on the radial maze and in fear conditioning: hippocampal processing and consolidation. Hippocampus *8*, 402–415.

Oliet, S.H., Malenka, R.C., and Nicoll, R.A. (1997). Two distinct forms of long-term depression coexist in CA1 hippocampal pyramidal cells. Neuron *18*, 969–982.

Orr, A.G., Orr, A.L., Li, X.-J., Gross, R.E., and Traynelis, S.F. (2009). Adenosine A(2A) receptor mediates microglial process retraction. Nat. Neurosci. *12*, 872–878.

Orr, A.G., Hsiao, E.C., Wang, M.M., Ho, K., Kim, D.H., Wang, X., Guo, W., Kang, J., Yu, G.-Q., Adame, A., et al. (2015). Astrocytic

adenosine receptor A2A and Gs-coupled signaling regulate memory. Nat. Neurosci. *18*, 423–434.

Otani, S., and Connor, J.A. (1998). Requirement of rapid Ca2+ entry and synaptic activation of metabotropic glutamate receptors for the induction of long-term depression in adult rat hippocampus. J. Physiol. *511 (Pt 3)*, 761–770.

Ouanounou, A., Zhang, L., Charlton, M.P., and Carlen, P.L. (1999). Differential modulation of synaptic transmission by calcium chelators in young and aged hippocampal CA1 neurons: evidence for altered calcium homeostasis in aging. J. Neurosci. Off. J. Soc. Neurosci. *19*, 906–915.

Pagnussat, N., Almeida, A.S., Marques, D.M., Nunes, F., Chenet, G.C., Botton, P.H.S., Mioranzza, S., Loss, C.M., Cunha, R.A., and Porciúncula, L.O. (2015a). Adenosine A(2A) receptors are necessary and sufficient to trigger memory impairment in adult mice. Br. J. Pharmacol. *172*, 3831–3845.

Pagnussat, N., Almeida, A.S., Marques, D.M., Nunes, F., Chenet, G.C., Botton, P.H.S., Mioranzza, S., Loss, C.M., Cunha, R.A., and Porciúncula, L.O. (2015b). Adenosine A(2A) receptors are necessary and sufficient to trigger memory impairment in adult mice. Br. J. Pharmacol. *172*, 3831–3845.

Pakkenberg, B., and Gundersen, H.J. (1997). Neocortical neuron number in humans: effect of sex and age. J. Comp. Neurol. *384*, 312–320.

Palmer, M.J., Irving, A.J., Seabrook, G.R., Jane, D.E., and Collingridge, G.L. (1997). The group I mGlu receptor agonist DHPG induces a novel form of LTD in the CA1 region of the hippocampus. Neuropharmacology *36*, 1517–1532.

Paoletti, P., Bellone, C., and Zhou, Q. (2013). NMDA receptor subunit diversity: impact on receptor properties, synaptic plasticity and disease. Nat. Rev. Neurosci. *14*, 383–400.

Parfitt, K.D., Hoffer, B.J., and Browning, M.D. (1991). Norepinephrine and isoproterenol increase the phosphorylation of

synapsin I and synapsin II in dentate slices of young but not aged Fisher 344 rats. Proc. Natl. Acad. Sci. U. S. A. *88*, 2361–2365.

Peters, A., Leahu, D., Moss, M.B., and McNally, K.J. (1994). The effects of aging on area 46 of the frontal cortex of the rhesus monkey. Cereb. Cortex N. Y. N 1991 *4*, 621–635.

Piccolino, M. (1997). Luigi Galvani and animal electricity: two centuries after the foundation of electrophysiology. Trends Neurosci. *20*, 443–448.

Pierrot, N., Ghisdal, P., Caumont, A.-S., and Octave, J.-N. (2004). Intraneuronal amyloid-beta1-42 production triggered by sustained increase of cytosolic calcium concentration induces neuronal death. J. Neurochem. *88*, 1140–1150.

Pierrot, N., Santos, S.F., Feyt, C., Morel, M., Brion, J.-P., and Octave, J.-N. (2006). Calcium-mediated transient phosphorylation of tau and amyloid precursor protein followed by intraneuronal amyloid-beta accumulation. J. Biol. Chem. *281*, 39907–39914.

Pin, J.P., and Duvoisin, R. (1995). The metabotropic glutamate receptors: structure and functions. Neuropharmacology *34*, 1–26.

Pinar, C., Fontaine, C.J., Triviño-Paredes, J., Lottenberg, C.P., Gil-Mohapel, J., and Christie, B.R. (2017). Revisiting the flip side: Long-term depression of synaptic efficacy in the hippocampus. Neurosci. Biobehav. Rev. *80*, 394–413.

Pinho, J., Vale, R., Batalha, V.L., Costenla, A.R., Dias, R., Rombo, D., Sebastião, A.M., de Mendonça, A., and Diógenes, M.J. (2017). Enhanced LTP in aged rats: Detrimental or compensatory? Neuropharmacology *114*, 12–19.

Pitler, T.A., and Landfield, P.W. (1990). Aging-related prolongation of calcium spike duration in rat hippocampal slice neurons. Brain Res. *508*, 1–6.

Pittaluga, A., Fedele, E., Risiglione, C., and Raiteri, M. (1993). Age-related decrease of the NMDA receptor-mediated noradrenaline release in rat hippocampus and partial restoration by D-cycloserine. Eur. J. Pharmacol. *231*, 129–134.

Pliássova, A., Canas, P.M., Xavier, A.C., da Silva, B.S., Cunha, R.A., and Agostinho, P. (2016). Age-Related Changes in the Synaptic Density of Amyloid-β Protein Precursor and Secretases in the Human Cerebral Cortex. J. Alzheimers Dis. JAD *52*, 1209–1214.

Pousinha, P.A., Mouska, X., Raymond, E.F., Gwizdek, C., Dhib, G., Poupon, G., Zaragosi, L.-E., Giudici, C., Bethus, I., Pacary, E., et al. (2017). Physiological and pathophysiological control of synaptic GluN2B-NMDA receptors by the C-terminal domain of amyloid precursor protein. ELife *6*.

Prediger, R.D.S., Batista, L.C., and Takahashi, R.N. (2005). Caffeine reverses age-related deficits in olfactory discrimination and social recognition memory in rats. Involvement of adenosine A1 and A2A receptors. Neurobiol. Aging *26*, 957–964.

Pyapali, G.K., and Turner, D.A. (1996). Increased dendritic extent in hippocampal CA1 neurons from aged F344 rats. Neurobiol. Aging *17*, 601–611.

Raza, M., Deshpande, L.S., Blair, R.E., Carter, D.S., Sombati, S., and DeLorenzo, R.J. (2007). Aging is associated with elevated intracellular calcium levels and altered calcium homeostatic mechanisms in hippocampal neurons. Neurosci. Lett. *418*, 77–81.

Rebola, N., Pinheiro, P.C., Oliveira, C.R., Malva, J.O., and Cunha, R.A. (2003a). Subcellular localization of adenosine A(1) receptors in nerve terminals and synapses of the rat hippocampus. Brain Res. *987*, 49–58.

Rebola, N., Sebastião, A.M., de Mendonca, A., Oliveira, C.R., Ribeiro, J.A., and Cunha, R.A. (2003b). Enhanced adenosine A2A receptor facilitation of synaptic transmission in the hippocampus of aged rats. J. Neurophysiol. *90*, 1295–1303.

Rebola, N., Canas, P.M., Oliveira, C.R., and Cunha, R.A. (2005a). Different synaptic and subsynaptic localization of adenosine A2A receptors in the hippocampus and striatum of the rat. Neuroscience *132*, 893–903.

Rebola, N., Rodrigues, R.J., Lopes, L.V., Richardson, P.J., Oliveira, C.R., and Cunha, R.A. (2005b). Adenosine A1 and A2A receptors are

co-expressed in pyramidal neurons and co-localized in glutamatergic nerve terminals of the rat hippocampus. Neuroscience *133*, 79–83.

Rebola, N., Lujan, R., Cunha, R.A., and Mulle, C. (2008). Adenosine A2A receptors are essential for long-term potentiation of NMDA-EPSCs at hippocampal mossy fiber synapses. Neuron *57*, 121–134.

Reitz, C., Brayne, C., and Mayeux, R. (2011). Epidemiology of Alzheimer disease. Nat. Rev. Neurol. *7*, 137–152.

Reppert, S.M., Weaver, D.R., Stehle, J.H., and Rivkees, S.A. (1991). Molecular cloning and characterization of a rat A1-adenosine receptor that is widely expressed in brain and spinal cord. Mol. Endocrinol. Baltim. Md *5*, 1037–1048.

Rex, C.S., Kramár, E.A., Colgin, L.L., Lin, B., Gall, C.M., and Lynch, G. (2005). Long-term potentiation is impaired in middle-aged rats: regional specificity and reversal by adenosine receptor antagonists. J. Neurosci. Off. J. Soc. Neurosci. *25*, 5956–5966.

Ribeiro, J.A., and Sebastião, A.M. (2010). Modulation and metamodulation of synapses by adenosine. Acta Physiol. Oxf. Engl. *199*, 161–169.

Ritchie, K., Carrière, I., de Mendonca, A., Portet, F., Dartigues, J.F., Rouaud, O., Barberger-Gateau, P., and Ancelin, M.L. (2007). The neuroprotective effects of caffeine: a prospective population study (the Three City Study). Neurology *69*, 536–545.

Rodrigues, R.J., Tomé, A.R., and Cunha, R.A. (2015). ATP as a multi-target danger signal in the brain. Front. Neurosci. *9*, 148.

Rombo, D.M., Newton, K., Nissen, W., Badurek, S., Horn, J.M., Minichiello, L., Jefferys, J.G.R., Sebastiao, A.M., and Lamsa, K.P. (2015). Synaptic mechanisms of adenosine A2A receptor-mediated hyperexcitability in the hippocampus. Hippocampus *25*, 566–580.

Rose, G.M., Ong, V.S., and Woodruff-Pak, D.S. (2007). Efficacy of MEM 1003, a novel calcium channel blocker, in delay and trace eyeblink conditioning in older rabbits. Neurobiol. Aging *28*, 766–773.

Roselli, F., Tirard, M., Lu, J., Hutzler, P., Lamberti, P., Livrea, P., Morabito, M., and Almeida, O.F.X. (2005). Soluble beta-amyloid1-40 induces NMDA-dependent degradation of postsynaptic density-95 at glutamatergic synapses. J. Neurosci. Off. J. Soc. Neurosci. *25*, 11061–11070.

Rosenmund, C., Stern-Bach, Y., and Stevens, C.F. (1998). The tetrameric structure of a glutamate receptor channel. Science *280*, 1596–1599.

Rosenzweig, E.S., and Barnes, C.A. (2003). Impact of aging on hippocampal function: plasticity, network dynamics, and cognition. Prog. Neurobiol. *69*, 143–179.

Rosenzweig, E.S., Rao, G., McNaughton, B.L., and Barnes, C.A. (1997). Role of temporal summation in age-related long-term potentiation-induction deficits. Hippocampus *7*, 549–558.

Sankar, R., Shin, D., Mazarati, A.M., Liu, H., Katsumori, H., Lezama, R., and Wasterlain, C.G. (2000). Epileptogenesis after status epilepticus reflects age- and model-dependent plasticity. Ann. Neurol. *48*, 580–589.

Santiago, A.R., Baptista, F.I., Santos, P.F., Cristóvão, G., Ambrósio, A.F., Cunha, R.A., and Gomes, C.A. (2014). Role of microglia adenosine A(2A) receptors in retinal and brain neurodegenerative diseases. Mediators Inflamm. *2014*, 465694.

Sarantis, K., Tsiamaki, E., Kouvaros, S., Papatheodoropoulos, C., and Angelatou, F. (2015). Adenosine A_2A receptors permit mGluR5-evoked tyrosine phosphorylation of NR2B (Tyr1472) in rat hippocampus: a possible key mechanism in NMDA receptor modulation. J. Neurochem. *135*, 714–726.

Sariyer, I.K. (2013). Transfection of neuronal cultures. Methods Mol. Biol. Clifton NJ *1078*, 133–139.

Satrústegui, J., Villalba, M., Pereira, R., Bogónez, E., and Martínez-Serrano, A. (1996). Cytosolic and mitochondrial calcium in synaptosomes during aging. Life Sci. *59*, 429–434.

Scheff, S.W., Price, D.A., Schmitt, F.A., and Mufson, E.J. (2006). Hippocampal synaptic loss in early Alzheimer's disease and mild cognitive impairment. Neurobiol. Aging *27*, 1372–1384.

Scheff, S.W., Price, D.A., Schmitt, F.A., DeKosky, S.T., and Mufson, E.J. (2007). Synaptic alterations in CA1 in mild Alzheimer disease and mild cognitive impairment. Neurology *68*, 1501–1508.

Scheibel, M.E., Lindsay, R.D., Tomiyasu, U., and Scheibel, A.B. (1976). Progressive dendritic changes in the aging human limbic system. Exp. Neurol. *53*, 420–430.

Schiffmann, S.N., and Vanderhaeghen, J.J. (1993). Adenosine A2 receptors regulate the gene expression of striatopallidal and striatonigral neurons. J. Neurosci. Off. J. Soc. Neurosci. *13*, 1080–1087.

Schiffmann, S.N., Libert, F., Vassart, G., and Vanderhaeghen, J.J. (1991). Distribution of adenosine A2 receptor mRNA in the human brain. Neurosci. Lett. *130*, 177–181.

Schmittgen, T.D., and Livak, K.J. (2008). Analyzing real-time PCR data by the comparative C(T) method. Nat. Protoc. *3*, 1101–1108.

Schnabel, R., Palmer, M.J., Kilpatrick, I.C., and Collingridge, G.L. (1999). A CaMKII inhibitor, KN-62, facilitates DHPG-induced LTD in the CA1 region of the hippocampus. Neuropharmacology *38*, 605–608.

Schultz, C., and Engelhardt, M. (2014). Anatomy of the hippocampal formation. Front. Neurol. Neurosci. *34*, 6–17.

Sebastião, A.M., Stone, T.W., and Ribeiro, J.A. (1990). The inhibitory adenosine receptor at the neuromuscular junction and hippocampus of the rat: antagonism by 1,3,8-substituted xanthines. Br. J. Pharmacol. *101*, 453–459.

Sebastião, A.M., Macedo, M.P., and Ribeiro, J.A. (2000). Tonic activation of A(2A) adenosine receptors unmasks, and of A(1) receptors prevents, a facilitatory action of calcitonin gene-related peptide in the rat hippocampus. Br. J. Pharmacol. *129*, 374–380.

Selkoe, D.J. (2002). Alzheimer's disease is a synaptic failure. Science *298*, 789–791.

Serra, M., Ghiani, C.A., Foddi, M.C., Motzo, C., and Biggio, G. (1994). NMDA receptor function is enhanced in the hippocampus of aged rats. Neurochem. Res. *19*, 483–487.

Shankar, G.M., Li, S., Mehta, T.H., Garcia-Munoz, A., Shepardson, N.E., Smith, I., Brett, F.M., Farrell, M.A., Rowan, M.J., Lemere, C.A., et al. (2008). Amyloid-beta protein dimers isolated directly from Alzheimer's brains impair synaptic plasticity and memory. Nat. Med. *14*, 837–842.

Shindou, T., Nonaka, H., Richardson, P.J., Mori, A., Kase, H., and Ichimura, M. (2002). Presynaptic adenosine A2A receptors enhance GABAergic synaptic transmission via a cyclic AMP dependent mechanism in the rat globus pallidus. Br. J. Pharmacol. *136*, 296–302.

Silva, A.J., Kogan, J.H., Frankland, P.W., and Kida, S. (1998). CREB and memory. Annu. Rev. Neurosci. *21*, 127–148.

Smith, A. (2002). Effects of caffeine on human behavior. Food Chem. Toxicol. Int. J. Publ. Br. Ind. Biol. Res. Assoc. *40*, 1243–1255.

Snyder, E.M., Nong, Y., Almeida, C.G., Paul, S., Moran, T., Choi, E.Y., Nairn, A.C., Salter, M.W., Lombroso, P.J., Gouras, G.K., et al. (2005). Regulation of NMDA receptor trafficking by amyloid-beta. Nat. Neurosci. *8*, 1051–1058.

Stanton, P.K., Winterer, J., Bailey, C.P., Kyrozis, A., Raginov, I., Laube, G., Veh, R.W., Nguyen, C.Q., and Müller, W. (2003). Long-term depression of presynaptic release from the readily releasable vesicle pool induced by NMDA receptor-dependent retrograde nitric oxide. J. Neurosci. Off. J. Soc. Neurosci. *23*, 5936–5944.

Staubli, U., and Scafidi, J. (1997). Studies on long-term depression in area CA1 of the anesthetized and freely moving rat. J. Neurosci. Off. J. Soc. Neurosci. *17*, 4820–4828.

Stone, E.A., Slucky, A.V., Platt, J.E., and Trullas, R. (1985). Reduction of the cyclic adenosine 3',5'-monophosphate response to

catecholamines in rat brain slices after repeated restraint stress. J. Pharmacol. Exp. Ther. *233*, 382–388.

Strange, B.A., Witter, M.P., Lein, E.S., and Moser, E.I. (2014). Functional organization of the hippocampal longitudinal axis. Nat. Rev. Neurosci. *15*, 655–669.

Sweatt, J.D. (2010). Mechanisms of memory (Amsterdam: Academic).

Takagi, N., Besshoh, S., Morita, H., Terao, M., Takeo, S., and Tanonaka, K. (2010). Metabotropic glutamate mGlu5 receptor-mediated serine phosphorylation of NMDA receptor subunit NR1 in hippocampal CA1 region after transient global ischemia in rats. Eur. J. Pharmacol. *644*, 96–100.

Tamaru, M., Yoneda, Y., Ogita, K., Shimizu, J., and Nagata, Y. (1991). Age-related decreases of the N-methyl-D-aspartate receptor complex in the rat cerebral cortex and hippocampus. Brain Res. *542*, 83–90.

Tanila, H., Shapiro, M., Gallagher, M., and Eichenbaum, H. (1997). Brain aging: changes in the nature of information coding by the hippocampus. J. Neurosci. Off. J. Soc. Neurosci. *17*, 5155–5166.

Tebano, M.T., Martire, A., Rebola, N., Pepponi, R., Domenici, M.R., Grò, M.C., Schwarzschild, M.A., Chen, J.F., Cunha, R.A., and Popoli, P. (2005). Adenosine A2A receptors and metabotropic glutamate 5 receptors are co-localized and functionally interact in the hippocampus: a possible key mechanism in the modulation of N-methyl-D-aspartate effects. J. Neurochem. *95*, 1188–1200.

Tebano, M.T., Martire, A., Potenza, R.L., Grò, C., Pepponi, R., Armida, M., Domenici, M.R., Schwarzschild, M.A., Chen, J.F., and Popoli, P. (2008). Adenosine A(2A) receptors are required for normal BDNF levels and BDNF-induced potentiation of synaptic transmission in the mouse hippocampus. J. Neurochem. *104*, 279–286.

Tetzlaff, W., Schubert, P., and Kreutzberg, G.W. (1987). Synaptic and extrasynaptic localization of adenosine binding sites in the rat hippocampus. Neuroscience *21*, 869–875.

Thibault, O., and Landfield, P.W. (1996). Increase in single L-type calcium channels in hippocampal neurons during aging. Science *272*, 1017–1020.

Thibault, O., Hadley, R., and Landfield, P.W. (2001). Elevated postsynaptic [Ca2+]i and L-type calcium channel activity in aged hippocampal neurons: relationship to impaired synaptic plasticity. J. Neurosci. Off. J. Soc. Neurosci. *21*, 9744–9756.

Tokuyasu, K.T. (1980). Immunochemistry on ultrathin frozen sections. Histochem. J. *12*, 381–403.

Tombaugh, G.C., Rowe, W.B., Chow, A.R., Michael, T.H., and Rose, G.M. (2002). Theta-frequency synaptic potentiation in CA1 in vitro distinguishes cognitively impaired from unimpaired aged Fischer 344 rats. J. Neurosci. Off. J. Soc. Neurosci. *22*, 9932–9940.

Tonkikh, A., Janus, C., El-Beheiry, H., Pennefather, P.S., Samoilova, M., McDonald, P., Ouanounou, A., and Carlen, P.L. (2006). Calcium chelation improves spatial learning and synaptic plasticity in aged rats. Exp. Neurol. *197*, 291–300.

Topic, B., Willuhn, I., Palomero-Gallagher, N., Zilles, K., Huston, J.P., and Hasenöhrl, R.U. (2007). Impaired maze performance in aged rats is accompanied by increased density of NMDA, 5-HT1A, and alpha-adrenoceptor binding in hippocampus. Hippocampus *17*, 68–77.

Tsien, J.Z., Huerta, P.T., and Tonegawa, S. (1996). The essential role of hippocampal CA1 NMDA receptor-dependent synaptic plasticity in spatial memory. Cell *87*, 1327–1338.

Turner, D.A., and Deupree, D.L. (1991). Functional elongation of CA1 hippocampal neurons with aging in Fischer 344 rats. Neurobiol. Aging *12*, 201–210.

Tyebji, S., Saavedra, A., Canas, P.M., Pliassova, A., Delgado-García, J.M., Alberch, J., Cunha, R.A., Gruart, A., and Pérez-Navarro, E. (2015). Hyperactivation of D1 and A2A receptors contributes to cognitive dysfunction in Huntington's disease. Neurobiol. Dis. *74*, 41–57.

Udagawa, R., Nakano, M., and Kato, N. (2006). Blocking L-type calcium channels enhances long-term depression induced by low-frequency stimulation at hippocampal CA1 synapses. Brain Res. *1124*, 28–36.

Uemura, E. (1985). Age-related changes in the subiculum of Macaca mulatta: synaptic density. Exp. Neurol. *87*, 403–411.

Uylings, H.B.M., and de Brabander, J.M. (2002). Neuronal changes in normal human aging and Alzheimer's disease. Brain Cogn. *49*, 268–276.

Valadas, J.S., Batalha, V.L., Ferreira, D.G., Gomes, R., Coelho, J.E., Sebastião, A.M., Diógenes, M.J., and Lopes, L.V. (2012). Neuroprotection afforded by adenosine A2A receptor blockade is modulated by corticotrophin-releasing factor (CRF) in glutamate injured cortical neurons. J. Neurochem. *123*, 1030–1040.

Varani, K., Vincenzi, F., Tosi, A., Gessi, S., Casetta, I., Granieri, G., Fazio, P., Leung, E., MacLennan, S., Granieri, E., et al. (2010). A2A adenosine receptor overexpression and functionality, as well as TNF-alpha levels, correlate with motor symptoms in Parkinson's disease. FASEB J. Off. Publ. Fed. Am. Soc. Exp. Biol. *24*, 587–598.

Veng, L.M., and Browning, M.D. (2002). Regionally selective alterations in expression of the alpha(1D) subunit (Ca(v)1.3) of L-type calcium channels in the hippocampus of aged rats. Brain Res. Mol. Brain Res. *107*, 120–127.

Veng, L.M., Mesches, M.H., and Browning, M.D. (2003). Age-related working memory impairment is correlated with increases in the L-type calcium channel protein alpha1D (Cav1.3) in area CA1 of the hippocampus and both are ameliorated by chronic nimodipine treatment. Brain Res. Mol. Brain Res. *110*, 193–202.

Verkhratsky, A., and Toescu, E.C. (1998). Calcium and neuronal ageing. Trends Neurosci. *21*, 2–7.

Viana da Silva, S., Haberl, M.G., Zhang, P., Bethge, P., Lemos, C., Gonçalves, N., Gorlewicz, A., Malezieux, M., Gonçalves, F.Q., Grosjean, N., et al. (2016). Early synaptic deficits in the APP/PS1

mouse model of Alzheimer's disease involve neuronal adenosine A2A receptors. Nat. Commun. *7*, 11915.

Villa, A., and Meldolesi, J. (1994). The control of Ca2+ homeostasis: role of intracellular rapidly exchanging Ca2+ stores. Cell Biol. Int. *18*, 301–307.

Walsh, D.M., and Selkoe, D.J. (2004). Deciphering the molecular basis of memory failure in Alzheimer's disease. Neuron *44*, 181–193.

Walton, M.R., and Dragunow, I. (2000). Is CREB a key to neuronal survival? Trends Neurosci. *23*, 48–53.

Wang, S.J., and Gean, P.W. (1999). Long-term depression of excitatory synaptic transmission in the rat amygdala. J. Neurosci. Off. J. Soc. Neurosci. *19*, 10656–10663.

Wang, Y., Rowan, M.J., and Anwyl, R. (1997). Induction of LTD in the dentate gyrus in vitro is NMDA receptor independent, but dependent on Ca2+ influx via low-voltage-activated Ca2+ channels and release of Ca2+ from intracellular stores. J. Neurophysiol. *77*, 812–825.

Wenk, G.L., Walker, L.C., Price, D.L., and Cork, L.C. (1991). Loss of NMDA, but not GABA-A, binding in the brains of aged rats and monkeys. Neurobiol. Aging *12*, 93–98.

West, M.J. (1993). New stereological methods for counting neurons. Neurobiol. Aging *14*, 275–285.

Williams, M. (1989). Adenosine: The prototypic neuromodulator. Neurochem. Int. *14*, 249–264.

Williams, R.S., and Matthysse, S. (1986). Age-related changes in Down syndrome brain and the cellular pathology of Alzheimer disease. Prog. Brain Res. *70*, 49–67.

Wong, T.P., Howland, J.G., Robillard, J.M., Ge, Y., Yu, W., Titterness, A.K., Brebner, K., Liu, L., Weinberg, J., Christie, B.R., et al. (2007). Hippocampal long-term depression mediates acute stress-induced spatial memory retrieval impairment. Proc. Natl. Acad. Sci. U. S. A. *104*, 11471–11476.

Yang, M., Soohoo, D., Soelaiman, S., Kalla, R., Zablocki, J., Chu, N., Leung, K., Yao, L., Diamond, I., Belardinelli, L., et al. (2007). Characterization of the potency, selectivity, and pharmacokinetic profile for six adenosine A2A receptor antagonists. Naunyn. Schmiedebergs Arch. Pharmacol. *375*, 133–144.

Yang, S.N., Tang, Y.G., and Zucker, R.S. (1999). Selective induction of LTP and LTD by postsynaptic [Ca2+]i elevation. J. Neurophysiol. *81*, 781–787.

Yang, W., Zhou, X., Zimmermann, H.R., Cavener, D.R., Klann, E., and Ma, T. (2016). Repression of the eIF2α kinase PERK alleviates mGluR-LTD impairments in a mouse model of Alzheimer's disease. Neurobiol. Aging *41*, 19–24.

Yu, L., Shen, H.-Y., Coelho, J.E., Araújo, I.M., Huang, Q.-Y., Day, Y.-J., Rebola, N., Canas, P.M., Rapp, E.K., Ferrara, J., et al. (2008). Adenosine A2A receptor antagonists exert motor and neuroprotective effects by distinct cellular mechanisms. Ann. Neurol. *63*, 338–346.

Zhang, Y., Li, P., Feng, J., and Wu, M. (2016). Dysfunction of NMDA receptors in Alzheimer's disease. Neurol. Sci. Off. J. Ital. Neurol. Soc. Ital. Soc. Clin. Neurophysiol. *37*, 1039–1047.

Appendix

Molecular Psychiatry
https://doi.org/10.1038/s41380-018-0110-9

ARTICLE

Age-related shift in LTD is dependent on neuronal adenosine A_{2A} receptors interplay with mGluR5 and NMDA receptors

Mariana Temido-Ferreira[1] · Diana G. Ferreira[1,2,3,4] · Vânia L. Batalha[1] · Inês Marques-Morgado[1] · Joana E. Coelho[1] · Pedro Pereira[5] · Rui Gomes[1,6] · Andreia Pinto[1] · Sara Carvalho[1] · Paula M. Canas[7,8] · Laetitia Cuvelier[9] · Valerie Buée-Scherrer[10] · Emilie Faivre[10] · Younis Baqi[11,12] · Christa E. Müller[11] · José Pimentel[5] · Serge N. Schiffmann[9] · Luc Buée[10] · Michael Bader[13,14,15] · Tiago F. Outeiro[2,16,17,18] · David Blum[10] · Rodrigo A. Cunha[7,8] · Hélène Marie[19] · Paula A. Pousinha[19] · Luísa V. Lopes[1]

Received: 20 November 2017 / Revised: 2 May 2018 / Accepted: 14 May 2018

Abstract

Synaptic dysfunction plays a central role in Alzheimer's disease (AD), since it drives the cognitive decline. An association between a polymorphism of the adenosine A_{2A} receptor ($A_{2A}R$) encoding gene—*ADORA2A*, and hippocampal volume in AD patients was recently described. In this study, we explore the synaptic function of $A_{2A}R$ in age-related conditions. We report, for the first time, a significant overexpression of $A_{2A}R$ in hippocampal neurons of aged humans, which is aggravated in AD patients. A similar profile of $A_{2A}R$ overexpression in rats was sufficient to drive age-like memory impairments in young animals and to uncover a hippocampal LTD-to-LTP shift. This was accompanied by increased NMDA receptor gating, dependent on mGluR5 and linked to enhanced Ca^{2+} influx. We confirmed the same plasticity shift in memory-impaired aged rats and APP/PS1 mice modeling AD, which was rescued upon $A_{2A}R$ blockade. This $A_{2A}R$/mGluR5/NMDAR interaction might prove a suitable alternative for regulating aberrant mGluR5/NMDAR signaling in AD without disrupting their constitutive activity.

Introduction

Synaptic dysfunction plays a central role in Alzheimer's disease (AD), since it drives the cognitive decline [1]. In age-related neurodegeneration, cognitive decline has a stronger correlation to early synapse loss than neuronal loss in patients [2]. Despite the many clinical trials conducted to identify drug targets that could reduce protein toxicity in AD, such targets and such strategies proven unsuccessful. Therefore, efforts focused on identifying the early mechanisms of disease pathogenesis, driven or exacerbated by the aging process, may prove more relevant to slow the progression rather than the current disease-based models.

The array of synaptic proteins is complex and the mechanisms underlying excitatory synaptic transmission are finely tuned by synaptic activity. The activation of *N*-methyl-D-aspartate (NMDA) receptors plays a pivotal role, because it can induce either long-term potentiation (LTP) or long-term depression (LTD), depending on the extent of the resultant intracellular [Ca^{2+}] rise in the dendritic spines and the downstream activation of specific intracellular cascades [3]. Indeed, the Aβ-triggered synaptic failure involves the removal of AMPA receptors from the synaptic membrane and the degradation of PSD95 protein at glutamatergic synapses [4, 5]. In addition to NMDA receptors and AMPA receptors, an involvement of the metabotropic glutamate receptors (mGlu receptors) in Aβ mediated synaptic dysfunction has been suggested [6]. Shankar and colleagues [6] demonstrated that different sources of Aβ (synthetic, extracted from human brain or from cells) can facilitate mGlu receptor-mediated LTD and can inhibit LTP leading to a reduced dendritic spine density.

The role of LTP has been extensively studied in learning and memory [7–9]. However, much less is known about LTD and memory, either in physiological or pathological

Electronic supplementary material The online version of this article (https://doi.org/10.1038/s41380-018-0110-9) contains supplementary material, which is available to authorized users.

✉ Luísa V. Lopes
lvlopes@medicina.ulisboa.pt

Extended author information available on the last page of the article

Published online: 27 June 2018

conditions. LTD is defined as a long-lasting weakening of a synapse in response to a repeated low-frequency stimulation [10, 11], being required for consolidation of hippocampal-dependent spatial memory [12]. The trigger for inducing activity-dependent LTD is predominantly an increase in postsynaptic calcium (Ca^{2+}). Since postsynaptic rises in Ca^{2+} are implicated in the induction of both LTP and LTD [13], it is widely accepted that larger rises in intracellular Ca^{2+} result in LTP induction, while more modest increases lead to LTD induction [14]. Some authors report increased susceptibility to LTD during aging [15], whereas others fail to observe alterations in LTD magnitude in aged animals [16]. These discrepancies can be explained by differences in animal strain, stimulation pattern or Ca^{2+}/Mg^{2+} ratio. Accordingly, age-related differences in LTD induction could be rescued by manipulating the extracellular Ca^{2+}/Mg^{2+} ratio, consistent with the idea that changes in Ca^{2+} regulation with advanced age may trigger increased susceptibility to LTD [15, 17, 18]. However, the mechanisms leading to calcium alterations in LTD during normal aging and age-related diseases remain mostly unexplored. Recently, an association between a polymorphism of the adenosine A_{2A} receptor ($A_{2A}R$) encoding gene—*ADORA2A*, with hippocampal volume (synaptic loss) in mild cognitive impairment and AD was reported [19]. This polymorphism occurs in a non-coding region, upstream to the coding sequence and it was just suggested, but not studied, that it could imply alterations in $A_{2A}R$ expression.

There is compelling evidence from animal models of a cortical and hippocampal upsurge of $A_{2A}R$ in glutamatergic synapses upon aging and AD [20–26]. Such $A_{2A}R$ overactivation induces glutamate release via PKA/cAMP/CREB signaling [23, 25, 27, 28], calcium influx [29] and leads to hippocampus-dependent cognitive deficits [30, 31]. Conversely, the blockade of $A_{2A}R$, with either caffeine or more selective antagonists (SCH 58261, KW6002, or MSX-3), prevents hippocampus-dependent memory deficits and LTP impairments in aged animals [32, 33] and in several AD models [34–37]. Furthermore, knocking-out $A_{2A}R$ can rescue stress and AD-related synaptic dysfunction [38, 39]. Accordingly, in humans, several epidemiological studies have shown that regular caffeine consumption attenuates memory disruption during aging and decreases the risk of developing memory impairments in AD patients [34, 40–43]. Altogether, these data suggest that $A_{2A}R$ might be a good candidate as trigger to synaptic dysfunction in aging and AD.

We now explored the role of $A_{2A}R$ in hippocampal function in age-related conditions. We showed a significant upsurge of $A_{2A}R$ in hippocampal neurons of aged humans, a phenotype aggravated in AD patients. Increased expression of $A_{2A}R$ driven by the CaMKII promoter selectively in rat forebrain neurons was sufficient to mimic aging-like memory impairments and to uncover an LTD-to-LTP shift in the hippocampus. This shift was due to an increased NMDA receptor gating and associated to increased Ca^{2+} influx. We identified the mGluR5-NMDAR interplay as key player in the observed $A_{2A}R$-induced synaptic dysfunction. Importantly, the same LTD-to-LTP shift was observed in memory-impaired aged rats and APP/PS1 mice modeling AD, a phenotype rescued upon $A_{2A}R$ blockade.

We not only prove that $A_{2A}R$ overexpression in young animals is sufficient to drive age-like synaptic impairments, but also explored this newly found interaction as a suitable alternative for regulating aberrant mGluR5/NMDA signaling without disrupting their constitutive activity. Due to the aberrant $A_{2A}R$ signaling in pathological conditions (reviewed in ref. [44]), their blockade is particularly relevant for long-term therapies, since the alternative option of targeting directly either mGluR5 or NMDAR interferes with basal neuronal function and memory, as these proteins are crucial components of the postsynaptic density.

Results

Increased levels of $A_{2A}R$ in human aged and Alzheimer's disease (AD) brain

There is a genetic association of the adenosine A_{2A} receptor encoding gene (*ADORA2A*) with hippocampal volume in mild cognitive impairment and Alzheimer's disease [19]. Plus, $A_{2A}R$ upregulation in cortex and hippocampus is associated with memory dysfunction in different animal models [45, 46]. We now probed this increase in human brain of aged and AD subjects. $A_{2A}R$ expression was measured in young (20–40 years old), aged (60–75 years old) and AD (60–75 years old, Braak stages 5–6) forebrain. There was a significant increase in $A_{2A}R$ protein levels in the aged forebrain that was further enhanced in samples from AD patients (Fig. 1a, b). The messenger RNA (mRNA) quantification by quantitative PCR (qPCR) indicates a 4.9 ± 0.3 ($n = 3$) fold increase in $A_{2A}R$ transcripts in AD samples compared to aged samples (Fig. 1c). To assess the cellular origin of this $A_{2A}R$ upregulation, we performed a histological analysis of the hippocampi from AD patients and age-matched controls. We detected a DAB-specific staining for $A_{2A}R$ in aging and AD sections (Fig. 1d, e), absent in the negative control (Supplementary Fig. 1a). In both conditions, we observed a neuron-specific $A_{2A}R$ positive staining (brown arrows; characterized by a large hypochromatic nucleus with nucleolar inclusions). We did not detect any significant $A_{2A}R$ signal in astrocytes (black arrows; nuclei typically have pale, finely granular chromatin patterns and relatively small or indistinct nucleoli), oligodendrocytes (blue arrows; small, round, relatively dark nuclei) or microglia (green arrows; rod-shaped and often irregularly contoured nuclei) [47] (Fig. 1d).

Physiopathological levels of $A_{2A}R$ in neurons impair hippocampus-dependent spatial memory

Given that $A_{2A}R$ upregulation is associated with decreased cognitive performance characteristic of aging and AD, we studied a rat transgenic model with physiopathological levels of $A_{2A}R$ expression to address the underlying mechanism. These transgenic rats selectively overexpress the human $A_{2A}R$ in neurons under the control of the CaMKIIα promoter [Tg(CaMKII-hA_{2A}R); Fig. 1f], mainly in the cortex and hippocampus, in an aging-like pattern of expression [23, 30]. The hippocampus displays a significant overexpression of $A_{2A}R$, particularly the DG and CA1, as reported by the in situ $A_{2A}R$ mRNA human probe (Fig. 1f) and immunostaining (Fig. 1g) and negligible expression in other brain areas (see also [30]). Importantly, at 12–16 weeks of age, Tg(CaMKII-hA_{2A}R) animals present a 5–8-fold increase of hippocampal $A_{2A}R$ immunoreactivity [30], which is of the same magnitude as the increase found in our human aged and AD samples (Fig. 1b), and equivalent to that of aged rats [22]. To further evaluate the profile of $A_{2A}R$ expression, co-staining for $A_{2A}R$, GFAP, and MAP2 was performed in hippocampal slices, confirming the upsurge in the neuropil and discarding the possibility of astrocytic $A_{2A}R$ expression in this model (Fig. 1g). Biochemical fractionation of hippocampal tissue revealed a clear enrichment of $A_{2A}R$ in the SNAP25 positive fraction, in contrast to the low levels in the PSD95-enriched fraction, favoring a mainly presynaptic localization (Fig. 1h), as occurs for native $A_{2A}R$ in the rodent hippocampus [21, 48]. This was further confirmed by immunohistochemical analysis of the CA1 area of the hippocampus, in which the $A_{2A}R$ signal overlaps with that of SNAP25, and not with PSD95 signal (Supplementary Figs. 1b, c and 2a). This is not due to lack of resolution since our system was able to resolve a control section labeled for both a pre- and a postsynaptic protein (Supplementary Fig. 2b).

Accordingly, immunoelectron micrographs of the CA1 area of Tg(CaMKII-hA_{2A}R) reveal a preferential presynaptic localization of $A_{2A}R$ (Fig. 1i). We then evaluated hippocampus-dependent spatial memory using the Morris water maze (MWM) test. Transgenic animals displayed a decrease in acquisition (Fig. 2a) and a lack of preference for the target quadrant during the probe test (Fig. 2b). We did not find differences in swimming speed between groups (Fig. 2c).

Increased levels of $A_{2A}R$ enhance glutamate release probability

To further dissect the mechanism by which $A_{2A}R$ impair memory performance, whole-cell patch-clamp recordings were performed. We first measured the intrinsic excitability of CA1 neurons from Tg(CaMKII-hA_{2A}R) and WT rats. No changes were observed in passive properties (resting membrane potential or membrane resistance), nor in single spike analysis of the studied populations of neurons (Supplementary Fig. 3a, b). Moreover, neurons from WT and Tg(CaMKII-hA_{2A}R) animals exhibited similar behavior when submitted to steps of current injection (Supplementary Fig. 3c–h). Thus, $A_{2A}R$ overexpression does not impact on the studied passive or intrinsic excitability properties of CA1 neurons. We then performed afferent-evoked EPSCs from CA1 pyramidal neurons ($V_h = -70$ mV), in the presence of $GABA_A$ receptor antagonist picrotoxin (50 μM). $A_{2A}R$ blockade significantly inhibited excitatory postsynaptic currents (EPSCs), an effect that was not observed in WT animals (Fig. 2d, e). Thus, there is a gain of function of $A_{2A}R$ upon their overexpression, whereby $A_{2A}R$ tonically control basal synaptic transmission in Tg (CaMKII-hA_{2A}R) animals, which does not occur in WT animals.

To test if tonic $A_{2A}R$ modulation of neuronal function occurs at a presynaptic level, we evaluated the glutamate release probability. A facilitation of the paired-pulse ratio (PPR) was observed in neurons from WT animals at all inter-stimulation intervals, more evident for the shorter intervals (Supplementary Fig. 3i). The magnitude of facilitation was reduced in Tg(CaMKII-hA_{2A}R) rats when compared to WT neurons (Supplementary Fig. 3i), albeit maintaining the same facilitatory profile. These data suggest that neuronal $A_{2A}R$ overexpression increases glutamate release probability [49, 50]. These PPR alterations in Tg (CaMKII-hA_{2A}R) rats were completely rescued by the $A_{2A}R$ selective antagonist, SCH 58261 (Supplementary Fig. 3i). As expected, $A_{2A}R$ blockade does not alter PPR values in WT animals (Supplementary Fig. 3i).

$A_{2A}R$ increase NMDAR-mediated currents in CA1 pyramidal neurons

$A_{2A}R$ were proposed to mainly modulate NMDA receptors (NMDAR) [51–53], which are minor contributors to excitatory synaptic transmission under basal conditions in the hippocampus [54]. We tested possible alterations of the AMPA and NMDA receptor contribution, by quantifying the AMPA/NMDA receptor ratio. The AMPA/NMDA receptor ratio was decreased in Tg(CaMKII-hA_{2A}R) vs. WT animals (Fig. 2f). To assess if this could be attributed to changes in the gating properties of the receptors, we performed current–voltage (I–V) relationships in pharmacologically isolated AMPAR and NMDAR responses. While the I–V relationships of the NMDAR were significantly increased in neurons from Tg(CaMKII-hA_{2A}R) animals (Fig. 2g), the AMPAR voltage-dependency was unaltered in Tg(CaMKII-hA_{2A}R) neurons (Supplementary Fig. 3j).

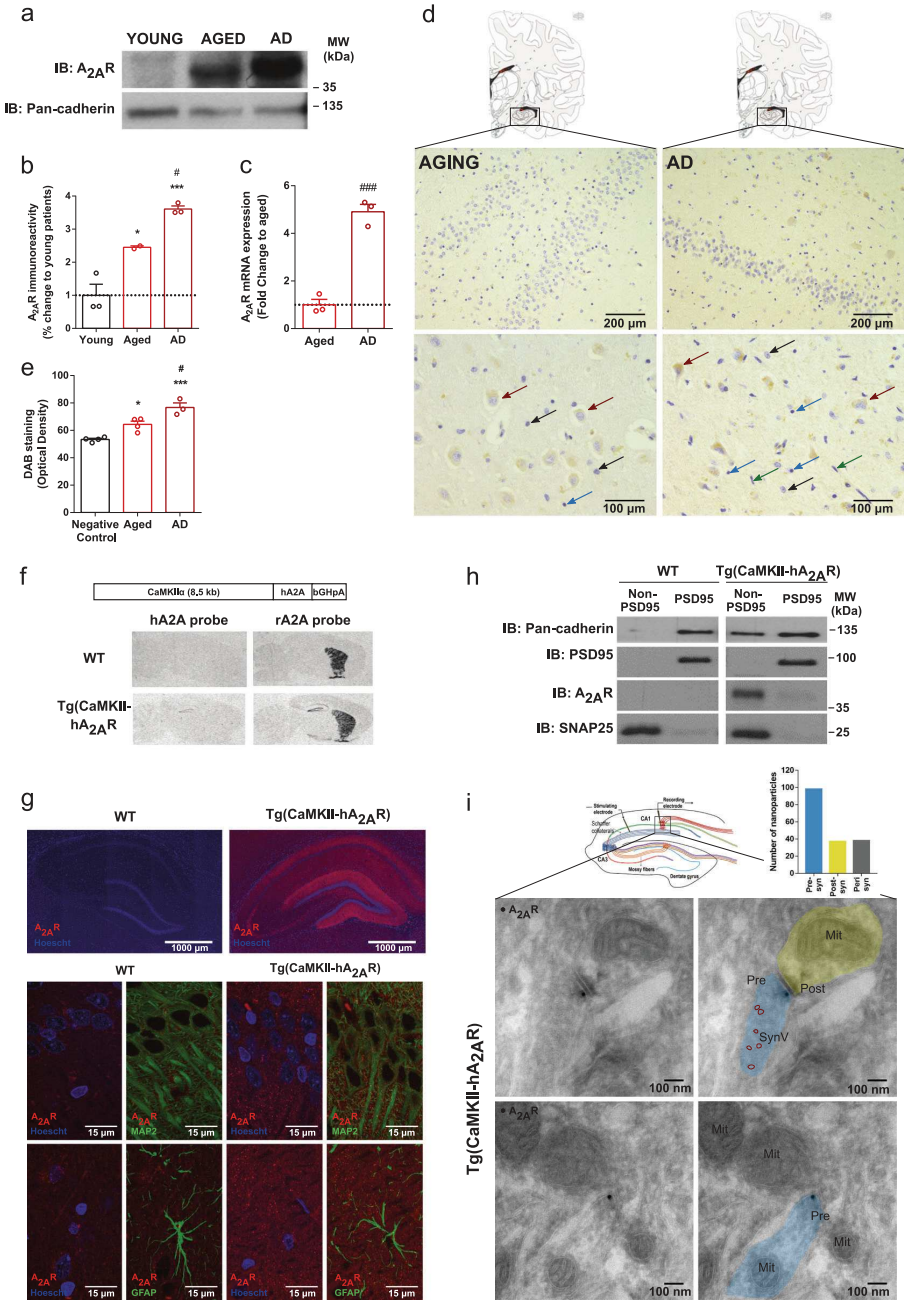

Moreover, we calculated the ratio between NMDAR current recorded at + 40 mV and at −60 mV, and observed it was significantly increased in Tg(CaMKII-hA_{2A}R) neurons (Fig. 2h).

In the hippocampus, NMDARs are heteromeric assemblies mainly composed of a constitutive GluN1 subunit and GluN2A or GluN2B subunits [55]. The deactivation time course of GluN1/GluN2B heteromers is higher than the one

◀ **Fig. 1** Increased levels of $A_{2A}R$ in human aged and Alzheimer's disease (AD) brain. **a** Representative image of the western blot for $A_{2A}R$ in human prefrontal cortex and the internal control Pan-cadherin. **b** $A_{2A}R$ immunoreactivity in young, aged, and AD human cortex ($^{*}p < 0.05$, $^{***}p < 0.001$ comparing to young subjects, $^{\#}p < 0.05$ comparing to aged subjects, one-way ANOVA followed by a Tukey's multiple comparisons post hoc test) ($n = 3$, 2, and 3, respectively). **c** Increase in $A_{2A}R$ mRNA in AD human brain when compared with age-matched control subjects ($^{\#\#\#}p < 0.001$ comparing to healthy age-matched subjects, unpaired *t*-test) ($n = 3$). **d** In human AD and age-matched control hippocampal sections, positive staining for $A_{2A}R$ is present (scale bar: 200 µm). Within hippocampus, $A_{2A}R$ upsurge is neuronal specific, since positive labeling is observed in neurons (brown arrows; cells with large hypochromatic nucleus with nucleolar inclusions), while in astrocytes (black arrows; astrocytic nuclei typically have pale, finely granular chromatin patterns and relatively small or indistinct nucleoli), oligodendrocytes (blue arrows; characterized by small, round, relatively dark nuclei) and microglia (green arrows; cells with rod-shaped and often irregularly contoured nuclei) $A_{2A}R$ is not detected (scale bar: 100 µm). **e** DAB immunostaining quantification in negative control, aged, and AD samples ($^{*}p < 0.05$, $^{***}p < 0.001$ comparing to negative control, $^{\#}p < 0.05$ comparing to aged, one-way ANOVA followed by a Bonferroni's multiple comparisons post hoc test) ($n = 4$, 4, and 3, respectively). **f** Construct used to generate Tg(CaMKII-hA_{2A}R) rats; Tg(CaMKII-hA_{2A}R) animals present an overexpression of total $A_{2A}R$ in the hippocampus evaluated by in situ hybridization (both with the hA_{2A}R probe and through cross-hybridization of the rat $A_{2A}R$ probe to the human $A_{2A}R$ mRNA). **g** Compositional images of fluorescence immunohistochemistry of hippocampus of WT and Tg(CaMKII-hA_{2A}R) animals (scale bar: 1000 µm). Nuclei are labeled in blue (with Hoechst) and $A_{2A}R$ in red. $A_{2A}R$ staining is present in hippocampal areas of Tg(CaMKII-hA_{2A}R) animals but not in WT littermates. Within the hippocampus, positive labeling can be observed in CA3 axonal projections and strong staining is also observed in the neuropil of DG and CA1 areas. On the top, z-stack maximum intensity projection images taken at 100× magnification in CA1 area of hippocampus are presented (scale bar: 15 µm). MAP2 positive cells are identified by green fluorescence. $A_{2A}R$ staining can be observed in the neuropil of CA1 area in Tg(CaMKII-hA_{2A}R) hippocampal slices. At the middle and bottom panels, a z-stack maximum intensity projection image taken at 100× magnification in CA1 area of hippocampus is presented (scale bar: 15 µm). GFAP positive cells are identified by green fluorescence. No co-localization is found between $A_{2A}R$ and GFAP staining. **h** Immunoblotting analysis after subcellular fractionation of hippocampal tissue from WT and Tg(CaMKII-hA_{2A}R) animals. **i** Electron micrographs of the area where the recordings were conducted in the hippocampus of Tg(CaMKII-hA_{2A}R) animals showing immunogold particles for $A_{2A}R$ in the presynaptic neuron. On top, intracellular distribution of nanoparticles reveal a preferential presynaptic localization of $A_{2A}R$. On the right, duplicates of the images with the identification of the subcellular structures. Pre presynaptic neuron, Post postsynaptic neuron, Mit mitochondria, SynV synaptic vesicle. Uncropped gels and blots with molecular weight standards are provided in Supplementary Fig. 6. All values are mean ± SEM

observed for GluN1/GluN2A heteromers [56]. To test if NMDAR overactivation was due to alterations in NMDAR subunit composition, we analyzed the deactivation kinetics of pharmacologically isolated NMDAR EPSCs. Time constants for fast, slow and weighted components (τ_{fast}, τ_{slow}, and $\tau_{weighted}$) were obtained by fitting the pharmacologically isolated NMDAR EPSCs ($V_h = +40$ mV) to a double exponential function (Levenberg-Marquandt method). No differences were found between groups for all parameters evaluated (Fig. 2i), suggesting that the enhancement of NMDAR conductance observed in Tg(CaMKII-hA_{2A}R) neurons is not related to alterations in NMDAR subunit composition.

Physiopathological levels of $A_{2A}R$ lead to a NMDAR-mediated LTD-to-LTP shift

In view of the key role of NMDAR in the control of synaptic plasticity we next focused on the impact of $A_{2A}R$ overexpression on long-term depression (LTD) in the CA1 area of the dorsal hippocampus. LTD is altered in association with memory deficits in aging [57] and animal models of stress [58] or AD [59]. In the hippocampus, LTD can be experimentally induced using several different protocols, including both electrical and pharmacological stimulation [60]. For our purpose, we selected a low-frequency stimulation (LFS) protocol particularly efficient in inducing robust LTDs in adult animals—three trains of 1200 pulses, 2 Hz, 10-min interval [39, 61].

We observed a significant alteration of the pattern of induction of LTD: whereas this protocol triggered a typical LTD in WT animals, it generated instead a significant LTP in Tg(CaMKII-hA_{2A}R) animals (Fig. 3a).

The pattern of activation of NMDAR controls the entry of calcium into the postsynaptic compartment, determining the output of plasticity [14, 62]. The robust recruitment of NMDAR causes a large calcium influx driving LTP, whereas the engagement of a lower number of NMDAR causes a more discrete calcium influx culminating in LTD [14, 62]. To confirm a greater NMDAR role in this LTD-to-LTP shift in Tg(CaMKII-hA_{2A}R) animals, we induced LTD and titrated the recruitment of NMDAR using increasing concentrations of the NMDAR antagonist, AP5 (Fig. 3b, c). With a low concentration of AP5 (15 µM), the LTP observed in Tg(CaMKII-hA_{2A}R) animals was abolished. Further increase of the AP5 concentration to 50 µM converted the LTP into LTD, fully rescuing the abnormal plasticity profile in Tg(CaMKII-hA_{2A}R) to a WT-like phenotype. Further increase of AP5 concentration to a supramaximal value of 100 µM abolished LTD, confirming that LTD in Tg(CaMKII-hA_{2A}R) animals is still strictly NMDAR-dependent (Fig. 3c). In WT animals, LTD magnitude did not change with 15 µM of AP5 (Fig. 3c), but when NMDAR were blocked with AP5 at 50 µM, no LTD was elicited, as expected (Fig. 3c). Consistent with an aberrant NMDAR contribution to basal transmission in Tg(CaMKII-hA_{2A}R) animals, we observed a decrease in fEPSPs slope with AP5 (50 µM) in Tg(CaMKII-hA_{2A}R) animals, but not in WT animals (Fig. 3d). Acute blockade of $A_{2A}R$ directly on slices rescued the LTD shift observed in

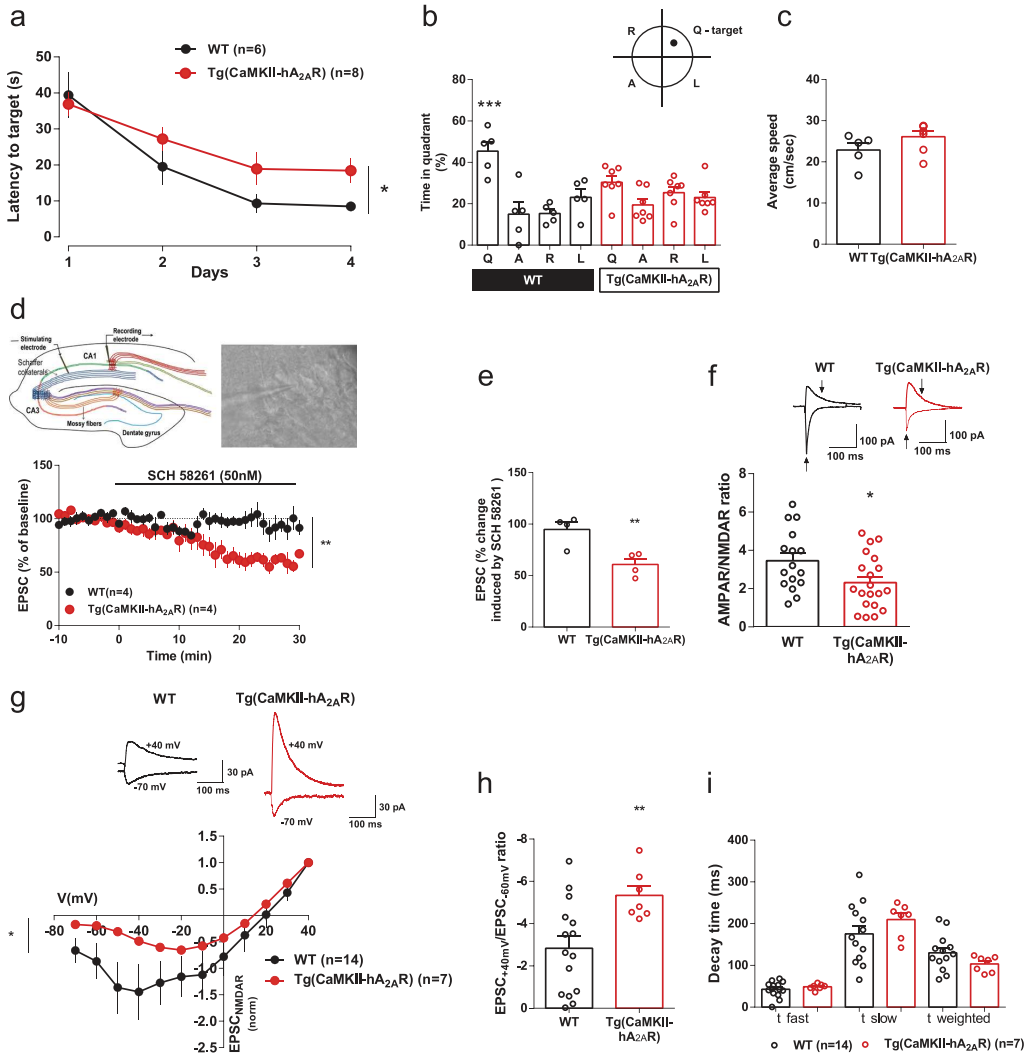

Fig. 2 Physiopathological levels of $A_{2A}R$ in neurons impair hippocampus-dependent spatial memory and increase NMDAR currents in CA1 pyramidal neurons. **a**, **b** Hippocampal-dependent memory performance was assessed by the MWM test, in which acquisition (**a**) ($*p < 0.05$, two-way ANOVA) ($n = 6$ and 8, respectively) and retention (**b**) ($***p < 0.001$, one-way ANOVA followed by a Bonferroni's multiple comparisons post hoc test within groups) ($n = 6$ and 8, respectively) were evaluated. **c** No changes in swimming speed during probe test between WT and Tg(CaMKII-hA_{2A}R) animals ($n = 6$ and 8, respectively). **d** Top left, schematic representation of the simplified circuitry of the hippocampus. A stimulation electrode was placed in the Schaffer collaterals and the recording electrode patching a pyramidal cell of the CA1 area. Top right, pyramidal area of the CA1 with a recording electrode patching one cell. Graph: Averaged time course of excitatory postsynaptic currents after perfusion with SCH 58261 (50 nM) for 30 min, in neurons from WT and Tg(CaMKII-hA_{2A}R) animals ($**p < 0.01$, unpaired *t*-test) ($n = 4$). Black traces represent baseline, while gray traces correspond to the EPSCs 20–30 min after SCH 58261 perfusion. **e** Averaged EPSCs (change in EPSCs from the last 10 min of SCH 58261 application) from acute SCH 58261 perfusion experiments. ($**p < 0.01$, unpaired *t*-test) ($n = 4$). **f** AMPAR/NMDAR ratio in neurons from WT and Tg(CaMKII-hA_{2A}R) animals ($*p < 0.05$, unpaired *t*-test) ($n = 16$ and 20, respectively); representative traces of EPSCs recorded at −70 mV and + 40 mV, arrows indicate the amplitudes considered to calculate AMPAR/NMDAR ratio. **g** Plots of normalized $EPSC_{NMDA}$ current–voltage relationships recorded in the presence of DNQX (100 μM) from WT and Tg(CaMKII-hA_{2A}R) neurons ($*p < 0.05$, two-way ANOVA) ($n = 14$ and 7, respectively); representative traces of NMDAR EPSCs recorded at −70 mV and + 40 mV. **h** NMDAR $EPSC_{+40mV}/EPSC_{-60mV}$ ratio from WT and Tg(CaMKII-hA_{2A}R) neurons ($**p < 0.01$, unpaired *t*-test) ($n = 14$ and 7, respectively). **i** Average time constants for fast and slow components (τ_{fast} and τ_{slow}) of NMDAR EPSC recorded in neurons from WT and Tg(CaMKII-hA_{2A}R) animals ($n = 14$ and 7, respectively). All values are mean ± SEM

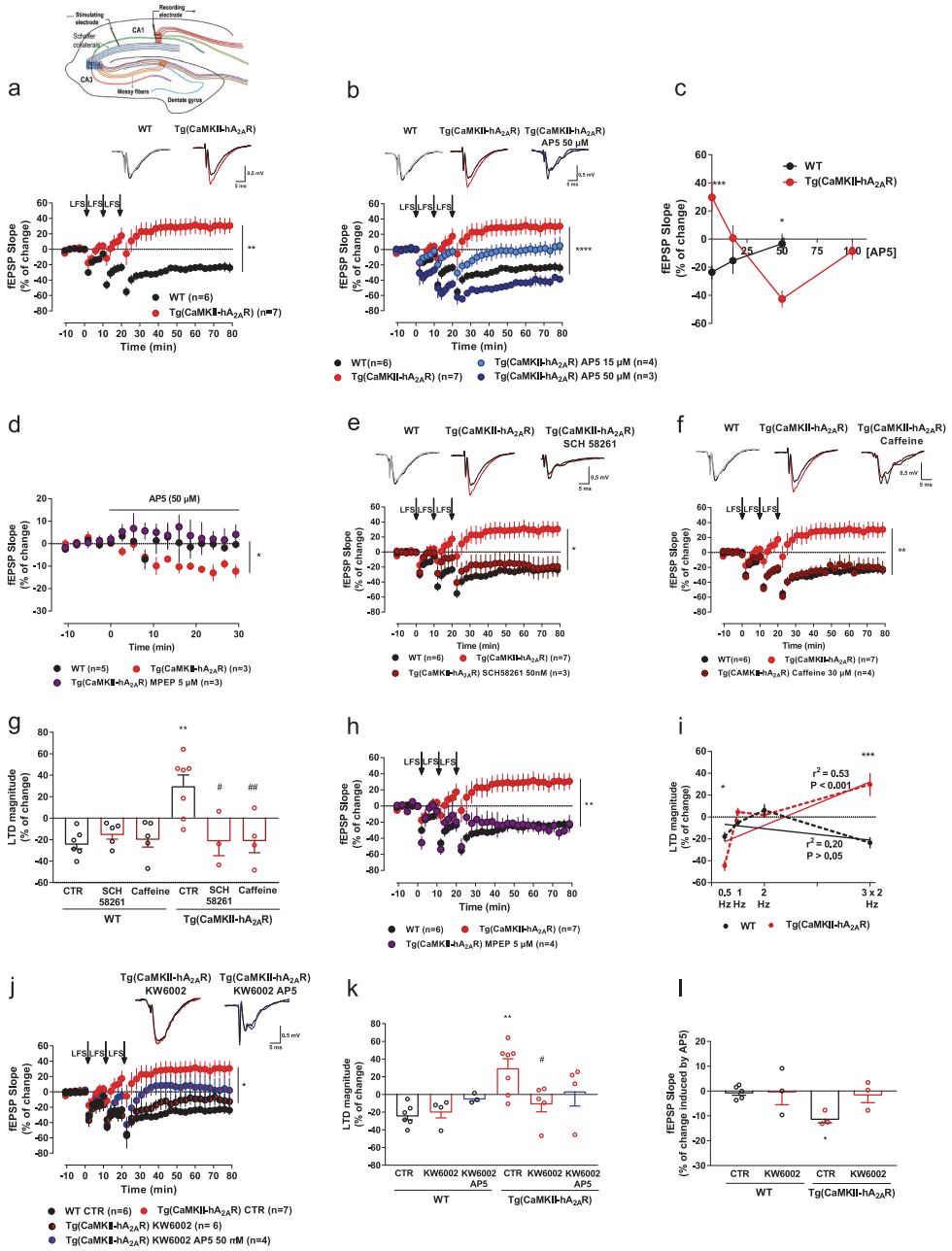

Tg(CaMKII-hA_{2A}R) animals. In fact, LFS stimulation of Tg (CaMKII-hA_{2A}R) slices with either SCH 58261 (50 nM) or the non-selective adenosine antagonist, caffeine (30 µM) triggered an LTD similar to that found in WT animals (Fig. 3e–g). As expected, in WT animals, this A_{2A}R blockade did not change LTD magnitude (Fig. 3g). Accordingly, SCH 58261, 50 nM, significantly decreased basal field excitatory post-synaptic potentials (fEPSPs) in Tg(CaMKII-hA_{2A}R) animals, while no effect was observed in WT (Supplementary Fig. 3k), confirming that the effects

◀ **Fig. 3** Physiopathological levels of $A_{2A}R$ lead to a NMDAR-mediated LTD-to-LTP shift. **a** Top, schematic representation of the simplified circuitry of the hippocampus. A stimulation electrode was placed in the Schaffer collaterals and the recording electrode in the pyramidal layer of the CA1 area. Graph: Changes in fEPSP slope induced by LFS stimulation (three trains of 1200 pulses, 2 Hz) recorded from WT and Tg(CaMKII-hA_{2A}R) hippocampal slices (**$p < 0.01$, unpaired *t*-test) ($n = 6$ and 7, respectively); representative traces of fEPSPs before (black) and 50–60 min after (gray, red) LTD induction in WT and Tg (CaMKII-hA_{2A}R) animals. **b** Changes in fEPSP slope induced by LFS stimulation (three trains of 1200 pulses, 2 Hz) recorded from WT and Tg(CaMKII-hA_{2A}R) hippocampal slices after partial and complete NMDAR blockade with AP5 (15 and 50 μM, respectively) (****$p <$ 0.0001 comparing to Tg(CaMKII-hA_{2A}R), two-way ANOVA followed by Bonferroni's multiple comparisons post hoc test) ($n = 4$ and 3, respectively); representative traces of fEPSPs before (black) and 50–60 min after (gray, red, blue) LTD induction in WT, Tg(CaMKII-hA_{2A}R) and Tg(CaMKII-hA_{2A}R) animals with NMDAR complete blockade. **c** Effect of increasing AP5 concentrations (0–100 μM) on synaptic strength after low-frequency stimulation (changes after 50-60 min) in WT and Tg(CaMKII-hA_{2A}R) animals (*$p < 0.05$, ***$p <$ 0.001, two-way ANOVA followed by Bonferroni's multiple comparisons post hoc test) (WT: $n = 6$, 4, and 4, respectively; Tg(CaMKII-hA_{2A}R): $n = 7$, 4, 3, and 3, respectively). **d** mGluR5 blockade rescues the effect of AP5 on basal transmission in Tg(CaMKII-hA_{2A}R) animals (*$p < 0.05$ comparing to WT, one-way ANOVA followed by Bonferroni's multiple comparisons post hoc test) ($n = 3$). **e** Changes in fEPSP slope induced by LFS stimulation recorded from WT, Tg (CaMKII-hA_{2A}R) and Tg(CaMKII-hA_{2A}R) hippocampal slices perfused with SCH 58261 (50 nM) (*$p < 0.05$ comparing to Tg(CaMKII-hA_{2A}R), two-way ANOVA followed by Bonferroni's multiple comparisons post hoc test) ($n = 6$, 7, and 3, respectively); representative traces of fEPSPs before (black) and 50–60 min after (gray, red, dark red) LTD induction in WT, Tg(CaMKII-hA_{2A}R) and Tg(CaMKII-hA_{2A}R) animals with SCH 58261. **f** Changes in fEPSP slope induced by LFS stimulation recorded from WT, Tg(CaMKII-hA_{2A}R) and Tg (CaMKII-hA_{2A}R) hippocampal slices perfused with caffeine (30 μM) (**$p < 0.01$ comparing to Tg(CaMKII-hA_{2A}R), two-way ANOVA followed by Bonferroni's multiple comparisons post hoc test) ($n = 6$, 7, and 4, respectively); representative traces of fEPSPs before (black) and 50–60 min after (gray, red, dark red) LTD induction in WT, Tg (CaMKII-hA_{2A}R) and Tg(CaMKII-hA_{2A}R) animals with caffeine. **g** Changes in fEPSP slope induced by LFS stimulation recorded from WT and Tg(CaMKII-hA_{2A}R) perfused with SCH 58261 (50 Mn) or caffeine (30 μM) (**$p < 0.01$ comparing to WT, $^{\#}p < 0.05$, $^{\#\#}p < 0.01$ comparing to Tg(CaMKII-hA_{2A}R), two-way ANOVA followed by Bonferroni's multiple comparisons post hoc test) (WT: $n = 5$). **h** Changes in fEPSP slope induced by LFS stimulation recorded from WT, Tg(CaMKII-hA_{2A}R) and Tg(CaMKII-hA_{2A}R) hippocampal slices perfused with mGluR5 antagonist MPEP (5 μM) (**$p < 0.01$ comparing to Tg(CaMKII-hA_{2A}R), two-way ANOVA followed by Bonferroni's multiple comparisons post hoc test) ($n = 6$, 7, and 4, respectively). **i** Changes in fEPSP slope induced by increasing frequencies of LFS stimulation in WT and Tg(CaMKII-hA_{2A}R) animals (*$p < 0.05$, ***$p < 0.001$, two-way ANOVA followed by Bonferroni's multiple comparisons post hoc test) (WT: $n = 4$, 3, 3, and 6, respectively; Tg(CaMKII-hA_{2A}R): 4, 4, 4, and 7, respectively). **j** Changes in fEPSP slope induced by LFS stimulation (three trains of 1200 pulses, 2 Hz) in WT and Tg(CaMKII-hA_{2A}R) animals non-treated (CTR) and treated with KW6002 (**$p < 0.01$ comparing to Tg(CaMKII-hA_{2A}R, two-way ANOVA followed by Bonferroni's multiple comparisons post hoc test) ($n = 6$). AP5, 50 μM, abolished LTD in Tg(CaMKII-hA_{2A}R) animals treated with KW6002 ($n = 4$); representative traces of fEPSPs before (black) and 50–60 min after (red, blue) LTD induction in Tg(CaMKII-hA_{2A}R) chronically treated with KW6002 in the absence and presence of AP5. **k** Changes in fEPSP slope induced by LFS stimulation recorded from WT and Tg(CaMKII-hA_{2A}R) animals non-treated (CTR) and treated with KW6002, in the presence and absence of AP5 (50 μM). (**$p < 0.01$ comparing to WT, $^{\#}p < 0.05$ comparing to Tg(CaMKII-hA_{2A}R), two-way ANOVA followed by Bonferroni's multiple comparisons post hoc test) (WT: $n = 6$, 4, and 3, respectively; Tg(CaMKII-hA_{2A}R): $n = 7$, 5, and 4, respectively). **l** Chronic KW6002 treatment reverts the effect of AP5 on basal transmission in Tg(CaMKII-hA_{2A}R) animals (*$p < 0.05$ comparing to WT, one-way ANOVA followed by Bonferroni's multiple comparisons post hoc test) ($n = 3$). All values are mean ± SEM

seen in Tg(CaMKII-hA_{2A}R) animals are indeed due to $A_{2A}R$ overactivation.

Group I metabotropic glutamate receptors, namely mGluR5, are postsynaptic and tightly coupled to NMDA receptors [51, 63, 64], conferring them the ability to exacerbate NMDAR-mediated toxicity. Upon activation by glutamate release, preferentially upon strong synaptic activation, they increase NMDAR-mediated Ca^{2+} currents [65]. When we blocked mGluR5 with MPEP, 5 μM, the LTD-to-LTP shift observed in Tg(CaMKII-hA_{2A}R) animals was prevented (Fig. 3h). Consistent with their activation upstream of NMDAR, the aberrant NMDAR component in Tg(CaMKII-hA_{2A}R) disappeared upon mGluR5 blockade (Fig. 3d), disclosing mGluR5 as a player in the observed $A_{2A}R$-induced synaptic dysfunction. MPEP does not change AP5-induced basal transmission or LTD magnitude in WT animals (Supplementary Fig. 3l, m).

To further study the alterations in the threshold for LTD in Tg(CaMKII-hA_{2A}R) animals, we elicited LTD using decreasing frequencies of stimulation maintaining the total number of pulses of one train (1200): 2, 1, and 0.5 Hz. In contrast to what we observed for 3 × trains of 1200 pulses (2 Hz), a lower 0.5 Hz frequency was more effective in inducing LTD in Tg(CaMKII-hA_{2A}R) than in WT animals (Fig. 3i and Supplementary Fig. 4a). Furthermore, frequencies of 1 and 2 Hz failed to elicit LTD in both WT and Tg(CaMKII-hA_{2A}R) (Supplementary Fig. 4b, c). More importantly, the magnitude of LTD in Tg(CaMKII-hA_{2A}R) animals correlated significantly with the frequency of stimulation (Fig. 3i), consistent with a shift to the left in the LTD threshold.

Blockade of $A_{2A}R$ activation in vivo rescues the LTD-to-LTP shift in Tg(CaMKII-hA_{2A}R) animals

To establish that $A_{2A}R$ overactivation is indeed the trigger for the aberrant NMDAR recruitment, we treated Tg (CaMKII-hA_{2A}R) animals with the $A_{2A}R$ selective antagonist KW6002 (5 mg/kg/day), in the drinking water for 4 weeks. In Tg(CaMKII-hA_{2A}R)-treated animals, LFS induced an LTD comparable to WT animals, rescuing the LTD-to-LTP shift (Fig. 3j, k). Furthermore, the KW6002 treatment normalized NMDAR overactivation, as confirmed

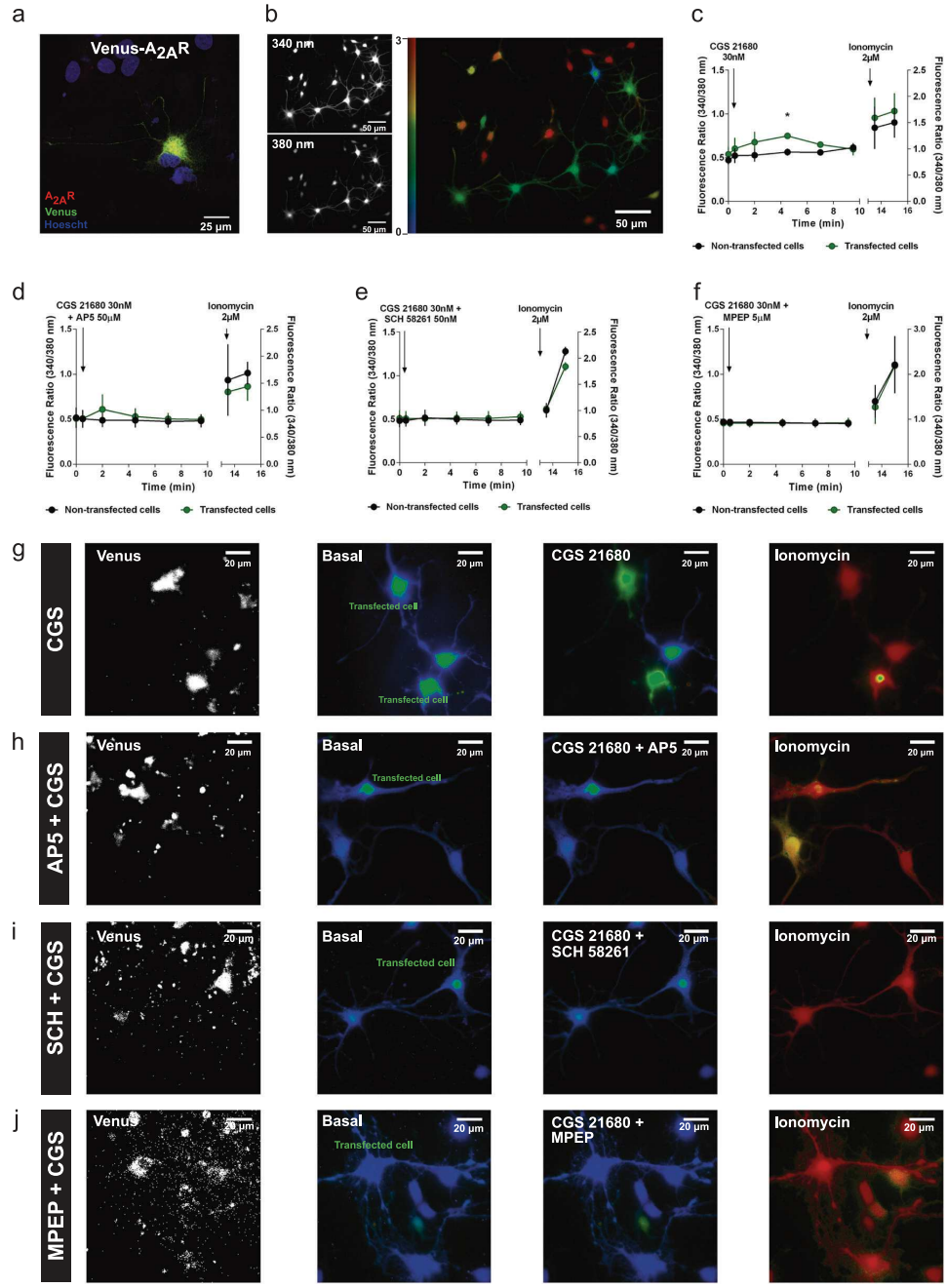

by the reinstatement of AP5 ability to fully block LTD in Tg (CaMKII-hA_{2A}R) (Fig. 3j, k). The treatment with KW6002 did not change LTD magnitude in WT animals (Fig. 3k), nor A_{2A}R mRNA relative expression in both WT and Tg (CaMKII-hA_{2A}R) (Supplementary Fig. 4d). The increased NMDAR contribution to basal transmission observed in Tg (CaMKII-hA_{2A}R) animals disappeared upon chronic KW6002 treatment (Fig. 3l).

◀ **Fig. 4** Increased levels of $A_{2A}R$ impair calcium homeostasis. **a** Control immunocytochemistry analysis of neurons transfected with Venus-$A_{2A}R$ construct confirmed co-expression of Venus and $A_{2A}R$. **b** Representative images of Ca^{2+} imaging. Bright regions indicate the location of cytoplasm and organelles, where the concentration of Ca^{2+} is higher than in the dark regions indicating the extracellular medium, where diffusion processes take place. The right image corresponds to the ratio between the radiation emitted at 510 nm, when cells are excited at 340 nm, over emission upon excitation at 380 nm (F340/F380). **c** Time course of Ca^{2+}-dependent fluorescence recorded and averaged per minute from Fura-2 AM neurons transfected with Venus-$A_{2A}R$ construct in response to CGS 21680, 30 nM, and ionomycin, 2 µM. Application of $A_{2A}R$ agonist CGS 21680, 30 nM, elevated intracellular Ca^{2+} levels in Venus-$A_{2A}R$ transfected neurons, whereas lower changes in fluorescence were detected in non-transfected neurons (*$p < 0.05$, unpaired *t*-test). Time of application of drugs are shown by arrows. (4–15 responsive cells per experimental condition from three independent cultures). **d** Time course of Ca^{2+}-dependent fluorescence recorded and averaged from Fura-2 AM neurons transfected with Venus-$A_{2A}R$ construct in response to AP5, 50 µM, CGS 21680, 30 nM, and ionomycin, 2 µM. The $A_{2A}R$-evoked increase in $[Ca^{2+}]i$ observed in **c**) was prevented by NMDAR antagonism (4–15 responsive cells per experimental condition from two independent cultures). Time of application of drugs are shown by arrows. **e** Time course of Ca^{2+}-dependent fluorescence recorded and averaged from Fura-2 AM neurons transfected with Venus-$A_{2A}R$ construct in response to SCH 58261, 50 nM, CGS 21680, 30 nM, and ionomycin, 2 µM. The $A_{2A}R$-evoked increase in $[Ca^{2+}]i$ observed in **c**) was prevented by $A_{2A}R$ antagonism (4–15 responsive cells per experimental condition from two independent cultures). Time of application of drugs are shown by arrows. **f** Time course of Ca^{2+}-dependent fluorescence recorded and averaged from Fura-2 AM neurons transfected with Venus-$A_{2A}R$ construct in response to MPEP, 5 µM, CGS 21680, 30 nM, and ionomycin, 2 µM. The $A_{2A}R$-evoked increase in $[Ca^{2+}]i$ observed in **c**) was prevented by mGluR5 antagonism (4–15 responsive cells per experimental condition from three independent cultures). Time of application of drugs are shown by arrows. **g**, **h**, **i**, **j** Representative images of the different conditions showed in (**c**, **d**, **e**), and **f**, respectively. All values are mean ± SEM

Increased levels of $A_{2A}R$ impair calcium homeostasis

To investigate whether $A_{2A}R$-mediated NMDAR hyperactivation disrupted Ca^{2+} signaling, we measured variations in intracellular calcium concentrations ($[Ca^{2+}]i$) in primary neuronal cultures transfected with $A_{2A}R$. For this, we used a construct encoding a Venus-$A_{2A}R$ fusion protein. We confirmed the co-localization of the Venus signal with the immunostaining for $A_{2A}R$ (Fig. 4a). Changes in $[Ca^{2+}]i$ were detected by Ca^{2+} imaging using Fura 2-acetoxymethyl ester (Fura-2 AM) (Fig. 4b). Application of the $A_{2A}R$ agonist CGS 21680, 30 nM, elevated intracellular Ca^{2+} levels in Venus-$A_{2A}R$ transfected neurons, whereas in non-transfected neurons lower changes in fluorescence were detected (Fig. 4c, g and Supplementary Video 1). This $A_{2A}R$-evoked increase in $[Ca^{2+}]i$ was prevented by the NMDAR antagonist, AP5, 50 µM (Fig. 4d, h), the $A_{2A}R$ antagonist, SCH 58261, 50 nM (Fig. 4e, i) or mGluR5 antagonist MPEP, 5 µM (Fig. 4f, j). These results show for the first time a crosstalk between $A_{2A}R$ and NMDAR that impacts on Ca^{2+} influx in glutamatergic neurons.

LTD-to-LTP shift in aged and APP/PS1 animals is rescued by $A_{2A}R$ blockade

Aging and AD are associated with an upregulation of $A_{2A}R$ in the hippocampus as we report here (Fig. 1) and others have shown previously [20, 21, 23, 66]. We evaluated putative LTD impairments in aged animals and in an APP/PS1 mouse model of AD, both models displaying $A_{2A}R$ increased levels (Supplementary Fig. 4e, f).

Aged animals displayed the same LTD-to-LTP shift to that observed in our Tg(CaMKII-h$A_{2A}R$) animals, while in young animals a robust LTD was achieved (Fig. 5a, b). The LTD-to-LTP shift was completely rescued with $A_{2A}R$ blockade by SCH 58261 (Fig. 5a, b), whereas SCH 58261 did not alter LTD profile in young animals (Fig. 5b). Within the aged group, we identified a subset of age-impaired animals that performed worse than young rats in the Y-maze test, revealing no preference for the novel arm (Fig. 5c). Interestingly, these same animals seem to be distinguished by an LTD-to-LTP shift, also observed in Tg (CaMKII-h$A_{2A}R$) (Fig. 5d). In contrast, age-unimpaired animals performed within the range of young rats (Fig. 5c) and could be distinguished their lack of response to LFS (Fig. 5d). Consistent with the enhanced role of $A_{2A}R$ upon aging [23, 25, 28], SCH 58261 decreased basal transmission in hippocampal slices of aged animals, while no effect was observed in young animals (Supplementary Fig. 4g). We observed a tendency towards an increased effect of SCH 58261 in age-impaired subset (Supplementary Fig. 4h), when compared with age-unimpaired animals, in spite of the lower *n*. This larger tonic effect of adenosine suggests an increased $A_{2A}R$ activation in age-impaired animals. Importantly, we found that plasticity profile correlated significantly with the behavioral memory index in aged rats (Fig. 5e), whereby a higher LTD-to-LTP shift corresponded to a worse Y-maze performance. Notably, a 3-week treatment with the selective $A_{2A}R$ antagonist (KW6002; 5 mg/Kg/day; oral) restored memory impairments, as observed by the increased time spent in the novel arm (Fig. 5c). This KW6002 treatment did not affect $A_{2A}R$ mRNA expression in aged animals (Supplementary Fig. 4e), consistent to what was observed for Tg(CAMKII-h$A_{2A}R$) animals (Supplementary Fig. 4d).

In 11–12 months old APP/PS1 mice, these animals display memory deficits [67] and LFS elicited LTP instead of LTD (Fig. 5f, g), as seen in Tg(CaMKII-h$A_{2A}R$) animals. Importantly, acute blockade of $A_{2A}R$ with 100 nM SCH 58261, was able to revert the LTD-to-LTP shift back to the LTD characteristic of WT mice (Fig. 5f, g).

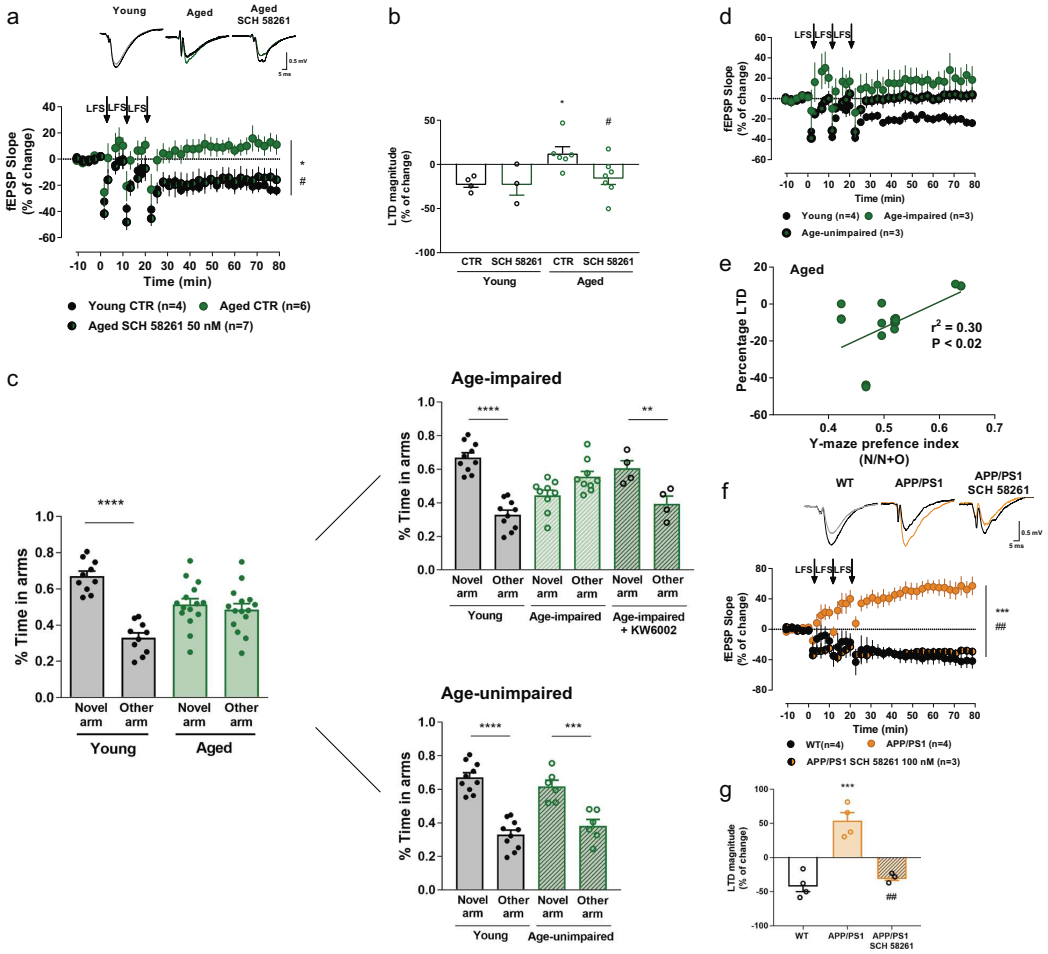

Fig. 5 LTD-to-LTP shift in aged and APP/PS1 animals is rescued by $A_{2A}R$ blockade. **a**, **b** Changes in fEPSP slope induced by LFS stimulation recorded from young and aged animals upon acute $A_{2A}R$ blockade (SCH 58261, 50 nM) ($^{*}p < 0.05$ comparing to young, $^{\#}p < 0.05$ comparing to aged, two-way ANOVA followed by Tukey's multiple comparisons post hoc test) (Young: 3 and 4, respectively; Aged: 6 and 7, respectively); representative traces of fEPSPs before (black) and 50–60 min after (gray, green, dark green) LTD induction in young, aged, and aged animals treated with SCH 58261, respectively. **c** Spatial memory performance was assessed by the Y-Maze test. Aged animals displayed a loss of preference for the novel arm ($^{***}p < 0.001$, $^{****}p < 0.0001$, novel arm comparing to other arm, two-way ANOVA followed by Bonferroni's multiple comparisons post hoc test) (young: $n = 10$; aged: $n = 15$). The pool of aged rats included a substantial subset of rats that performed within the range of young rats, labeled age-unimpaired rats ($n = 6$), while other clearly showed impairment, labeled age-impaired rats ($n = 9$), that is rescued upon chronic KW6002 treatment ($^{**}p < 0.01$, novel arm comparing to other arm, two-way ANOVA followed by Bonferroni's multiple comparisons post hoc test) ($n = 4$). **d** Age-impaired animals exhibited a LTD-to-LTP shift ($^{*}p < 0.05$ comparing to WT, one-way ANOVA followed by a Bonferroni's multiple comparisons post hoc test) ($n = 3$). Age-unimpaired animals can be distinguished by their lack of response to LFS ($n = 3$). **e** LTD magnitude observed in aged animals significantly correlates with Y-maze preference index (three replicates of $n = 6$ animals, $r^2 = 0.30$, $p < 0.05$). **f**, **g** Changes in fEPSP slope induced by LFS stimulation recorded from WT, APP/PS1 mice, and APP/PS1 hippocampal slices perfused with SCH 58261 (100 nM) ($^{***}p < 0.001$ comparing to WT, $^{\#\#}p < 0.01$ comparing to APP/PS1, one-way ANOVA followed by a Bonferroni's multiple comparisons post hoc test) ($n = 4$, 4, and 3, respectively); representative traces of fEPSPs before (black) and 50–60 min after (gray, orange) LTD induction in WT, APP/PS1 and APP/PS1 SCH 58261 100 nM. All values are mean ± SEM

Discussion

We show that the $A_{2A}R$ upsurge, described in different pathological situations in rodent models, such as hypoxia, ischemia, stress, diabetes, and even upon aging [44], is also characteristic of the human aged brain and is aggravated in AD [68]. Moreover, we describe that an increase in neuronal $A_{2A}R$ is sufficient to drive deficits in synaptic

plasticity, leading to an LTD-to-LTP shift and impairments of hippocampal-dependent learning and memory. This is a consequence of an $A_{2A}R$-induced increase in postsynaptic Ca^{2+} influx via NMDAR, which is dependent on mGluR5 activation (see Supplementary Fig. 5 for a summary). We reveal that the same synaptic plasticity shift occurs in the hippocampus of aged and APP/PS1 animals, which is rescued upon $A_{2A}R$ blockade.

The findings in human hippocampal samples confirm the observations made in animal models, in which $A_{2A}R$ density is increased upon aging [20, 22–24, 69]. Accordingly, in humans, several epidemiological studies have shown that regular caffeine consumption attenuates memory disruption during aging and decreases the risk of developing memory impairments in AD patients [34, 40–43]. Furthermore, in animal models of several other pathologies, there is a clear correlation of hippocampal $A_{2A}R$ upregulation with cognitive deficits, such as in acute or chronic stress [38, 45, 70], Alzheimer's [26], Parkinson's [71], or Huntington's diseases [72, 73]. However, the exact mechanism by which neuronal $A_{2A}R$ overactivation could trigger or increase the susceptibility for memory dysfunction in these multiple pathologies was not known.

A previous study using a model of $A_{2A}R$ overexpression under the control of the neuron-specific enolase promoter reported working memory deficits [74]. However, that study could not distinguish $A_{2A}R$-related embryonic effects from those elicited by postnatal alterations. In contrast, our model of overexpression, driven by a CaMKII promoter, allows a progressive postnatal and forebrain-specific expression, bypassing developmental effects and closer to an age-like $A_{2A}R$ distribution. These animals exhibit depressive-like behavior, hyperlocomotion, and altered exploratory behavior, consistent with the depressive signs found in aging, chronic stress, and AD [75]. Importantly, they do not present changes in adenosine A_1 receptor levels nor adenosine levels in the hippocampus [30]. Furthermore, at 12 week-old, the Tg(CaMKII-h$A_{2A}R$) animals display a 5–8-fold increase of $A_{2A}R$ immunoreactivity [30], which is in the same magnitude of that found in our human aged and AD samples, and equivalent to that of aged rats [20–22, 25]. Importantly, this $A_{2A}R$ overexpression occurs in the hippocampus and cortex, recapitulating the pattern observed in our aged and AD human samples and consistent with previous reports [68]. In the Tg(CaMKII-h$A_{2A}R$) model there is no evidence of $A_{2A}R$ overexpression in astrocytes, strengthening the idea that the observed memory and synaptic impairments are due to a neuronal-specific $A_{2A}R$ overexpression. The fact that in aged and AD human samples we observed a clear $A_{2A}R$ overexpression in neurons further emphasizes neuronal $A_{2A}R$ as key mediators in synaptic glutamatergic dysfunction observed in aging and AD [76]. Aberrant astrocytic $A_{2A}R$ expression in late-stage AD has been associated to cognitive decline, and indeed astrocytic $A_{2A}R$ can lead to alterations of synaptic $A_{2A}R$-mediated functions [77]. However, neuronal contribution is highlighted by recent evidence showing that stimulation of neuronal opto-$A_{2A}R$ in the hippocampus induces changes in synaptic plasticity and CREB activation [27]. Moreover, silencing $A_{2A}R$ in neurons of the associative/commissural pathway rescues the aberrant LTP in APP/PS1 mice in a non-NMDAR-dependent mechanism [26, 27]. Our findings demonstrate that neuronal A_{2A} overactivation is sufficient to induce synaptic dysfunction and cognitive impairments. This suggests that synaptic dysfunction in aging and early stages of AD may be driven predominantly by a neuronal $A_{2A}R$ progressive dysfunction, whereas at later Braak stages of AD, astrocytic $A_{2A}R$ and inflammation might become more relevant [39, 76].

Both aging and AD comprehend functional and structural alterations in the hippocampus that drive cognitive decline [1, 78]. Furthermore, they are also characterized by an abnormal Ca^{2+} signaling. Several studies reported an age-associated increase in basal $[Ca^{2+}]i$ levels [79, 80] and action potential-evoked calcium influx [81] and a reduction in the expression of calcium-buffering proteins. In AD mouse models, increased levels of intracellular Ca^{2+} [82] distorts the normal Ca^{2+} signaling and Ca^{2+}-dependent mechanisms and can indeed trigger the amyloidogenic pathway [83–85]. Concretely, the AD brain is characterized by a clear loss of synaptic processes and neuronal cell bodies in the limbic and association cortices (reviewed in ref. [1]). In normal aging, there is still a considerable structural preservation in several brain areas including the hippocampus [78, 86–88]. Therefore it is conceivable to hypothesize that the shift from normal aging to AD could be related to dysregulation of the integrated homeostatic network caused by differences either in the levels of the endogenous ligand —adenosine [89], or in the expression of $A_{2A}R$ that are increased upon aging and are further exacerbated in AD (Fig. 1). To specifically check the endogenous activation of $A_{2A}R$, we have quantified the effect of blocking $A_{2A}R$ in CA1 basal transmission, in age-impaired and age-unimpaired animals. The fact that we observe a tendency towards an increased effect of SCH 58261 in age-impaired subset, without significant differences in the bulk mRNA $A_{2A}R$ levels within the aged group, supports the first hypothesis.

$A_{2A}R$ and A_1R form heteromers and, under physiological conditions, adenosine preferentially activate A_1R [90, 91] in the hippocampus, which control glutamatergic neurotransmission, namely by a decrease in NMDAR-mediated responses [92, 93]. In conditions where hippocampal transmission is dysfunctional, there is an upregulation of $A_{2A}R$ (reviewed in ref. [44]) together with an increased release of ATP as a danger signal [94], which is the main source of the extracellular adenosine activating $A_{2A}R$ [95].

The signaling of these upregulated $A_{2A}R$ is shifted from a PKC-dependent, controlled by inhibitory adenosine A_1 receptors, towards a more disinhibited PKA-dependent mechanism in aging and pathology [25, 30, 96], leading to impaired synaptic plasticity and compromised memory performance [26, 38, 39, 45]

This dysfunction is associated to an excitatory effect on glutamatergic transmission, which we can postulate that it may be mediated by non-heteromerized $A_{2A}R$. Our results in Tg(CaMKII-h$A_{2A}R$) are in line with this hypothesis, since we observe an aberrant constitutive activation of $A_{2A}R$, dependent on PKA [30], and consequent NMDAR, both contributing to basal synaptic transmission, that could not be observed in WT animals.

Long-term synaptic plasticity processes (LTP and LTD) are the main neurophysiological correlate of memory [7, 97]. Although the relation between hippocampal LTP and memory is the most explored [98], there is also robust evidence that altered hippocampal LTD affects memory performance [12, 99], as shown in animal models of stress [58] or of AD [59, 61]. We now report that Tg(CaMKII-h$A_{2A}R$) animals display memory impairments together with a newly described LTD-to-LTP shift as a result of an increase in Ca^{2+} influx dependent on NMDAR activation. In fact, we observed a dose-dependent rescue of LTD in slices from Tg(CaMKII-h$A_{2A}R$) rats with the NMDAR antagonist AP5. The concentration that fully restored LTD in Tg(CaMKII-h$A_{2A}R$) prevented it in WT animals. This LTD in Tg(CaMKII-h$A_{2A}R$) is NMDAR-dependent, since a higher concentration of AP5, 100 μM, was able to completely abolish LTD. Accordingly, in primary cultures of hippocampal neurons, $A_{2A}R$ activation directly increased Ca^{2+} intracellular levels through NMDAR activation, blocked by its selective antagonist AP5. These data strongly indicate an $A_{2A}R$–NMDAR interaction, consistent with our synaptic plasticity results. Although in our paper we observe a Ca^{2+} influx-dependent LTD-to-LTP shift, there are reports that metabotropic NMDAR activity, independent of calcium influx, can also induce LTD [100]. More relevant, we have shown that the blockade of $A_{2A}R$ can restore a similar LTD-to-LTP shift in aged and AD mice models, strongly emphasizing $A_{2A}R$ as the pathophysiological mediator involved in this synaptic shift.

We can postulate that NMDA receptor gating properties are directly modulated by such an increase in glutamate available to activate the ionotropic receptor. In such a case, however, AMPA-mediated currents in Tg(CaMKII-h$A_{2A}R$) would be similarly increased, which we do not find. Moreover, when we transfected neurons with $A_{2A}R$ we could only observe an increase in Ca^{2+} transients in transfected cells, but not in the adjacent non-transfected neurons. If an overall increase in glutamate were the only mechanism, then we might expect some non-transfected neurons to be affected. Therefore, other postsynaptic modifications due to an $A_{2A}R$-related increase in glutamate release and/or postsynaptic $A_{2A}R$ contribution must be considered. Indeed, a postsynaptic activation of $A_{2A}R$ can lead to downstream activation of CREB in the hippocampus [27], and $A_{2A}R$ and mGluR5 can directly interact and regulate NMDAR activity [53, 101].

Group I metabotropic glutamate receptors, namely mGluR5, are postsynaptic and tightly coupled to NMDA receptors [63, 64, 102], conferring them the ability to either protect or exacerbate NMDAR-mediated toxicity depending upon the model or cell type [103]. Upon activation by glutamate release, preferentially upon strong synaptic activation, mGluR5 increase NMDAR-mediated Ca^{2+} currents [65], by reducing the Mg^{2+} block [103] and triggering the phosphorylation of NMDAR [64]. Previous studies hinted at a possible $A_{2A}R$-NMDAR crosstalk, since $A_{2A}R$ can control expression [51, 102], recruitment [52] and the rate of desensitization [53] of NMDAR. We and others have provided compelling evidence of an $A_{2A}R$-mGluR5 synergistic interaction in the modulation of NMDAR-mediated effects [53, 101, 102, 104]. Thus, mGluR5 is a likely candidate to act as a switch between $A_{2A}R$ and NMDAR, by sensing glutamate and translating it into NMDAR overactivation. Consistent with this hypothesis, we observe that mGluR5 blockade prevents the downstream NMDAR aberrant contribution in basal transmission and the LTD-to-LTP shift, supporting the mGluR5-NMDAR interplay as key player in the observed $A_{2A}R$-induced physiopathology.

Aging is associated with a decline in cognitive function that can, in part, be explained by changes in the mechanisms of plasticity [78]. While some studies report increased susceptibility to LTD during aging [15], others do not observe alterations in LTD magnitude between young and aged animals [16]. These discrepancies can be easily explained by differences in rat strain, stimulation pattern and Ca^{2+}/Mg^{2+} ratio. In fact, the stimulation pattern used in those studies (900 pulses, 1 Hz) does not elicit LTD in young animals [15, 105], while we and others observe a robust LTD with our LFS protocol [39, 61]. Moreover, those age differences were reverted under elevated Ca^{2+}/Mg^{2+} ratio suggesting that aging is associated with a shift in the threshold for LTD-induction rather than in the LTD intrinsic capacity [16, 57]. Notably, the significant correlation between LTD magnitude and the frequency of LFS in Tg(CaMKII-h$A_{2A}R$) animals confirms an age-associated decrease in the threshold for LTD induction.

The fact that in aged CA1 pyramidal neurons there is an increased duration of NMDAR-mediated responses [106] which display an altered Ca^{2+} metabolism typified by larger increases upon repeated stimulation [81, 107] further strengthens our hypothesis. This increase in Ca^{2+} observed in aging can lead to CREB dephosphorylation due to an increase in calcineurin (PP2B) activity, strongly suggesting

differential phosphatases and kinases activation as a key mediator in these impairments [108, 109]. Alterations in phosphatases and kinases could directly account for the observed LTD-to-LTP shift. Importantly, we not only showed that susceptibility to induction of LTD is associated with memory impairments in aging, but also that the LTD magnitude could be positively correlated with behavior performance, consistent with previous data [57, 110].

The fact that an acute $A_{2A}R$ blockade is sufficient to rescue the LTD-to-LTP shift favors the hypothesis that $A_{2A}R$ blockade reestablishes the physiological signaling of adenosine, rather than the receptor expression, which is unlikely to occur at such a short time frame. Accordingly, we have prior data showing that chronic KW6002 treatment rescues cognitive and synaptic impairments induced by stress, without altering $A_{2A}R$ levels [45].

There is a growing awareness of AD beginning as a synaptic pathology [111], but very little is known concerning LTD in these animals [112–114]. We now demonstrate that, as our Tg(CaMKII-hA_{2A}R) model, APP/PS1 animals exhibit this LTD-to-LTP shift. Alterations in NMDAR have been consistently linked to AD pathology [59, 115–119] that we now report to be dependent on $A_{2A}R$ activation. This abnormal $A_{2A}R$/NMDAR crosstalk may underlie the efficiency of $A_{2A}R$ blockade in reverting memory deficits in animal models of AD [26, 35, 39].

The combined evidence of an increased $A_{2A}R$ expression in hippocampal neurons from humans (aged individuals and AD patients) and from animal models of these physiopathological conditions (Fig. 1; [26, 46, 68]) and the complete rescue of the LTD-to-LTP shift upon $A_{2A}R$ acute blockade stresses out $A_{2A}R$ as a putative pathological mediator involved in calcium dysfunction underlying age- and AD-related cognitive deficits, involving an aberrant recruitment of mGluR5/NMDAR coupled to an altered Ca^{2+} influx (see Supplementary Fig. 5 for a summary).

Methods

Human samples

The use of human samples was conducted in accordance with the Helsinki Declaration as well as national ethical guidelines. Protocols were approved by the Local Ethics Committee and the National Data Protection Committee. Human AD samples were provided by Valerie Buée-Scherrer (INSERM UMR-S1172 "Alzheimer & Tauopathies", Lille Neurobank, Jean-Pierre Aubert Research Center Univ. Lille-Nord de France, France) or by Pedro Pereira and José Pimentel (Laboratório de Neuropatologia, Hospital de Santa Maria, CHLN, EPE, Lisboa, Portugal). Samples were collected from brains at 36 h post mortem. Aged and young human samples were collected by Beatriz S. da Silva (National Institute of Legal Medicine and Forensic Sciences, Coimbra, Portugal) and prepared by Paula M. Canas (CNC-Center for Neurosciences and Cell Biology, Univ. Coimbra, Coimbra, Portugal). After validation of their quality (Pliássova et al. 2016 [141]) young (20–40 years old), aged (60–75 years old) and AD (60–75 years old, Braak stages 5–6) human forebrain and hippocampus were used for histological analysis, Western blotting and qPCR as indicated.

Animals

Animal procedures were performed in accordance with the European Community guidelines (Directive 2010/63/EU), Portuguese law on animal care (DL 113/2013), and approved by the *Instituto de Medicina Molecular* Internal Committee and the Portuguese Animal Ethics Committee (*Direcção Geral de Veterinária*). Environmental conditions were kept constant: food and water ad libitum, 21 ± 0.5 °C, 60 ± 10% relative humidity, 12 h light/dark cycles, 2 to 3 rats per cage or 3 to 4 mice per cage. Only male animals were used in all experiments. Mice were sacrificed by cervical dislocation and rats were sacrificed by decapitation after anesthesia under halothane atmosphere. Male Tg (CaMKII-hA_{2A}R) Sprague-Dawley rats and their WT littermates with matched age (8–14 weeks old) or aged WT males (18–20 months old) were used for behavior and electrophysiology experiments. Male WT and APP/PS1 mice (11–12 months old) were used for electrophysiology experiments.

Generation and maintenance of transgenic animals

Transgenic rats with an overexpression of human $A_{2A}R$ cDNA under the control of the Ca^{2+}/calmodulin-dependent protein kinase II (CaMKII) promoter, Tg(CaMKII-hA_{2A}R), were generated as previously described [30]. Expression of $A_{2A}R$ was achieved in forebrain areas, mainly in the hippocampus and cortex. Relevantly, the endogenous r$A_{2A}R$ mRNA levels were not modified in the hippocampus [30]. Furthermore, there was no changes in adenosine A_1 receptor levels in the hippocampus of Tg(CaMKII-hA_{2A}R) animals [30].

Genotyping

Transgenic rats were identified by PCR (30 cycles, 58 °C annealing temperature) of their genomic DNA isolated from ear biopsies by the use of the CaMKII-hA2AR transgene-specific primers and rat β-actin primers as an internal control (Invitrogen, USA; see Supplementary Table 1). APP/PS1dE9 transgenic mice on C57Bl6/J background have been described elsewhere [120].

Genotyping was done by PCR analysis of tail DNA (30 cycles, 60 °C annealing temperature) using transgene-specific primers (APP and PrP) and tau as an internal control (Supplementary Table 1).

Oral administration of the drug

KW6002 (istradefylline), a selective $A_{2A}R$ antagonist [121, 122], was diluted in the drinking water (0.025% methylcellulose) and was orally administered to WT, Tg(CaMKII-h$A_{2A}R$) and aged animals, being continuously available. The experimenter was blinded to genotype for the duration of KW6002 administration. The weight of the animals and the volume intake were assessed twice a week and the concentration of the solution was adjusted so that the drug intake was maintained at 5 mg kg^{-1} per day. The treatment started at 5–7 weeks of age in WT and Tg(CaMKII-h$A_{2A}R$) and at 16 months of age in aged animals, and lasted for 1 month or 3 weeks, respectively, until sacrifice.

RNA extraction and quantitative real-time PCR analysis (RT-qPCR)

Total RNA was extracted and purified using the RNeasy Lipid Tissue Mini Kit (Qiagen, Germany). RNA quality was assessed by NanoDrop 2000 (Thermo Scientific, USA) analysis ($A_{260}/A_{280} \approx 2$; $A_{260}/A_{235} > 1.8$). Total RNA (2 µg) was reverse-transcribed using random primers and SuperScript™ First-Strand Synthesis System for RT-PCR (Invitrogen). RT-qPCR analysis was performed on a Corbett Rotor-gene 6000 apparatus (Qiagen, Germany) using Power SYBR Green PCR Master Mix (Applied Biosystems, UK), 0.2 µM of each primer and 1/20 dilutions of total cDNA (final concentration 0.4 ng/µl). The thermal cycler conditions were 10 min at 95 °C, 40 cycles of a two-step PCR, 95 °C for 15 s followed by 60 °C for 25 s with a final thermal ramp from 72 to 95 °C. Primer efficiencies ($E = 1 \pm 0.02$) were obtained from standard curves of serial dilutions (slope and R^2 around −3.3 and 0.99, respectively). The sequences of the primers used (all from Invitrogen, HPLC purified) are listed in Supplementary Table 1. Reference genes were PPIA (cyclophilin A) and β-actin for human tissues and PPIA, β-actin, Rpl13A and Pgk1 for rat tissue. Amplifications were carried out in triplicate in two independent runs, and according to the MIQE guidelines [123]. The relative expression of target genes was determined by the comparative CT method [124].

In situ hybridization

The in situ hybridization technique was adapted from previously described methods [125]. The sections mounted on RNAse free poly-L-lysine-coated slides were fixed in freshly prepared 4% paraformaldehyde solution for 30 min and rinsed in phosphate-buffered saline (PBS: 130 mM NaCl, 7 mM Na_2HPO_4, 3 mM NaH_2PO_4). All sections were dehydrated and dipped for 3 min in chloroform. After air drying, the sections were incubated overnight at 42 °C with 0.35×10^6 cpm per section of ^{35}S-labeled probes diluted in hybridization buffer, which consisted of 50% formamide, 4xSSC (1xSSC: 0.15 M NaCl, 0.015 M sodium citrate, pH 7.4), 1 × Denhardt's solution (0.02% polyvinylpyrrolidone, 0.02% bovine serum albumin (BSA), 0.02% Ficoll, 1% sarcosyl, 0.02 M sodium phosphate at pH 7.4, 10% dextran sulfate, 500 µg/ml yeast tRNA, 100 µg/ml salmon sperm DNA, and 60 mM dithiothreitol). After hybridization, the sections were rinsed for 4 × 15 min in 1xSSC at 55 °C, dehydrated and covered with Hyperfilm-βmax film (Amersham, Belgium) for 2 or 3 weeks. The oligonucleotide probes were synthesized using an Applied Biosystems 381A DNA synthesizer or Eurogentec (Belgium) with a GC to AT ratio between 45 and 65%. The human $A_{2A}R$ oligonucleotide probe (CAGCCCTGGGAGTGGTTCTTGC CCTCCTTTGGCTGACC-GCA) is complementary to nucleotides 123–166 in a partial human cDNA sequence [126] and has been previously used on human brain sections [127]. The rat $A_{2A}R$ probe (CCGCTCCCCTGGCA GGGGCTGGCTCTCCATC-TGCTTCAGCTG) is complementary to nucleotides 604–645 of the rat cDNA sequence [128]. Oligonucleotides were labeled with α-^{35}S dATP (DuPont-NEN, Belgium) at their 3' end by terminal DNA deoxynucleotidylexotransferase (Gibco, Belgium) and purified with a G50 column (Pharmacia, Belgium) according to the manufacturer's instructions.

Behavioral assessments

Rats were first handled for 5 days prior to behavioral tests. Mazes were cleaned with a 30% ethanol solution between each animal. Animals were randomized prior to behavioral assessment and the experimenter blinded to genotype for the duration of behavioral testing. All behavioral tests were performed during the light phase between 8:00 a.m. and 6:00 p.m. in a sound attenuated room.

Morris water maze (MWM)

Spatial memory ability was evaluated in the MWM test, as previously described [45]. WT and Tg(CaMKII-h$A_{2A}R$) animals were randomized and the experimenter blinded to genotype for the duration of behavioral testing. The test was performed over the course of 5 consecutive days and consisted of a 4-day acquisition phase and a 1 day probe test. The test was performed in a circular pool (1.8 m diameter, 0.6 m height), filled with water opacified with non-toxic black paint and kept at 25 ± 2 °C. A round 8-cm in diameter

platform was hidden 1 cm beneath the surface of the water at a fixed position. Four positions around the edge of the tank were used, dividing the tank into four quadrants: target quadrant (T, quadrant where the platform was hidden), left quadrant (L, quadrant on the left of the target quadrant), right quadrant (R, quadrant of the right of the target quadrant) and opposite quadrant (O, quadrant on the opposite side of the target quadrant). During the acquisition phase, each animal was given four swimming trials per day (30-mins inter-trial interval). A trial consisted of placing the animal into the water facing the outer edge of the pool and allowing the animal to explore and reach for the hidden platform. If the animal reached the platform before 60 s, it was allowed to remain there for 10 s. If the animal failed to find the target before 60 s, it was manually guided to the platform, where it was allowed to remain for 20 s. After the end of each trial, animals were removed from the pool and placed back to their home cages beneath heat lamps in order to prevent temperature loss. During the probe test, the platform was removed and animals were allowed to swim freely for 60 s while recording the percentage of time spent on each quadrant. The latency to find the platform during the acquisition phase and the percentage of time in the platform quadrant during the probe test were recorded and analyzed using the Smart 2.5 tracking system (PanLab, Barcelona) to evaluate hippocampal-dependent memory. Swimming speed was also registered, as a measure of possible motor deficits that could interfere with the ability to perform the task.

Y-maze behavior test

Short-term reference memory was assessed in a spontaneous novelty-based spatial preference Y-maze test. The Y-maze was performed in a two-trial recognition test in a Y-shaped maze with three arms (each with 35 cm length x 10 cm width x 20 cm height), angled at 120° and with opaque walls. Different cues were placed on the surrounding walls. Allocation of arms was counterbalanced within each group. On the first trial (learning trial), the animal explored the maze for 10 min with only two arms opened ("start" and "other" arm). Access to the third arm of the maze ("novel" arm) was blocked by an opaque door. The rat was then removed from the maze and returned to its home cage. After 1 h, the animal was placed again in the "start" arm of the maze, the door of the "novel" arm was removed and the rat was allowed to explore the maze for 5 min (test trial). Rat tracings were continuously monitored by an automated tracking system (Smart 2.5, PanLab, Barcelona). Preference for the novel arm is considered a measure of short-term reference memory. To exclude the possible confounding effect of alterations of locomotor activity, we used the frequency of entrance into the arms (number of transitions) as an indirect indicator of the general locomotor activity.

Electrophysiology experiments

After decapitation, the brain was rapidly removed and the hippocampi were dissected free in ice-cold Krebs solution, which is composed of (mM): NaCl 124; KCl 3; NaH_2PO_4 1.25; $NaHCO_3$ 26; $MgSO_4$ 1; $CaCl_2$ 2 and D-glucose 10, continuously gassed with 95% O_2 and 5% CO_2, pH 7.4. Transverse hippocampal slices (400 µm thick) were obtained with a McIlwain tissue chopper and field excitatory postsynaptic potentials (fEPSPs) were recorded in the *stratum radiatum* of the CA1 area at 32 °C, as previously described [45]. Tested drugs, SCH 58261 (50 and 100 nM), caffeine (30 µM), MPEP (5 µM) or AP5 (15, 50 and 100 µM), were added to the Krebs superfusion solution (3 ml/min) after obtaining a stable 10 min baseline. LTD was induced as previously [39] with three trains of 2 Hz during 10 min separated by a 10-min interval, or 1200 pulses at 0.5, 1, and 2 Hz, with baseline fEPSPs of 0.5 mV/ms. The magnitude of synaptic plasticity was calculated as percentage of change of fEPSP slope 50–60 min after LTD induction compared to baseline fEPSP (10 min before LTD induction). Recordings were performed at 32 °C, 3 ml/min.

For patch-clamp recordings, transverse hippocampal slices (300 µm) were cut in an oxygenated ice-cold solution containing (mM): 234 sucrose, 2.5 KCl, 1.25 NaH_2PO_4, 0.5 $CaCl_2$, 10 $MgSO_4$, 11 glucose, 26 $NaHCO_3$. They were incubated at 37 °C for 1 h and then maintained at room temperature (RT) for 0.5–5 h in an oxygenated physiological solution (ACSF) containing (in mM): 119 NaCl, 2.5 KCl, 1.25 NaH_2PO_4, 2.5 $CaCl_2$, 1.3 $MgSO_4$, 11 glucose, 26 $NaHCO_3$, pH 7.4. For recording, slices were transferred into a submerged recording chamber perfused with oxygenated ACSF at 3 ml/min at 32 °C and visualized under IR-DIC on a slidescope at x60 magnification (Scientifica Ltd., UK). Recordings were made using a patchstar micromanipulator (Scientifica Ltd.) connected to a Multiclamp700B amplifier and Digidata 1440 acquisition system controlled by the pClamp 10 software (Axon instruments, Molecular Devices Ltd., USA). Patch pipettes were made of borosilicate glass and shaped to a final resistance of approximately 5 MΩ.

Current clamp experiments

Whole-cell patch-clamp experiments were performed in the current clamp configuration [129] using a pipette solution containing (mM): 135 gluconic acid (potassium salt: K-gluconate), 5 NaCl, 2 $MgCl_2$, 10 HEPES, 0.5 EGTA, 2

ATP-Tris, and 0.4 Tris-GTP. After a tight seal (> 1 GΩ) on the cell body of the selected neuron was obtained, whole-cell patch-clamp configuration was established, and cells were left to stabilize for approximately 2 min before recordings began. The resting (V_m) membrane potential was first measured in the absence of any spontaneous firing, and only cells with V_m −55 mV were considered. We then injected a minimum amount of current (150 pA) to stimulate a sustained firing that we recorded for a few minutes. Using this tonic firing, we measured the fast and medium afterhyperpolarization potentials (fAHP and mAHP, respectively) (Supplementary Fig. 3a, b). The maximum rising slope, the overshoot and the action potential (AP) half-width were also considered (Supplementary Fig. 3a, b). The half-width value was calculated considering the AP width measured at 50% of the peak amplitude. These AP parameters were estimated without taking into account the voltage drop across the pipette resistance. To study the relationship between firing frequency and current input (Supplementary Fig. 3c, d), we first adjusted the membrane potential to −60 mV and then injected 16 pulses of increasing intensity (from 100 to 850 pA, 200 ms duration). We also used these recordings to measure the instantaneous firing frequency at the beginning (onset frequency, f_o, corresponding to the firing frequency measured between the first and second APs in the spike train) and at the end of the spike train (steady-state frequency, f_{ss}, corresponding to the firing frequency measured between the last two APs in the spike train) (Supplementary Fig. 3c). By plotting f_o and f_{ss} as a function of injected current (Supplementary Fig. 3e, f), we obtained information on the spike frequency adaptation of these neurons. To quantify the inward rectification time-dependent potential, we first adjusted the membrane potential (V_h) to −60 mV and injected 20 pulses of increasing intensity (from −100 pA to −2 nA, 600 ms duration). During the pulse, we observed that the hyperpolarization reached a maximum value (peak) and then decreased to stabilize to a steady-state value (Supplementary Fig. 3g). We plotted the difference between the peak and the steady-state values as a function of injected current to obtain indirect information on the hyperpolarization-activated inward current (Ih) (Supplementary Fig. 3h).

Voltage-clamp experiments

Whole-cell patch-clamp experiments were performed in the voltage-clamp configuration [117, 130] using a pipette solution containing (in mM): 117.5 cesium methanesulfonate, 15 CsCl, 10 tetraethylammonium chloride (TEACl), 8 NaCl, 10 HEPES, 0.25 EGTA, 4 MgATP, 0.3 NaGTP; the pH was adjusted to 7.3 with CsOH. For all experiments, slices were superfused with the oxygenated ACSF at 32 °C in the continuous presence of 50 µM picrotoxin (dissolved in Dimethylsulfoxide (DMSO), Sigma-Aldrich, France) to block GABAergic transmission. The Schaffer collateral pathway was stimulated at 0.10 Hz using electrodes (glass pipettes filled with ACSF) placed in the *stratum radiatum*. After a tight seal (> 1 GΩ) on the cell body of the selected neuron was obtained, whole-cell patch-clamp configuration was established, and cells were left to stabilize for approximately 2 min before recordings began. To measure the paired-pulse ratio (PPR), two stimuli were delivered with inter-spike intervals between 50 and 200 ms. PPRs were calculated as the ratio between the peak amplitude of $EPSC_2$ and of $EPSC_1$ (20 sweeps average per inter-spike interval) (Supplementary Fig. 3i). To calculate the AMPAR/NMDAR ratio (Fig. 2f), cells were held at −65 mV to record AMPAR EPSCs and at + 40 mV to record NMDAR EPSCs. AMPAR EPSCs amplitudes were calculated by averaging 30 consecutive EPSCs recorded at −65 mV and measuring the peak compared to the baseline. NMDAR EPSCs amplitudes were calculated by averaging 30 consecutive EPSCs recorded at + 40 mV and measuring the amplitude 60 ms after EPSC onset compared to the baseline. Before starting *I-V* relationship measurements, stimulus intensity was set to evoke an EPSC of approximately 100 pA at −60 mV, normalizing the response and thus the number of recruited fibers. Liquid junction potential was not corrected for whole-cell voltage-clamp recordings. For $EPSC_{NMDAR}$ *I-V* relationship measurements (Fig. 2g), pharmacologically isolated NMDAR EPSCs were obtained in the presence of 6,7-dinitroquinoxaline-2,3-dione (DNQX, 100 µM dissolved in 1% DMSO, Sigma-Aldrich). NMDAR EPSCs amplitudes were calculated by averaging 15 consecutive EPSCs recorded at voltages ranging from −70 mV to + 40 mV in 10 mV steps. *I–V* relationships were normalized to the NMDAR EPSC amplitude at + 40 mV (as + 1). AMPAR *I–V* relationships were recorded using an identical procedure, but in presence of R-2-amino-5-phosphonopentanoate (AP5, 50 µM dissolved in DMSO, Sigma-Aldrich) and were normalized to the AMPAR EPSC amplitude at −70 mV (as -1). The decay time of pharmacologically isolated NMDAR EPSC, recorded from cells voltage clamped at + 40 mV, was fit with a double exponential function, using Clampfit software, to calculate both slow and fast decay time constants, τ_{slow} and τ_{fast}, respectively (Fig. 2i). The weighted time constant ($\tau_{weighted}$) was calculated using the relative contribution from each of these components, applying the formula: $\tau_w = [(a_f . \tau_f) + (a_s . \tau_s)]/(a_f + a_s)$, where a_f and a_s are the relative amplitudes of the two exponential components, and τ_f and τ_s are the corresponding time constants (Fig. 2i).

Primary neuronal cultures

Hippocampal neurons were cultured from 18 day Sprague-Dawley rat embryos (Harlan, Barcelona, Spain) as previously described [131]. Briefly, embryos were collected in Hank's Balanced Salt Solution (HBSS, Corning, USA) and rapidly decapitated. Meninges were removed, and whole cortices (hippocampi and attached cortex) were dissociated and incubated for 15 min in HBSS with 0.025% trypsin. Cells were washed once with HBSS with 30% fetal bovine serum (FBS), centrifuged three times, re-suspended in Neurobasal Medium (Gibco–Life Technologies, USA) supplemented with 2% B-27 supplement, 25 μM Glutamate, 0.5 mM glutamine, and 2 U/ml penicillin/streptomycin, gently dissociated and filtered through a 70 μm strainer (VWR, USA). Cells were plated on poly-D-lysine-coated plates and grown for 14 days at 37 °C in a 5% CO_2-humidified atmosphere in the previously described supplemented Neurobasal medium, in the absence of any positive selection for neurons.

Transfection of primary neuronal cultures

At DIV (day in vitro) 13, neurons were transfected as previously described [132]. A 33 ± 4% efficiency of transfection was obtained. At DIV 14, Ca^{2+} imaging experiments and immunocytochemistry to confirm transfection were performed.

Construct generation

Venus-A_{2A}R construct was generated with the In-fusion HD Cloning Kit (Clontech Takara, USA). Venus and A_{2A}R fragments were produced by using, respectively, the pair of primers 5'-GTTTAAACTTAAGCTTATGGTGAGCAAGG GCGAG-3' and 5'-GCTGCCCATGGTGGCCTTGTAC AGCTCGTCCATG-3', and the pair of primers 5'-GCCAC-CATGGGCAGCAGC-3' and 5'-AAACGGGCCCTCTAG ATCAGCTGGGGGCGAACTC-3'. PCR fragments were cloned into the vector pcDNA3.1(+) linearized with *Hin*dIII and *Xba*I, and the resulting construct was verified by DNA sequencing (GATC Biotech, Germany).

Ca^{2+} imaging

Primary neuronal cultures were plated at a density of 50×10^3 cells per well in 35 mm glass bottom culture dishes (MatTek Corporation, USA) previously coated with poly-D-lysine. At DIV 14, neurons were loaded with Fura-2 AM (5 μM, in external physiological solution with the following composition in mM: NaCl 125, KCl 3, NaH_2PO_4 1.25, $CaCl_2$ 2, $MgSO_4$ 1, D-(+)-glucose 10 and HEPES 10; pH 7.4 adjusted with NaOH) and incubated at 37 °C for 1 h. Cells were then placed on a heated chamber installed in an inverted microscope with epifluorescent optics and equipped with a high speed multiple excitation fluorimetric system (Lambda DG4, with a 175 W Xenon arc lamp). Fura-2 AM loaded neurons were sequentially excited both at 340 and 380 nm, for 250 ms at each wavelength, and the emission fluorescence was recorded at 510 nm with a charge-coupled device (CDD) camera. Experiments were performed on cells with a baseline fluorescence ratio around 0.5, which corresponds approximately to a $[Ca^{2+}]$i of about 100 nM, considered the normal $[Ca^{2+}]_I$ [133, 134]. Cells with a baseline fluorescence ratio above 1 were discarded. Experiments were performed at 37 °C in a 5% CO_2-humidified atmosphere. Drugs were applied directly to the cells medium. All cells were challenged with ionomycin (a Ca^{2+} ionophore; 2 μM) at the end of the experiment and only those that responded were included, confirming neuronal viability. Image data were recorded and analyzed using the MetaFluor software (Universal Imaging, West Chester, PA, USA).

Immunocytochemistry

Twenty-four hours after transfection, primary neurons were washed with PBS and fixed with 4% paraformaldehyde for 10 min at RT, followed by a permeabilization step with 0.5% Triton X-100 (Sigma–Aldrich) for 20 min at RT. After blocking in 10% FBS for 30 min, the cells were incubated with mouse anti-A_{2A}R primary antibody (1:100, mouse monoclonal, mab70192, Covalab, France) overnight at 4 °C. After a 30-min washing with PBS, cells were incubated with the secondary antibody Alexa Fluor 568 goat anti-mouse IgG (Life Technologies-Invitrogen) for 1 h at RT. Finally, the cells were stained with Hoechst 33258 (1 mg/mL, Life Technologies;1:5000 in PBS) for 5 min and mounted in Dako mounting medium. Z-stack images at 63 × magnification were acquired with a Zeiss LSM 880 confocal microscope.

Immunohistochemistry

Brains were removed, stored in formaldehyde 4% aqueous solution (VWR, USA) for 3 days, embedded in paraffin, and cut into coronal sections of 2 μm. Slides were deparaffinized, rehydrated and antigen retrieval was performed by microwave heating in 0.01 M citrate buffer pH = 6.0. For fluorescence analysis, slices were then incubated with primary antibodies selective for A_{2A}R (1:100, mouse monoclonal, mab70192, Covalab) and GFAP (1:250, rabbit polyclonal, G9269, Sigma-Aldrich), MAP2 (1:500, rabbit polyclonal, ab32454, Abcam, UK), SNAP25 (1:5000, rabbit polyclonal, S9684, Sigma-Aldrich), synaptophysin (1:200, mouse monoclonal, S7568, Sigma-Aldrich) or PSD95 (1:100, rabbit polyclonal, D27E11, Cell Signaling Technology, UK) overnight at RT and washed

for 20 min with PBS before being incubated overnight at RT with secondary antibodies (Alexa Fluor 488 donkey anti-rabbit and Alexa Fluor 568 donkey anti-mouse 1:400, Life Technologies, USA). After washing for 20 min, the sections were incubated with Hoechst 33342 (12 µg/ml final concentration; Thermo Scientific, USA), washed once and mounted in Dako Mounting Medium (Agilent, USA). Z-stack images at 63 × magnification were acquired with a Zeiss LSM 880 Confocal Microscope with Airyscan. The images were acquired with a 63 × objective, model Plan-Apochromat, a numerical aperture of 1.40 and a working distance of 0.19 mm. The images were acquired with a voxel size of *x*:132 nm, *y*:132 nm, *z*:316 nm, and the point spread function (PSF) monitored with beads of 175 nm was $XY = \min\ 205 \pm 4$ nm, max 234 ± 3 nm, and Z 478 ± 30 nm (emission wavelength 525 nm). Co-localization analysis between A_{2A}R and SNAP25/PSD95 was performed in single plans with co-localization threshold tool in Fiji software [135], which calculates several co-localization parameters and generates an image with co-localized pixels stained in white (Supplementary Fig. 2a, b). Compositional images of hippocampal formation were produced by tile stitching of images at 10 × magnification acquired using Zeiss Axio Observer Widefield microscope. For human samples, coronal sections were stained with an anti-A_{2A}R (1:100, mab70192, Covalab) and developed using amplification (NovoLink™ Polymer Detection System, Leica Biosystems, Germany) and horseradish peroxidase–diaminobenzidine (HRP-DAB) detection systems. In parallel, an age-matched control section was used as a negative control, where no primary antibody was used. Samples were then mounted in Entellan® mounting medium (Sigma-Aldrich). Optical density was measured using ImageJ software in one field of 20 × magnification and three fields of 40 × magnification.

Electron microscopy

Tg(CaMKII-hA_{2A}R) animals were anesthetized using isoflurane and fixed using perfusion pump with 0.1 M phosphate buffer containing 2% paraformaldehyde and 0.2% glutaraldehyde. After removal of the brain, 500 µm slices of hippocampus were collected using a Vibratome (Leica, Germany). Immunoelectron microscopy of hippocampal slices was performed according to Tokuyasu [136]. Slides were chemically fixed in 0.1 M phosphate buffer containing 2% paraformaldehyde and 0.2% glutaraldehyde, embedded in gelatine (Royal® food grade gelatine) and cryo-preserved in 2.3 M sucrose. Gelatine blocks were frozen in liquid nitrogen and sectioned at −120 °C using an cryo-ultramicrotome (UC7 and FC7, Leica) to generate 70 nm sections, sections were collected and thaw in a mixture of 2.3 M sucrose and 2% methylcellulose. Immunolabeling was done in 1% bovine serum albumin and 0.8% gelatine from cold water fish skin in PBS with polyclonal rabbit anti-A_{2A}R primary antibody (pab70273, 1:50, Covalab) and 15 nm gold coupled Protein A (CMC Utrecht, 1:50). After immuno-labeling, the sections were stained and mounted in a mixture of 3% (aq.) uranyl acetate and 2% methylcellulose. Images were taken using a Hitachi H-7650 electron microscope at 100 kV acceleration. We counted the immunogold particles in 40 micrographs (total of 72 synapses) of the CA1 area of Tg (CaMKII-hA_{2A}R) animals (according to ref. [137]) and evaluated blindly by two pathologists. We found an average of 2.4 particles/synapse. The gold labeling in synapses elements was categorized into pre or post (< 30 nm within the active zone) and perisynaptic (< 30 nm outside the active zone). No particles were found in the nucleus.

Fractionation

Subcellular fractionation was performed as described previously [138]. Briefly, WT and Tg(CaMKII-hA_{2A}R) frozen hippocampi were homogenized with Potter in a buffer containing sucrose 0.32 M and HEPES 10 mM. After centrifugation (1000 g for 10 min), the pellet was dissolved in a buffer containing HEPES 4 mM and EDTA 1 mM. After centrifugation (12,000 × *g* for 20 min), the pellet was dissolved in a buffer containing HEPES 20 mM, NaCl 100 mM, triton X-100 0.5%. After centrifugation (12,000 × *g* for 20 min), the supernatant is the non-postsynaptic density membrane fraction (non-PSD95-enriched fraction), as confirmed by the detection of enriched SNAP25 and the absence of PSD95 (Fig. 1h). The pellet was dissolved in a buffer containing HEPES 20 mM, NaCl 0.15 mM, triton X-100 1%, deoxycholic acid 1%, SDS 1% and centrifuged for 15 min at 10,000 × *g*. The supernatant is the postsynaptic density membrane fraction (PSD95-enriched fractions), as demonstrated by the detection of enriched PSD95 and sparse SNAP25. Equal volumes of non-PSD95 and PSD95-enriched fractions were diluted in sample buffer (see western blotting section) and denatured by heating to 65 °C for 20 min and used for western blot analysis.

Western blotting

Tissue was homogenized by sonication using RIPA buffer (50 mM Tris, 1 mM EDTA, 150 mM NaCl, 0.1% SDS, 1% Tergitol-type NP-40, pH 8.0). The protein concentration was determined using a BioRad DC Protein assay kit [based on ref. [139])]. The appropriate volume of each sample was diluted in water and sample buffer (70 mM Tris pH 6.8, 6% glycerol, 2% SDS, 120 mM dithiothreitol and 0.0024% Bromophenol blue). The samples were denatured at 65 °C for 20 min. Based on the protocol of Towbin et al. [140], samples and molecular weight markers were separated by sodium dodecyl sulfate polyacrylamide gel electrophoresis (10% for resolving and a 5% for stacking gels) in denaturing conditions and electro-transferred to Polyvinylidene fluoride (PVDF) membranes (GE Healthcare, UK). Membranes were blocked with 3% BSA in TBS-T

0.1% (Tris-buffered saline with 0.1% Tween-20 solution, 200 nM Tris, 1.5 M NaCl) for 1 h and incubated with primary antibody (diluted in TBS-T, 3% BSA and 0.1% NaN_3) overnight at 4 °C. Primary antibodies were mouse anti-$A_{2A}R$ (1:2000, 05-717, Upstate/Millipore, Germany), rabbit anti-SNAP25 (1:10,000, S9684, Sigma), rabbit anti-pan-cadherin (1:20,000, ab6529, Abcam), rabbit anti-PSD95 (1:1000, D27E11 Cell Signaling Technology) and mouse anti-α-tubulin (1:1000, sc-8035, Santa Cruz Biotechnology, USA). After three washing periods of 10 min with TBS-T, membranes were incubated with horseradish peroxidase (HRP)—conjugated anti-mouse or anti-rabbit secondary antibodies (1:10 000; Santa Cruz Biotechnology) (in 5% nonfat dry milk) for 1 h at RT. After 30 min of washing with TBS-T, chemiluminescent detection was performed with Enhanced chemiluminescence (ECL) western blotting detection reagent (GE Healthcare) using X-Ray films (Fujifilm, Japan). Optical density was determined with Image-J software and normalized to the respective pan-cadherin or tubulin band density.

Drugs

The $A_{2A}R$ selective antagonist, 2-(2-furanyl)-7-(2-phenylethyl)-7H-pyrazolo[4,3-e][1,2,4]triazolo[1,5-c]¬pyrimi¬din-5-amine (SCH 58261) and the $A_{2A}R$ selective agonist 2-[*p*-(2-Carboxyethyl)-phenylethylamino]-5'-*N*-ethylcarboxamidoadenosine (CGS 21680) were purchased from Tocris (UK). GABA receptor antagonist picrotoxin, AMPA receptor antagonist 6,7-dinitroquinoxaline-2,3-dione (DNQX) and NMDA receptor antagonist (2 *R*)-amino-5-phosphonovaleric acid (AP5) were purchased from Sigma-Aldrich. mGluR5 antagonist 6-Methyl-2-(phenylethynyl)-pyridine hydrochloride (MPEP) was purchased from Enzo Life Sciences (USA). These drugs were diluted in the assay solution from 5 mM or 1 mM stock aliquots made in DMSO or water stored at –20 °C. All other reagents used were of the highest purity available either from Merck or Sigma–Aldrich.

Statistical analysis

All statistical analyses were performed with GraphPad Prism software. Values are presented as mean ± s.e.m. in figure legends. Statistical analyses were designed using the assumption of normal distribution and similar variance among groups, as previously tested. Statistical comparisons included two-sided unpaired *t*-test, one or two-way ANOVA followed by a Bonferroni's or Tukey's multiple comparison post hoc tests as specified in the figure legends. *P*-values of < 0.05 were considered to be statistically significant. The sample size was determined based on Power Analysis or similar experiments carried out in the past. Power Analysis was performed using G-power in order to estimate the number of animals required, for a signal-to-noise ratio of 1.4 and 80% to 90% power assuming a 5% significance level.

Data availability

For detailed information on experimental design please see the provided Reproducibility Checklist. Full-length gels and blots with molecular weight standards are provided in Supplementary Fig. 6. All the software used to data analysis is commercially available and the respective information is provided in each respective section. The data that support the findings of this study are available from the corresponding authors upon reasonable request.

Acknowledgements MT-F is an FCT/PhD Fellow (IMM Lisbon BioMed PhD program; SFRH/BD/52228/2013); VLB, DGF and JEC were supported by a fellowship from Fundação para a Ciência e Tecnologia (FCT, Portugal); LVL is an Investigator FCT. TFO is supported by the DFG Center for Nanoscale Microscopy and Molecular Physiology of the Brain, Goettingen, Germany. RAC is supported by Maratona da Saúde, Santa Casa da Misericórdia and ERDF, through Centro 2020 (project CENTRO-01-0145-FEDER-000008: BrainHealth 2020), and through FCT (projects POCI-01-0145-FEDER-007440 and PTDC/NEU-NMC/4154/2016). DB, VBS, EF, and LB are supported by Région Hauts de France (PARTNAIRR COGNADORA), ANR (ADORATAU and SPREADTAU), LECMA/Alzheimer Forschung Initiative, Programs d'Investissements d'Avenir LabEx (excellence laboratory) DISTALZ (Development of Innovative Strategies for a Transdisciplinary approach to AD), France Alzheimer/Fondation de France, the FHU VasCog research network (Lille, France), Fondation pour la Recherche Médicale, Fondation Plan Alzheimer, INSERM, CNRS, Université Lille 2, Lille Métropole Communauté Urbaine, FEDER, DN2M, LICEND, and CoEN. LVL and DB are supported by AAP Internationalization, Université de Lille. EF is supported by ANR and Université de Lille. We would like to thank the Lille Neurobank for providing human brain tissues. HM and PAP supported by ATIP/AVENIR program (Center National de la Recherche Scientifique—CNRS), by the Foundation Plan Alzheimer (Senior Innovative Grant 2010) and PP by the Fondation pour la Recherche Médicale (FRM post-doctoral fellowship). Funded by LISBOA-01-0145-FEDER-007391, project co-financed by FEDER, POR Lisboa 2020—Programa Operacional Regional de Lisboa, from PORTUGAL 2020 and by Fundação para a Ciência e a Tecnologia (PTDC/BIM-MEC/47778/2014). We acknowledge Varsha Prabhakar and iMM Rodent and Bioimaging Facilities—especially to José Rino, for critical review of the manuscript-, and Histology and Comparative Pathology Laboratory for technical assistance.

Author contributions MT-F has written the draft, designed and performed most of the experimental work. VB and DGF performed the behavior assays and some electrophysiological experiments. MT-F and PAP performed whole-cell patch-clamp recordings. JEC performed some calcium influx experiments. JP, PP, PC, EF, and VB-S provided and processed the human samples. IM-M performed the immunohistochemistry assays. RG performed the qPCR. AP performed the electron microscopy experiments. SC performed the fractionation protocol. MB generated the Tg(CaMKII-h$A_{2A}R$); SS and LC performed the in situ hybridization. MT-F and RG made the in-frame Venus-$A_{2A}R$ construct starting from a Venus plasmid (provided by TFO) and the $A_{2A}R$ plasmid (provided by DB). YB and CEM synthesized, analyzed, and provided KW6002. MT-F, TFO, LB, DB,

RAC, HM, PAP, and LVL designed the experiments and wrote the manuscript. LVL coordinated the project. All authors revised the manuscript and discussed the experimental findings. The manuscript has been read and approved by all named authors

Compliance with ethical standards

Conflict of interest RAC is a scientific consultant for the non-profit organization Institute for Scientific Information. All other authors declare that they have no conflict of interest.

References

1. Walsh DM, Selkoe DJ. Deciphering the molecular basis of memory failure in Alzheimer's disease. Neuron. 2004;44:181–93.
2. DeKosky ST, Scheff SW. Synapse loss in frontal cortex biopsies in Alzheimer's disease: correlation with cognitive severity. Ann Neurol. 1990;27:457–64.
3. Kullmann DM, Lamsa KP. Long-term synaptic plasticity in hippocampal interneurons. Nat Rev Neurosci. 2007;8:687–99.
4. Roselli F, Tirard M, Lu J, Hutzler P, Lamberti P, Livrea P, et al. Soluble beta-amyloid1-40 induces NMDA-dependent degradation of postsynaptic density-95 at glutamatergic synapses. J Neurosci Off J Soc Neurosci. 2005;25:11061–70.
5. Almeida CG, Tampellini D, Takahashi RH, Greengard P, Lin MT, Snyder EM, et al. Beta-amyloid accumulation in APP mutant neurons reduces PSD-95 and GluR1 in synapses. Neurobiol Dis. 2005;20:187–98.
6. Shankar GM, Li S, Mehta TH, Garcia-Munoz A, Shepardson NE, Smith I, et al. Amyloid-beta protein dimers isolated directly from Alzheimer's brains impair synaptic plasticity and memory. Nat Med. 2008;14:837–42.
7. Lynch MA. Long-term potentiation and memory. Physiol Rev. 2004;84:87–136.
8. Malenka RC, Nicoll RA. Long-term potentiation-a decade of progress? Science. 1999;285:1870–4.
9. Martin SJ, Grimwood PD, Morris RG. Synaptic plasticity and memory: an evaluation of the hypothesis. Annu Rev Neurosci. 2000;23:649–711.
10. Christie BR, Kerr DS, Abraham WC. Flip side of synaptic plasticity: long-term depression mechanisms in the hippocampus. Hippocampus. 1994;4:127–35.
11. Collingridge GL, Peineau S, Howland JG, Wang YT. Long-term depression in the CNS. Nat Rev Neurosci. 2010;11:459–73.
12. Ge Y, Dong Z, Bagot RC, Howland JG, Phillips AG, Wong TP, et al. Hippocampal long-term depression is required for the consolidation of spatial memory. Proc Natl Acad Sci USA. 2010;107:16697–702.
13. Bliss TV, Collingridge GL. A synaptic model of memory: long-term potentiation in the hippocampus. Nature. 1993;361:31–9.
14. Lisman J. A mechanism for the Hebb and the anti-Hebb processes underlying learning and memory. Proc Natl Acad Sci USA. 1989;86:9574–8.
15. Norris CM, Korol DL, Foster TC. Increased susceptibility to induction of long-term depression and long-term potentiation reversal during aging. J Neurosci Off J Soc Neurosci. 1996;16:5382–92.
16. Kumar A, Thinschmidt JS, Foster TC, King MA. Aging effects on the limits and stability of long-term synaptic potentiation and depression in rat hippocampal area CA1. J Neurophysiol. 2007;98:594–601.
17. Foster TC. Involvement of hippocampal synaptic plasticity in age-related memory decline. Brain Res Brain Res Rev. 1999;30:236–49.
18. Foster TC, Norris CM. Age-associated changes in Ca(2+)-dependent processes: relation to hippocampal synaptic plasticity. Hippocampus. 1997;7:602–12.
19. Horgusluoglu-Moloch E, Nho K, Risacher SL, Kim S, Foroud T, Shaw LM, et al. Targeted neurogenesis pathway-based gene analysis identifies ADORA2A associated with hippocampal volume in mild cognitive impairment and Alzheimer's disease. Neurobiol Aging. 2017;60:92–103.
20. Canas PM, Duarte JMN, Rodrigues RJ, Köfalvi A, Cunha RA. Modification upon aging of the density of presynaptic modulation systems in the hippocampus. Neurobiol Aging. 2009;30:1877–84.
21. Costenla AR, Diógenes MJ, Canas PM, Rodrigues RJ, Nogueira C, Maroco J, et al. Enhanced role of adenosine A(2A) receptors in the modulation of LTP in the rat hippocampus upon ageing. Eur J Neurosci. 2011;34:12–21.
22. Diógenes MJ, Assaife-Lopes N, Pinto-Duarte A, Ribeiro JA, Sebastião AM. Influence of age on BDNF modulation of hippocampal synaptic transmission: interplay with adenosine A2A receptors. Hippocampus. 2007;17:577–85.
23. Lopes LV, Cunha RA, Ribeiro JA. Increase in the number, G protein coupling, and efficiency of facilitatory adenosine A2A receptors in the limbic cortex, but not striatum, of aged rats. J Neurochem. 1999;73:1733–8.
24. Lopes LV, Sebastião AM, Ribeiro JA. Adenosine and related drugs in brain diseases: present and future in clinical trials. Curr Top Med Chem. 2011;11:1087–101.
25. Rebola N, Sebastião AM, de Mendonca A, Oliveira CR, Ribeiro JA, Cunha RA. Enhanced adenosine A2A receptor facilitation of synaptic transmission in the hippocampus of aged rats. J Neurophysiol. 2003;90:1295–303.
26. Viana da Silva S, Haberl MG, Zhang P, Bethge P, Lemos C, Gonçalves N, et al. Early synaptic deficits in the APP/PS1 mouse model of Alzheimer's disease involve neuronal adenosine A2A receptors. Nat Commun. 2016;7:11915.
27. Li P, Rial D, Canas PM, Yoo J-H, Li W, Zhou X, et al. Optogenetic activation of intracellular adenosine A2A receptor signaling in the hippocampus is sufficient to trigger CREB phosphorylation and impair memory. Mol Psychiatry. 2015;20:1339–49.
28. Lopes LV, Cunha RA, Kull B, Fredholm BB, Ribeiro JA. Adenosine A(2A) receptor facilitation of hippocampal synaptic transmission is dependent on tonic A(1) receptor inhibition. Neuroscience. 2002;112:319–29.
29. Gonçalves ML, Cunha RA, Ribeiro JA. Adenosine A2A receptors facilitate 45Ca2 + uptake through class A calcium channels in rat hippocampal CA3 but not CA1 synaptosomes. Neurosci Lett. 1997;238:73–7.
30. Batalha VL, Ferreira DG, Coelho JE, Valadas JS, Gomes R, Temido-Ferreira M, et al. The caffeine-binding adenosine A2A

receptor induces age-like HPA-axis dysfunction by targeting glucocorticoid receptor function. Sci Rep. 2016;6:31493.
31. Pagnussat N, Almeida AS, Marques DM, Nunes F, Chenet GC, Botton PHS, et al. Adenosine A(2A) receptors are necessary and sufficient to trigger memory impairment in adult mice. Br J Pharmacol. 2015;172:3831–45.
32. Costa MS, Botton PH, Mioranzza S, Souza DO, Porciúncula LO. Caffeine prevents age-associated recognition memory decline and changes brain-derived neurotrophic factor and tirosine kinase receptor (TrkB) content in mice. Neuroscience. 2008;153:1071–8.
33. Prediger RDS, Batista LC, Takahashi RN. Caffeine reverses age-related deficits in olfactory discrimination and social recognition memory in rats. Involvement of adenosine A1 and A2A receptors. Neurobiol Aging. 2005;26:957–64.
34. Arendash GW, Cao C. Caffeine and coffee as therapeutics against Alzheimer's disease. J Alzheimers Dis Jad. 2010;20 (Suppl 1):S117–26.
35. Dall'Igna OP, Fett P, Gomes MW, Souza DO, Cunha RA, Lara DR. Caffeine and adenosine A(2a) receptor antagonists prevent beta-amyloid (25-35)-induced cognitive deficits in mice. Exp Neurol. 2007;203:241–5.
36. Laurent C, Eddarkaoui S, Derisbourg M, Leboucher A, Demeyer D, Carrier S, et al. Beneficial effects of caffeine in a transgenic model of Alzheimer's disease-like tau pathology. Neurobiol Aging. 2014;35:2079–90.
37. Cunha GMA, Canas PM, Melo CS, Hockemeyer J, Müller CE, Oliveira CR, et al. Adenosine A2A receptor blockade prevents memory dysfunction caused by beta-amyloid peptides but not by scopolamine or MK-801. Exp Neurol. 2008;210:776–81.
38. Kaster MP, Machado NJ, Silva HB, Nunes A, Ardais AP, Santana M, et al. Caffeine acts through neuronal adenosine A2A receptors to prevent mood and memory dysfunction triggered by chronic stress. Proc Natl Acad Sci USA. 2015;112:7833–8.
39. Laurent C, Burnouf S, Ferry B, Batalha VL, Coelho JE, Baqi Y, et al. A2A adenosine receptor deletion is protective in a mouse model of Tauopathy. Mol Psychiatry. 2016;21:97–107.
40. Eskelinen MH, Ngandu T, Tuomilehto J, Soininen H, Kivipelto M. Midlife coffee and tea drinking and the risk of late-life dementia: a population-based CAIDE study. J Alzheimers Dis Jad. 2009;16:85–91.
41. van Gelder BM, Buijsse B, Tijhuis M, Kalmijn S, Giampaoli S, Nissinen A, et al. Coffee consumption is inversely associated with cognitive decline in elderly European men: the FINE Study. Eur J Clin Nutr. 2007;61:226–32.
42. Maia L, de Mendonça A. Does caffeine intake protect from Alzheimer's disease? Eur J Neurol. 2002;9:377–82.
43. Ritchie K, Carrière I, de Mendonca A, Portet F, Dartigues JF, Rouaud O, et al. The neuroprotective effects of caffeine: a prospective population study (the Three City Study). Neurology. 2007;69:536–45.
44. Cunha RA. How does adenosine control neuronal dysfunction and neurodegeneration? J Neurochem. 2016;139:1019–55.
45. Batalha VL, Pego JM, Fontinha BM, Costenla AR, Valadas JS, Baqi Y, et al. Adenosine A(2A) receptor blockade reverts hippocampal stress-induced deficits and restores corticosterone circadian oscillation. Mol Psychiatry. 2013;18:320–31.
46. Espinosa J, Rocha A, Nunes F, Costa MS, Schein V, Kazlauckas V, et al. Caffeine consumption prevents memory impairment, neuronal damage, and adenosine A2A receptors upregulation in the hippocampus of a rat model of sporadic dementia. J Alzheimers Dis Jad. 2013;34:509–18.
47. Garman RH. Histology of the central nervous system. Toxicol Pathol. 2011;39:22–35.
48. Rebola N, Canas PM, Oliveira CR, Cunha RA. Different synaptic and subsynaptic localization of adenosine A2A receptors in the hippocampus and striatum of the rat. Neuroscience. 2005;132:893–903.
49. Cunha RA, Milusheva E, Vizi ES, Ribeiro JA, Sebastião AM. Excitatory and inhibitory effects of A1 and A2A adenosine receptor activation on the electrically evoked [3H]acetylcholine release from different areas of the rat hippocampus. J Neurochem. 1994;63:207–14.
50. Rombo DM, Newton K, Nissen W, Badurek S, Horn JM, Minichiello L, et al. Synaptic mechanisms of adenosine A2A receptor-mediated hyperexcitability in the hippocampus. Hippocampus. 2015;25:566–80.
51. Ferreira DG, Batalha VL, Vicente Miranda H, Coelho JE, Gomes R, Gonçalves FQ, et al. Adenosine A2A receptors modulate α-synuclein aggregation and toxicity. Cereb Cortex N Y N 1991. 2017;27:718–30.
52. Rebola N, Lujan R, Cunha RA, Mulle C. Adenosine A2A receptors are essential for long-term potentiation of NMDA-EPSCs at hippocampal mossy fiber synapses. Neuron. 2008;57:121–34.
53. Sarantis K, Tsiamaki E, Kouvaros S, Papatheodoropoulos C, Angelatou F. Adenosine A_2A receptors permit mGluR5-evoked tyrosine phosphorylation of NR2B (Tyr1472) in rat hippocampus: a possible key mechanism in NMDA receptor modulation. J Neurochem. 2015;135:714–26.
54. Collingridge GL, Kehl SJ, McLennan H. Excitatory amino acids in synaptic transmission in the Schaffer collateral-commissural pathway of the rat hippocampus. J Physiol. 1983;334:33–46.
55. Rosenmund C, Stern-Bach Y, Stevens CF. The tetrameric structure of a glutamate receptor channel. Science. 1998;280:1596–9.
56. Paoletti P, Bellone C, Zhou Q. NMDA receptor subunit diversity: impact on receptor properties, synaptic plasticity and disease. Nat Rev Neurosci. 2013;14:383–400.
57. Foster TC, Kumar A. Susceptibility to induction of long-term depression is associated with impaired memory in aged Fischer 344 rats. Neurobiol Learn Mem. 2007;87:522–35.
58. Wong TP, Howland JG, Robillard JM, Ge Y, Yu W, Titterness AK, et al. Hippocampal long-term depression mediates acute stress-induced spatial memory retrieval impairment. Proc Natl Acad Sci USA. 2007;104:11471–6.
59. Lanté F, Chafai M, Raymond EF, Pereira ARS, Mouska X, Kootar S, et al. Subchronic glucocorticoid receptor inhibition rescues early episodic memory and synaptic plasticity deficits in a mouse model of Alzheimer's disease. Neuropsychopharmacol Publ Am Coll Neuropsychopharmacol. 2015;40:1772–81.
60. Abraham WC, Mason-Parker SE, Logan B. Low-frequency stimulation does not readily cause long-term depression or depotentiation in the dentate gyrus of awake rats. Brain Res. 1996;722:217–21.
61. Ahmed T, Blum D, Burnouf S, Demeyer D, Buée-Scherrer V, D'Hooge R, et al. Rescue of impaired late-phase long-term depression in a tau transgenic mouse model. Neurobiol Aging. 2015;36:730–9.
62. Yang SN, Tang YG, Zucker RS. Selective induction of LTP and LTD by postsynaptic [Ca2 +]i elevation. J Neurophysiol. 1999;81:781–7.
63. Jia Z, Lu Y, Henderson J, Taverna F, Romano C, Abramow-Newerly W, et al. Selective abolition of the NMDA component of long-term potentiation in mice lacking mGluR5. Learn Mem Cold Spring Harb N. 1998;5:331–43.
64. Takagi N, Besshoh S, Morita H, Terao M, Takeo S, Tanonaka K. Metabotropic glutamate mGlu5 receptor-mediated serine phosphorylation of NMDA receptor subunit NR1 in hippocampal CA1 region after transient global ischemia in rats. Eur J Pharmacol. 2010;644:96–100.
65. Mannaioni G, Marino MJ, Valenti O, Traynelis SF, Conn PJ. Metabotropic glutamate receptors 1 and 5 differentially regulate

CA1 pyramidal cell function. J Neurosci Off J Soc Neurosci. 2001;21:5925–34.
66. Diógenes MJ, Costenla AR, Lopes LV, Jerónimo-Santos A, Sousa VC, Fontinha BM, et al. Enhancement of LTP in aged rats is dependent on endogenous BDNF. Neuropsychopharmacol Publ Am Coll Neuropsychopharmacol. 2011;36:1823–36.
67. Cramer PE, Cirrito JR, Wesson DW, Lee CYD, Karlo JC, Zinn AE, et al. ApoE-directed therapeutics rapidly clear β-amyloid and reverse deficits in AD mouse models. Science. 2012;335:1503–6.
68. Albasanz JL, Perez S, Barrachina M, Ferrer I, Martín M. Up-regulation of adenosine receptors in the frontal cortex in Alzheimer's disease. Brain Pathol Zur Switz. 2008;18:211–9.
69. Cunha RA, Constantino MC, Sebastião AM, Ribeiro JA. Modification of A1 and A2a adenosine receptor binding in aged striatum, hippocampus and cortex of the rat. Neuroreport. 1995;6:1583–8.
70. Cunha GMA, Canas PM, Oliveira CR, Cunha RA. Increased density and synapto-protective effect of adenosine A2A receptors upon sub-chronic restraint stress. Neuroscience. 2006;141:1775–81.
71. Varani K, Vincenzi F, Tosi A, Gessi S, Casetta I, Granieri G, et al. A2A adenosine receptor overexpression and functionality, as well as TNF-alpha levels, correlate with motor symptoms in Parkinson's disease. FASEB J Publ Fed Am Soc Exp Biol. 2010;24:587–98.
72. Li W, Silva HB, Real J, Wang Y-M, Rial D, Li P, et al. Inactivation of adenosine A2A receptors reverses working memory deficits at early stages of Huntington's disease models. Neurobiol Dis. 2015;79:70–80.
73. Tyebji S, Saavedra A, Canas PM, Pliassova A, Delgado-García JM, Alberch J, et al. Hyperactivation of D1 and A2A receptors contributes to cognitive dysfunction in Huntington's disease. Neurobiol Dis. 2015;74:41–57.
74. Giménez-Llort L, Schiffmann SN, Shmidt T, Canela L, Camón L, Wassholm M, et al. Working memory deficits in transgenic rats overexpressing human adenosine A2A receptors in the brain. Neurobiol Learn Mem. 2007;87:42–56.
75. Coelho JE, Alves P, Canas PM, Valadas JS, Shmidt T, Batalha VL, et al. Overexpression of Adenosine A2A receptors in rats: Effects on depression, locomotion, and anxiety. Front Psychiatry. 2014;5:67.
76. Orr AG, Hsiao EC, Wang MM, Ho K, Kim DH, Wang X, et al. Astrocytic adenosine receptor A2A and Gs-coupled signaling regulate memory. Nat Neurosci. 2015;18:423–34.
77. Matos M, Shen H-Y, Augusto E, Wang Y, Wei CJ, Wang YT, et al. Deletion of adenosine A2A receptors from astrocytes disrupts glutamate homeostasis leading to psychomotor and cognitive impairment: relevance to schizophrenia. Biol Psychiatry. 2015;78:763–74.
78. Burke SN, Barnes CA. Neural plasticity in the ageing brain. Nat Rev Neurosci. 2006;7:30–40.
79. Hajieva P, Kuhlmann C, Luhmann HJ, Behl C. Impaired calcium homeostasis in aged hippocampal neurons. Neurosci Lett. 2009;451:119–23.
80. Raza M, Deshpande LS, Blair RE, Carter DS, Sombati S, DeLorenzo RJ. Aging is associated with elevated intracellular calcium levels and altered calcium homeostatic mechanisms in hippocampal neurons. Neurosci Lett. 2007;418:77–81.
81. Oh MM, Oliveira FA, Waters J, Disterhoft JF. Altered calcium metabolism in aging CA1 hippocampal pyramidal neurons. J Neurosci Off J Soc Neurosci. 2013;33:7905–11.
82. Lopez JR, Lyckman A, Oddo S, Laferla FM, Querfurth HW, Shtifman A. Increased intraneuronal resting [Ca2 +] in adult Alzheimer's disease mice. J Neurochem. 2008;105:262–71.
83. Pierrot N, Ghisdal P, Caumont A-S, Octave J-N. Intraneuronal amyloid-beta1-42 production triggered by sustained increase of cytosolic calcium concentration induces neuronal death. J Neurochem. 2004;88:1140–50.
84. Pierrot N, Santos SF, Feyt C, Morel M, Brion J-P, Octave J-N. Calcium-mediated transient phosphorylation of tau and amyloid precursor protein followed by intraneuronal amyloid-beta accumulation. J Biol Chem. 2006;281:39907–14.
85. Querfurth HW, Selkoe DJ. Calcium ionophore increases amyloid beta peptide production by cultured cells. Biochem (Mosc). 1994;33:4550–61.
86. Keuker JIH, Luiten PGM, Fuchs E. Preservation of hippocampal neuron numbers in aged rhesus monkeys. Neurobiol Aging. 2003;24:157–65.
87. Pakkenberg B, Gundersen HJ. Neocortical neuron number in humans: effect of sex and age. J Comp Neurol. 1997;384:312–20.
88. Merrill DA, Roberts JA, Tuszynski MH. Conservation of neuron number and size in entorhinal cortex layers II, III, and V/VI of aged primates. J Comp Neurol. 2000;422:396–401.
89. Sebastião AM, Cunha RA, de Mendonça A, Ribeiro JA. Modification of adenosine modulation of synaptic transmission in the hippocampus of aged rats. Br J Pharmacol. 2000;131:1629–34.
90. Ciruela F, Casadó V, Rodrigues RJ, Luján R, Burgueño J, Canals M, et al. Presynaptic control of striatal glutamatergic neurotransmission by adenosine A1-A2A receptor heteromers. J Neurosci Off J Soc Neurosci. 2006;26:2080–7.
91. Ferré S, Ciruela F, Quiroz C, Luján R, Popoli P, Cunha RA, et al. Adenosine receptor heteromers and their integrative role in striatal function. Scientific World J. 2007;7:74–85.
92. Canhão P, de Mendonça A, Ribeiro JA. 1,3-Dipropyl-8-cyclopentylxanthine attenuates the NMDA response to hypoxia in the rat hippocampus. Brain Res. 1994;661:265–73.
93. Klishin A, Lozovaya N, Krishtal O. A1 adenosine receptors differentially regulate the N-methyl-D-aspartate and non-N-methyl-D-aspartate receptor-mediated components of hippocampal excitatory postsynaptic current in a Ca2 + /Mg(2 +)-dependent manner. Neuroscience. 1995;65:947–53.
94. Rodrigues RJ, Tomé AR, Cunha RA. ATP as a multi-target danger signal in the brain. Front Neurosci. 2015;9:148.
95. Augusto E, Matos M, Sévigny J, El-Tayeb A, Bynoe MS, Müller CE, et al. Ecto-5'-nucleotidase (CD73)-mediated formation of adenosine is critical for the striatal adenosine A2A receptor functions. J Neurosci Off. J Soc Neurosci. 2013;33:11390–9.
96. Lopes LV, Cunha RA, Ribeiro JA. Cross talk between A(1) and A(2A) adenosine receptors in the hippocampus and cortex of young adult and old rats. J Neurophysiol. 1999;82:3196–203.
97. Citri A, Malenka RC. Synaptic plasticity: multiple forms, functions, and mechanisms. Neuropsychopharmacol Publ Am Coll Neuropsychopharmacol. 2008;33:18–41.
98. Marchetti C, Marie H. Hippocampal synaptic plasticity in Alzheimer's disease: what have we learned so far from transgenic models? Rev Neurosci. 2011;22:373–402.
99. Dong Z, Bai Y, Wu X, Li H, Gong B, Howland JG, et al. Hippocampal long-term depression mediates spatial reversal learning in the Morris water maze. Neuropharmacology. 2013;64:65–73.
100. Nabavi S, Kessels HW, Alfonso S, Aow J, Fox R, Malinow R. Metabotropic NMDA receptor function is required for NMDA receptor-dependent long-term depression. Proc Natl Acad Sci USA. 2013;110:4027–32.
101. Tebano MT, Martire A, Rebola N, Pepponi R, Domenici MR, Grò MC, et al. Adenosine A2A receptors and metabotropic glutamate 5 receptors are co-localized and functionally interact in the hippocampus: a possible key mechanism in the modulation of N-methyl-D-aspartate effects. J Neurochem. 2005;95:1188–200.
102. Ferreira DG, Temido-Ferreira M, Miranda HV, Batalha VL, Coelho JE, Szegö ÉM, et al. α-synuclein interacts with PrP(C) to

induce cognitive impairment through mGluR5 and NMDAR2B. Nat Neurosci. 2017;20:1569–79.
103. Lea PM, Custer SJ, Vicini S, Faden AI. Neuronal and glial mGluR5 modulation prevents stretch-induced enhancement of NMDA receptor current. Pharmacol Biochem Behav. 2002;73:287–98.
104. Kouvaros S, Papatheodoropoulos C. Major dorsoventral differences in the modulation of the local CA1 hippocampal network by NMDA, mGlu5, adenosine A2A and cannabinoid CB1 receptors. Neuroscience. 2016;317:47–64.
105. Kumar A, Foster TC. Intracellular calcium stores contribute to increased susceptibility to LTD induction during aging. Brain Res. 2005;1031:125–8.
106. Jouvenceau A, Dutar P, Billard JM. Alteration of NMDA receptor-mediated synaptic responses in CA1 area of the aged rat hippocampus: contribution of GABAergic and cholinergic deficits. Hippocampus. 1998;8:627–37.
107. Thibault O, Hadley R, Landfield PW. Elevated postsynaptic [Ca2 +]i and L-type calcium channel activity in aged hippocampal neurons: relationship to impaired synaptic plasticity. J Neurosci Off. J Soc Neurosci. 2001;21:9744–56.
108. Norris CM, Halpain S, Foster TC. Alterations in the balance of protein kinase/phosphatase activities parallel reduced synaptic strength during aging. J Neurophysiol. 1998;80:1567–70.
109. Foster TC, Sharrow KM, Masse JR, Norris CM, Kumar A. Calcineurin links Ca2 + dysregulation with brain aging. J Neurosci Off J Soc Neurosci. 2001;21:4066–73.
110. Lee H-K, Min SS, Gallagher M, Kirkwood A. NMDA receptor-independent long-term depression correlates with successful aging in rats. Nat Neurosci. 2005;8:1657–9.
111. Selkoe DJ. Alzheimer's disease is a synaptic failure. Science. 2002;298:789–91.
112. Chang EH, Savage MJ, Flood DG, Thomas JM, Levy RB, Mahadomrongkul V, et al. AMPA receptor downscaling at the onset of Alzheimer's disease pathology in double knockin mice. Proc Natl Acad Sci USA. 2006;103:3410–5.
113. D'Amelio M, Cavallucci V, Middei S, Marchetti C, Pacioni S, Ferri A, et al. Caspase-3 triggers early synaptic dysfunction in a mouse model of Alzheimer's disease. Nat Neurosci. 2011;14:69–76.
114. Yang W, Zhou X, Zimmermann HR, Cavener DR, Klann E, Ma T. Repression of the eIF2α kinase PERK alleviates mGluR-LTD impairments in a mouse model of Alzheimer's disease. Neurobiol Aging. 2016;41:19–24.
115. Auffret A, Mariani J, Rovira C. Age-related progressive synaptic dysfunction: the critical role of presenilin 1. Rev Neurosci. 2010;21:239–50.
116. Auffret A, Gautheron V, Mattson MP, Mariani J, Rovira C. Progressive age-related impairment of the late long-term potentiation in Alzheimer's disease presenilin-1 mutant knock-in mice. J Alzheimers Dis Jad. 2010;19:1021–33.
117. Pousinha PA, Mouska X, Raymond EF, Gwizdek C, Dhib G, Poupon G, et al. Physiological and pathophysiological control of synaptic GluN2B-NMDA receptors by the C-terminal domain of amyloid precursor protein. eLife. 2017;6:1–29.
118. Zhang Y, Li P, Feng J, Wu M. Dysfunction of NMDA receptors in Alzheimer's disease. Neurol Sci Off J Ital Neurol Soc Ital Soc. Clin Neurophysiol. 2016;37:1039–47.
119. Snyder EM, Nong Y, Almeida CG, Paul S, Moran T, Choi EY, et al. Regulation of NMDA receptor trafficking by amyloid-beta. Nat Neurosci. 2005;8:1051–8.
120. Jankowsky JL, Slunt HH, Ratovitski T, Jenkins NA, Copeland NG, Borchelt DR. Co-expression of multiple transgenes in mouse CNS: a comparison of strategies. Biomol Eng. 2001;17:157–65.
121. Hockemeyer J, Burbiel JC, Müller CE. Multigram-scale syntheses, stability, and photoreactions of A2A adenosine receptor antagonists with 8-styrylxanthine structure: potential drugs for Parkinson's disease. J Org Chem. 2004;69:3308–18.
122. Yang M, Soohoo D, Soelaiman S, Kalla R, Zablocki J, Chu N, et al. Characterization of the potency, selectivity, and pharmacokinetic profile for six adenosine A2A receptor antagonists. Naunyn Schmiede Arch Pharmacol. 2007;375:133–44.
123. Bustin SA, Benes V, Garson JA, Hellemans J, Huggett J, Kubista M, et al. The MIQE guidelines: minimum information for publication of quantitative real-time PCR experiments. Clin Chem. 2009;55:611–22.
124. Schmittgen TD, Livak KJ. Analyzing real-time PCR data by the comparative C(T) method. Nat Protoc. 2008;3:1101–8.
125. Schiffmann SN, Vanderhaeghen JJ. Adenosine A2 receptors regulate the gene expression of striatopallidal and striatonigral neurons. J Neurosci Off J Soc Neurosci. 1993;13:1080–7.
126. Libert F, Parmentier M, Lefort A, Dinsart C, Van Sande J, Maenhaut C, et al. Selective amplification and cloning of four new members of the G protein-coupled receptor family. Science . 1989;244:569–72.
127. Schiffmann SN, Libert F, Vassart G, Vanderhaeghen JJ. Distribution of adenosine A2 receptor mRNA in the human brain. Neurosci Lett. 1991;130:177–81.
128. Fink JS, Weaver DR, Rivkees SA, Peterfreund RA, Pollack AE, Adler EM, et al. Molecular cloning of the rat A2 adenosine receptor: selective co-expression with D2 dopamine receptors in rat striatum. Brain Res Mol Brain Res. 1992;14:186–95.
129. Marcantoni A, Raymond EF, Carbone E, Marie H. Firing properties of entorhinal cortex neurons and early alterations in an Alzheimer's disease transgenic model. Pflug Arch. 2014;466:1437–50.
130. Marchetti C, Tafi E, Middei S, Rubinacci MA, Restivo L, Ammassari-Teule M, et al. Synaptic adaptations of CA1 pyramidal neurons induced by a highly effective combinational antidepressant therapy. Biol Psychiatry. 2010;67:146–54.
131. Valadas JS, Batalha VL, Ferreira DG, Gomes R, Coelho JE, Sebastião AM, et al. Neuroprotection afforded by adenosine A2A receptor blockade is modulated by corticotrophin-releasing factor (CRF) in glutamate injured cortical neurons. J Neurochem. 2012;123:1030–40.
132. Sariyer IK. Transfection of neuronal cultures. Methods Mol Biol Clifton NJ. 2013;1078:133–9.
133. Barhoumi R, Qian Y, Burghardt RC, Tiffany-Castiglioni E. Image analysis of Ca2 + signals as a basis for neurotoxicity assays: promises and challenges. Neurotoxicol Teratol. 2010;32:16–24.
134. Knot HJ, Laher I, Sobie EA, Guatimosim S, Gomez-Viquez L, Hartmann H, et al. Twenty years of calcium imaging: cell physiology to dye for. Mol Interv. 2005;5:112–27.
135. Costes SV, Daelemans D, Cho EH, Dobbin Z, Pavlakis G, Lockett S. Automatic and quantitative measurement of protein-protein colocalization in live cells. Biophys J. 2004;86:3993–4003.
136. Tokuyasu KT. Immunochemistry on ultrathin frozen sections. Histochem J. 1980;12:381–403.
137. Elsaesser A, Barnes CA, McKerr G, Salvati A, Lynch I, Dawson KA, et al. Quantification of nanoparticle uptake by cells using an unbiased sampling method and electron microscopy. Nanomed . 2011;6:1189–98.
138. Burnouf S, Martire A, Derisbourg M, Laurent C, Belarbi K, Leboucher A, et al. NMDA receptor dysfunction contributes to impaired brain-derived neurotrophic factor-induced facilitation of hippocampal synaptic transmission in a Tau transgenic model. Aging Cell. 2013;12:11–23.
139. Lowry OH, Rosebrough NJ, Farr AL, Randall RJ. Protein measurement with the Folin phenol reagent. J Biol Chem. 1951;193:265–75.
140. Towbin H, Staehelin T, Gordon J. Electrophoretic transfer of proteins from polyacrylamide gels to nitrocellulose sheets:

procedure and some applications. Proc Natl Acad Sci USA. 1979;76:4350–4.
141. Pliássova A, Canas PM, Xavier AC, da Silva BS, Cunha RA, Agostinho P. (2016) Age-Related Changes in the Synaptic Density of Amyloid-β Protein Precursor and Secretases in the Human Cerebral Cortex. J Alzheimers Dis. 2016;52:1209–14. https://doi.org/10.3233/JAD-160213.

Affiliations

Mariana Temido-Ferreira[1] · Diana G. Ferreira[1,2,3,4] · Vânia L. Batalha[1] · Inês Marques-Morgado[1] · Joana E. Coelho[1] · Pedro Pereira[5] · Rui Gomes[1,6] · Andreia Pinto[1] · Sara Carvalho[1] · Paula M. Canas[7,8] · Laetitia Cuvelier[9] · Valerie Buée-Scherrer[10] · Emilie Faivre[10] · Younis Baqi[11,12] · Christa E. Müller[11] · José Pimentel[5] · Serge N. Schiffmann[9] · Luc Buée[10] · Michael Bader[13,14,15] · Tiago F. Outeiro[2,16,17,18] · David Blum[10] · Rodrigo A. Cunha[7,8] · Hélène Marie[19] · Paula A. Pousinha[19] · Luísa V. Lopes[1]

1 Instituto de Medicina Molecular, Faculdade de Medicina de Lisboa, Universidade de Lisboa, 1649-028 Lisbon, Portugal

2 Department of Experimental Neurodegeneration, Center for Nanoscale Microscopy and Molecular Physiology of the Brain, Center for Biostructural Imaging of Neurodegeneration, University Medical Center Göttingen, Waldweg 33, 37073 Göttingen, Germany

3 Department of Pharmacology and Therapeutics, Faculty of Medicine, University of Porto, Porto, Portugal

4 MedInUP—Center for Drug Discovery and Innovative Medicines, University of Porto, 4200-450 Porto, Portugal

5 Laboratory of Neuropathology, Department of Neurosciences, Hospital de Santa Maria, CHLN, EPE, 1649-035 Lisbon, Portugal

6 Faculdade de Ciências da Universidade de Lisboa, 1749-016 Lisbon, Portugal

7 CNC-Center for Neuroscience and Cell Biology, University of Coimbra, 3004-504 Coimbra, Portugal

8 Faculty of Medicine, University of Coimbra, 3004-504 Coimbra, Portugal

9 Laboratory of Neurophysiology, ULB Neuroscience Institute, Université Libre de Bruxelles (ULB), 1070 Brussels, Belgium

10 Université de Lille, Institut National de la Santé et de la Recherche Medicale (INSERM), CHU Lille, UMR-S 1172 JPArc, "Alzheimer & Tauopathie", LabEx DISTALZ, Lille, France

11 PharmaCenter Bonn, Pharmazeutische Chemie I, Pharmazeutisches Institut, University of Bonn, Bonn, Germany

12 Department of Chemistry, Faculty of Science, Sultan Qaboos University, PO Box 36, Postal Code 123 Muscat, Oman

13 Max-Delbrück-Center for Molecular Medicine (MDC), 13125 Berlin, Germany

14 Charité-University Medicine, 10117 Berlin, Germany

15 Institute of Biology, University of Lübeck, 23652 Lübeck, Germany

16 Max Planck Institute for Experimental Medicine, 37075 Göttingen, Germany

17 CEDOC, Chronic Diseases Research Center, NOVA Medical School, Faculdade de Ciências Médicas, Universidade NOVA de Lisboa, 1150-082 Lisbon, Portugal

18 Institute of Neuroscience, The Medical School, Newcastle University, Framlington Place, Newcastle Upon Tyne NE2 4HH, United Kingdom

19 Université Côte d'Azur, CNRS UMR7276, IPMC, 06560 Valbonne, France